

Fluorescent Biodegradable Block Copolymer Nano-Assemblies for Bioimaging and Drug Delivery

A THESIS

SUBMITTED IN PARTIAL FULFILMENT OF THE

REQUIREMENTS

OF THE DEGREE OF

DOCTOR OF PHILOSOPHY

BY

Bhagyashree Kulkarni

Registration Number: 20123198



**DEPARTMENT OF CHEMISTRY
INDIAN INSTITUTE OF SCIENCE EDUCATION AND
RESEARCH (IISER), PUNE
PUNE 411 008, MAHARASTRA, INDIA**

OCTOBER 2018

Dedicated to

My Beloved Parents

My Lovely Husband

and

Little Son

for their endless support and encouragement




भारतीय विज्ञान शिक्षा एवं अनुसंधान संस्थान पुणे
INDIAN INSTITUTE OF SCIENCE EDUCATION AND RESEARCH PUNE
(An Autonomous Institution of Ministry of Human Resource Development, Govt. of India)
Dr. Homi Bhabha Road, Pune - 411 008.

Prof. Manickam Jayakannan
Department of Chemistry

CERTIFICATE

Certified that the work incorporated in the thesis entitled "*Fluorescent Biodegradable Block Copolymer Nano-Assemblies for Bioimaging and Drug Delivery*" submitted by Ms. Bhagyashree Kulkarni was carried out by the candidate under my supervision. The work presented here or any part of it has not been included in any other thesis submitted previous for the award of any degree or diploma from any other University or Institution


Date: 17th October 2018
Pune, Maharashtra, India


Professor M. Jayakannan
(Thesis Supervisor)
17/10/2018

DECLARATION

I affirm that this written thesis document represent my own ideas in words and the ideas that adopted from others' have been adequately cited and referenced the original sources. I also declare that, I have obeyed to all principles of scientific honesty, integrity and have not misrepresented or fabricated or falsified any idea/data/fact/source in my submission. I understand that violation of the above will be cause for disciplinary action by the institute and can also suggest penal action from the sources which have thus not been properly cited or from whom proper permission has not been taken when desired.

Date: 17th October 2018
Pune, Maharashtra, India


Bhagyashree Kulkarni
Roll No: 20123198

Acknowledgements

I take this opportunity to extend my great appreciation to all the people who helped and supported me to complete my Ph. D. thesis.

First of all, I would like to express my sincere gratitude and special appreciation to my thesis supervisor Prof. **M. Jayakannan** who accepted me as Ph. D. student and offered his mentorship. It would not have been able to accomplish this journey without his valuable guidance, continuous support and motivation. I thank him for putting his all efforts to shape my research life and encouraging me to explore my scientific potential. Working with him was a great pleasure and I could not have imagined having better mentor for my research study.

I would like to express my sincere thanks to former Director **Prof. K.N. Ganesh**, and **Prof. Jayant B. Udgaonkar**, present Director, IISER-Pune for providing world class research facility at IISER Pune carrying out this research work.

I would like to thank **Dr. Prakash Wadgaonkar** and **Dr. S. Britto** for being my research advisory committee (RAC) members and providing me valuable comments and suggestions during RAC meetings, to improve my research work.

I wish to thank **Dr. Asha, S. K.** as I have benefited greatly from her for valuable scientific discussion and suggestions that have been helpful for this study and extending research facilities in her laboratory.

I extend my sincere thanks to faculty members in the department of chemistry, IISER Pune for interactive scientific discussions and teaching me various chemistry courses.

I take the opportunity to give my heartfelt thanks to my present and former lab mates for providing their support, cooperation and stimulating environment which made my life memorable at IISER, Pune especially Dr. Mahima, Dr. Bala, Dr. Smita, Dr. Ananthraj, Dr. Pramod, Dr. Bapu, Dr. Narsimha, Dr. Rajendra, Moumita, Sonashree, Nilesh, Mehak, Uma, Vikas, Thameez, Maitreyee, Lipi, Khushboo, Shraddha, Nithish, Hemlata, yogita, Sharda, Mishika, Rasika, Khuddoos, Dheeraj, Ruma, Sharaffudin, Anu, uttareshwar, Pranav, Caroline, Rekha, Kaushal, Nagesh,

Chinmay, Shekhar, Nisha, Senthil, Saibal, Prajitha, Swapnil, Sandeep, Moumita, Shrikant and Sarabjot.

Special thanks to Dr. Bapurao, who have had an important academic influence on me. He has been wonderful colleague and I have learned a lot about how to do interesting research and overcome the difficulties in research work.

I would like to extend special thanks to Mehak, Sonashree and Nilesh for their immense help to provide me cytotoxicity studies, cellular uptake studies and confocal microscopy imaging and FACS analysis. Without these data I would not be able to finish my thesis work.

I would like to thank all instrument technicians of IISER Pune for their support: Pooja, Deepali, Chinmay (NMR), Swati (MALDI), Sandeep (HRMS), Megha (AFM), Anil, Yatish (FE-SEM). I thank National Chemical Laboratory (NCL) Pune for HR TEM facilities.

I am indebted to many other friends for providing an inspiring and fun filled environment in IISER Pune, especially Madhuri, Nagesh, Trimbak, Prabhakar and all other friends. I also thank all the staff members in administration, finance, accounts, stores, and library, canteen especially, Ms. Naina, Mr. Mayuresh, Mr. Nitin and Mr. Tushar for their immediate help whenever I needed them. I also thank the entire cleaning depot to keeping campus clean and clear.

I would like to express the deepest gratitude to my parents for unconditional love, affection and support. They always encouraged me to pursue my dreams. I would not be who I am today without them. Their patience and sacrifices will always remain my inspiration through-out my life. I wish to give my heartfelt thanks to my brothers Gajanan, Gaurav, my sister in law Amruta and my princess Aarya for their unwavering support, encouragement and prayers.

I owe my deepest gratitude and appreciation to a very special person, my husband, Shailesh who always been my strength. His unconditional love, patience, understanding, and eternal support made the completion of this journey possible. I greatly value his every little thing done for me and deeply appreciate his contribution. I would like to extend my gratitude towards my little bundle of joy, sweet son, Sparsh whose arrival made this journey more wonderful. He contributed to my work by

Acknowledgements

encouraging me with his bright little smile. Words cannot express how grateful I am to both of you.

Financial support from UGC and IISER Pune is greatly acknowledged.

Bhagyashree

Synopsis

Fluorescent polymer nano-scaffolds provide unique opportunity to delivery cargoes as well as facilitate the real-time monitoring of nano-carriers under biological conditions. The combination of fluorescent properties in associating with enzymatic-biodegradation further enhance their potential as intercellular carrier-cum-bioprobes or theranostics for cellular level drug delivery and bio-imaging together in single nano-platform. The thesis is aimed to make new classes of amphiphilic block copolymer nano-system based on fluorescent polycaprolactone (PCL) using blue or red luminescent π -conjugated chromophores as fluorophores in the backbone. The resultant polymer nano-architectures were employed for loading and delivering anticancer drug like doxorubicin. Fluorescent tri-block copolymer was designed to chemical conjugation of Pt-drugs. These block copolymers were also explored for the development of FRET bio-probes for cancer cell imaging. The fluorescent block copolymer approach provides unique opportunity to understand the polymer chains self-organization phenomena as well their drug/bio-imaging applications. The thesis is divided into five chapters and their details are as follows:

Chapter 1: The introduction chapter provides detail literature survey on the polymer drug delivery, the role of macromolecular architectures in drug delivery, application of different types of block copolymers in drug delivery, π -conjugated polymer system in bio-imaging applications, the unique advantages of combining the π -conjugated polymer + biodegradable polymer systems in single platform for theranostics applications and put forward the concept for the aim of the thesis.

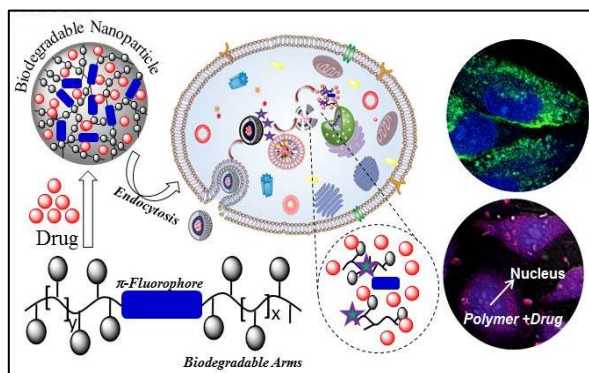
Chapter 2: Blue-luminescent biodegradable PCL block copolymers were designed and developed through ring opening polymerization process. A new polymerization π -conjugated blue fluorescent initiator was tailor-made based on oligo-phenylenevinylene chromophores. The OPV-containing blue fluorescent block nano-carrier was employed for intracellular delivery of delivering doxorubicin. Both bio-imaging and delivery was accomplished simultaneously at the intracellular level.

Chapter 3: Enzyme-responsive fluorescence resonance energy transfer probe (FRET-probe) was constructed using the OPV-tagged blue luminescent nano-scaffold as donor and Nile red fluorophore as acceptor. FRET probe was demonstrated for imaging in cancer cells and the photophysical properties were confirmed by details steady state and time-resolved spectroscopic studies.

Chapter 4: Red-luminescence PCL block copolymer were designed using perylenebisimide macro-initiator via ring opening polymerization process. The amphiphilic block copolymers readily dispersed in water and its aqueous nanoparticle was employed for bio-imaging in cancer cells.

Chapter 5: New triblock PCL copolymer was synthesized using the perylene-initiator. In this design, the carboxylic substituted PCL placed in the interior and PEG-chain anchored PCL as exterior to bring core-shell type nano-assemblies. Cisplatin was chemically conjugated in the CPCL part which produced water soluble fluorescent Pt-drug for treatment in cancer cells.

In chapter 2, new polymer drug delivery concept based on biodegradable polycaprolactone (PCL) and highly luminescent π -conjugated fluorophore is reported as dual functional nano-carrier for cellular imaging and delivery vehicles for



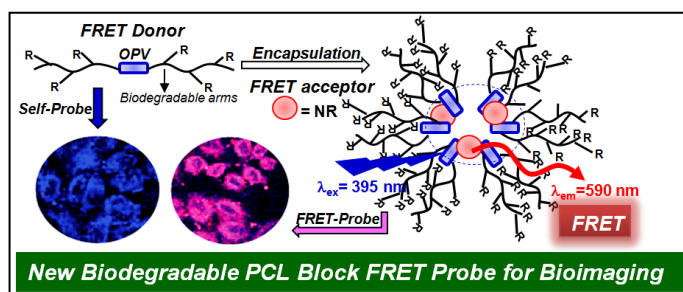
anticancer drug to cancer cells. To accomplish this goal, a new substituted caprolactone monomer was designed and it was subjected to ring opening polymerization using a blue luminescent bishydroxyl oligo-phenylenevinylene (OPV) fluorophore as an initiator. A series

of A-B-A triblock copolymer building blocks with a fixed OPV π -core and variable chain biodegradable PCL arm length were tailor-made. These triblocks self-assembled in organic solvents to produce well defined helical nanofibers whereas in water they produced spherical nanoparticles (size \sim 150 nm) with blue luminescence. The hydrophobic pocket of the polymer nanoparticle was found to be an efficient host for loading water insoluble anticancer drug such as doxorubicin (DOX). *In vitro* studies revealed that the biodegradable PCL arm was susceptible to enzymatic cleavage at the intracellular lysosomal esterase under physiological conditions to release the loaded drugs. The nascent nanoparticles were found to be non-toxic to cancer cells whereas the DOX loaded nanoparticles accomplished more than 80 % killing in HeLa cells. Confocal microscopic analysis confirmed the cell penetrating ability of the blue luminescent polymer nanoparticles and their accumulation preferably in the cytoplasm. The DOX loaded red luminescent polymer nanoparticles were also taken

up by the cells and the drug was found to be accumulated at the peri-nuclear environment.

In chapter 3, fluorophore-tagged biodegradable polycaprolactone (PCL) block copolymer FRET-probe for intracellular imaging in cancer therapy. This blue-

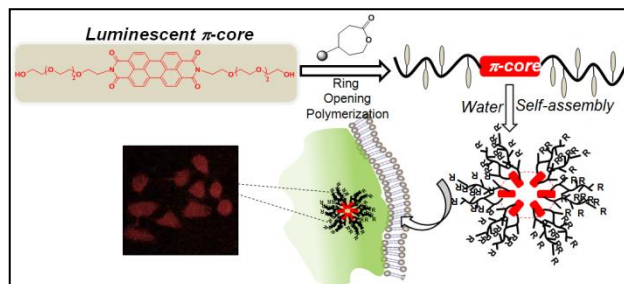
luminescent OPV-PCL triblock spherical nanoparticles (FRET donor) and it encapsulated water insoluble Nile red (NR, FRET acceptor) combinations



produce unique OPV-NR FRET probe. Selective photo excitation of OPV chromophore in block copolymer nano-assemblies enabled the excitation energy transfer from the OPV to NR and facilitated the efficient FRET process in aqueous medium. Time-correlated fluorescent decay dynamics and detail photophysical studies were carried out to estimate the Förster distance, donor-acceptor distance and the excitation energy transfer efficiency. The PCL chains in the FRET probe was susceptible for enzymatic biodegradation at the intracellular environment and the degradation process controlled the FRET on/off mechanism. Cytotoxicity studies revealed that the FRET probe was biocompatible and non-toxic to cells and the FRET-probe was found to be readily taken up by the cancer cells and it was internalized in the cytoplasm and peri-nuclear environment. Selective photo excitation of OPV chromophore in confocal microscope exhibited dual emission from the FRET probe. The cancer cells exhibited blue luminescence (self-emission) with respect to the OPV chromophore (in blue channel) and bright red-luminescence from the NR dye followed by the FRET process at the cellular level (in red channel). The dual luminescence characteristics, biodegradation and biocompatibility makes the newly designed PCL-OPV-NR FRET probe as an excellent biomedical nano-device for bioimaging application

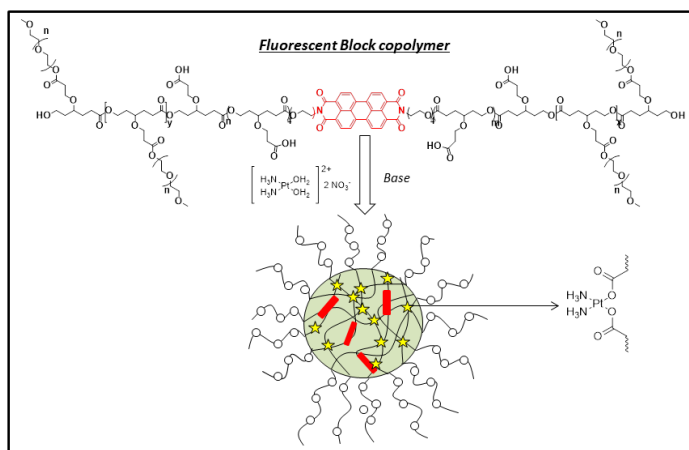
In chapter 4, water soluble highly fluorescent PBI derivatives with enzyme responsive amphiphilic biodegradable block copolymer was designed for cellular imaging in cancer cells. The carboxyl substituted polycaprolactone was incorporated as hydrophilic and biodegradable substituent on the imide position of PBI via ring opening polymerization. The amphiphilic block copolymers self-assembled as spherical nanoparticles of ~ 100 nm in aqueous medium. The hydrophilic PCL arms

ensured the water solubility and expected to hinder the aggregation of PBI chromophore in block copolymers. Importantly the desired photophysical properties of the PBI chromophore were retained in



aqueous medium. Enzyme responsive biodegradation studies revealed the possible degradation of polymer nanoparticles into small molecules which can be subsequently removed from the body after the intended purpose. The block copolymer nanoparticles with prominent features including high fluorescence, biodegradability and low toxicity were demonstrated for bioimaging application in cancer cells and exhibited good cellular uptake concurrently observed by inherent red fluorescence for the PBI chromophore. Hence, current polymer design with attractive photophysical properties of PBI and biodegradability of PCL backbone provided new opportunity for development of efficient nano-assemblies for bioimaging application.

In chapter 5, dual functional highly luminescent, biodegradable, cisplatin conjugated amphiphilic block copolymer nanocarriers was developed and it was



demonstrated for therapeutic and diagnostic application in cancer cells. New PBI-CPCL-PEGPCL block copolymer was designed and synthesized by ring opening polymerization. The polymer design comprises carboxylic acid is functionalized

polycaprolactone block to facilitate chemical conjugation of cisplatin and hydrophilic PEG substituted polycaprolactone block to obtain required amphiphilicity in the block copolymer. Moreover, highly fluorescent PBI chromophore provides opportunity to directly monitor fate of the drug inside the cells. The polymer nanocarriers prevented undesirable interactions of cisplatin with PBS, saline and GSH and protected the drug inside polymer-cisplatin conjugated nanoparticles. The *in vitro* drug release studies demonstrated that esterase enzyme triggered the cleavage of polymer-cisplatin conjugated nanoparticles to release cisplatin in to the medium. Cytotoxicity studies

confirmed high biocompatibility of the nascent polymer and hence utilized as fluorescent probe to track the non-fluorescent cisplatin delivery inside the cancer cells using non-invasive bioimaging tool. Further, Polymer-cisplatin conjugated NP exhibited comparable cell killing to that of free cisplatin in cancer cells. The cellular uptake followed by accumulation of the drug conjugated nanoparticles inside the cytoplasm was confirmed from the red fluorescence of PBI chromophore in the polymer by CLSM imaging. Thus,

The last chapter summarizes the thesis work and put forward the direction for future research. The new classes of fluorescent PCL block copolymers designed and developed in this thesis are new entries as enzymatic-biodegradable polymers in the literature; hence they would be expected to be very important nano-carriers for long-term application in the biomedical field. Further, the multifunctional block copolymer nanocarriers are promising candidates for simultaneous delivery and direct tracking of cisplatin inside the cancer cells. Thus, the work described in the thesis opens up opportunities in biomaterials arena based on fluorescent block copolymers.

TABLE OF CONTENTS

Chapter 1: Introduction	1
1.1. Introduction to drug delivery	2
1.2. Block Copolymers	14
1.3. Block copolymers in drug delivery	26
1.4. π -conjugated polymers in bioimaging	39
1.5. π -conjugate tagged block copolymer nanocarriers	49
1.6. Aim of the Thesis	53
1.7. References	55
Chapter 2: Dual Functional Nanocarriers for Cellular Imaging and Drug delivery to Cancer cells Based on π-Conjugated Core and Biodegradable Polymer Arms	
2.1. Introduction	63
2.2. Experimental Section	67
2.2.1 Materials	67
2.2.2. General Procedures	67
2.3. Results and Discussion	76
2.3.1. Synthesis and Characterization of Polymers	76
2.3.2. Self-Assemblies of polymers	80
2.3.3. Encapsulation Capabilities of BPCLx nanoparticles	84
2.3.4. <i>In vitro</i> drug release and cytotoxicity	87
2.3.5. Confocal microscope imaging and cellular uptake	91
2.4. Conclusion	93
2.5. References	94
Chapter 3: Fluorescent-Tagged Biodegradable Polycaprolactone Block Copolymer FRET Probe for Intracellular Imaging in Cancer Cells Nano-assemblies	
3.1. Introduction	98
3.2. Experimental Section	102
3.2.1. Materials	102

3.2.2. Methods	102
3.3. Results and Discussion	106
3.3.1. Synthesis, Self-assembly of fluorescent block copolymers	106
3.3.2. Encapsulation of acceptor and FRET process	110
3.3.3. Energy transfer and FRET distance	114
3.3.4. Enzyme responsiveness and FRET process	117
3.3.5. Cytotoxicity and FRET process in cancer cells	120
3.4. Conclusion	124
3.5. References	125

Chapter 4: Enzymatically Biodegradable Perylene Bisimide Carboxylic Polycaprolactone Fluorescent Block Copolymers for Bioimaging in Cancer Cells

4.1. Introduction	130
4.2. Experimental Section	135
4.2.1. Materials	135
4.2.2. Methods	135
4.3. Results and Discussion	140
4.3.1. Synthesis of fluorescent Block Copolymers	140
4.3.2. Self-assembly of fluorescent amphiphilic block copolymers	147
4.3.3. Photophysical characterization	150
4.3.4. Enzyme responsive biodegradation of block copolymers	152
4.3.5. Cytotoxicity and cellular uptake	155
4.4. Conclusion	156
4.5. References	158

Chapter 5: Perylene-Tagged Fluorescent Theranostic Triblock Nanocarriers for Pt-Drug Delivery in Cancer Cells

5.1. Introduction	162
5.2. Experimental Methods	169
5.2.1. Materials	169
5.3. Results and Discussion	175
5.3.1. Synthesis of block copolymers	175

5.3.2. Synthesis of block copolymer-cisplatin prodrug	179
5.3.3. Self-assembly of polymer-Pt prodrug	180
5.3.4. Stability and enzyme responsive delivery of Pt-prodrug	182
5.3.5. Cytotoxicity and cellular uptake	186
5.4. Conclusion	189
5.5. References	190
6. Summary and Future Directions	192
7. List of Publications	195
8. Appendix	199

Chapter 1

Introduction

1.1 Introduction to drug delivery

Cancer is a widespread disease and one of the leading causes of death due to genetic effect, environmental pollutants, unhealthy habits etc.^{1,2} Majority of anticancer drugs are small molecules (molecular weight under 500 g mole^{-1}) and these drugs are administered in to the body using conventional drug administration methods including injection, infusion, inhalation. The drug molecules encounter several disadvantages in biomedical applications which includes: (i) poor solubility in the aqueous media as majority of drugs are hydrophobic, (ii) short half-life of drugs due to high phagocytic and renal clearance, (iii) rapid breakdown of the drug after administration in the body, (iv) drugs are rapidly diffused in the normal tissue resulting in dose limiting side effects, and (v) due to the even distribution of drug within the body relatively low concentration of the drug reaches target tissue resulting in reduced therapeutic efficacy.^{3,4} One of the way to overcome the shortcoming exhibited by existing drugs is to develop new drugs through discovery. However, bringing a new drug through drug invention process is synthetically and scientifically challenging process. Moreover, clinical testing, regulatory approval make the process time consuming and expensive.⁵ Therefore, to meet these challenges, improving the therapeutic index of the existing drugs utilizing drug delivery system is the most versatile and facile approach. The concept of drug delivery was introduced as 'magic bullets' by Paul Ehrlich in 1906.³ An effective drug delivery system offers controlled drug release improving therapeutic efficacy of the drug which is achieved by continuous delivery of drug at predetermined rate over an extended duration. Further during the controlled release the concentration of the drug can be maintained within the therapeutic window which is beneficial over the conventional drug therapy wherein the drug plasma level experiences periods of ineffectiveness and toxicity which is shown in figure 1.1 The controlled drug release using drug delivery system beneficial for the drugs which are rapidly metabolized and eliminated from the body after administration. The drug is delivered to the particular part of the body lowering systemic drug level. This indeed reduces number of doses of drug administration which improves patient compliance.^{5,6}

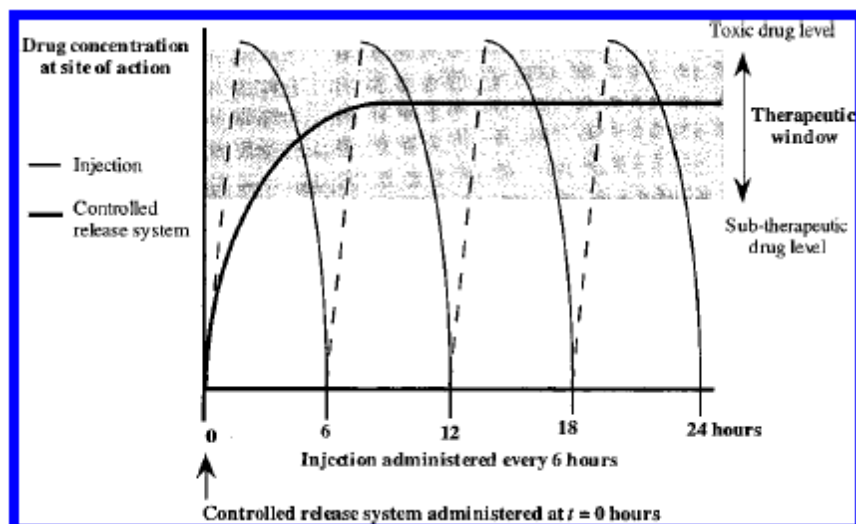


Figure 1.1. Drug concentration at site of therapeutic action after delivery as a conventional injection (thin line) and as controlled release system (bold line) (Adopted from Uhric et al *Chem. Rev.* **1999**, 99, 3181-3198)

An evolution in drug delivery capability has been witnessed by the development of nanotechnology by improving the therapeutic efficacy of the drug both in research as well as clinical settings.⁷ The term nanotechnology was first used by NarioTaniguchi in 1974 which refers to the ability of manipulating material at nanometer level.⁸ Nanotechnology aided drug delivery is concerned to the development of colloidal particles (hollow or solid structure) ranging from 1 to 100 nm size range in at least one dimension. The nanoscale sized materials exhibit distinct and significantly enhanced chemical, physical and biological properties unlike their bulk counterpart.⁸ These nanoscale materials offer suitable means of delivering therapeutic and imaging contrast agents to improve cancer diagnostics and therapeutics. The potential nanotherapeutic agent may help to achieve: (i) improving drug delivery of hydrophobic drug, (ii) reducing non-specific distribution (systemic toxicity) of drug by targeted delivery, (iii) effective intracellular delivery of macromolecular drug, (iv) improved half-life of drug by prolonged blood circulation time, (v) improved pharmacokinetic and pharmacodynamics of the therapeutic agent, (vi) controlled drug release over the required duration for optimal therapeutic efficacy, (vii) codelivery of two or more therapeutic modality for combination therapy, and (viii) enhanced drug absorption at the target site.^{7,9,10} Nanotherapeutic agents can be fabricated from small organic and polymeric or inorganic materials. The physicochemical properties of these therapeutic nanocarriers can be manipulated by

tailoring their chemical composition, size, shape, structure, morphology and surface properties.^{11,12} A wide range of nanotherapeutic agents available for drug delivery are shown in figure 1.2

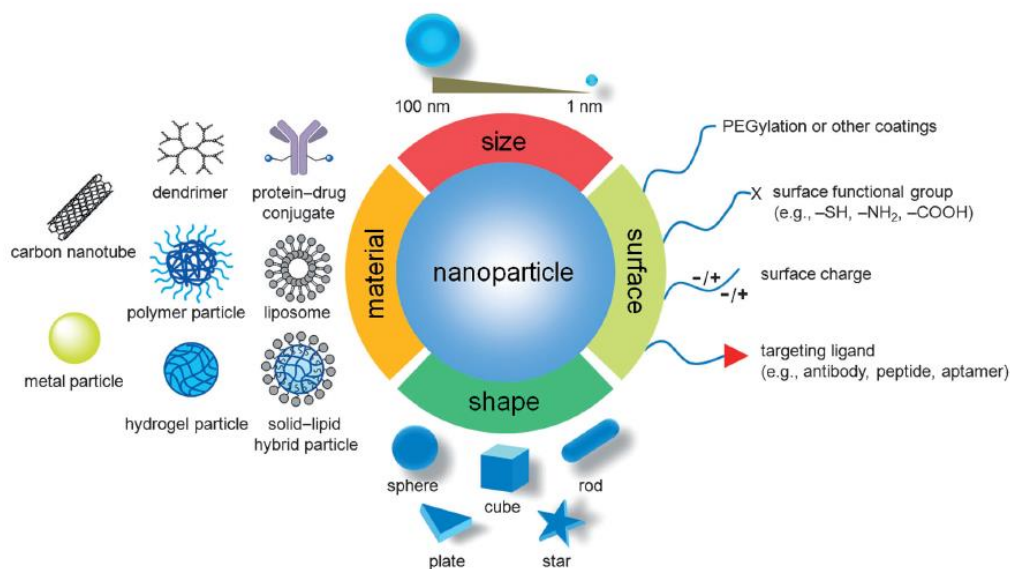


Figure 1.2. Different types of nanoparticles that have been explored as carriers for drug delivery in cancer therapy, together with illustration of physicochemical properties. (Adopted from Sun et al *Angew. Chem. Int. Ed.* **2014**, *53*, 12320-12364)

Liposomes, dendrimers, polymer nanocarriers and inorganic and other solid nanoparticles have been realized as promising drug delivery systems for effective cancer treatment. Liposomes are one of the most versatile nanocarriers available for drug delivery which have been known since 1960s. Liposomes consist of phospholipids offer distinct advantages including (i) they are composed of naturally occurring substances therefore they are nontoxic and nonimmunogenic (ii) unique ability to encapsulate hydrophobic and hydrophilic drugs due to the hollow and spherical morphology consisting of aqueous core and lipophilic shell. The coating of liposomes with PEG (PEGylated liposomes) has been extensively studied to improve stability and circulation half-life and reduce opsonization in the blood.¹³ Several peg-liposomes are in clinical trial whereas few of them have become successful for application in the cancer treatment. Liposomal anthracycline DOXIL was the first PEGylated liposome based nanomedicine approved for the treatment of breast cancer, ovarian cancer and Kaposi's sarcoma. DOX encapsulated pegylated liposomes reduces the dose limiting cardiac toxicity associated with free drug counterpart and it

has circulation half-life 100 folds longer than free DOX which eventually improves tumor uptake and therapeutic index of DOX.^{14,15}

Dendrimers were first reported in 1980s but recently have been realised as promising drug delivery system. Dendrimers are well defined, three dimensional, tree-like, regularly branched, monodisperse spherical architectures. Dendrimers are synthesized via two major approaches; convergent and divergent approach. Divergent approach is the most commonly used approach based on synthesis of initiator core first followed by stepwise addition of shell to form periphery. In convergent approach synthesis starts from periphery by the synthesis of individual dendrons which are subsequently coupled to core molecule or group.¹⁶ Other than chemical synthesis, dendrimers can also be prepared from supramolecular assembly of amphiphilic dendrons. Drug delivery of the hydrophobic drugs can be achieved by entrapment of drug molecules through noncovalent interactions such as ionic, hydrogen bonding, vander waals interactions in the core to improve the aqueous solubility of the drug and control their release profile. In an alternative approach, surface groups on the dendrimers can be covalently conjugated with chemotherapeutic agent and or targeting ligand via direct coupling or the pH sensitive linkages. The dendrimers-drug conjugation has emerged as promising approach for preclinical trials.¹⁷ Minko and co-workers prepared poly(propylenimine tetrahexacontaamine) dendrimers generation 5 (PPIG5) and condensed with siRNA against B-cell lymphoma m-RNA (BCL-antiapoptotic). The PPIG5-siRNA were further coated with PEG chains through redox responsive disulphide linkage, dimethyl-3-3'-dithiobispropionimide-HCL (DTBP) to facilitate intracellular siRNA release in presence of glutathione. Subsequently the complexes were coated with luteinizing hormone-releasing hormone (LHRH) peptide as targeting moiety. The LHRH-PEG-DTBP-PPIG5-siRNA exhibited higher cellular uptake for LHRH positive A2780 human ovarian carcinoma cells than LHRH-negative SKOV-3 cells whereas nontargeted nanoparticles did not show significant cellular uptake in both the cell lines. Further *in vivo* investigations revealed that LHRH-PEG-DTBP-PPIG5-siRNA showed higher tumor targeting efficiency and lower clearance by the liver and kidney than nontargeted nanoparticles as shown in figure 1.3.¹⁸

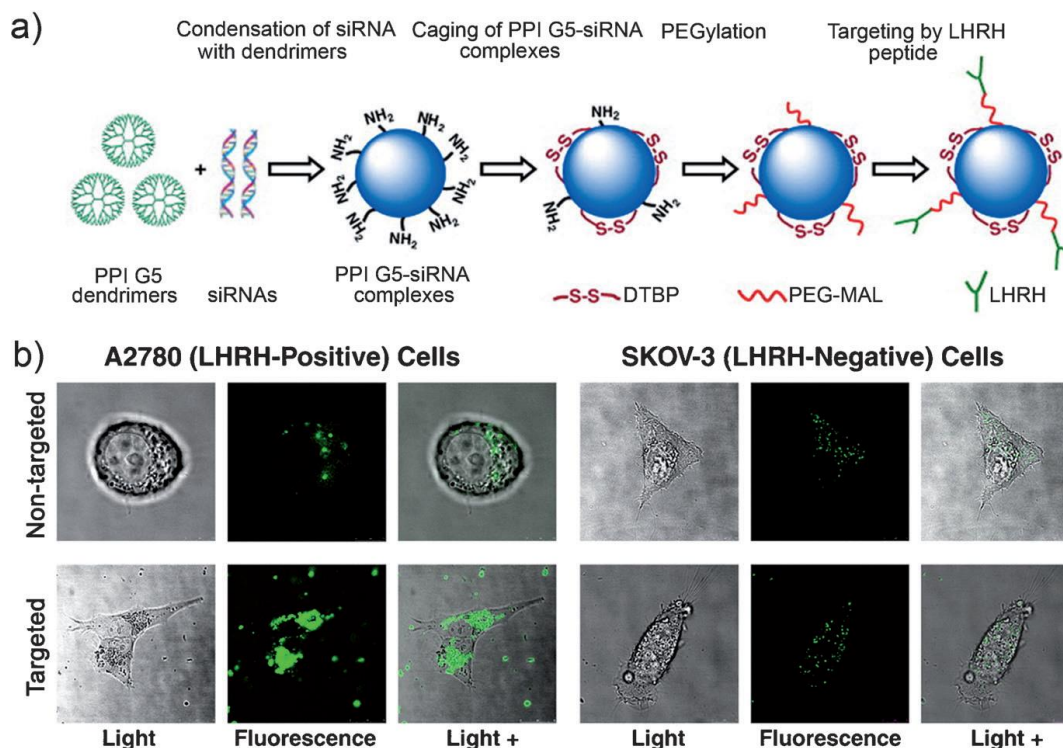


Figure 1.3. (a) Preparation of stable tumor targeted dendrimers nanoparticles for siRNA delivery (b) confocal microscopy images of LHRH-receptor positive A2780 and LHRH-receptor negative SKOV-3 human ovarian cancer cells incubated with fluorescence labelled nontargeted PEG-DTBP-PPIG5-siRNA-6-FAM green particles and targeted LHRH-PEG-DTBP-PPIG5-siRNA-6-FAM green particles (Adopted from Taratula et al *J. Controlled Release* **2009**, 140, 284-293)

The dendrimers-drug conjugation improved the half-life of the drug. In an example conjugation of methotrexate with poly(amidoamine) PAMAM dendrimers increased its half-life from 24 minutes to 24 h. The increased half-life improved the efficacy of drug which eventually reduces frequency of drug administration. This helps to improve patient's compliance.¹⁹ The polyglycerol dendrimers with 4-5 generations were synthesized and investigated for aqueous solubilisation of poorly water soluble paclitaxel drug.²⁰

Inorganic nanoparticles including gold, silver, iron oxide, silica, quantum dots, hydroxyapatite, carbon based nanostructures (grapheme oxide, carbon nanotubes, fullerenes) are an important category of drug delivery system due to precise control over size and shape, excellent physicochemical properties and functionality. In spite of their inability to degrade which limit their scope of application these materials have been extensively studied for diagnostic and therapeutic purposes^{8,11} as depicted in figure 1.4

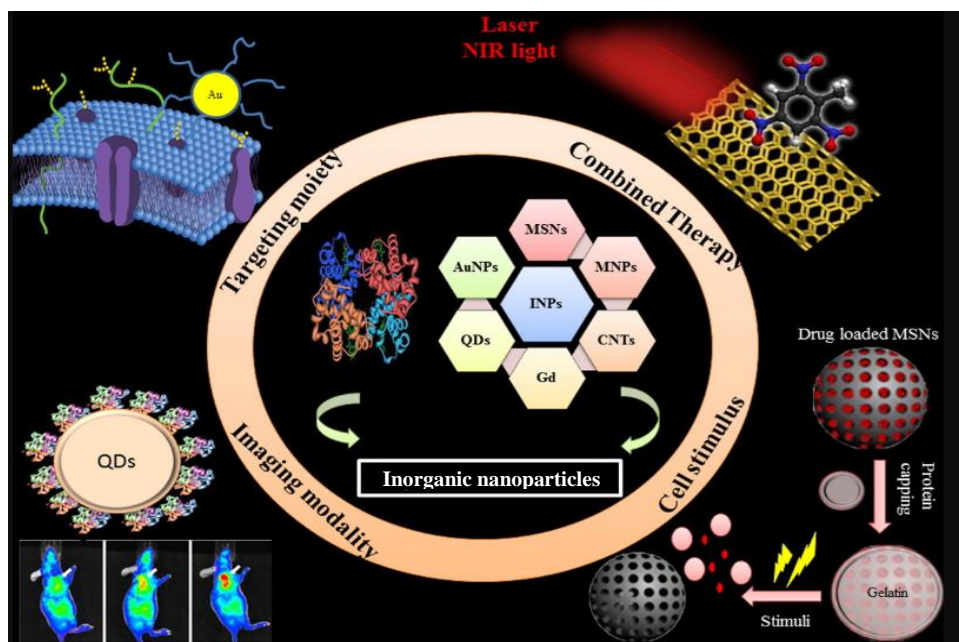


Figure 1.4. Different types of inorganic nanoparticles for drug delivery and cancer diagnostics. (Adopted from Elzoghby et al. *J. controlled Release* **2016**, 243,303-322)

Gold nanoparticles are widely used nanomedicines owing to their tuneable optical properties. Diverse range of gold nanoparticles have been investigated for hyperthermia application by modification of gold nanoparticles including gold nanorods, gold colloidal nanospheres, gold-silica nanoshells, gold-gold sulphide nanoparticles, hollow gold nanoshells, and smaller-diameter NIR-tunable gold nanocages. These gold nanoparticle designs for photothermal therapy application have been proved to be effective in preclinical studies and clinical examination of these nanoparticles is underway.²¹ Magnetic nanoparticles (MNP) are manufactured from maghemite ($\gamma\text{-Fe}_3\text{O}_2$) and magnetite (Fe_3O_4) and the drug is encapsulated or adsorbed on to the magnetic nanoparticles. These iron oxide magnetic nanoparticles facilitate cancer diagnosis through enhanced contrast and improve drug delivery by enhancing tumor cell death with magnetic hyperthermia.²² The water dispersibility of MNP is improved by surface coating with polymer materials which also helps to improve physical and chemical stability of the colloid.²³ Iron oxide MNP coated with oleic acid (OA) and pluronic F-127 which can be loaded with hydrophobic anticancer drug was evaluated for intravenous injection in rat to ensure their safe clinical use as these MNPs did not cause long-term changes in liver enzyme level or induce oxidative stress.²⁴

Carbon nanotubes have been used to deliver different types of therapeutic agents including anticancer drugs,²⁵ proteins,²⁶ DNA²⁷ and RNA.²⁸ Amine functionalized single walled carbon nanotubes (SWCNTs) were developed and demonstrated for platinum (IV) anticancer drug in testicular cancer cells. The efficient drug loading is achieved due to the extremely high specific surface area. Anticancer drug paclitaxel was conjugated to PEG substituted SWCNTs. *In Vivo* delivery of this drug CNT conjugate was studied in mice model bearing 4T1 breast tumor normally resistant to PTX treatment. These studies showed prolonged blood circulation with 10 fold higher drug uptake resulting in improved treatment efficacy than free paclitaxel.²⁵

Polymer nanocarriers have become an integral part of drug delivery in cancer treatment. The greatest advantage of polymers is their synthetic versatility which provides an opportunity to tune properties such as molecular weight, hydrophobicity, functionality in a controlled manner to optimize loading and release of the drug with improved pharmacokinetic properties. Compared to small molecule nanocarrier polymers exhibit higher stability and durability due to their mechanical and physical properties.¹¹ The polymer mediated drug delivery systems encompass polymer-drug conjugates, polyplexes, polymer hybrid systems, polymeric micelles, polymersomes for the targeted delivery of therapeutic agent to improve the efficiency of cancer treatment. The conjugation of drugs or proteins to water soluble polymer nanocarriers gained importance with development of Ringsdorf's model in 1975. The polymer-drug/protein conjugates are linked via spacer molecules such as anhydrides, hydrazone which are the predetermined breaking points for release of drug/proteins at the site of interest.³ The various polymers such as N-(hydroxypropyl)methacrylamide (HPMA), poly(glutamic acid) and poly(ethylene glycol) (PEG) and drug including doxorubicin, paclitaxol, camptothecin, methotrexate and platinum drugs have been explored for polymer-drug conjugation.²⁹ Doxorubicin conjugated to HPMA polymer through the amino sugar and tetra peptide spacer (PK1) as shown in figure 1.5 was first polymer-drug conjugate approved for clinical trials. The clinical studies revealed that the dose limiting side effects such as nausea, diarrhoea and carditoxicity were reduced to great extent as compared to free DOX and hence improved antitumor activity.^{30,31}

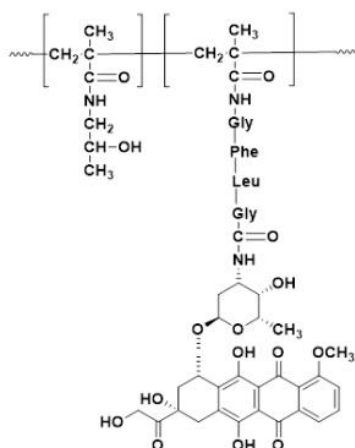


Figure 1.5 Chemical structure of the first clinically tested polymeric antitumor therapeutics PK1 (adopted from Haag and Kratz *et al.* *Angew. Chem. Int. Ed.* **2006**, *45*, 1198-1215)

Polymer directed enzyme prodrug therapy (PDEPT) is a combined antitumor approach involving polymeric prodrug and polymer-enzyme conjugate to facilitate enhanced drug release at the tumor site. PDEPT approach involves two steps; the administration of polymer-drug conjugate to enhance tumor targeting and subsequent administration of polymer-enzyme conjugate to promote the release of drug for improved therapeutics³² (see figure 1.6). In the PDEPT approach, the polymer-drug conjugate PK1 combined with (HPMA)-(cathepsin B) conjugate were utilized in the treatment of B16F10 melanoma tumors, which exhibited the antitumor activity for PDEPT approach of 168 % compared to 152 % for PK1 alone and 144 % for free DOX.³³

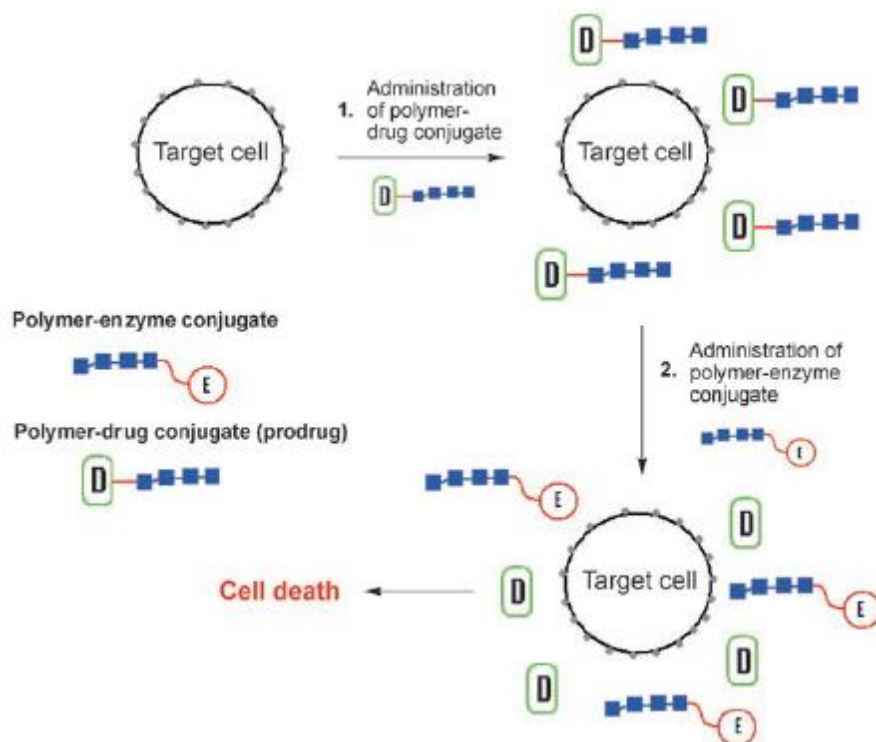


Figure 1.6. The PDEPT concept; After administration of the polymer-drug conjugate and uptake in the tissue, the polymer-enzyme conjugate is added to release the drug and induce cell death (adopted from Haag and Kratz et al. *Angew. Chem. Int. Ed.* **2006**, *45*, 1198-1215)

Li and co-workers prepared copolymers using monomethyl oligo(ethylene glycol) acrylate (OEGA), disulphide containing bis(2-acryloyloxyethyl) (BADS), acid labile 2-(5,5-dimethyl-1,3-dioxan-2-yioxy) ethyl acrylate (DMDEA) via miniemulsion copolymerization. These polymer nanogels exhibited thermoresponsive property and acid triggered hydrolysis of acid labile groups were observed upon incubation with weakly acidic medium (pH 4-6) or in response to 20 mM DTT at pH 7.4 due to the cleavage of disulphide linkage as shown in figure 1.7. The drugs such as PTX and DOX encapsulated nanogels revealed very slow drug release at physiological conditions (pH 7.4) and greatly accelerated in mild acidic conditions (pH 5-6). Further increase in drug release rate was observed in response to 20 mM DTT.³⁴

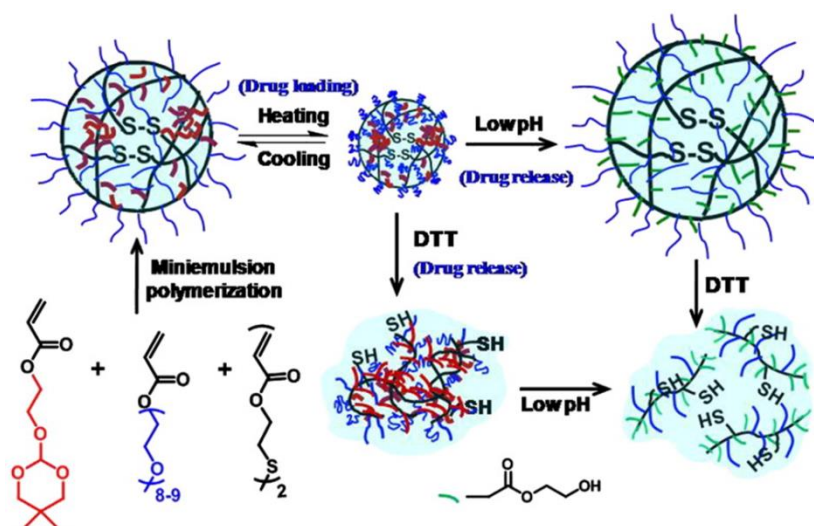


Figure 1.7. Temperature, pH and redox responsive polymer nanogels prepared by miniemulsion copolymerization for stimuli responsive delivery of drugs (adopted from Qiao et al. *J. Controlled Release* **2011**,152, 57-66)

The macromolecular-polymeric nanocarriers protect the drug from non-specific interaction during the transport through blood-stream and reticuloendothelial system (RES) offering reduced systemic toxicity.³⁵ These nanocarriers can access the target tissue by passive targeting through preferential accumulation at tumor site via well-known enhanced permeability and retention (EPR) effect. EPR effect is a result of the increased permeability of tumor vasculature to macromolecules and impaired lymphatic drainage in tumor tissue.¹⁵ The EPR effect was first observed by Maeda and coworkers while studying the inflammation induced by microbial infection and further the EPR effect was successfully demonstrated for tumor targeting for first time.³⁶ Unlike tight endothelial junctions of normal blood vessels the formation of large fenestration in tumor tissue due to the abnormal endothelial cells which leads to aberrant vascular architecture thereby increasing vascular permeability. This facilitates the selective extravasation of nanocarriers in tumor tissue. This increases the drug concentration in tumor tissue several folds higher than normal tissue. Further the lymphatic drainage system is either absent or dysfunctional facilitating the retention of nanocarriers are retained in the tumor tissue.³⁷ the EPR effect is schematically shown in figure 1.8

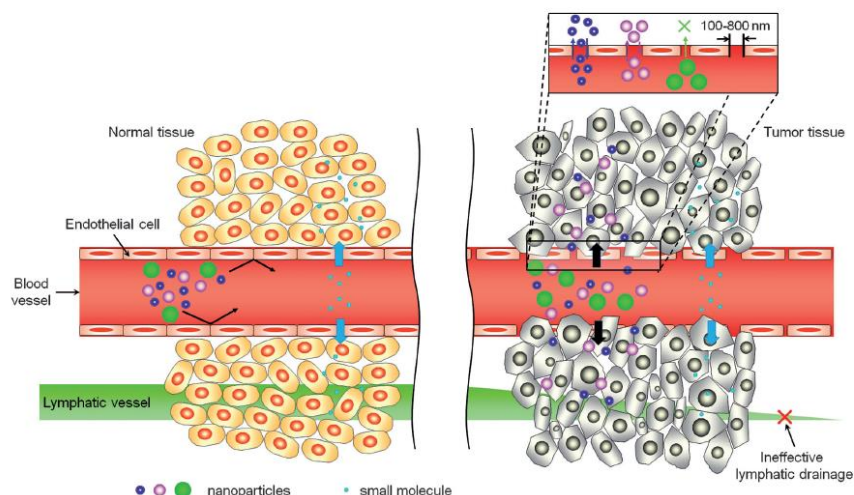


Figure 1.8. Transport of nanocarriers with different size and small molecules through normal and cancerous tissue. The enhanced permeability and retention (EPR) effect is a unique feature of most tumors, allowing nanocarriers of appropriate size to accumulate more in cancerous tissue than in normal tissues. . (Adopted from Sun et al *Angew. Chem. Int. Ed.* **2014**, 53, 12320-12364)

The active targeting can be achieved by ligand mediated targeting which utilizes the affinity ligand on the surface functionalization of nanocarriers which selectively binds to the receptors overexpressed in diseased cells.³⁸ (see figure 1.9) The commonly employed ligands include antibodies, proteins, peptides, nucleic acids, sugar, and vitamins. Proteins, sugars or lipids overexpressed on the cancer cells serves as target molecules.^{39,40} The active targeting nanocarriers should be in the close vicinity of their target substrate in order to recognize and interact with it and subsequently accumulate at the tumor tissue through ligand receptor interaction enhancing the internalization by the cells followed by release of the drug at the targeted site. Thus active targeting approach improves the intracellular concentration of drug in tumor tissue and reduces the toxic effects to the normal cells around the cancer tissue.¹⁰

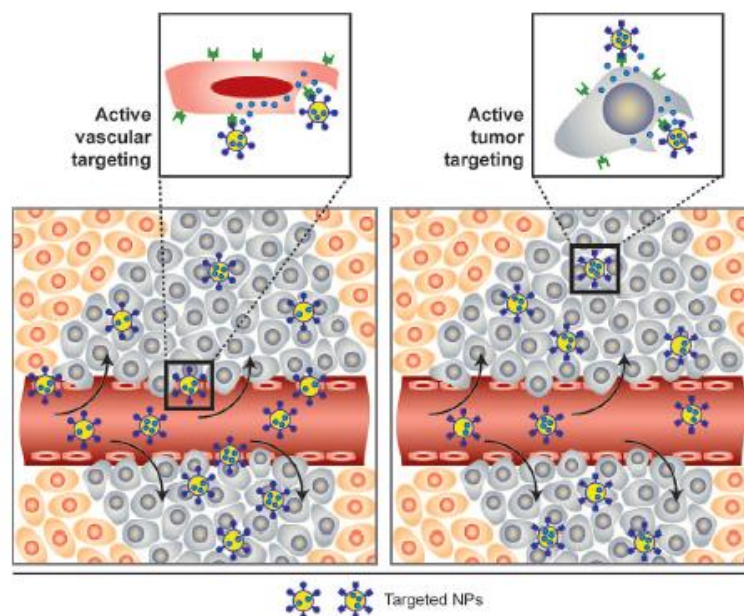


Figure 1.9. Active targeting of nanocarriers. The of ligands present on the particle surface which bind to receptors present on the target cell or the tissue resulting in enhanced accumulation and cellular uptake improving the therapeutic efficacy of drug.

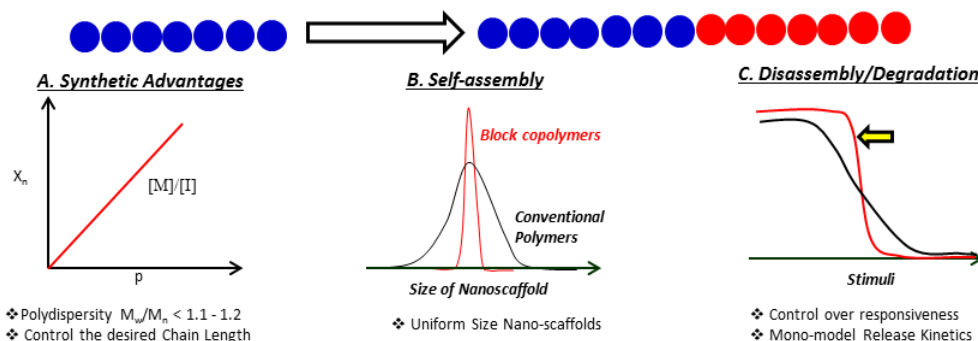


Figure 1.10. Schematic representation of features of block copolymers.

Among various Polymer nanocarriers block copolymers have gained significant interest in the drug delivery. The block copolymers have advantages over conventional polymers as follows; (i) block copolymers have well-defined structures with precise control over the molecular weight and narrow polydispersity (ii) desirable physicochemical properties as well as self-assembly behaviour can be achieved due to the well-defined structures which in turn results in controlled response against stimuli for delivery of drug. These features of block copolymers are schematically shown in figure 1.10.

1.2 Block copolymers

Block copolymers are an important class of polymers and the design, synthesis and properties of block copolymers is in high demand in academia as well as industry due to their unique ability to form a plethora of ordered nanoscale structures.⁴¹ The block copolymers are formed by two or more chemically distinct monomers attached together which can result in random or alternating copolymer depending upon the arrangement of different monomers within the polymer chain. Two or more monomers are arranged in random fashion to give random copolymer whereas the monomers are arranged in regular alternating fashion to form alternating copolymer. In addition to these arrangements of copolymer, sequential addition of different monomers leads to the formation of discrete block along the polymer chain to form block copolymer.^{42,43} The formation of different copolymers is schematically shown in figure 1.11.

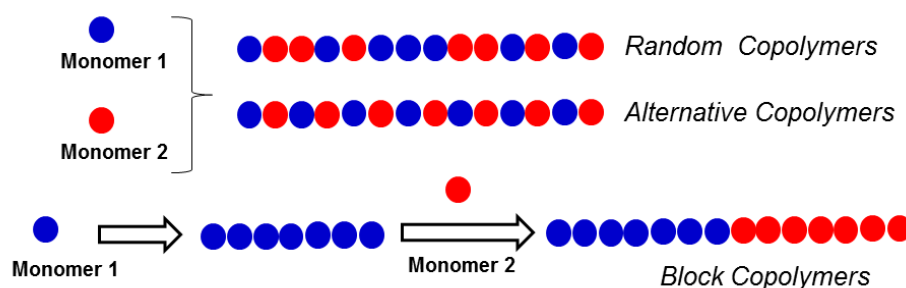


Figure 1.11. Schematic representation of types of copolymers

Further the number of monomers used in the polymerization results in diblock (two monomers) and triblock (three monomers) multi block (more than three monomers) copolymer formation. Further, apart from linear block copolymers nonlinear polymer topologies with wide range of architectures including miktorm, star, graft schematically shown in figure 1.12 have been prepared with extraordinary structural and compositional versatility to obtain extraordinary properties and variety of applications.^{44,45}

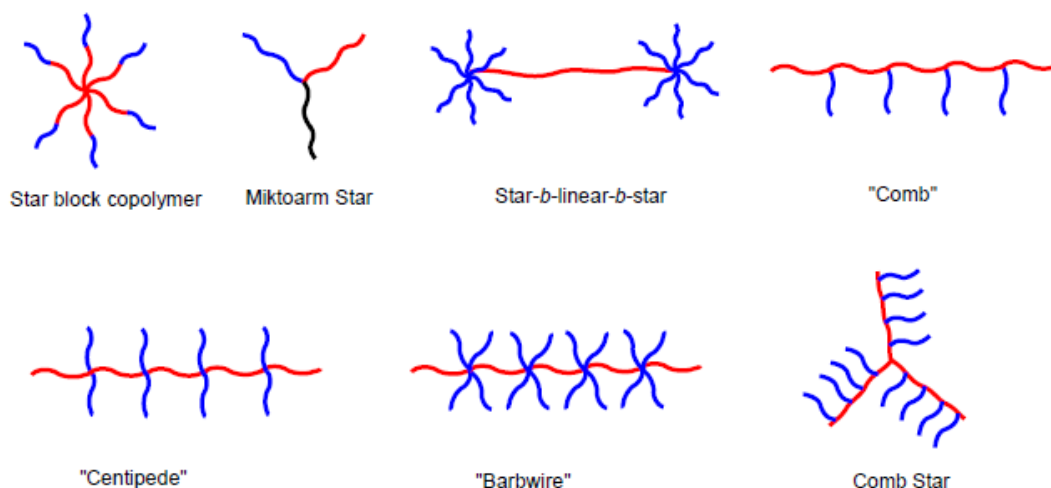


Figure 1.12. Complex nonlinear block copolymer architectures (adopted from Feng et al. *Polymers* **2017**, 9, 494)

Nevertheless, synthesis of different types of block copolymers including complex architectures is possible due to the advancement in polymer synthetic strategies after the ground-breaking discovery of living anionic polymerization by Szwarc in 1956.⁴⁶ This discovery opened up the way to synthesize structurally and compositionally well-defined homogeneous block copolymers by living or controlled-living polymerization.⁴⁴ The block copolymer synthetic strategies include sequential addition of monomers via conventional living anionic and cationic polymerization as well as promising controlled radical polymerization techniques such as atom transfer radical polymerization (ATRP), reversible addition-fragmentation chain transfer (RAFT) radical polymerization, nitroxide-mediated radical polymerization (NMP), controlled ring opening polymerization (ROP) and many other.⁴¹ Synthesis of block copolymers via Controlled radical polymerization techniques have gained increased interest owing to their compatibility with wide range of monomers, high tolerance of functional groups and relatively ambient reaction conditions. Further, dynamic equilibrium between active species and dormant species reduces the concentration of keeps the polymer chain end reactive for block copolymer synthesis which results in well-defined polymers with controlled molecular weight, composition, functionality, chain architecture and narrow polydispersity unlike conventional radical polymerization.⁴⁷ Edmond Fremy's discovery led to the development of Nitroxide-mediated polymerization (NMP) a type of reversible deactivation radical polymerization typically initiated by alkoxyamine compounds. Block copolymers prepared by NMP possess controlled stereochemistry and low polydispersity. Block

copolymers containing Polystyrene, poly(methylmethacrylate), poly(vinyl acetates) are generally synthesized via NMP. The block copolymerization of t-butyl acrylate and 1,3-butadiene using NMP is shown in figure 1.13. The polymerization was carried out in presence of alkoxyamine initiator based on 2,2,5-trimethyl-4-phenyl-3-azahexane-3-oxy skeleton. Further block copolymers of 1,3- dienes with variety of functionalized vinyl monomers such as styrene, acrylate and methacrylate derivatives. The block copolymers were obtained with well-defined controlled molecular weights and narrow polydispersity.^{48,49}

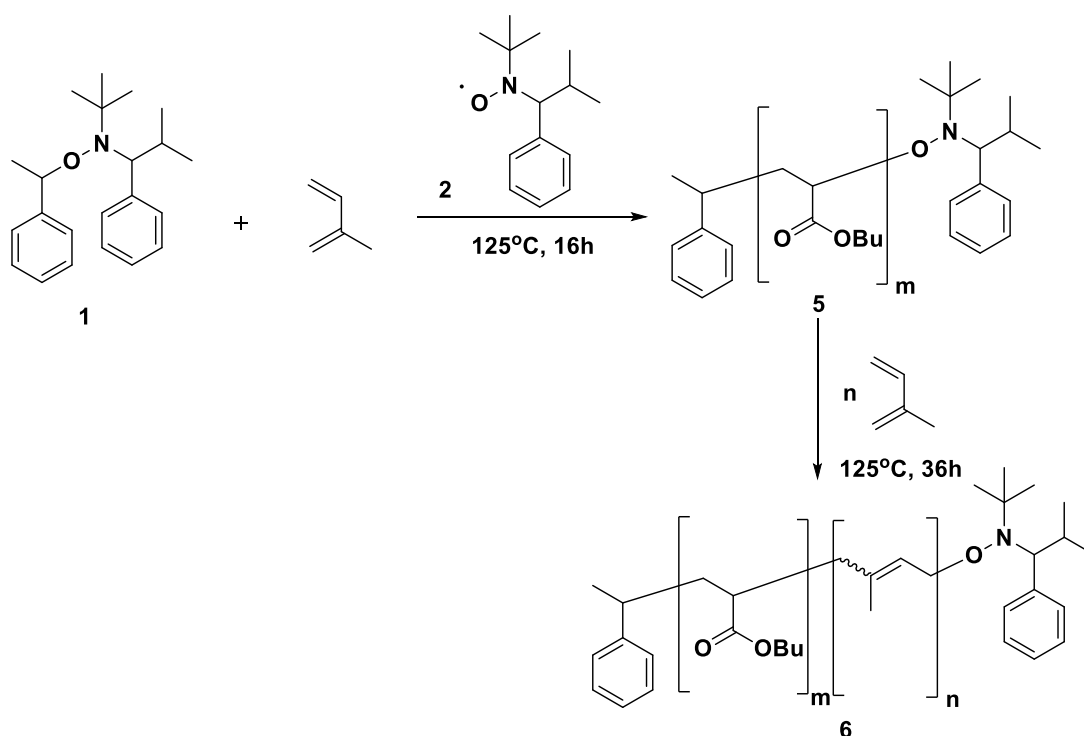


Figure 1.13. Synthesis of block copolymers via NMP

In atom-transfer radical polymerization (ATRP) radical is generated by reversible redox reaction of an organic halide catalysed by a transition metal compound for example cuprous halide under mild reaction conditions. Poly(ethylene oxide)-*b*-poly(2-(methacryloxy)ethyl phosphorylcholine) (PEO-*b*-PMPC) was synthesized via ATRP using near-monodisperse PEO macroinitiator with CuBr/ 2,2'-bipyridine as catalyst in isopropanol water mixture at 40 °C (see figure 1.14). Well defined block copolymers with targeted compositions were achieved by using this polymerization technique.^{50,51}

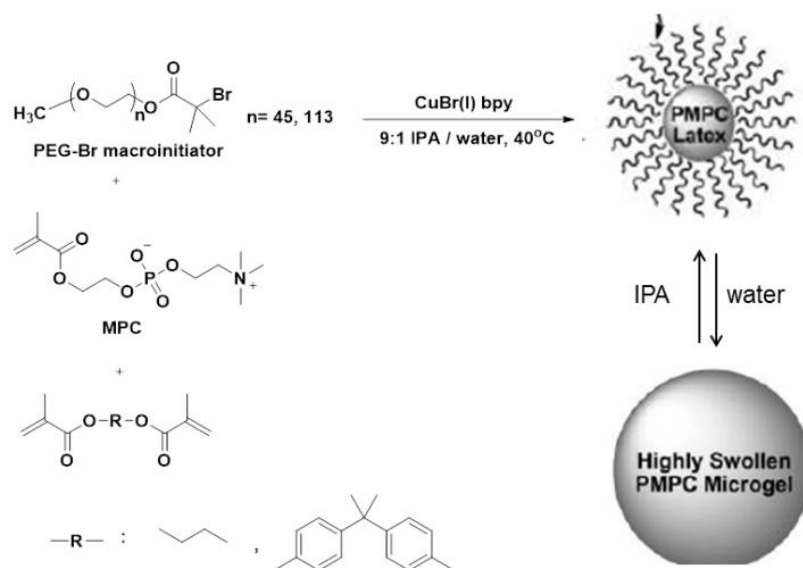


Figure 1.14. Synthesis of PEO-*b*-PMPC block copolymer via ATRP (Adopted from Sugihara et al *Macromolecules* **2010**, 43, 6321-6329)

Radical addition-fragmentation transfer (RAFT) polymerization is performed in presence of reversible addition-fragmentation chain transfer agent such as dithio compounds for example dithiobenzoates which reversibly transfer labile end group to propagating chain. Block copolymer of different acrylates with styrene were synthesized in water at 80°C in which poly(acrylic acid), poly(methacrylic acid) or poly(methacrylic acid-*co*-poly(ethylene oxide) methyl ether methacrylate) macroRAFTs were formed in water in presence of 4-cyano-4-thiothiopropylsulfanyl pentaneic acid (CTPPA) as chain transfer agent. The resulting hydrophilic macroRAFTs were immediately used without further purification to polymerize hydrophobic styrene in the same reactor as shown in figure 1.15. Well-defined amphiphilic block copolymers were successfully produced.^{52,53}

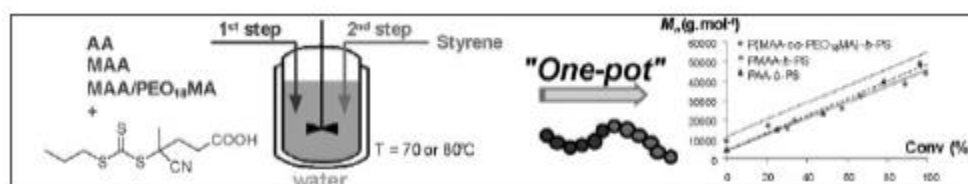


Figure 1.15. Synthesis of PMA-*b*-PS amphiphilic block copolymers by RAFT polymerization technique (adopted from Chaduc et al *Macromol. Rapid Commun.* **2011**, 32, 1270-1276)

Other than controlled radical polymerization, ring opening polymerization (ROP) has been one of the important widely practiced methods for synthesis of well-defined block copolymers using cyclic monomers including cyclic ethers, acetals, carbonates, phosphonites, lactams, lactones, and siloxanes. ROP is versatile and facile approach for synthesis of block copolymers due to the tolerance to a broad spectrum of functional groups and produces well-defined polymers with specific and controllable properties.⁵⁴ Combination of two different polymerization techniques can also be utilized for block copolymer synthesis. Using this approach, block copolymers can be synthesized without formation of substantial homopolymers moreover comparable polydispersities can be achieved as compared to sequential addition of monomers.⁴¹ PCL-*b*-PMMA block copolymers were prepared by concurrent ATRP and ROP processes simultaneously. One pot polymerization synthesis of structurally different vinyl and lactone monomers and bifunctional initiator with primary hydroxyl and tertiary bromide functionality was carried out without the necessity of any inorganic catalyst under natural sunlight as shown in figure 1.16. These two different polymerization processes do not interfere with each other in one reaction medium due to the nature of propagating species involved during polymerization. The block copolymers were prepared in controlled manner with narrow polydispersity and free from homopolymers.⁵⁵

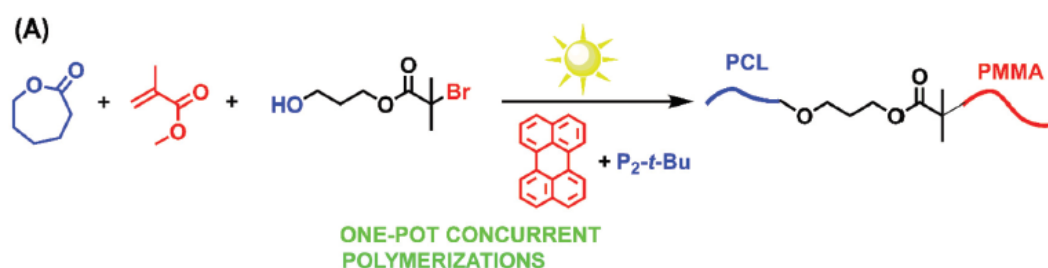


Figure 1.16. One pot polymerization of PCL-*b*-PMMA using combination of ATRP and ROP processes simultaneously (adopted from Aydogan et al *Polym. Chem.* **2017**, 8, 2899-2903)

Self-assembly of block copolymers

Block copolymers linked with constitutionally different monomer units allow combination of distinct properties within the macromolecular system which permits nanoscale assembly phenomena with dramatically unique macroscale behaviour.⁵⁶ Block copolymers undergo phase separation to produce various ordered

microstructures and nanostructures that have attracted scientific and technological interest in bulk as well as in solution state.^[57] The self-assembly of block copolymers is driven by unfavourable mixing enthalpy coupled with a small mixing entropy giving rise to ordered structures in bulk which result in wide range of morphologies including lamellar, bicontinuous, cylindrical and spherical as shown in figure 1.17.⁵⁸

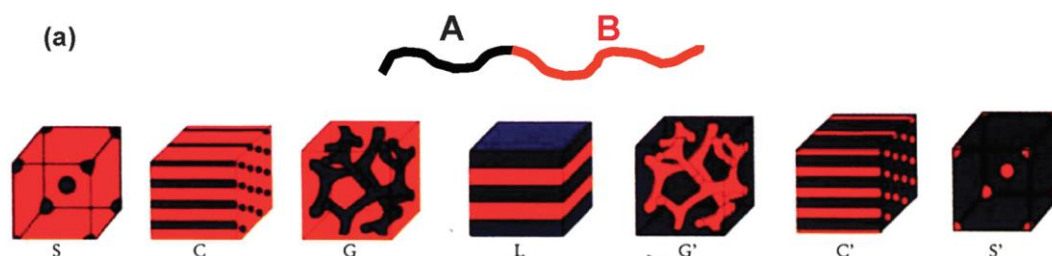


Figure 1.17. Morphologies of block copolymer in bulk (adopted from Mai et al Chem. Soc. Rev. 2012, 41, 5969-5985)

Owing to the fascinating morphologies, the block copolymers find application in broad range of areas including photonics,^[59] lithography,^[60] electronics,^[61] membranes,^[62] nanoreactors,^[63] and thermoplastic elastomers.^[64]

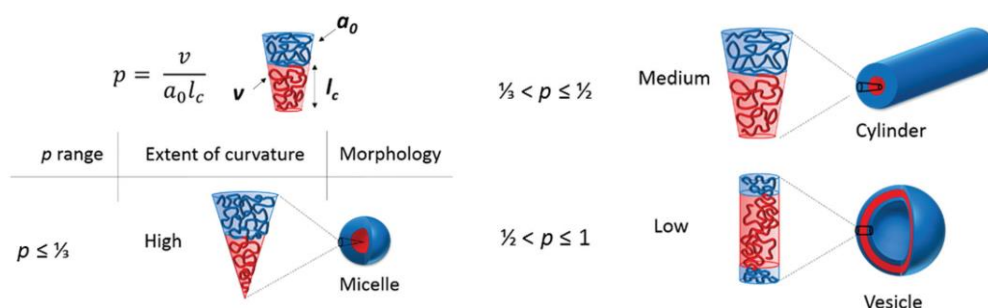


Figure 1.18. Different morphologies obtained by targeting different packing parameters (adopted from Doncom et al. Chem. Soc. Rev. 2017, 46, 4119-4134)

Further, amphiphilic block copolymers in which hydrophilic block is chemically tethered with hydrophobic block spontaneously undergo self-organization in aqueous medium to form various nanostructures including micelles, vesicles, nanocapsules, cylindrical micelles and nanoparticles which have seen tremendous progress in various applications including tissue engineering,^[65] bone engineering,^[66] water purification^[67] and drug delivery.^[68] The packing parameter for small molecular surfactants proposed by Israelachvili, Mitchell and Ninham governs the formation of

broad range of nanoscale morphologies.⁶⁹ The relation between surfactant molecular structure with inherent curvature and the resulting morphology can be understood from packing parameter p as given below;

$$p = v/a_0l_c$$

where v is volume of hydrophobic tail, a_0 is polar head group surface area, l_c is hydrophobic tail length. Hence, different morphologies are obtained with different p values such as spherical micelles are formed when $p \leq 1/3$, cylindrical micelles between $1/3 < p \leq 1/2$ and when $1/2 < p \leq 1$ vesicles are formed as shown in figure 1.18. Amphiphilic block copolymer structures are the imitates of small molecule surfactants where hydrophobic block represents the surfactant tail and hydrophilic block represents the polar head group and various morphologies are resulted by altering these parameters.^{70,71}

Among the various aqueous self-assembled nanostructures micelles and vesicles are the most studied morphologies.

Block copolymer micelles

The amphiphilic block copolymers with unique core-shell structure self-assemble in aqueous medium to form micelles above the critical micellar concentration. The driving force for the self-assembling behaviour is to decrease the interfacial area of hydrophobic-core forming segment to minimize interfacial free energy. The formation of block copolymer micelles is schematically shown in figure 1.19.

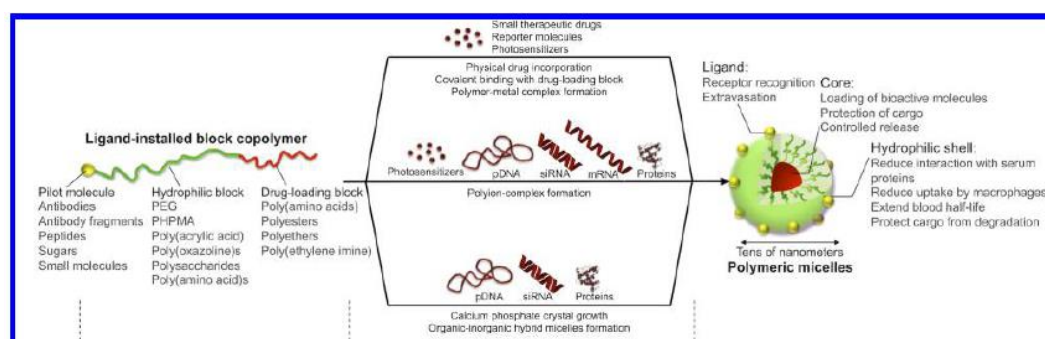


Figure 1.19. Formation and architecture of block copolymer micelles which spontaneously form by self-assembly in water (adopted from Cabral et al Chem. Rev. 2018, 118, 6844-6892)

Generally polymeric micelles have been designed for the delivery of poorly water soluble anticancer drugs and are better choice for drug delivery than small surfactant molecules generally due to the higher stability and longer circulation time of loaded drug. Furthermore micelle core can get additional stability from the interaction between the drug payload and core forming segment.⁷² A range of hydrophobic polymers utilized to form the core of the micelles include poly (ϵ -caprolactone) (PCL), poly (lactic acid) (PLA), poly(lactic-co-glycolic acid) (PLGA), poly(propylene oxide) (PPO), poly(sebacic acid) (PSA), and poly(aspartic acid) (PAsp). The hydrophilic blocks constitute the micelle shell which can prolong plasma circulation and modified with various functionalities to obtain the control over the drug release and effective therapeutic response. Frequently used hydrophilic shell-forming polymers are poly(ethylene glycol) (PEG), poly(vinyl alcohol) (PVA), poly(vinyl pyrrolidone) (PVP), poly(acrylamide) (PMA), poly(ethyleneimine) (PEI).⁷³ NK911 is DOX encapsulated supramolecular polymer micelle designed for enhanced delivery of doxorubicin is under clinical evaluation. PEG-*b*-poly(α,β -aspartic acid) copolymer prepared by ring opening polymerization of N-carboxyanhydride of benzyl-L-aspartate followed by debenzilation in basic condition. Further, the block copolymer was conjugated with DOX through amide bond and free DOX was physically encapsulated into the hydrophobic core of poly(α,β -aspartic acid-doxorubicin) to form stable micelles. Clinical trial studies have demonstrated the reduction of side effects related with free DOX and high efficacy.^{74, 75} Block copolymers with polyethylene glycol (PEG) and polyaspartate were used to physically incorporate PTX into polymeric micelles facilitated by hydrophobic interaction between PTX and aspartate chain. These polymer micelles with size 20 nm and 23% (w/w) of PTX were named as NK105 for clinical studies. Cisplatin conjugated (CDDP) micelles (NC6004) prepared by polyethylene glycol (PEG) block as hydrophilic shell and polymer-metal coordination complex of polyglutamic acid and cisplatin constituting the inner core of the micelle having remarkably high stability. SN-38 loaded polymeric micelles NK012 were constructed by self-assembly of amphiphilic PEG-*b*-polyglutamate block copolymer with 20 % (w/w) of SN-38. These are some of the micelles examples summarized in figure 1.20 under clinical trials demonstrating reduced side effects with promising efficacy even against triple-negative breast cancer and pancreatic cancer.⁷⁶

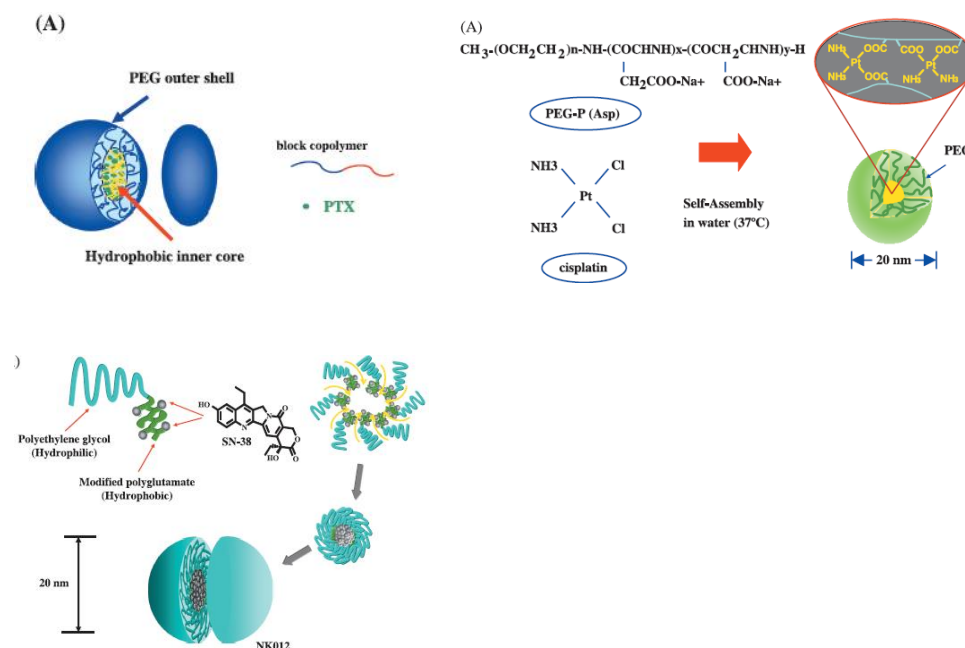


Figure 1.20. Block copolymer micelles encapsulated with various anticancer drugs under clinical trials (adopted from Matsumura et al *Cancer Sci.* **2009**, 100, 527-579).

Block copolymer vesicles

Vesicles are higher order self-organized spherical nanostructures with aqueous core enclosed by hydrophobic membrane. Polymersomes are the vesicles prepared using high molecular weight amphiphilic block copolymers with right hydrophobic-hydrophilic balance having superior morphological stability to their lipid counterparts, liposomes. Polymer vesicles have additional advantage in drug delivery owing to the morphological similarity to cellular membrane and viral capsids. The unique structural feature of polymer vesicles allows the encapsulation of hydrophobic drug in bilayer membrane core and hydrophilic drug in aqueous interior.^{77, 78} Discher and co-workers carried out pioneering work by exploring block copolymer, poly (ethylene oxide)-*b*-poly-(ethyl ethylene) (PEO-*b*-PEE) in the area of polymer vesicle.⁷⁹ Feijen and co-workers prepared vesicles based on PEG and polylactides block copolymers with variable sizes ranging from 70 nm to 50 μm and the size of the vesicles was tailored by extrusion through membrane with well-defined pore sizes.⁸⁰ Discher and co-workers demonstrated these PEG-PLA based polymersomes for systemic delivery of anticancer drugs hydrophobic drug PTX and hydrophilic drug DOX in combination therapy. The *in vitro* drug release was triggered by hydrolysis of PLA in the vesicle core to convert vesicles into wormlike micelles and spheres and subsequent release of the drugs (see figure 1.21). In *in vivo* studies the polymersome exhibited two fold

higher tumor cell deaths than free drug and showed qualitative increase in maximum tolerated dose and tumor accumulation of drugs.⁸¹

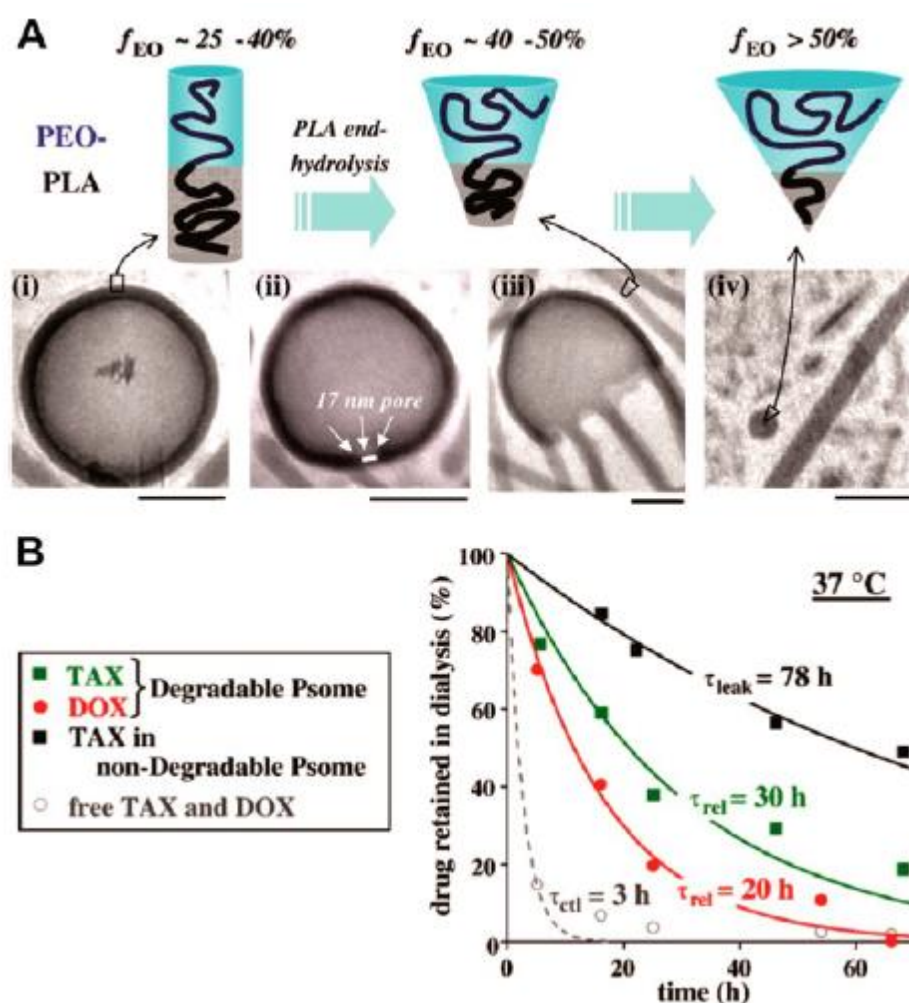


Figure 1.21. PEG-PLA based polymersome self-assembly, degradation, and drug release (A) Cryo-TEM images of empty aggregates. hydrolysis of PLA in the vesicle core triggers the growth of pores and conversion of vesicles into wormlike micelles and spheres.(B) In vitro release and leakage of DOX and PTX from the polymersomes (adopted from Ahmed et al. *J. Controlled Release* **2006**, 116,150-158)

Forster and co-workers synthesized amphiphilic polybutadiene-block-poly(L-glutamate) block copolymers by anionic polymerization and subsequent ring opening polymerization of N-carboxyanhydrides to form polymersomes or peptosomes composed of modified protein units. Further the pH dependent helix-coil transition of peptide units occur without altering the vesicular morphology as shown in figure 1.22⁸²

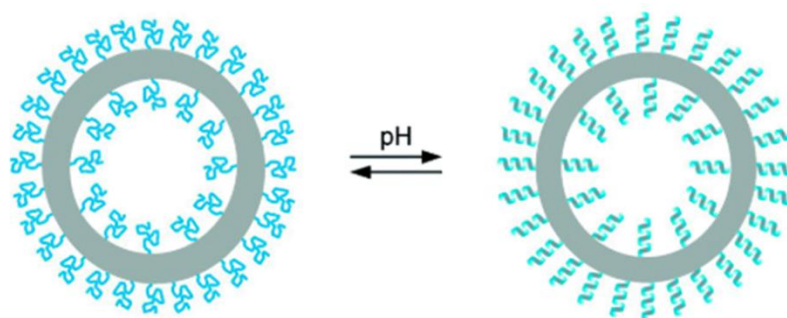


Figure 1.22. polybutadiene-block-poly(L-glutamate) block copolymer polymersomes with modified protein units can undergo pH dependent helix-coil transition without change in vesicle morphology (adopted from Kukulka et al. *J. Am. Chem. Soc.* **2002**, 124,1658-1663)

Lecommandoux and co-workers prepared zwitterionic poly(γ -benzyl-L-glutamate)-b-poly(N-trifluoroacetyl-L-lysine) (PBLG-b-PTFALys) block copolymers. The block copolymers spontaneously self-assembled to form reversible schizophrenic vesicles that can be reversibly produced in moderate acidic or basic aqueous solutions. At acidic pH (pH 3) poly(L-glutamic acid) (PGA) block is neutralized and changes from charged coil to neutral more compact α -helical structure therefore hydrophobic, neutral PGA forms the core and PLys form the shell of the vesicles. Under basic conditions (pH 12) protonated poly(L-lysine) block ($-\text{NH}_3^+$) is transformed into neutral and insoluble $-\text{NH}_2$ groups forming the core of aggregates (see figure 1.23).⁸³

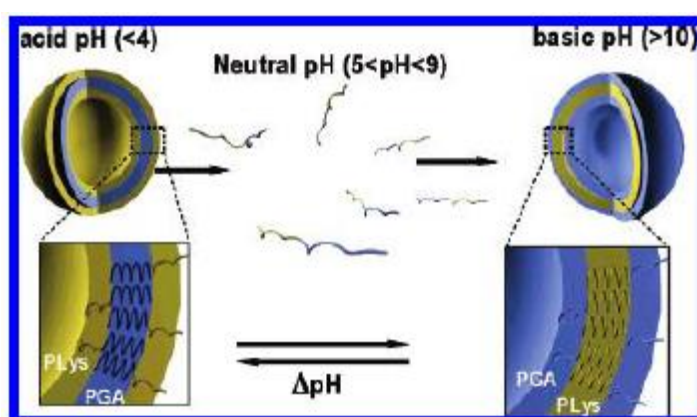


Figure 1.23 Schematic representation of the self-assembly into vesicles of diblock copolymer PGA-b-PLys as function of pH (adopted from Hernandez et al. *J. Am. Chem. Soc.* **2005**, 127,2026-2027)

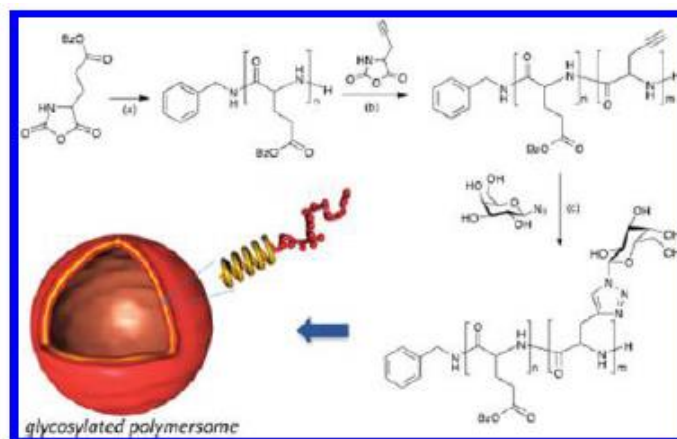


Figure 1.24. Synthesis of (PBLG-*b*-PGG) block copolymers; conditions: (a) DMF, benzylamine, 0 °C; (b) DMSO, *r. t.*; (c) $\text{Cu}(\text{PPh}_3)_3\text{Br}$, Et_3N , DMSO, 30 °C (adopted from Huang *et al.* *J. Am. Chem. Soc.* **20012**, 134,119-122)

Heise, Lecommandoux and co-workers prepared well-defined amphiphilic galactose containing amino acid block copolymers (PBLG-*b*-PGG) by sequential ring opening polymerization of benzyl-L-glutamate and propargylglycine (PG) N-carboxyanhydrides followed by glycosylation of PG block via Huisgen's cycloaddition "click" reaction using azide functionalized galactose. The block copolymers self-assembled to obtain wormlike micelles as well as polymersomes depending upon the block length ratio and the nanoprecipitation conditions as shown in figure 1.24.⁸⁴

1.3. Block Copolymers in drug delivery

Polymer-based drug delivery has paved the way to improve therapeutic efficacy and specific targeting of the drugs. In this regard, use of biodegradable polymers in drug delivery system has become prominent due to their ability to exhibit controlled/programmed release of drug in targeted cancer cells induced by degradation in response to the external stimuli (eg. redox, pH or enzyme). Moreover, the degradation of polymer inside the body produces non-toxic natural biproducts and eliminated from the body ensuring the clearance of empty device when their support is not needed.^{85,86} Various natural as well as synthetic biodegradable polymers have been explored for effective targeted delivery of drugs. Natural biodegradable polymers including collagen, albumin, gelatin, polysaccharides such as hyaluronic acid (HA), cyclodextrines, carrageenan, dextran, alginate, agarose have been used for drug delivery application. In spite of being highly biodegradable, their use is limited by batch to batch variation and broad molecular weight distribution, lack of suitable physical properties and undesirable immune response. Synthetic biodegradable polymers such as poly(amides), poly(esters), poly(anhydrides), poly(phosphoesters) which are degraded under enzymatic or hydrolytic conditions have also realized as promising biodegradable polymers for controlled drug delivery.⁸⁷ Different biodegradable block copolymers with varying environmental stability and enzymatic biodegradability is shown in figure 1.25. Polylactides possess very high biodegradation rate and very less environmental stability whereas polycaprolactone possess very high environmental stability but very poor biodegradability. Polypeptides and polyhydroxybutyrate show moderate environmental stability and biodegradability.

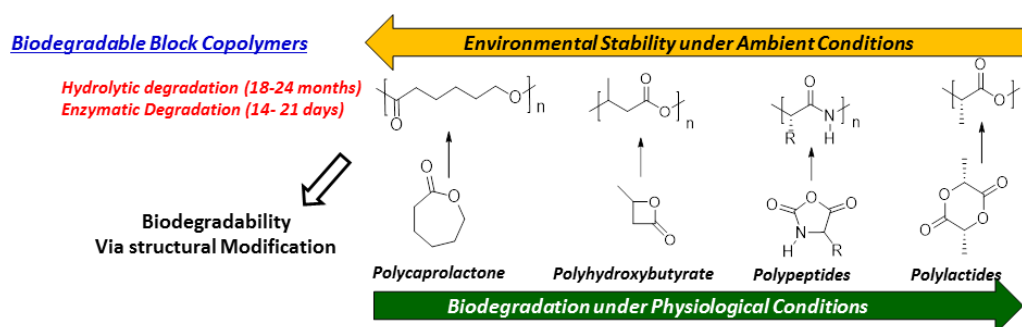


Figure 1.25. Biodegradable block copolymers with varying environmental stability and biodegradation rate.

Among various biodegradable polymers, polyesters have shown outstanding progress in the various biomedical applications including drug delivery owing to the hydrolysable backbone, ease of synthesis via ROP and tuneable physical, mechanical and biological properties. Polyesters including poly(lactic acids) (PLA), poly(glycolic acids) (PGA) and poly(ϵ -caprolactone) (PCL) contain aliphatic ester bonds linkages in carbon backbone which can be cleaved by enzymes present in the body and produce natural degradation products lactic acid, glycolic acid and 6-hydroxyl caproic acid respectively and eliminated from the body via citric acid cycle^{88,89}. Due to these advantages of polyesters have become popular commercially available biodegradable polymers. PGA is investigated for very promising application such as degradable suture DEXON as well as scaffold for bone, cartilage, tooth, vaginal, intestinal and spinal regeneration.^{90,91,92} However, PGA has limited use in drug delivery devices due to the fast degradation rate and limited solubility.⁹³ Poly(lactic acids) (PLA) are found in various forms such as poly(D-lactic acid) (PDLA), poly(L-lactic acid) (PLLA), poly(D, L-lactic acid) (PDLLA) a racemic mixture of PLLA and PDLA due to the presence of chiral monomer molecule. Properties of PLA can be tuned by varying L- and D-isomer ratio. Due to the presence of methyl group on the backbone PLA has higher hydrophobicity and hence lower degradation rate compared to PGA.⁸⁵ Therefore, to obtain the control over the degradation rate copolymers of lactides and glycolides poly(lactide-co-glycolide) (PLGA) began to be explored for biomedical applications such as sutures and implants, drug delivery vehicles and tissue engineering scaffolds. The degradation rate of PLGA is influenced by change in the lactide to glycolide ratio (L:G) i. e. decrease in the ratio of L:G decreases the degradation rate of PLGA. Thus these PLGA polymers exhibit improved *in vivo* circulation and biocompatibility compared to their homopolymers and employed for controlled drug release.^{94,95}

Polycaprolactone block copolymers

Poly(ϵ -caprolactone) PCL being one of the earliest polymer synthesized by ring opening polymerization (ROP) of ϵ -caprolactone monomer by Carothers group in early 1930s has recently gained attention for their potential use in biomedical applications among various biodegradable aliphatic polyesters. Generally PCL is synthesized by ROP of ϵ -caprolactone monomer using a broad range of cationic, anionic and coordination catalyst. In addition to this conventional route, PCL is

prepared via free radical ring opening polymerization of 2-methylene-1, 3-dioxepane. PCL is semicrystalline hydrophobic polymer with melting point of 55-60 °C and glass transition temperature of -60 °C and longer degradation time of 12 to 24 months.⁸⁸ PCL has been extensively investigated for biomedical application including tissue engineering, bone scaffold packaging and controlled drug release owing to its good biocompatibility, biodegradability and non-immunogenicity. Moreover, FDA has approved use of PCL for variety of medical products including sutures for surgeries, bone screws, tissue engineering scaffolds and drug delivery systems. One-year implantable contraceptive device-Capronor containing PCL is available in the market and the toxicological investigations have shown the material to be safe for its use. Due to the flexible mechanical properties PCL also find paramedical applications such as wound dressing and dentistry. In addition to biodegradability and biocompatibility, PCL is superior for drug delivery application as compared to other aliphatic polyesters- polyglycolides (PGA) and polylactides (PLA) due to its high permeability to drugs under physiological conditions and less acidic degradation products.^{96,97} However, hydrophobicity, lack of functionality, longer degradation time limits its widespread application in drug delivery. Nevertheless, due to the synthetic versatility, PCL offers a myriad of opportunities for substitution with functional groups which provides possibilities to obtain desired physicochemical properties including hydrophilicity and degradation rate and the functional groups could be utilized to conjugate drugs, targeting agents and stimuli responsive molecules.^{89,98} In addition, amphiphilic block copolymers containing hydrophilic segment combined with hydrophobic PCL block can self-assemble into various nanocarrier architectures for drug delivery application. Ren-Shen Lee and co-workers amphiphilic block copolymers MPEG-ONB-PXCL. Difunctional, photocleavable *ortho*-nitrobenzene (ONB) was used as initiator for ROP of 4-phenyl/methyl substituted caprolactone. This hydrophobic block was connected hydrophilic MPEG block through photochemically sensitive ONB linker via click reaction as shown in figure 1.26. The biodegradable and biocompatible amphiphilic block copolymer self-assembled as micelle and anticancer drug DOX was encapsulated into the core of the micelle. The photodegradable DOX loaded MPEG-ONB-PXCL micelles showed light triggered release of DOX due to disruption of micelles. Further DOX loaded micelles facilitated improved uptake of DOX by HeLa cells.⁹⁹

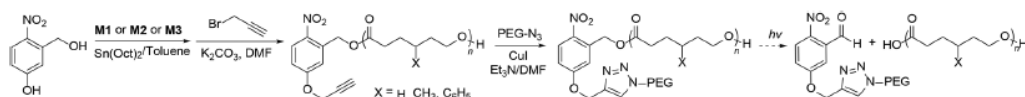


Figure 1.26. Synthesis of the photo-cleavable MPEG-ONB-PXCL and their photodegradation (adopted from Peng et al. *RSC Advances* **2013**, 3, 18453-18463)

Meidong Lang and co-workers prepared pH sensitive copolymers from 2-/6-benzyloxycarbonylmethyl substituted ϵ -caprolactone monomer and PEG-OH as macroinitiator by ROP. Further benzyl carboxylate groups were deprotected to generate carboxylic functionality which improves the water solubility and can be used for further modification as shown in figure 1.27. Formation of the self-assembly was driven by the pH wherein below the pK_a carboxylic groups were protonated to form micelles and above the pK_a polymer self-assembly was disrupted due to deprotonation.¹⁰⁰

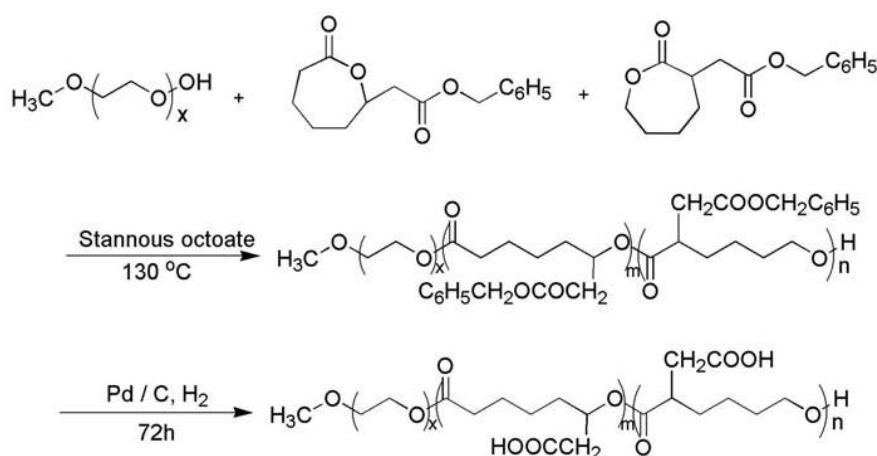


Figure 1.27. Synthesis of pH responsive block copolymers (adopted from Zhang et al. *J. Polym. Chem.* **2014**, 52, 188-199)

Guerry et al. prepared series of chitosan oligosaccharide-grafted caprolactone polymers (PCL-g-Cos) coupling through click reaction between azide substituted polycaprolactone polymer (PCL-N3) and alkynyl modified chitosan oligosaccharides (CO-alkynyl). PCL-g-Cos polymers containing PCL as hydrophobic core and Cos as hydrophilic shell undergo self-organization in aqueous medium to form micelles and further core cross linking with disulphide containing bis alkynyl cystamine to form redox responsive nanocarriers schematically shown in figure 1.28. The encapsulation of DOX and its release properties of DOX loaded redox sensitive micelles were investigated in response to intracellular glutathione level.¹⁰¹

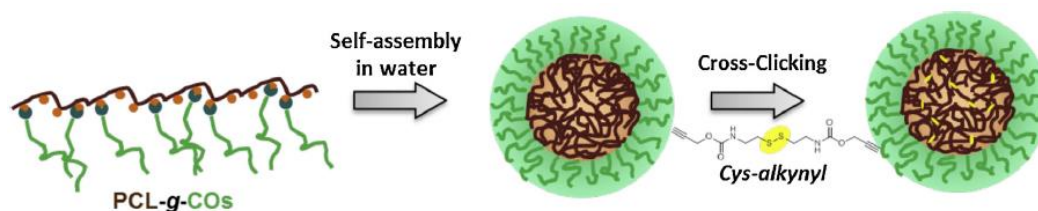


Figure 1.28. Synthesis of amphiphilic PCL-g-Cos polymers and their self-assembly in aqueous medium followed by core-cross linking with the disulphide cys-alkynyl to give redox stimuli responsive nano-vehicles (adopted from Guerry et al. *Carbohydr. Polym.* **2014**, 112,746-752)

Zhu and co-workers prepared salt/pH dual responsive amphiphilic brush copolymers poly(2-hydroxyethyl methacrylate)-g-(poly(ϵ -caprolactone)-adnine:uracil-poly(ethylene glycol)) (PHEMA-g-(PCL-A:U-PEG)). The block copolymers formed supramolecular micelles loaded with anticancer drug DOX. The low pH and high salt concentration of tumor tissue was exploited to study the drug release from the micelles showing controlled drug release against salt and pH stimuli (see figure 1.29).¹⁰²

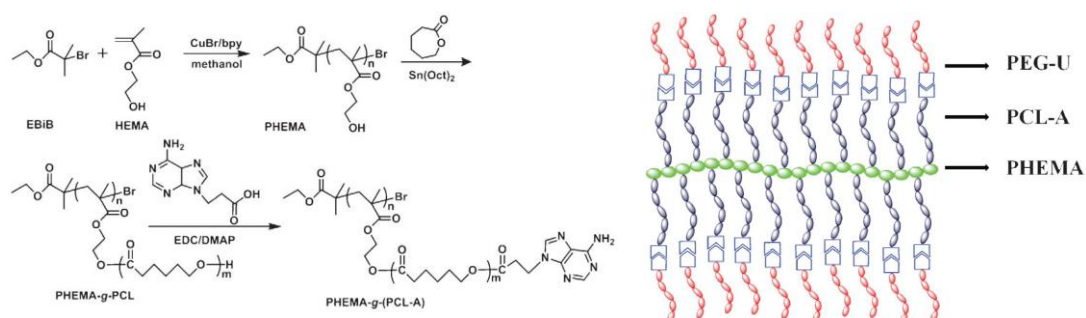


Figure 1.29. Synthesis and schematic supramolecular structure of brush copolymers PHEMA-g-(PCL-A:U-PEG)(adopted from Wang et al. *RSC Adv.* **2012**, 2,11953-11962)

Stefan and co-workers prepared 4-octyloxy and oligoethylene glycol substituted caprolactone monomers and utilized them for synthesis of amphiphilic block copolymers (PMEEECL-*b*-POCTCL) under ROP process. The octyloxy-containing PCL act as hydrophobic segment and oligoethylene glycol containing PCL behaves as hydrophilic segment to form micelles in aqueous medium. Further these block copolymers exhibited thermoresponsive behaviour due to the oligoethylene glycol substituted polycaprolactone block and the LCST can be tuned by changing the molar ratios between the hydrophilic and hydrophobic substituted caprolactone monomers as well as by varying the chain length of oligoethylene glycol functional

groups attached to the caprolactone monomer. In the continuation of this work, the above mentioned amphiphilic block copolymers exhibited LCST of 38 °C. This LCST value enables to sense the elevated tumor tissue temperature due to faster metabolism or induced hyperthermia and release the drug in controlled manner. The polymer micelles were loaded with anticancer drug DOX and exhibited in vitro thermoresponsive release when the temperature was above the LCST. The cellular uptake of the drug loaded micelles against MCF-7 cells showed comparatively higher cytotoxicity at temperature above the LCST (see figure 1.30).^{103,104}

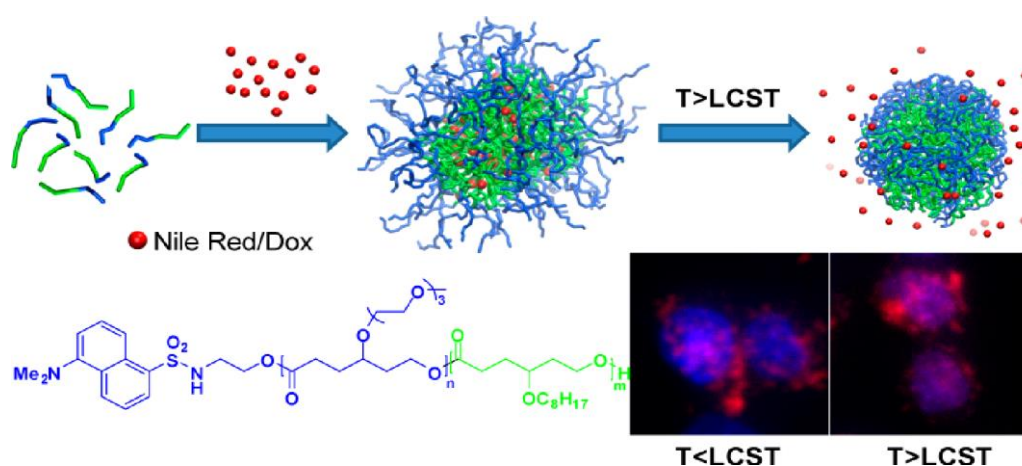


Figure 1.30. DOX/nile red loaded micelles showing its LCST properties (adopted Cheng et al. *Biomacromolecules* **2012**, *13*, 2163-2173)

Same authors prepared a very short ethylene glycol chain substituted caprolactone monomer γ -2-(methoxyethoxy)-3-caprolactone (MECL) to employ as hydrophobic segment as shown in figure 1.41 which may improve the interaction with encapsulated drug as compared to alkoxy counterpart. The amphiphilic block copolymers were synthesized by using this newly synthesized monomer and above mentioned oligoethylene glycol substituted caprolactone monomer. The amphiphilic copolymers were self-assembled in aqueous medium with highly tuneable thermoresponsive behaviour in the range of 31–43 °C. Further modification of end group position and alteration of hydrophobic block composition by using caprolactone as well as MECL monomer was carried out to prepare triblock copolymers (see figure 1.31) to improve the thermodynamic stability, thermoresponsive properties and drug loading of the above mentioned diblock copolymers.^{105,106}

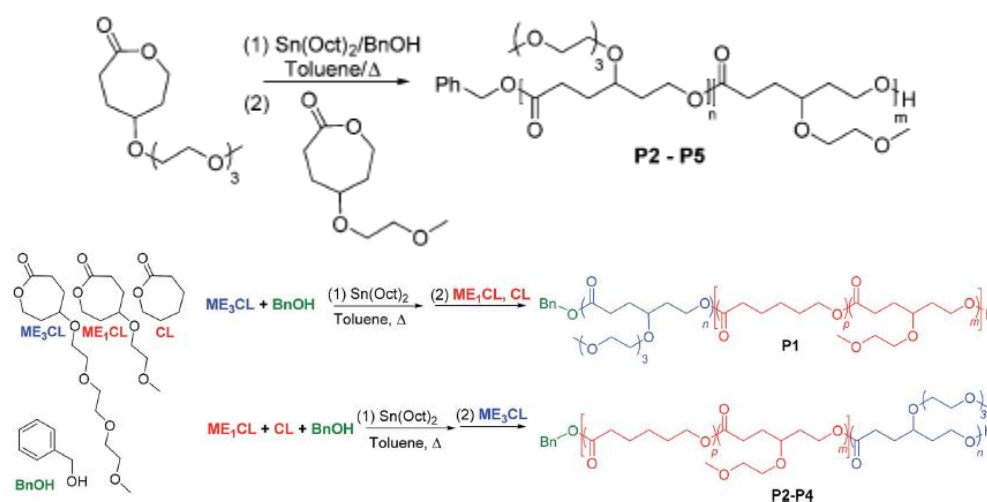


Figure 1.31. Synthesis of diblock and triblock copolymers from γ -substituted caprolactone monomers having tuneable thermoresponsive properties (adopted from Rainbolt et al. *J. Mater. Chem. B* **2013**, *1*, 6532-6537 and *J. Mater. Chem. B* **2015**, *3*, 1779-1787)

In further studies, 4- and 6-arm thermoresponsive star like block copolymers were synthesized using pentaerythritol and myoinositol as multifunctional initiators by ring opening polymerization with ethoxy and oligoethylene glycol substituted caprolactone monomers as shown in figure 1.32. These star copolymer micelles having LCST at 39 °C were demonstrated as promising drug carrier with temperature controlled doxorubicin release.¹⁰⁷



Figure 1.32. Synthesis of 4- and 6-arm star-like PECL-*b*-PMEEECL amphiphilic diblock copolymers (adopted from Washington et al. *J. Mater. Chem. B* **2017**, *5*, 5632-5640)

Jerome and coworkers synthesized γ -keto substituted caprolactone polymers (polyKCL) by ROP using $\text{Al}(\text{iOPr})_3$ as a catalyst at ambient temperature. Cheng et al adopted this approach to prepare methoxy poly(ethylene glycol)-b-poly(ϵ -caprolactone-co- γ -hydroxyl- ϵ -caprolactone) (mPEG-b-P(CL-co-HCL)) bearing pendant hydroxyl groups on the PCL back bone. The hydroxyl groups were obtained by the reduction of ketone group present on polyKCL polymer using sodium borohydride. The block copolymers self-assembled and DOX was encapsulated into the micelles as shown in figure 1.33. The pendant hydroxyl groups played very important role in loading and releasing DOX from the micelles because of the hydrogen bond formation between DOX and hydroxyl group. Further better cellular uptake of DOX loaded micelles was observed compared to free DOX against HepG2 cells.^{108,109}

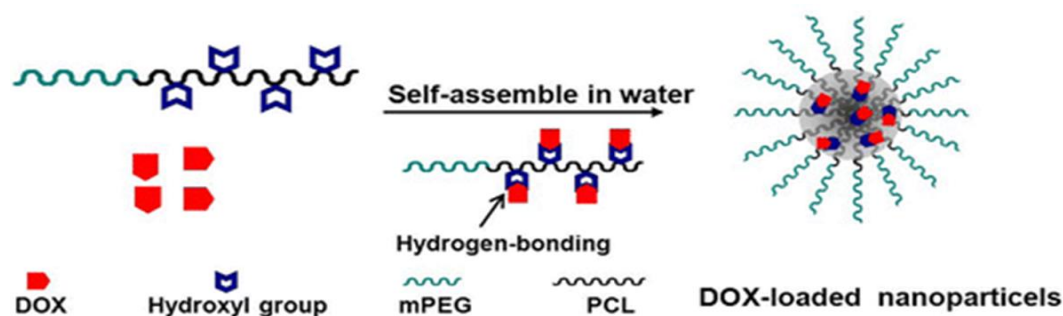


Figure 1.33. Synthesis of DOX loaded micelles based on hydroxy PEG-b-PPCL block copolymers (adopted from Chang et al. *Biomacromolecules*, **2012**, 13, 3301–3310).

Chen and Wang co-workers synthesized chondroitin sulphate-g-poly(caprolactone) (CP) polymers via atom transfer radical addition (ATRA) by using CL-Br as ATRP initiator. The polymer self-assembled into micelles in water to encapsulate hydrophobic anticancer drug camptothecin (CPT). The *in vitro* release studies showed that active lactone form of CPT was preserved against hydrolysis under stimulated physiological conditions. Cellular uptake studies revealed significantly better cell killing and apoptosis inducing effects than free CPT. The *in vivo* therapeutic efficacy of CPT loaded micelles was studied in non-small-cell-lung cancer xenograft animal model and showed good inhibition in tumor growth (see figure 1.34).¹¹⁰

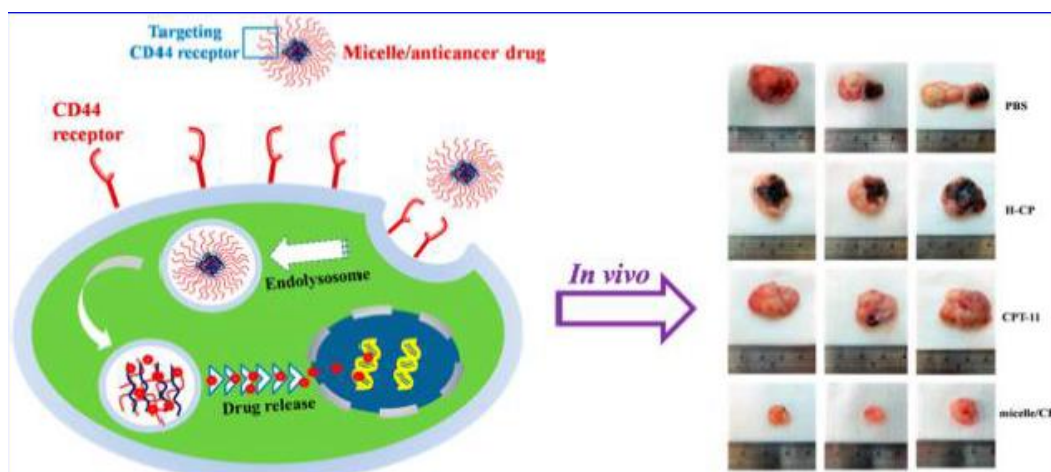


Figure 1.34. *schematical representation of chondroitin sulphate-g-poly(ϵ -caprolactone) polymer micelles loaded with CPT for improved in vivo therapeutic efficacy (adopted from Liu et al. Mol. Pharmaceutics 2014, 11, 1164-1175)*

Stepfan and coworkers prepared diblock copolymers by ring opening polymerization of γ -4-phenylbutyrate- ϵ -caprolactone (PBACL) and γ -valproate- ϵ -caprolactone (VPACL) and ϵ -caprolactone using PEG macroinitiator as shown in figure 1.35. The advantage of pendant chains on the caprolactone backbone is that 4-phenylbutyric acid and valproic acid possess anticancer properties by acting as histone deacetylase inhibitors (HDACis). DOX was encapsulated get into the HDAC inhibitor conjugated prodrug micelles. The DOX loaded micelles enabled to show sustained drug release in a concentration dependent manner over time to expand therapeutic window of small molecule drug.¹¹¹

In the continuation of this work pendant PBA HDACi containing poly(γ -4-phenylbutyrate- ϵ -caprolactone)(PPBCL) homopolymer was synthesized using $\text{NdCl}_3 \cdot 3\text{TEP}/\text{TIBA}$ (TEP = triethyl phosphate TIBA = triisobutylaluminium) catalytic system because commonly utilized catalysts failed to produce homopolymers. The homopolymer nanoparticles loaded with DOX were prepared by using PEG surfactant. These DOX loaded nanoparticles exhibited release of both DOX and PBA at endosomal pH conditions. The dual action of DOX and PBA HDACi showed enhanced cytotoxicity compared to free DOX (see figure 1.36).¹¹²

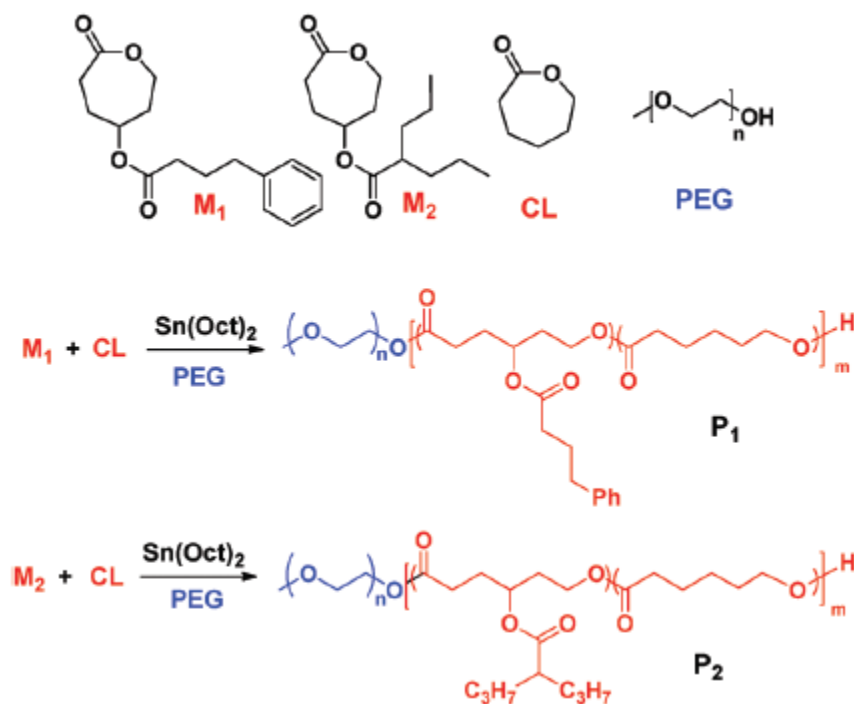


Figure 1.35. Synthesis of poly(ethylene glycol)-*b*-poly(γ -2-propylpentanoate- ϵ -cprolactone-*ran*- ϵ -cprolactone) and poly(ethylene glycol)-*b*-poly(γ -4-phenylbutyrate- ϵ -cprolactone-*ran*- ϵ -cprolactone) diblock copolymers (adopted from Senevirathne et al. *J. Mater. Chem. B* **2017**, 5, 2106-2114).

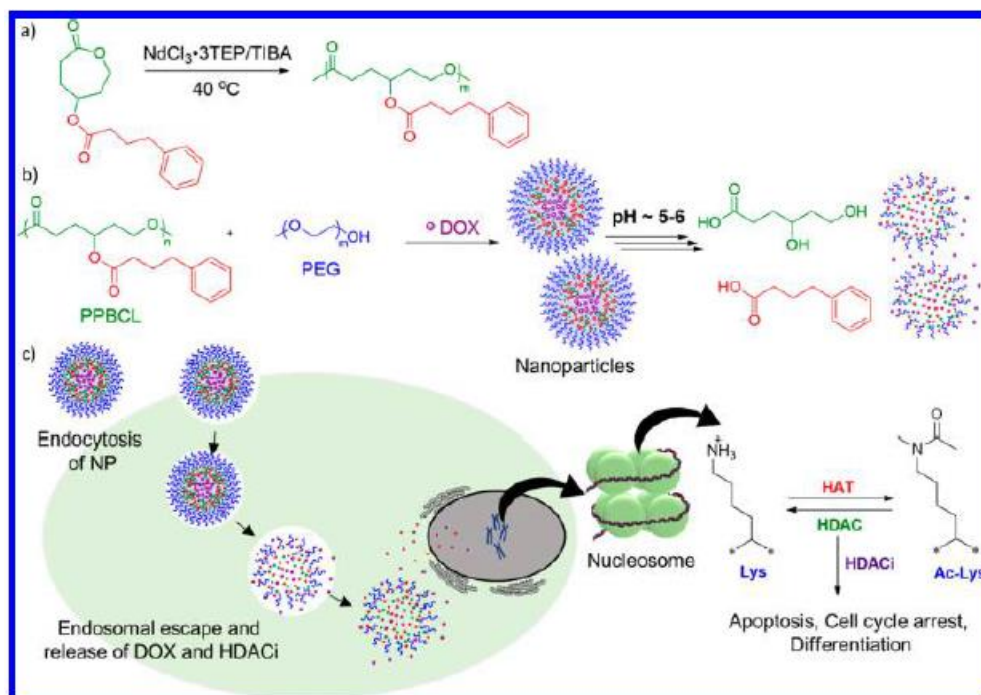


Figure 1.36. Schematic diagram of (a) synthesis of PPBCL polymer with $\text{NdCl}_3 \cdot 3\text{TEP/TIBA}$ catalytic system (b) formation of DOX loaded NP using PEG and release of DOX and PBA upon the introduction of acidic medium and (c) endocytosis and subsequent release of DOX and PBA in cancer cells (adopted from Kularatne et al. *Biomacromolecules* **2018**, 19, 1082-1089)

Kim and co-workers prepared AB₂ miktoarm block copolymers with hydrophilic PEG as A constituent and hydrophobic polycaprolactone as B component containing singlet oxygen (¹O₂)-labile region and stereospecific β-aminoacrylate linkage. ¹O₂ responsive amphiphilic copolymers self-assembled as micelles and hydrophobic photosensitizer chlorin e6 (Ce6) and DOX were encapsulated into the core as shown in figure 1.37. The cellular uptake of co-loaded micelles was studied in human breast cancer (MDA-MB-231) cancer cells. Upon red laser irradiation, the singlet oxygen generated by the photosensitizer triggered photocleavage of β-aminoacrylate linkage inducing micelle disassembly facilitated intracellular DOX release for effective therapy.¹¹³

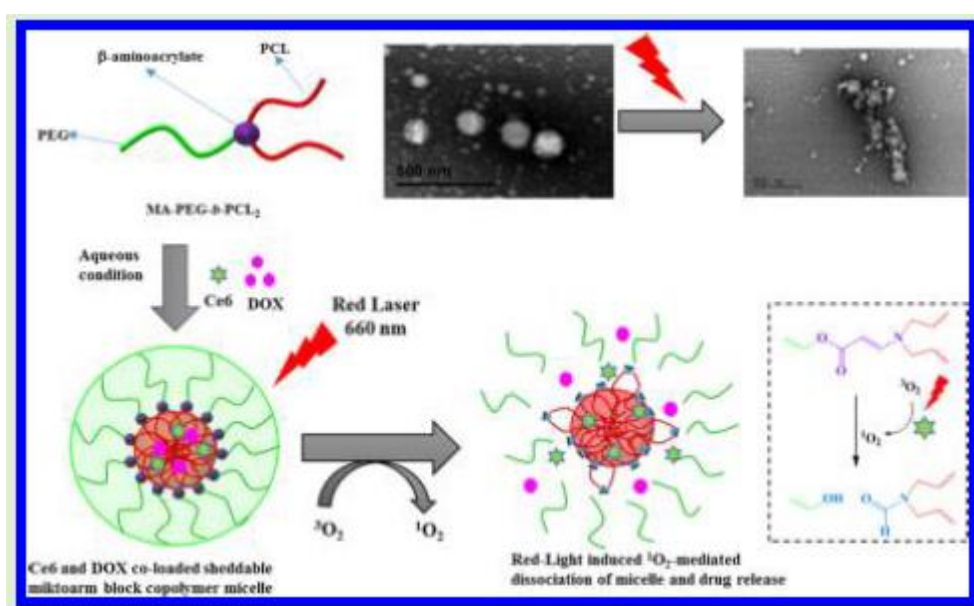


Figure 1.37. Schematic illustration of self-assembly and red laser induced ¹O₂-mediated dissociation of MA-PEG-*b*-PCL₂ micelles (adopted from Saravanakumar *et al. Biomacromolecules* **2018**, *19*, 2202-2213)

Bapurao *et al.* from our laboratory designed and developed carboxyl functionalized block copolymer by ring opening polymerization of newly designed 4-*t*-butyl ester substituted ε-caprolactone monomer using PEG-OH as macroinitiator. The *t*-butyl ester present on the backbone of the polymer was selectively deprotected to obtain carboxylic acid substituted amphiphilic PEG-*b*-CPCL block copolymers. These amphiphilic block copolymers formed vesicular self-assemblies in water and efficiently encapsulated hydrophilic molecules such as Rh-B as well as hydrophobic drugs ibuprofen (IBF) and camptothecin (CPT). pH responsive behaviour of the drug loaded vesicles was observed as they were stable under strong acidic conditions of

stomach and disassemble to release the loaded drugs under neutral or basic pH conditions similar to small intestine. Thus these PEG-b-CPCL block copolymer vesicles were demonstrated for stimuli responsive drug delivery under GI tract as shown in figure 1.38.¹¹⁴

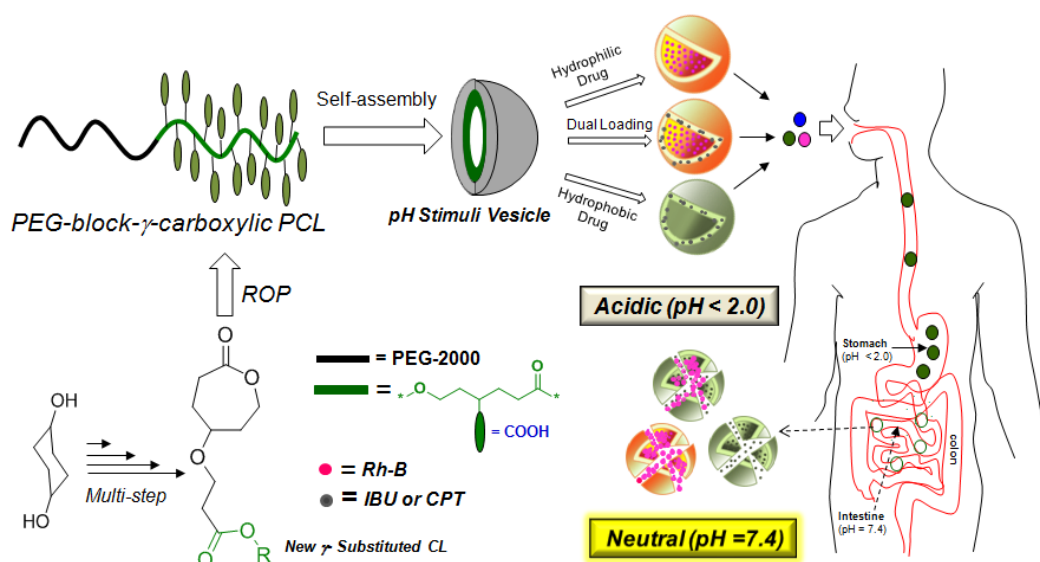


Figure 1.38. Carboxylic substituted PCL block copolymer vesicles and their pH stimuli responsive delivery under the GI tract (adopted from Bapurao et al. *Biomacromolecules* 2013,14,4377-4387)

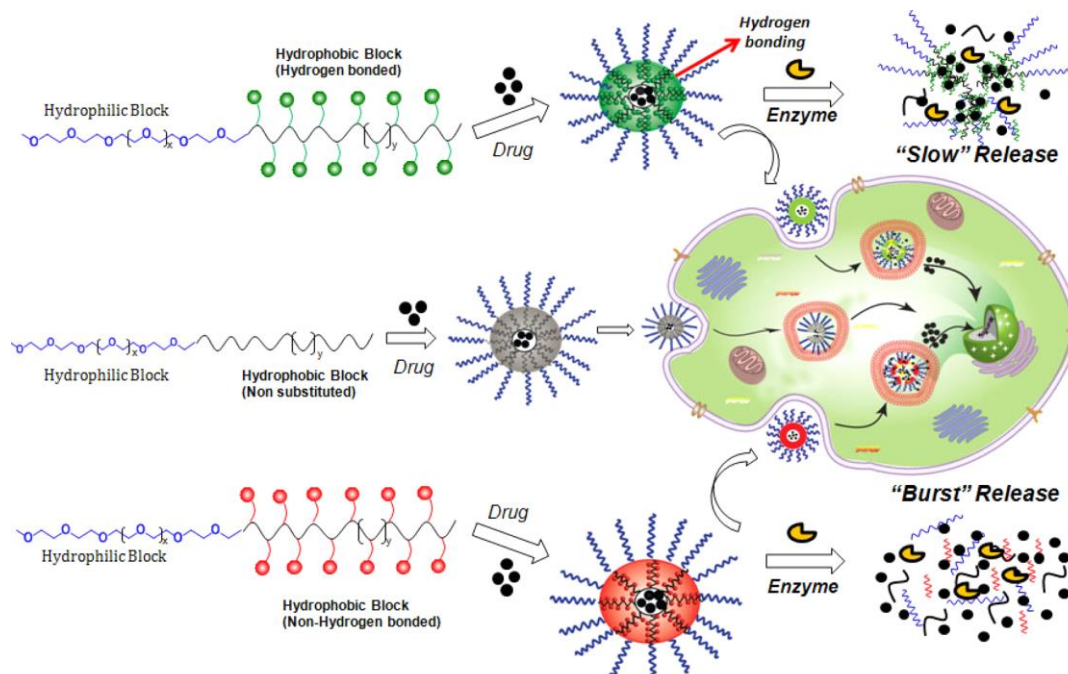


Figure 1.39. Hydrogen bond-controlled drug delivery in cancer cells from enzyme responsive polycaprolactone diblock copolymer nano-assemblies (adopted from Bapurao et al. *ACS Biomater. Sci. Eng.* 2016, 2, 1926-1941)

Further these block copolymers with different PEG chain length were also investigated for cisplatin conjugation through carboxylic acid pendent chains to form cisplatin conjugated core shell nanoparticles. The influence of the length of hydrophilic PEG shell on detoxification of drug by GSH was studied which showed that longer PEG shell protected cisplatin against GSH detoxification.^{115,116}

Same authors prepared amide and ester side chain substituted ϵ -caprolactone monomers and utilized for the synthesis of amide and ester substituted polycaprolactone-b-PEG (amide-PCL and ester-PCL) block copolymers by ROP process. These block copolymers self-assembled as stable nanoparticles in aqueous medium and were capable of loading multiple anticancer drugs including DOX, curcumin (CUR), camptothecin (CPT), methotrexate (MTX). The influence of hydrogen bonding on the drug release kinetics was studied for hydrogen bond containing amide-PCL block and non-hydrogen bonded ester block copolymers. The drug release studies revealed that hydrogen bonded amide-PCL block copolymers exhibited controlled drug release compared to that of nonhydrogen bonded ester-PCL block copolymers and schematically shown in figure 1.39.¹¹⁷

1.4 π -Conjugated polymers in Bioimaging

Drug delivery systems with fluorescence imaging probes such as organic dyes and quantum dots (QDs) have been explored to monitor the real-time drug distribution during drug delivery. However, photobleaching, low signal intensities and cellular cytotoxicity restrict their reliability and sensitivity. Although quantum dots often show superior brightness and photostability in *in vitro* and *in vivo* studies however surface oxidation and leaking of harmful toxic metal ions (Cd and Se) induce severe cytotoxicity. Further aggregation of QDs in the biological systems restricts their practical application in live cell imaging. These limitations of conventional fluorescent materials inspired to develop new fluorescent probes with improved performance. Conjugated polymers exhibit high fluorescence quantum yield, good photostability low cytotoxicity which are the prime concern for cellular imaging application. Moreover, the conjugated polymers have advantage of emission colour tuneability across the entire visible region and near IR which can be achieved by tuning the HOMO (highest occupied molecular orbital)-LUMO (lowest unoccupied molecular orbital) band gap of the π -conjugated backbone as shown in figure 1.40



Figure 1.40. *Tuning of optical properties in conjugated polymers*

Owing to these appealing photophysical properties, water soluble conjugated polymers which can load therapeutic agent along with molecular imaging capability have emerged as promising multifunctional candidates for drug delivery in the cancer treatment.^{118,119} Bin Liu and co-workers prepared fluorescent AIEgens such as TPE, TPETPAFN and BTPEBT containing polymeric nanorods via nanoprecipitation under ultrasound sonication (see figure 1.41). Depending upon the sonication time the nanodots converted into nanorods. The *in vivo* tumor imaging revealed that nanorods possess higher tumor accumulation, deeper tumor penetration and more efficient cellular uptake as compared to nanodots.¹²⁰

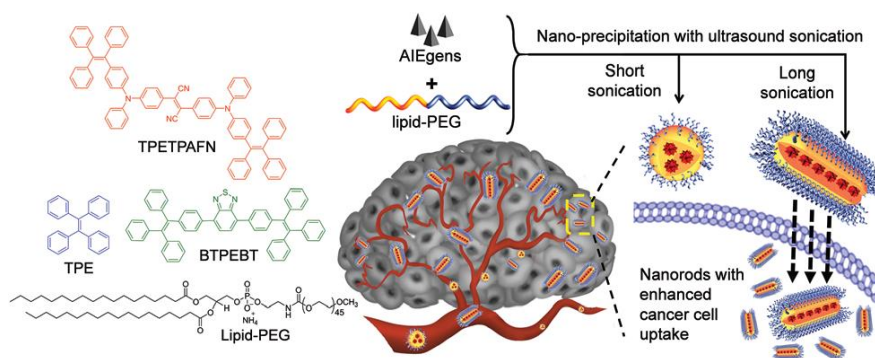


Figure 1.41. Schematic illustration of ultrasound sonication induced nanodot-to-nanorod transition and the enhanced tumor accumulation and cancer cell uptake of nanorods (Adopted from Feng et al. *Nanoscale* **2018**, *10*, 5869-5874)

Same authors developed nanoplatform containing photothermal conjugated polymer PFTTQ co-loaded with anticancer drug DOX in to an amphiphilic brush copolymer having photoresponsive group (DNQ) as encapsulation matrix. The surface modification of these nanoparticles with cRGD tripeptide improves tumor targeting ability by enhancing the cellular uptake in $\alpha_v\beta_3$ integrin overexpressed cancer cells. Upon NIR two photon laser irradiation, conjugated polymer PFTTQ rapidly converts laser energy into thermal energy for PTT moreover upon laser irradiation the photoresponsive hydrophobic 2-diazo-1,2-naphthoquinone (DNQ) moieties could be transformed to hydrophilic 3-indene carboxylate moiety and ultimately results in NP disassembly to release the drug. The chemotherapy and PPT resulted in synergistic cell killing to achieve improved therapeutic effects in cancer treatment.¹²¹

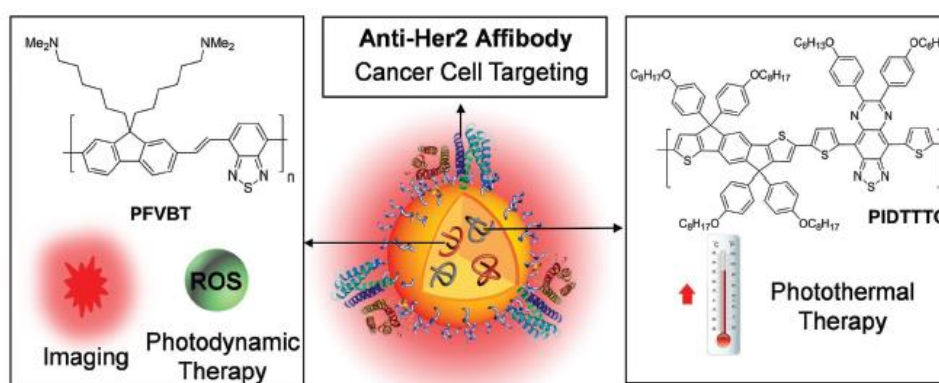


Figure 1.42. Schematic illustration of the components and functions of anti-HER2-CPNs (Adopted from Feng et al. *Small* **2017**, *13*, 1602807)

Same authors developed conjugated polymer nanoparticles for tumor targeting, fluorescence detection, photodynamic therapy (PDT) and photo-thermal

therapy (PTT) functions for cancer treatment. Two specially designed conjugated polymer, (PFVBT) with bright red and efficient ROS production capability and PIDTTTQ as shown in figure 1.42 with high near-infrared (NIR) absorption and light to heat conversion efficiency were synthesized and encapsulated by PEG matrix to form nanoparticles. The nanoparticle surface was modified with anti-HER2 affibody. The obtained nanoparticles showed excellent targeting ability towards HER2 overexpressed SKBR3 breast cancer cells. The *in vivo* tumor targeting and accumulation ability was visualized by fluorescence and infrared thermal imaging. Upon light illumination the synergistic combination effect of PDT and PTT largely suppressed the tumor growth.¹²²

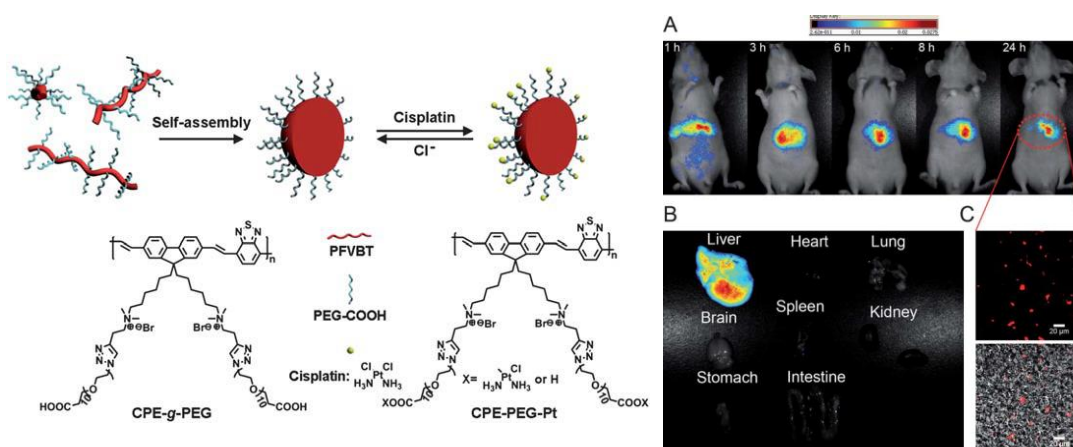


Figure 1.43. (a) Schematic illustration of synthesis of CPE-PEG-CP nanoparticles. (b) *In vivo* noninvasive fluorescence imaging of a nude mouse after intravenous injection of CPE-PEG-CP nanoparticles. (c) Fluorescence imaging of various organs at 24h post administration. (d) CLSM images of liver slices at 24h post administration. The red fluorescence (upper) from the CPE-PEG-CP nanoparticles distributed in the liver tissue is overlaid with the optical image (lower). (adapted from Ding et al. *Nanoscale* **2011**, 3, 1997-2002)

Liu and co-workers prepared PEG-grafted red fluorescent polyelectrolyte based nanoparticles conjugated with anticancer drug cisplatin (CPE-PEG-Pt) for simultaneous imaging and drug tracking. The *in vitro* cellular uptake of CPE-PEG-Pt in HepG2 cancer cells demonstrated the internalization into the cell nuclei by observing bright red fluorescence in the entire cells. The CPE-PEG-Pt nanoparticles were injected into the nude mice through intravenous administration to obtain real time information of the *in vivo* biodistribution and excretion profile of the nanoparticles using noninvasive live animal fluorescence technology. The

accumulation of nanoparticles in liver tissue showed their potential for liver cancer treatment (see figure 1.43).¹²³

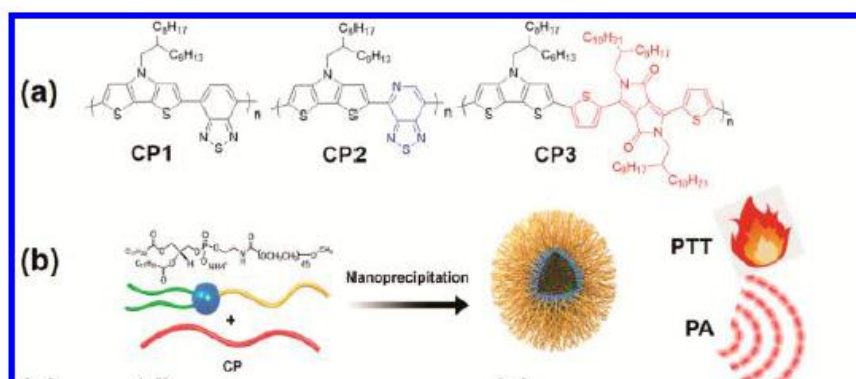


Figure 1.44. Chemical structures of CP1-3 and illustration of nanoparticle formation (adopted from Guo et al. *ACS Nano* **2017**, *11*, 1024-1034.)

Same authors designed and synthesized three different conjugated polymers (CP) using different electron acceptors (A) and a planar electron donor (D) as shown in figure 1.44 and the effect of D-A strength on photophysical properties and PA and PTT performance was systematically studied. With increasing D-A strength CP nanoparticles exhibited stronger photoacoustic signal and highly efficient photothermal therapeutic efficacy *in vitro* and *in vivo* superior to other reported contrast agents.¹²⁴ Same authors developed light responsive AIE nanoparticles to overcome the drug resistance in cancer cells. Hydrophilic polyethylene glycol (PEG) was conjugated with hydrophobic photosensitizer an AIEgen (TPETP) via ROS cleavable thioketal (TK) linker to obtain polymer (TPETP-TK-PEG). The amphiphilic polymer self-assemble as micellar nanoparticle and DOX was encapsulated into it with high drug loading capacity. Upon white light irradiation, the ROS generated from AIE nanoparticle facilitate endo-lysosomal escape by inducing rupture of membrane. ROS also cleave the TK linker which resulted in disassembly of nanoparticle to release the drug into the cytosol. This improved the DOX accumulation and retention in drug resistant MDA-MB-231 breast cancer cells and significantly inhibited the growth of the cancer cells (see figure 1.45).¹²⁵

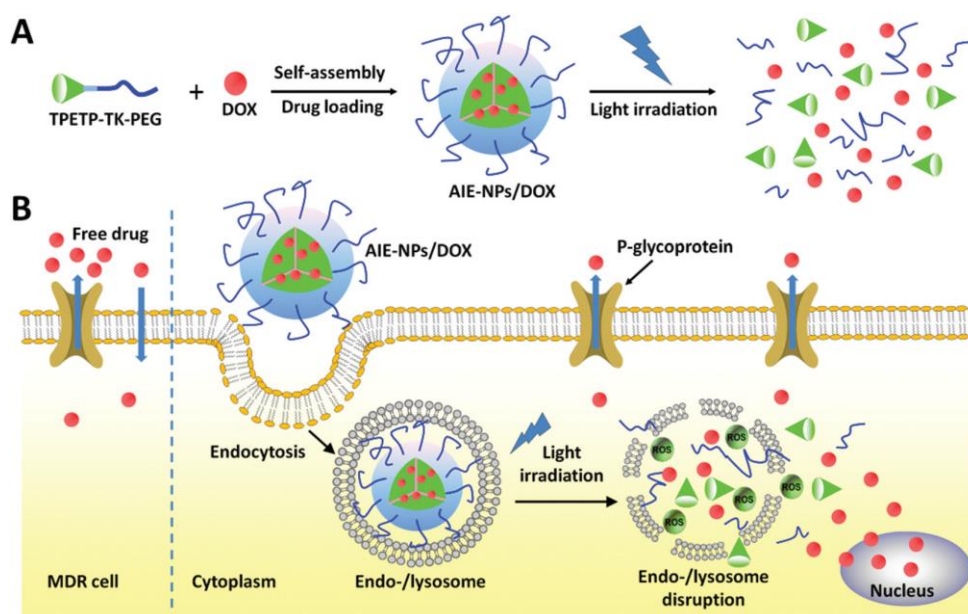


Figure 1.45. (a) Schematic illustration of light-responsive AIE-NPs encapsulated with DOX and visible light triggered drug release (b) the itinerary of AIE-NPs/DOX to overcome the drug resistance in cancer cells. For free DOX, the drug can be easily effluxed by the P-glycoprotein (P-gp) pump in drug resistant cancer cells. The drug loaded AIE-NPs were endocytosed by the cancer cells and entrapped in endo-/lysosomes. Upon white light irradiation, the ROS generated from the PS can enhance the membrane permeability of endo-/lysosomes to facilitate the NP escape to the cytosol and break the polymer to trigger the DOX release in the cytosol for nuclear entry to increase the drug retention in cancer cells and overcome the drug resistance (adopted from Yuan et al. *Polym. Chem.* 2016)

Same authors developed dual-prodrug with traceable activation for combination PDT and chemotherapy. AIE based photosensitizer TPEPYSH (PS) was linked to mitomycin C (MMC) through a disulphide bond to obtain TPEPY-S-MMC. The PS activity and fluorescence of TPEPY is blocked by quinine component in MMC. In addition, the cytotoxicity of MMC is inhibited by the electron withdrawing acyl at the nitrogen position of MMC. After glutathione activation, TPEPY-S-MMC can simultaneously release PDT active TPEPYSH and chemo-drug MMC. The turn on of the fluorescence of TPEPYSH can monitor the drug release as well as guide the photodynamic therapy (see figure 1.46).¹²⁶

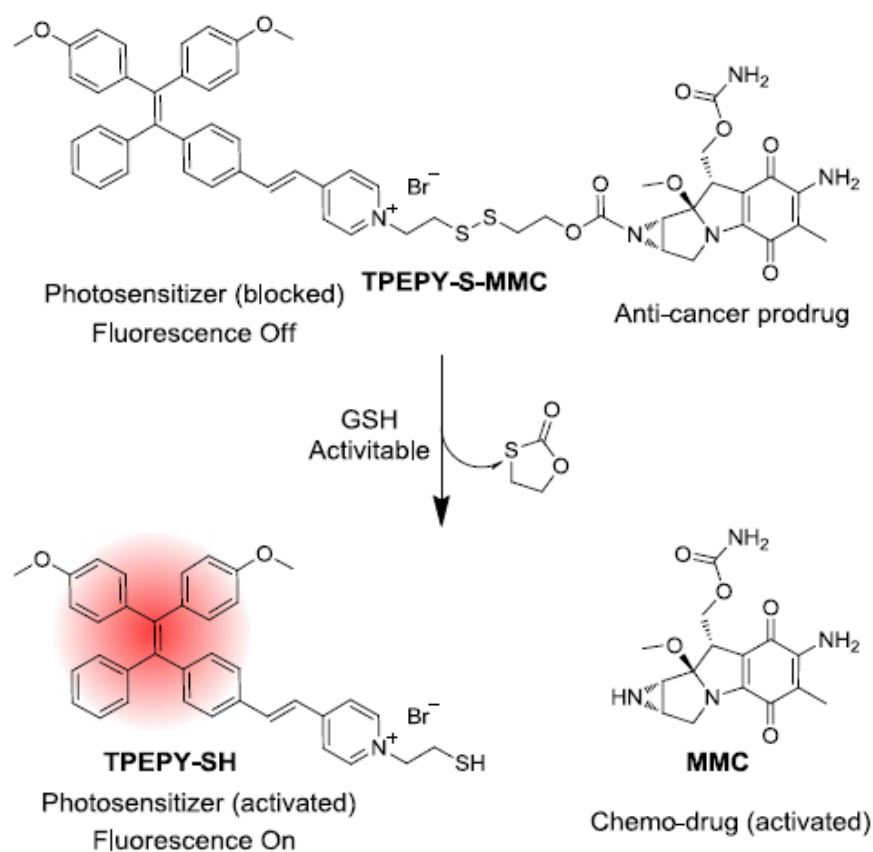


Figure 1.46. proposed route for the traceable activation of dual prodrug (adopted from Hu et al. *Biomaterials* **2017**, 144, 53-59)

Shu Wang and Guillermo C. Bazan group prepared multi-coloured (blue, green, yellow, red) conjugated polymer nanoparticles (CPN). Carboxyl functionalized CPN were prepared by co-precipitation of four conjugated polymers with poly(styrene-*co*-maleic anhydride) (PSMA). The CPN showing multicolour emission under single excitation over entire visible emission region were obtained. CPN-antibody conjugates were prepared by surface modification of CPN through amide coupling of antibody with carboxyl functionalized CPN. The antibody conjugated CPN were demonstrated for targeted cell imaging and specific cell detection of tumor cells as shown in figure 1.47.¹²⁷

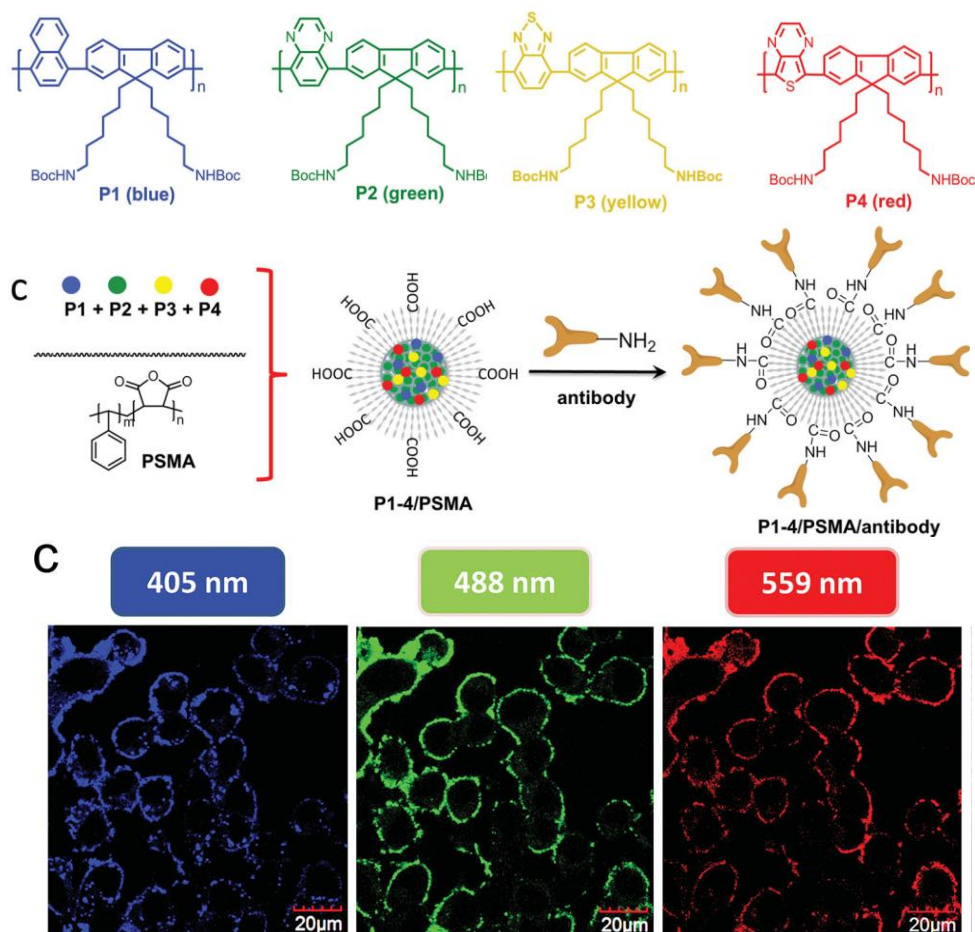


Figure 1.47. (a) Chemical structures of multicolour conjugated polymers (b) the preparation of multicolour conjugated polymer nanoparticles and their modification with antibody (c) multi-channel fluorescence images of MCF-7 cells with CPN-antibody conjugated nanoparticles. The excitation wavelengths are 405nm, 488nm, 559 nm.(adopted from Feng et al. *Adv. Mater.* **2014**, 26,3926-3930)

Libing Liu and Shu Wang group prepared aqueous nanoparticles containing fluorescent cationic conjugated polymer PFO which can form electrostatic assembly with negatively charged poly(l-glutamic acid) conjugated with anticancer drug doxorubicin (PFO/PG-DOX). The fluorescence of PFO in PFO/PG-DOX is in ‘turn off’ state due to electron transfer mechanism to DOX. The delivery of PFO/PG-DOX nanoparticles to lung cancer (A549) cells demonstrated that poly(l-glutamic acid) is hydrolysed to release DOX and inducing the fluorescence of PFO to ‘turn on’ state. Thus DOX release was monitored by fluorescence turn on signal from PFO which simultaneously images the cancer cells (see figure 1.48).¹²⁸

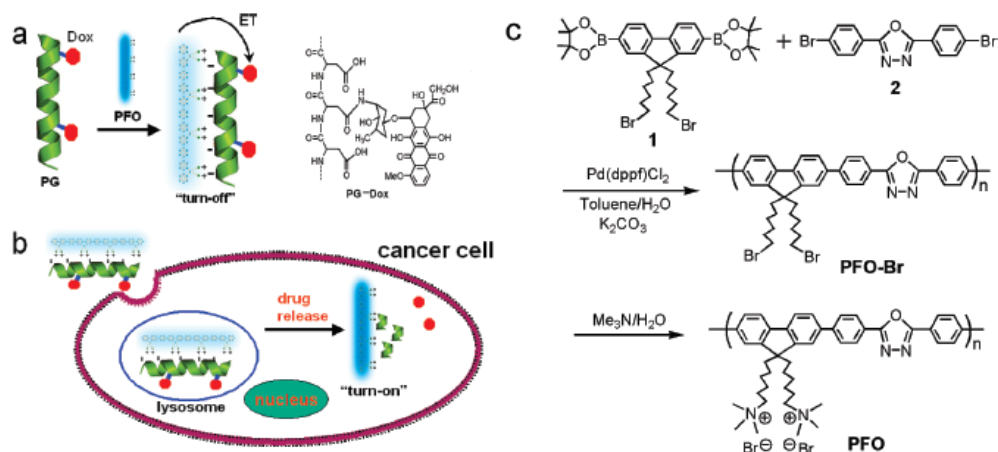


Figure 1.48. (a) Schematic illustration of PFO/PG-DOX complex system, where the fluorescence of PFO is highly quenched by DOX resulting in the fluorescence 'turn-off' state; chemical structures of PG-DOX conjugate and PFO are shown (b) Schematic representation of uptake of the electrostatic complex into cancer cells; hydrolysis of poly(l-glutamic acid) by hydrolase in lysosome releases the DOX to induce the activation of PFO fluorescence to 'turn on' state, thereby sensing the intracellular delivery of DOX and simultaneously achieving fluorescence imaging (c) synthetic route of cationic conjugated polymer PFO.

Same authors prepared hydrogel obtained by Michael addition between cysteine-terminated matrix metalloproteinase (MMP) cleavable oligopeptides and 4-arm vinyl sulfone-terminated polyethylene glycol (PEG-VS) as shown in figure 1.49. The hydrogel was functionalized with oligo(*p*-phenylenevinylene-*co*-benzothiazole) (OPV-BT) which act as photosensitizer (PS) to generate ROS upon light irradiation and cell adhesion peptide motif RGD to promote cell adhesion. In addition OPVBT was found to accumulate in mitochondria being effective for subcellular organelles-targeted PDT. Due to the overexpressed MMP in cancer cells, the MMP cleavable substrate in the hydrogel releases the OPVBT from hydrogel which selectively light up tumor cells and inhibit tumor cell growth by ROS generated from OPVBT upon light irradiation.¹²⁹

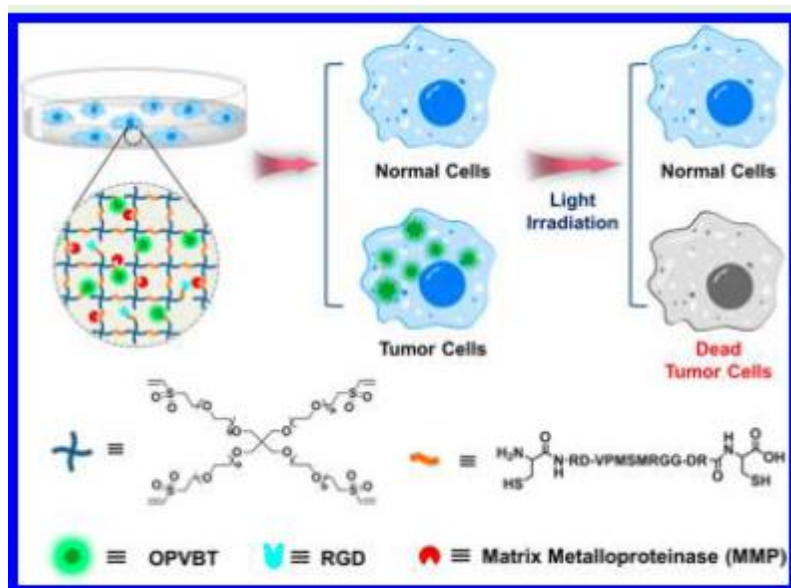
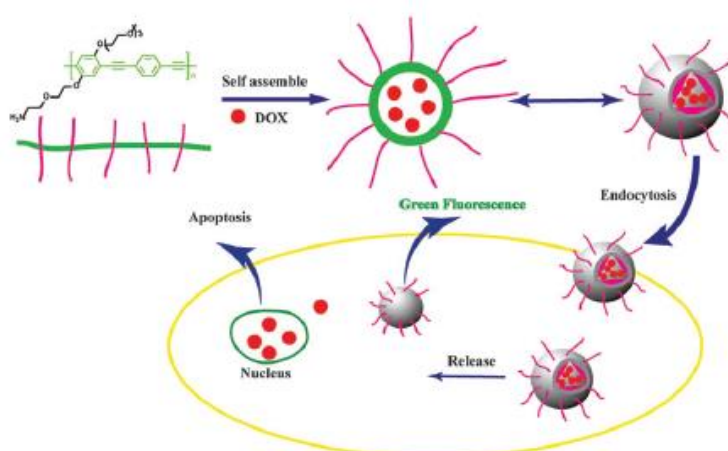


Figure 1.49. Illustration of MMP-sensitive hydrogel incorporated with OPVBT and RGD for tumor cell-specific imaging and photodynamic therapy (adopted from Li et al. *ACS Biomater. Sci. Eng.* **2018**, 4, 2037-2045)

Zhiyong Ke and Ruiyuan Liu group designed and synthesized amphiphilic poly(phenyleneethylene) which could self-assemble into nanoparticles (PPE) and anticancer drug DOX was encapsulated with high loading efficiency. The *in vitro* drug release study revealed efficient drug release from nanoparticle at endolysosomal pH (pH 5.5) as schemitally shown in figure 1.50. Live cell imaging demonstrated the successful cellular uptake followed by efficient drug release into the PC3 cancer cells. DOX loaded PPE nanoparticles exhibited improved cytotoxicity and cell apoptosis than free DOX in PC3cancer cells resulting in higher therapeutic efficiency.¹³⁰



Figutr 1.50. Schematic illustration of drug release of PPE nanoparticles in the cells (adopted from Chen et al. *J. Mater. Chem.* **2015**, 3, 3564-3572)

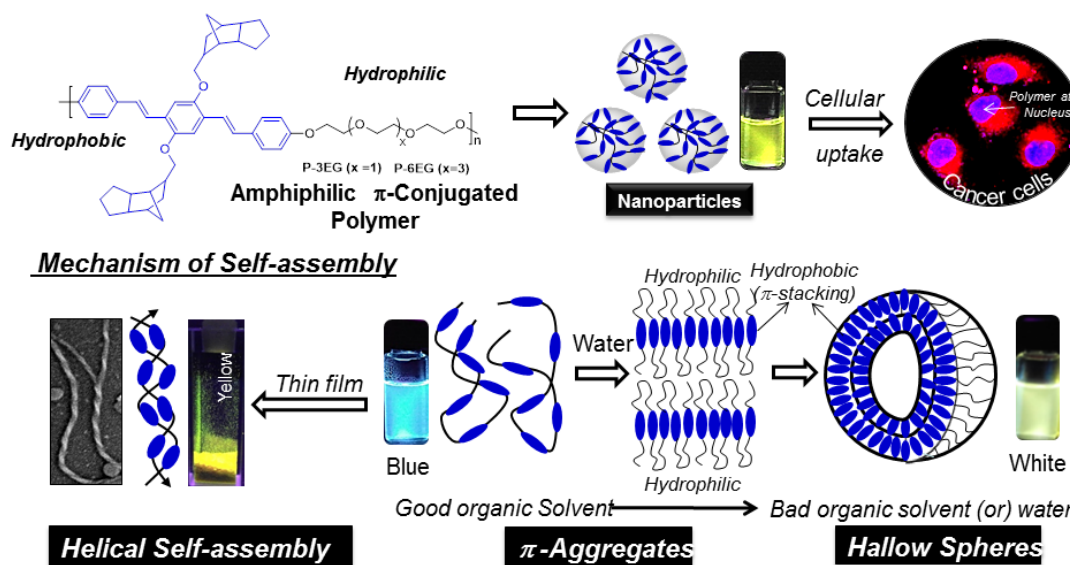


Figure 1.51. Segmented conjugated polymers for diverse polymer self-assembly and demonstrate their luminescent nano-assemblies as biomarkers in cancer cell imaging (adopted from Narasimha et al. *Macromolecules* **2016**, 49, 4102-4114)

Narasimha et al. developed amphiphilic segmented block copolymers containing rigid, luminescent oligophenylene vinylene (OPV) π -core and flexible oligo-ethyleneoxy spacer. Solvent induced aggregation of polymer chain revealed morphological transition from one dimensional helical nano-fibrous to three dimensional spherical nano-assemblies in THF/water solvent combinations followed by fluorescence colour change from blue-to-white-to-yellow as shown in figure 1.51. The polymers formed stable luminescent nanoparticles in aqueous medium. The cytotoxicity study confirmed non-toxic nature and biocompatibility of aqueous nanoparticles therefore the polymer nanoparticles were explored for bioimaging application in cervical (HeLa) and breast cancer (MCF-7) cells. Cellular uptake studies exhibited efficient internalization and accumulation of nanoparticles inside the cancer cells.¹³¹

1.5. π -Conjugate Tagged Block Copolymers Nano-carriers

Conjugated polymers with exceptional electrical and optical properties have been recognized as promising biomaterial for various biomedical applications. However, poor solubility and non-biodegradability are the prime concern to restrict their practical bioapplications and clinical translations. Owing to the inherent non-biodegradable nature of conjugated polymers, efforts have been taken to develop strategies to modify these polymers which can offer certain degree of biodegradability.¹³² The strategies to develop biodegradable conjugated polymers mainly include; direct blending of conjugated and biodegradable polymers to generate partially degradable polymeric composites and integration of conjugated oligomers and biodegradable monomers together to generate different macromolecular architectures^{133,134}

The direct blending approach is simple and straightforward strategy to obtain partially degradable composites wherein the conjugated polymers such as polythiophene, poly(3,4-ethylene dioxythiophene) (PEDOT), polyaniline, polypyrrole (PPy) blended with different synthetic polymers including polylactides, polycaprolactone, polyurethane, polyglycolide to form different nanocomposites. The desirable properties can be achieved through the selection of appropriate types as well as ratio of the degradable and conjugated polymers to be blended.^{135,136}

In the second approach conjugated oligomers are chemically conjugated to biodegradable polymers as conjugated oligomers also possess optoelectronic properties similar to their corresponding conjugated polymers. These polymers can be further modified with broad variety of functional groups which provides an opportunity to precisely control the amount of conjugated and biodegradable segment to obtain optimal performance. These polymers can be prepared different macromolecular architectures including linear, hyperbranched, star-shaped, and cross linked network architectures as shown in figure 1.52. These architectures also influences important properties of polymers such as morphology, mechanical and optical properties, biodegradability and hence the overall performance.^{137,138,139}

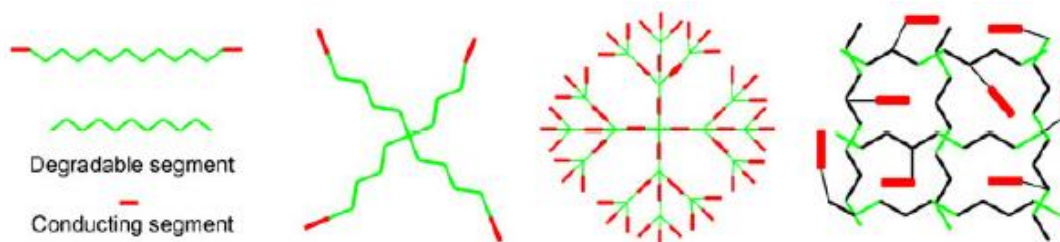


Figure 1.52. Degradable conjugated polymers with different architectures (adopted from BaoLin et al. *Sci. China: Chem.* **2014**, 57, 490-500)

In addition to the aforementioned approaches to develop biodegradable conjugated polymers, relatively recent strategy includes the modification of conjugated monomers and conjugation through biodegradable linkages (eg. imine) to prepare biodegradable conjugated polymers. Thus a large variety of biodegradable polymers with excellent morphological, optical and biological properties have been prepared following above mentioned strategies and extensively explored for biomedical applications including tissue engineering and regenerative medicine, biomedical implants, bioelectronics devices and consumer electronics.^{132,140,141} However, these conjugated biodegradable polymers are rarely utilized for bioimaging and drug delivery applications. Very few reports are known in the literature for the utility of biodegradable conjugated polymers in bioimaging and drug delivery applications. For example Wang and co-workers prepared fluorescent polycaprolactone grafted conjugated polymer bottle brushes (PFBT^{out}-g-PCL) and (PFBTⁱⁿ-g-PCL) with different positions of hexyl group on thiophene rings. These hydrophobic PFB-g-PCL polymers were encapsulated with amphiphilic block copolymers PCL-b-POEGMA using nanoprecipitation to form stable nanoparticles (nanoRED) in aqueous medium. These polymers exhibited broad emission at 635 nm with high fluorescence quantum yield and demonstrated for bioimaging application in L929 and HeLa cells with good biocompatibility (see figure 1.53).¹⁴²

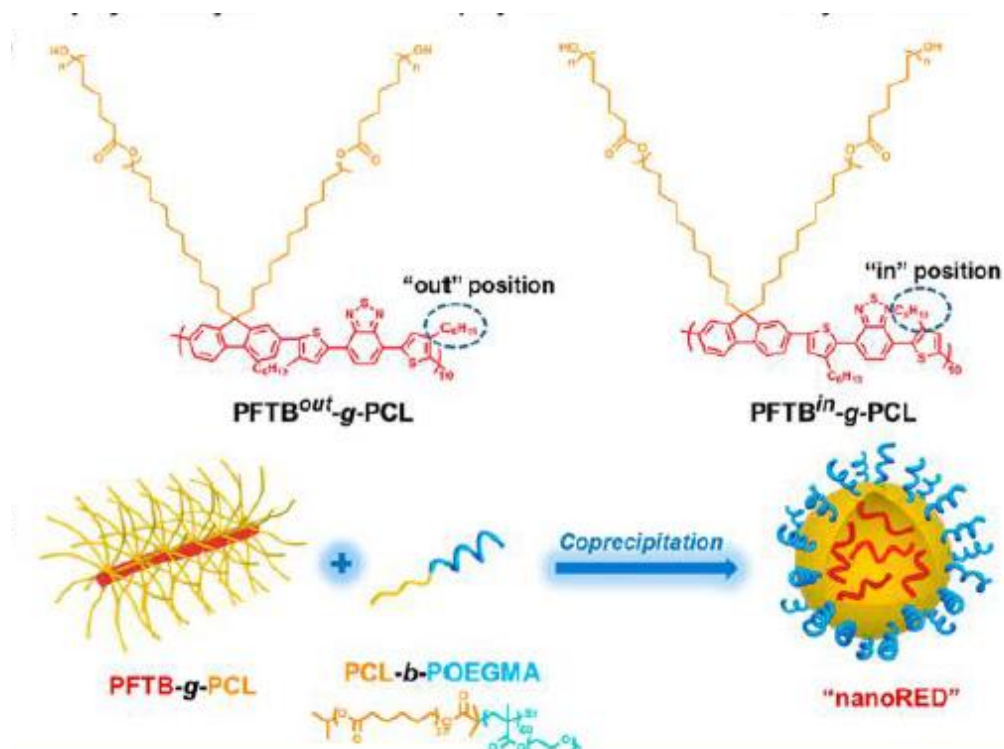


Figure 1.53. Chemical structure of PFTB-g-PCL with different hexyl side positioning on thiophene ring and schematic illustration of nanoRED formed by co-precipitation of PFTB-g-PCL and PCL-b-POEGMA as the stabilizer (adopted from Yang *et al.* 2016, 17, 1673-1683)

Twomey *et al.* synthesized biodegradable poly(p-phenyleneethylene)s (PPE) by polymerization of monomers including disulfide containing monomer which is reducible at intracellular glutathione concentrations. The mitochondrial targeting of PPE was improved by substitution of triphenylphosphine (TPP) on the side chains. The biodegradable fluorescent CP nanoparticles were demonstrated for active cellular internalization via variety of endocytosis and specifically localized to live tumor cells followed by intracellular degradation and trafficking (see figure 1.54)¹⁴³

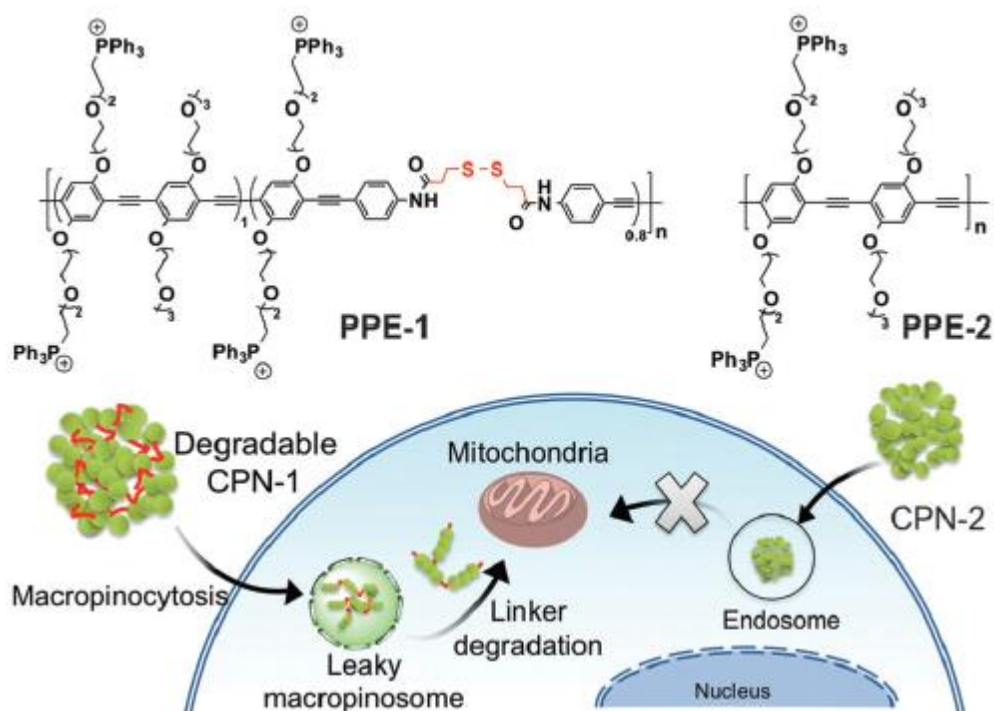


Figure 1.54. Chemical structures of PPEs with (PPE-1) and without (PPE-2) biodegradable linkers in the backbone and schematic illustration of cellular entry and mitochondrial localization biodegradable CPNs. CPN-1 and CPN-2 were fabricated with the corresponding PPEs via self-assembly in water (adopted from Twomey et al. *Chem. Commun.* **2016**, 52, 4910-4913)

Kuehne and co-workers reported fully conjugated polymer nanoparticles based on imidazole units having highly fluorescent and biodegradable particles. The polymer nanoparticles can be degraded upon exposure to ROS using hydrogen peroxide and the resulting degradation products are water soluble low molecular weight molecules as shown in figure 1.55. These conjugated polymer nanoparticles were demonstrated for cellular imaging.¹⁴⁴



Figure 1.55. Conjugated polymer synthesis; polymerization of thiophene monomers with imidazole monomers to produce degradable polymers (P1 and P3) and polymerization with benzene monomer to obtain non-biodegradable polymers (P2 and P4) and the degradative imidazole oxidation of particle by reactive oxygen species to decompose into methyl amino acid and amide terminated 2,5-diethynylene-3,4-methoxythiophene (adopted from Repenko et al. *Nat. Commun.* **2016**, 1-8)

The above study clearly outlined the huge potential of biodegradable polymers as well as conjugated polymers for efficient delivery of drugs and cellular imaging. However development of biodegradable conjugated polymers for practical drug delivery and cellular imaging applications is challenging task. Therefore there is need to develop nontoxic, biodegradable conjugated polymers for drug delivery and cellular imaging without losing their smart properties such as optical properties and biodegradability.

1.6. Aim of the thesis

Multipurpose polymer nano-scaffolds for cellular imaging and delivery of anticancer drug are urgently required for the treatment of cancer. The detail literature survey indicates that cationic polyelectrolytes based on π -conjugated oligomers and polymers were reported as promising candidates for cell imaging and diagnostics in cancer tissues. Despite, these fluorophores are excellent probes for cellular imaging; unfortunately, the highly rigid C-C or C-N backbones in these polymers render no biodegradation under physiological conditions. As a result, the cleavage of the polymer scaffold was impossible to achieve to employ these fluorophore containing polymers as a drug carrier while imaging. Hence, the development of new dual functional polymer nano-carriers by combining the design principles of biodegradable polymer and π -conjugated luminescent fluorophore in a single polymer system would open up new opportunity for simultaneous delivery and imaging in cancer treatment. To accomplish this goal, the present thesis work is emphasized to develop new class of block copolymer nano-carrier design consisting of π -conjugated fluorophore as a fixed core and variable length PCL biodegradable arms for cellular imaging and drug delivery vehicle (two-in-one design) in cancer cells. This new nano-scaffold design would allow one to achieve both therapeutic (or delivery) and cellular imaging (or diagnostics) in a single polymer system. For this purpose, our group expertise in biodegradable aliphatic polyester polycaprolactone (PCL) in drug delivery and π -conjugated oligo-phenylenevinylene chromophores is cleverly utilized for addressing the above problem. The new nano-carrier approach reported in the present work accomplishes both cellular imaging and delivering drugs to intracellular compartments. This concept is schematically shown in figure 1.56.

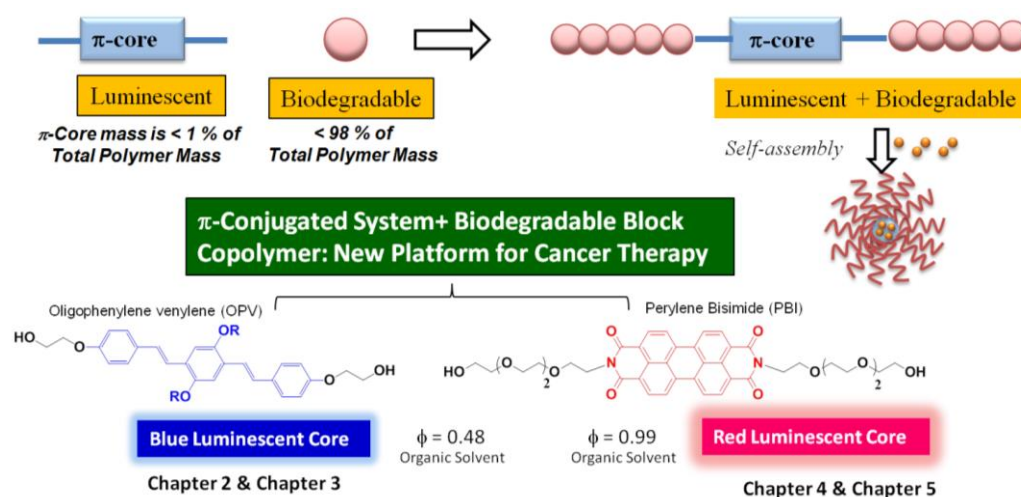


Figure 1.56. Schematic representation of the aim of the thesis work.

The thesis work is divided into four chapters. In chapter 2, blue-luminescent biodegradable PCL block copolymers were designed and developed through ring opening polymerization process. A new polymerization π -conjugated blue fluorescent initiator was tailor-made based on oligo-phenylenevinylene chromophores. The OPV-containing blue fluorescent block nano-carrier was employed for intracellular delivery of delivering doxorubicin. Both bio-imaging and delivery was accomplished simultaneously at the intracellular level. In chapter 3, enzyme-responsive fluorescence resonance energy transfer probe (FRET-probe) was constructed using the OPV-tagged blue luminescent nano-scaffold as donor and Nile red fluorophore as acceptor. FRET probe was demonstrated for imaging in cancer cells and the photophysical properties were confirmed by details steady state and time-resolved spectroscopic studies. In chapter 4, red-luminescence PCL block copolymer were designed using perylenebisimide macro-initiator via ring opening polymerization process. The amphiphilic block copolymers readily dispersed in water and its aqueous nanoparticle was employed for bio-imaging in cancer cells. In chapter 5, new triblock PCL copolymer was synthesized using the perylene-initiator. In this design, the carboxylic substituted PCL placed in the interior and PEG-chain anchored PCL as exterior to bring core-shell type nano-assemblies. Cisplatin was chemically conjugated in the CPCL part which produced water soluble fluorescent Pt-drug for treatment in cancer cells. The last chapter summarizes the thesis work and put forward the direction for

future research. The new classes of fluorescent PCL block copolymers designed and developed in this thesis are new entries as enzymatic-biodegradable polymers in the literature; hence they would be expected to be very important nano-carriers for long-term application in the biomedical field. The fluorescent block copolymer approach provides unique opportunity to understand the polymer chains self-organization phenomena as well their drug/bio-imaging applications.

1.7 References

1. Riehemann, K.; Schneider, S. W.; Luger, T. A.; Godin, B.; Ferrari, M.; Fuchs, H. *Angew. Chem. Int. Ed.* **2009**, *48*, 872-897
2. Ren, W. X.; Han, J.; Uhm, S.; Jang, Y. J.; Kang, C.; Kim, J. H.; Kim, J. S. *Chem. Commun.* **2015**, *51*, 10403-10418
3. Haag, R.; Kratz, F. *Angew. Chem. Int. Ed.* **2006**, *45*, 1198-1215
4. Allen, T. M.; Cullis, P. R. *Science* **2004**, *303*, 1818-1822
5. Langer, R. *Science* **1990**, *249*, 1527-1533
6. Uhrich, K. E.; Cannizzaro, S. M.; Langer, R.; Shakesheff, K. M. *Chem. Rev.* **1999**, *99*, 3181-3198
7. Torchilin, V. P. *Adv. Drug Deliv. Rev.* **2006**, *58*, 1532-1555
8. Davadasu, V. R.; Bhardwaj, V.; Ravi Kumar, M. N. V. *Chem. Rev.* **2013**, *113*, 1686-1735
9. Panyam, J.; Labhasetwar, V. *Adv. Drug Deliv. Rev.* **2003**, *55*, 329-347
10. Farokhzad, O. C.; Langer, R. *ACS Nano* **2009**, *3*, 16-20
11. Sun, T.; Zhang, Y. S.; Pang, B.; Hyun, D. C.; Yang, M.; Xia, Y. *Angew. Chem. Int. Ed.* **2014**, *53*, 12320-12364
12. Ferrari, M. *Nat. Rev. Cancer* **2005**, *5*, 161-171
13. Pattni, B. S.; Chupin, V. V.; Torchilin, V. P. *Chem. Rev.* **2015**, *115*, 10938-10966
14. Davis, M. E.; Chen, Z.G.; Shin, D.M. *Nat. Rev. Drug Discov.* **2008**, *7*, 771-782
15. Wang, A. Z.; Langer, R.; Farokhzad, O.C. *Annu. Rev. Med.* **2012**, *63*, 185-198
16. Sowinska, M.; Lipkowska, Z. U. *New J. Chem.* **2014**, *38*, 2168-2203
17. Medina, S.H.; El-Sayed, M. E. H. *Chem. Rev.* **2009**, *109*, 3141-3157
18. Taratula, O.; Garbuzenko, O.B.; Kirkpatrick, P.; Pandya, I.; Savla, R.; Pozharov, V. P.; He, H.; Minko, T. *J. Control. Release* **2009**, *140*, 284-293
19. Kojima, C.; Kono, K.; Maruyama, K.; Takagishi, T. *Bioconjugate Chem.* **2000**, *11*, 910-917
20. Ooya, T.; Lee, J.; Park, K. *Bioconjugate Chem.* **2004**, *15*, 1221-1229
21. Kennedy, L. C.; Bickford, L.R.; Lewinski, N.A.; Coughlin, A.J.; Hu, Y.; Day, E.S.; West, J.L.; Drezek, R.A. *Small* **2011**, *7*, 169-183
22. Foy, S.P.; Labhasetwar, V. *Biomaterials* **2011**, *32*, 9155-9158

23. Reddy, H.; Arias, J. L.; Nicolas, J.; Couvreur, P. *Chem. Rev.* **2012**, *112*, 5818-5878
24. Jain, T.K.; Reddy, M. K.; Morales, M.A.; Leslie-Pelecky, D.L.; Labhasetwar, V. *Mol. Pharmaceutics* **2007**, *5*, 316-327
25. Lui, Z.; Chein, K.; Davis, C.; Sherlock, S.; Cao, Q.; Chen, X.; Dai, H. *Cancer Res.* **2008**, *68*, 6652-6660
26. Kam, N. W. S.; Dai, H. *J. Am. Chem. Soc.* **2005**, *127*, 6021-6026
27. Lui, Y.; Wu, D.bC.; Zhang, W.D.; Jiang, X.; He, C.B.; Chung, T.S.; Gho, S.H.; Leong, K.W. *Angew. Chem. Int. Ed.* **2005**, *44*, 4782-4785
28. Kam, N.W. S.; Lui, Z.; Dai, H. *J. Am. Chem. Soc.* **2005**, *127*, 12492-12493
29. Liechty, W.B.; Peppas, N.A. *Eur. J. Pharm. Biopharm.* **2012**, *80*, 241-246
30. Vasey, P. A.; Kaye, S. B.; Morrison, R.; Twelves, C.; Wilson, P.; Duncan, R.; Thomson, A.H.; Murray, L.S.; Hilditch, T.E.; Murray, T.; Burtles, S.; Fraier, D.; Frigerio, E.; Cassidy, J. *Clin. Cancer Res.* **1999**, *5*, 83-94
31. Bilim, V. *Curr. Opin. Mol. Ther.* **2003**, *5*, 326-330
32. Duncan, R.; Gac-Breton, S.; Keane, R.; Musila, R.; Sat, Y.N.; Satchi, R.; Searle, F. *J. Control. Release* **2001**, *74*, 135-146
33. Satchi, R.; Connors, T.A.; Duncan, R. *Br. J. Cancer* **2001**, *85*, 1070-1076
34. Qiao, Z.Y.; Zhang, R.; Du, F.S.; Liang, D.H.; Li, Z.C. *J. Control. Release* **2011**, *152*, 57-66
35. Cabral, H.; Miyata, K.; Osada, K.; Katakoka, K. *Chem. Rev.* **2018**, *118*, 6844-6892
36. Matsumoto, K.; Yamamoto, T.; Kamata, R.; Maeda, H. *J. Biochem.* **1984**, *96*, 739-749
37. Fang, J.; Nakamura, H.; Maeda, H. *Adv. Drug Deliv. Rev.* **2011**, *63*, 136-151
38. Bertrand, N.; Wu, J.; Xu, X.; Kamaly, N.; Farokhzad, O.C. *Adv. Drug Deliv. Rev.* **2014**, *66*, 2-25
39. Yu, B.; Tai, H.C.; Xue, W.; Lee, L.J.; Lee, R.J. *Mol. Membr. Biol.* **2010**, *27*, 286-298
40. Saha, R.N.; Vasanthakumar, S.; Bende, G.; Snehalatha, M. *Mol. Membr. Biol.* **2010**, *27*, 215-231
41. Feng, H.; Wang, W.; Kang, N.G.; Mays, J.W. *Polymers* **2017**, *9*, 494
42. Hadjichristidis, N.; Pitsikalis, M.; Pispas, S.; Iatrou, H. *Chem. Rev.* **2001**, *101*, 3747-3792
43. Li, M.; Jahed, N. M.; Min, K.; Matyjaszewski, K. *Macromolecules* **2004**, *37*, 2434-2441
44. Hadjichristidis, N.; Iatrou, H.; Pitsikalis, M.; Mays, J. *Prog. Polym. Sci.* **2006**, *31*, 1068-1132.
45. Wang, H.; Lu, W.; Wang, W.; Shah, P. N.; Misichronis, K.; Kang, N. G.; Mays, J. W. *Macromol. Chem. Phys.* **2018**, *219*, 1700254.
46. Szwarc M. *Nature* **1956**, *176*, 1168.
47. Matyjaszewski, K.; Spanswick, J. *Mater. Today.* **2005**,
48. Grubbs, R. B.; Grubbs, R. H. *Macromolecules* **2017**, *50*, 6979-6997.

49. Benoit, D.; Harth, E.; Fox, P.; Waymouth, R. M.; Hawker, C. J. *Macromolecules* **2000**, *33*, 363-370.
50. Sugihara, s.; Sugihara, K.; Armes, S. P.; Ahmad, H.; Lewis, A. L. *Macromolecules* **2010**, *43*, 6321-6329.
51. Li, M.; Jahed, N.M.; Min, K.; Matyjaszewski, K. *Macromolecules* **2004**, *37*, 2434-2441.
52. Chong, Y. K.; Le, P. T.; Moad, G.; Tang, S.H. *Macromolecules* **1999**, *32*, 2071-2074.
53. Chaduc, I.; Zhang, W.; Rieger, J.; Lansalot, M.; Agosto, F.D.; Charleux, B. *Macromolecules*, **2011**, *32*, 1270-1276.
54. Nuyken, O.; Pask, S.D. *Polymers* **2013**, *5*, 361-403.
55. Aydogan, J.; Kutaya, C.; Allushi, A.; Yilmaz, G.; Yagci, Y. *Polym Chem* **2017**, *8*, 2899-2903.
56. Epps, T. E.; O'Reilly, R. K. *Chem Sci* **2016**, *7*, 1674-1689.
57. Jenekhe, S. A.; Chen, X. L. *Science* **1998**, *279*, 1903.
58. Mai, Y.; Eisenberg, A. *Chem. Soc. Rev*, **2012**, *41*, 5969-5985.
59. Ruiz, R.; Kang, H. M.; Detcheverry, F. A.; Dobisz, E.; Kercher, D. S.; Albrecht, T. R.; de Pablo, J. J.; Nealey, P. F. *Science* **2008**, *321*, 936-939.
60. Paquet, C.; Kumacheva, E. *Mater. Today* **2008**, *11*, 48-56. (4) Kim, H. C.; Park, S. M.; Hinsberg, W. D. *Chem. Rev.* **2010**, *110* (1), 146-177.
61. Jackson, E. A.; Hillmyer, M. A. *ACS Nano* **2010**, *4*, 3548- 3553.
62. Lu, A.; O'Reilly, R. K. *Curr. Opin. Biotechnol.* **2013**.
63. Munoz-Bonilla, A.; Ali, S. I.; del Campo, A.; Fernandez-Garcia, M.; van Herk, A. M.; Heuts, J. P. A. *Macromolecules* **2011**, *44*, 4282-4290.
64. Luo, Y. W.; Wang, X. G.; Zhu, Y.; Li, B. G.; Zhu, S. P. *Macromolecules* **2010**, *43*, 7472-7481.
65. Drury, J. L.; Mooney, D. J.; *Biomaterials* **2003**, *24*, 4337-4351
66. Khan, F.; Tanaka, M.; Ahmad, A. R. *J. Mater. Chem. B* **2015**, *3*, 8224.
67. Wang, G.; Henselwood, F.; Liu, G. *Langmuir* **1998**, *14*, 1554-1559
68. Adams, M. L.; Lavasanifar, A.; Kwon, G. S. *J. Pharm. Sci* **2003**, *92*, 1343
69. J. N. Israelachvili, D. J. Mitchell and B. W. Ninham, *Biochim. Biophys. Acta*, **1977**, *470*, 185-201.
70. Doncom, K. E. B.; Blackman, L. D.; Wright, D. B.; Gibson, M. I.; O'Reilly, R. K. *Chem Soc Rev* **2017**, *46*, 4119-4134.
71. Jain, S.; Bates, F. S. *Science* **2003**, *300*, 460-464.
72. Cabral, H.; Miyata, K.; Osada, K.; Kataoka, K. *Chem Rev* **2018**, *118*, 6844-6892.
73. Guo, X.; Wang, L.; Wei, X.; Zhou, S. *Polymer Chemistry* **2016**, *54*, 3525-3550.
74. Cabral, H.; Kataoka, K. *Journal of Controlled Release* **2014**, *190*, 463-476.
75. Matsumura, Y.; Hamaguchi, T.; Ura, T.; Muro, K.; Yamada, Y.; Shimada, Y.; Okusaka, T.; Ueno, H.; Lkeda, M.; Watanabe, N. *British J. Cancer* **2004**, *91*, 1775- 1781.
76. Matsumura, Y.; Kataoka, K. *Cancer Sci* **2009**, *100*, 572-579.

77. Hu, X.; Zhang, Y.; Xie, Z.; Jing, X.; Billotti, A.; Gu, Z. *Biomacromolecules* **2017**, *18*, 649-673.
78. Feng, A.; Yuan J. *Macromol. Rapid Commun* **2014**, *35*, 767-779.
79. Discher, D. E.; Ahmed, F. *Annu. Rev. Biomed. Eng.* **2006**, *8*, 323-341
80. Meng, A.; Hiemstra, C.; Engbers, G. H. M.; Feijen J. *Macromolecules* **2003**, *36*, 3004-3006.
81. Ahmed, H.; Pakunlu, R. I. Brannan, A.; Bates, F.; Minko, T.; Discher, D. E. *Journal of Controlled Release* **2006**, *116*, 150-158.
82. Kukula, H.; Schlaad H.; Antonietti, M.; Forster, S.; *J. Am Chem. Soc* **2002**, *124*, 1658-16-63.
83. Rodríguez-Hernández, Juan.; Lecommandoux, S.; *J. Am Chem. Soc* **2005**, *127*, 2026-2027.
84. Huang, J.; Bonduelle, C.; Thévenot, J.; Lecommandoux, S.; Heise, A.; *J. Am Chem. Soc* **2012**, *134*, 119-122.
85. Kamaly, N.; Yameen, B.; Wu, J.; Farokzhad, O.C. *Chem. Rev.*, **2016**, *116*, 2602-2663.
86. Zhang, W.; Ko, N. R.; Oh, J. K. *Chem Commun.* **2012**, *48*, 7542-7552.
87. Pillai, O.; Pachagnula, R.; *Curr. Opin. Chem. Biol.* **2001**, *5*, 447-451.
88. Woodruff, M. A.; Hutmacher, D. W.; *Prog. Polym. Sci.* **2010**, *35*, 1217-1256.
89. Rainbolt, E. A.; Washington, K. E.; Biewer, M. C.; Stefan, M. C. *Polym. Chem.* **2015**, *6*, 2369-2381.
90. Maurus, P. B.; Kaeding, C. C. *Oper. Techn. Sports Med.* **2004**, *12*, 158-160.
91. Knight, S.; Erggelet, C.; Endres, M.; Sittinger, M.; Kaps, C.; Stussi, E. J. *Biomed. Mater. Res. Part B: Appl. Biomater.* **2007**, *83*, 50-57
92. Erggelet, C.; Neumann, K.; Endres, M.; Haberstroh, K.; Sittinger, M.; Kaps, C. *Biomaterials* **2007**, *28*, 5570-5580
93. Ulery, B. D.; Nair, L. S; Laurencin, C. T. J. *Polym, Sci., Part B: Polym. Phys.* **2011**, *49*, 832-864.
94. Middleton, J. C.; Tipton, A. *J. Med. Plast. Biomater.* **1998**, 31-38
95. Conn, J.; Oyasu, R.; Welsh, M.; Beal, J. M. *Am. J. Surg.* **1974**, *128*, 19-23
96. Li, Z.; Tan, B. H. *Mater. Sci. Eng. C* **2014**, *45*, 620-634.
97. Dash, T. K.; Konkimalla, V. B. *J. Control Release* **2012**, *158*, 15-33.
98. Williams, C. K. *Chem. Soc. Rev.*, **2007**, *36*, 1573-1580.
99. Peng, K-Y.; Wang, S-W.; Hua, M-Y.; Lee, R-S. *RSC Adv* **2013**, *3*, 18453-18463.
100. Peng, K-Y.; Wang, S-W.; Lee, R-S. *J. Polym. Sci., Polym Chem.* **2013**, *51*, 2769-2781.
101. Guerry, A.; Cottaz, S.; Fleury, E.; Bernard, J.; Halila, S. *Carbohydrate Polymers* **2014**, *112*, 746-752.
102. Wang, D.; Huan, X.; Zhu, L.; Liu, J.; Qiu, F.; Yan, D.; Zhu, X. *RSC Adv.*, **2012**, *2*, 11953-11962.
103. Hao, J.; Servello, J.; Sista, P.; Biewer, M. C.; Stefan, M. C. *J. Mater. Chem.*, **2011**, *21*, 10623-10628.

104. Cheng, Y.; Hao, J.; Lee, L. A.; Biewer, M. C.; Wang, Q. *Biomacromolecules* **2012**, *13*, 2163-2173.
105. Rainbolt, E. A.; Washington, K. E.; Biewer, M. C.; Stefan M. C. *J. Mater. Chem. B*, **2013**, *1*, 6532-6537.
106. Rainbolt, E. A.; Miller, J. B.; Washington, K. E.; Senevirathne, S. A.; Biewer, M. C.; Siegwart, D. J.; Stefan M. C. *J. Mater. Chem. B*, **2015**, *3*, 1779-1787.
107. Washington, K. E.; Kularatne, R. N.; Du, J.; Ren, Y.; Gillings, M. J.; Geng, C. X.; Biewer, M. C.; Stefan M. C. *J. Mater. Chem. B*, **2017**, *5*, 5632-5640.
108. Tian, D.; Halleux, O.; Dubois, P.; Jerome, R. *Macromolecules* **1998**, *31*, 924-927.
109. Chang, L.; Deng, L.; Wang, W.; Lv, Z.; Hu, F.; Dong, A.; Zhang, J. *Biomacromolecules* **2012**, *13*, 3301-3310.
110. Liu, Y-S.; Chiu, C-C.; Chen, H-Y.; Chen, S-H.; Wang, L-F. *Mol. Pharmaceutics* **2014**, *11*, 1164-1175.
111. Senevirathne, S. A.; Washington, K. E.; Miller, J. B.; Biewer, M. C.; Oupicky, D.; Siegwart, D. J.; Stefan M. C. *J. Mater. Chem. B*, **2017**, *5*, 2106-2114.
112. Kularatne, R. N.; Washington, K. E.; Bulumulla, C.; Calubaquib, E. L.; Biewer, M. C.; Oupicky, D.; Stefan M. C. *Biomacromolecules*, **2018**, *19*, 1082-1089.
113. Saravanakumar, G.; Park, H.; Kim, J.; Park, D.; Pramanick, S.; Kim, D. H.; Kim, W. J. *Biomacromolecules* **2018**, *19*, 2202-2213.
114. Surnar, B.; Jayakannan, M. *Biomacromolecules* **2013**, *14*, 4377-4387.
115. Surnar, B.; Subash, P. P.; Jayakannan, M. *Z. Anorg. Allg. Chem.* **2014**, *640*, 1119-1126.
116. Surnar, B.; Sharma, K.; Jayakannan, M. *Nanoscale*, **2015**, *7*, 17964-17979.
117. Surnar, B.; Jayakannan, M. *ACS Biomater. Sci. Eng.* **2016**, *2*, 1926-1941.
118. Li, K.; Liu, B. *J. Mater. Chem.* **2012**, *22*, 1257-1264.
119. Li, K.; Liu, B. *Chem. Soc. Rev.* **2014**, *43*, 6570-6597.
120. Feng, G.; Mao, D.; Liu, J.; Goh, C. C.; Ng, L. G.; Kong, D.; Tang, B. Z.; Liu, B. *Nanoscale* **2018**, *10*, 5869-5874.
121. Yuan, Y.; Wang, Z.; Cai, P.; Liu, J.; Liao, L-D.; Hong, M.; Chen, X.; Thakor, N.; Liu, B. *Nanoscale* **2015**, *7*, 3067-3076.
122. Feng, G.; Fang, Y.; Liu, J.; Geng, J.; Ding, D.; Liu, B. *Small* **2017**, *13*, 1602807.
123. Ding, D.; Li, K.; Zhu, Z.; Pu, K-Y.; Hu, Y.; Jiang, X.; Liu, B. *Nanoscale* **2011**, *3*, 1997-2002.
124. Guo, B.; Sheng, Z.; Hu, D.; Li, A.; Xu, S.; Manghnani, P. N.; Liu, C.; Guo, L.; Zheng, H.; Liu, B. *ACS Nano* **2017**, *11*, 10124-10134.
125. Yuan, Y.; Xu, X.; Zhang, C-J.; Liu, B. *Polym. Chem.* **2016**, *7*, 3530-3539.
126. Hu, F.; Yuan, Y.; Mao, D.; Wu, W.; Liu, B. *Biomaterials* **2017**, *144*, 53-59.

127. Feng, L.; Liu, L.; Lv, F.; Bazan, G. C.; Wang, S. *Adv. Mater.* **2014**, *26*, 3926-3930.
128. Feng, X.; Lv, F.; Liu, L.; Tang, H.; Xing, C.; Yang, Q.; Wang, S. *ACS Appl. Mater. Interfaces* **2010**, *2*, 2429-2435.
129. Li, M.; He, P.; Li, S.; Wang, X.; Liu, L.; Lv, F.; Wang, S. *ACS Biomater. Sci. Eng.* **2018**, *4*, 2037-2045.
130. Chen, T.; Xu, W.; Huang, Z.; Peng, H.; Ke, Z.; Lu, X.; Yan, Y.; Liu, R. *J. Mater. Chem. B*, **2015**, *3*, 3564-3572.
131. Narasimha, K.; Jayakannan, M. *Macromolecules* **2016**, *49*, 4102-4114.
132. Kenry; Liu, B. *Biomacromolecules* **2018**, *19*, 1783-1803.
133. Xue, J.; Xie, J.; Liu, W.; Xia, Y. *Acc. Chem. Res.* **2017**, *50*, 1976-1987.
134. Wei, Z.; Faul, C. F. J. *Macromol. Rapid. Commun.* **2008**, *29*, 280-292.
135. Kaur, G.; Adhikari, R.; Cass, P.; Bown, M.; Gunatillake, P. *RSC Adv.* **2015**, *5*, 37553-37567.
136. Guo, B.; Glavas, L.; Albertsson, A-C. *Prog. Polym. Sci.* **2013**, *38*, 1263-1286.
137. BaoLin, G.; Peter X, M. A. *Sci. China: Chem.* **2014**, *57*, 490-500.
138. Guo, B.; Finne-Wistrand, A.; Albertsson, A-C. *Macromolecules* **2010**, *43*, 4472-4480.
139. Guo, B.; Finne-Wistrand, A.; Albertsson, A-C. *Biomacromolecules* **2010**, *11*, 855-863.
140. Baolin, G.; Peter X, M. A. *Biomacromolecules* **2018**, *19*, 1764-1782.
141. Balint, R.; Cassidy, N. J.; Cartmell, S. H. *Acta Biomater.* **2014**, *10*, 2341-2353.
142. Yang, C.; Liu, H.; Zhang, Y. Xu, Z.; Wang, X.; Cao, B.; Wang, M. *Biomacromolecules* **2016**, *17*, 1673-1683.
143. Twomey, M.; Mendez, E.; Manian, R. K.; Lee, S.; Moon, J. H. *Chem. Commun.* **2016**, *52*, 4910-4913.
144. Repenko, T.; Rix, A.; Ludwanowski, S.; Go, D.; Kiessling, F.; Lederle, W.; Kuehne, A. J. C. *Nat. Commun.* **2017**, *8*, 470.

Chapter 2

Dual Functional Nanocarrier for Cellular Imaging and Drug Delivery in Cancer Cells based on π -Conjugated Core and Biodegradable Polymer Arms

Abstract

Multipurpose polymer nano-scaffolds for cellular imaging and delivery of anticancer drug are urgently required for the cancer therapy. The present investigation reports a new polymer drug delivery concept based on biodegradable polycaprolactone (PCL) and highly luminescent π -conjugated fluorophore as dual functional nano-carrier for cellular imaging and delivery vehicles for anticancer drug to cancer cells. To accomplish this goal, a new substituted caprolactone monomer was designed and it was subjected to ring opening polymerization using a blue luminescent bishydroxyl oligo-phenylenevinylene (OPV) fluorophore as an initiator. A series of A-B-A triblock copolymer building blocks with a fixed OPV π -core and variable chain biodegradable PCL arm length were tailor-made. These triblocks self-assembled in organic solvents to produce well defined helical nanofibers whereas in water they produced spherical nanoparticles (size \sim 150 nm) with blue luminescence. The hydrophobic pocket of the polymer nanoparticle was found to be an efficient host for loading water insoluble anticancer drug such as doxorubicin (DOX). The photophysical studies revealed that there was no cross-talking between the OPV and DOX chromophores and their optical purity was retained in the nanoparticle assembly for cellular imaging. *In vitro* studies revealed that the biodegradable PCL arm was susceptible to enzymatic cleavage at the intracellular lysosomal esterase under physiological conditions to release the loaded drugs. The nascent nanoparticles were found to be non-toxic to cancer cells whereas the DOX loaded nanoparticles accomplished more than 80 % killing in HeLa cells. Confocal microscopic analysis confirmed the cell penetrating ability of the blue luminescent polymer nanoparticles and their accumulation preferably in the cytoplasm. The DOX loaded red luminescent polymer nanoparticles were also taken up by the cells and the drug was found to be accumulated at the peri-nuclear environment. The new nano-carrier approach reported in the present manuscript accomplishes both cellular imaging and delivering drugs to intracellular compartments in a single polymer system. The present investigation is one of the first examples to demonstrate the dual functional biodegradable luminescence nano-carrier concept in the literature and the studies established this proof-of-concept in cellular imaging and drug delivery in cancer cells.

2.1 Introduction

The development of new polymer scaffolds for diagnosing the disease site and delivering anticancer drug molecules have been emerging as important protocol in the treatment of cancers.^{1,2} In recent years, luminescent π -conjugated polymers (or oligomers) were made into nanoparticulate dispersion in aqueous medium and they were employed as fluorescent probe for cellular imaging and diagnosis.³⁻⁵ Most often, these π -conjugated nanoparticles were produced by the miniemulsion method or reprecipitation of polymers in the organic solvents into water. The optical properties of the nanoparticles were tuned by the varying the chemical structure of the π -conjugated backbone or altering their HOMO-LUMO band gaps.^{6,7}

To enhance the cellular uptake, these π -conjugated nanoparticles were further modified with cationic charges to increase their intracellular administration and binding to DNA for imaging.⁸ Cationic polyelectrolytes based on polyfluorenes and their copolymers⁹⁻¹⁴ (see figure 2.1), poly(phenylene ethynylene)s¹⁵⁻¹⁶ and poly(phenylenevinylene)s¹⁷⁻²¹ are some of the important examples. They were employed as probes for Heparin sensing,²² NIR fluorescence imaging²³ and targeted imaging of HER2-positive cells,²⁴ etc. Two-photon imaging and two-photon photodynamic therapeutic techniques were also developed for these π -conjugated polymers in living cells.²⁵⁻²⁹

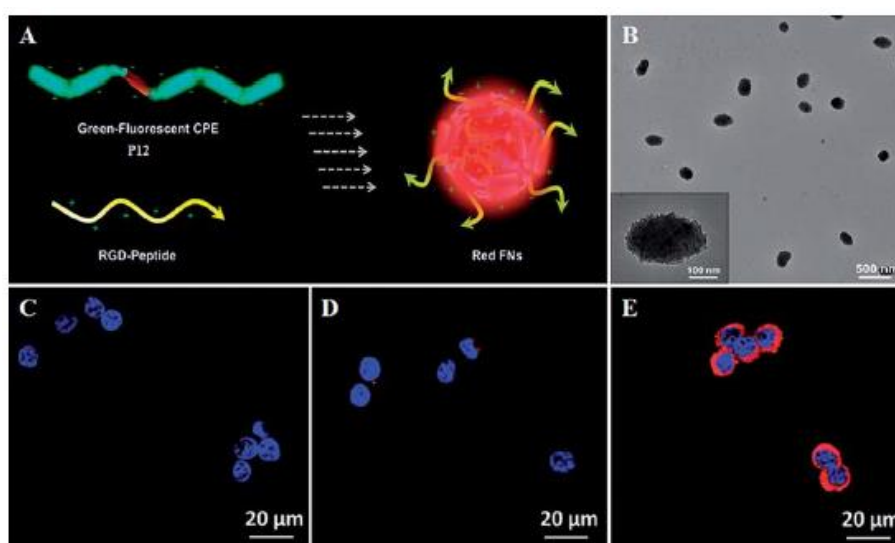


Figure 2.1(a)Schematic illustration of green fluorescent CPE/peptide nanoparticle formation, (b)TEM images of CPE/peptide nanoparticles. Confocal fluorescence images of HT29 cells with (c) polymer (D) and (E)polymer/peptide nanoparticles.

Bioluminescence resonance energy transfer process between luminal and cationic oligo-phenylenevinylene (OPV) chromophores was also achieved for anticancer, antifungal activities and combating drug resistance of cancer cells.³⁰⁻³¹

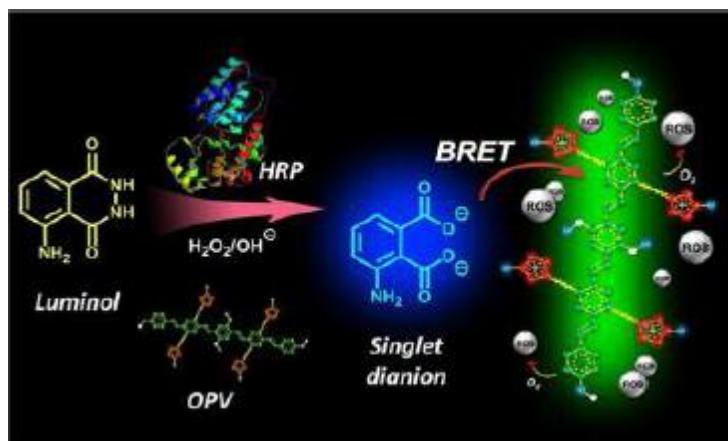


Figure 2.2. Schematic illustration of bioluminescence resonance energy transfer process between luminal and cationic oligo-phenylenevinylene (OPV) chromophores for PDT (Adopted from Yuan et al. *J. Am. Chem. Soc.* **2012**, 134, 13184-13187)

Few attempts were also made to blend or complex these π -conjugated polymers (or oligomer) were polystyrene-co-maleic anhydride,³² poly(L-glutamic acid)³³ or lipids,³⁴ antibodies³⁵ or cucurbituril³⁶ (see figure 2.3) to bring appropriate bio-compatibility and nano-shape for drug administration. Cationic polyfluorene polyelectrolyte-cisplatin complex was also developed for imaging and drug tracking in HepG2 cells.³⁷

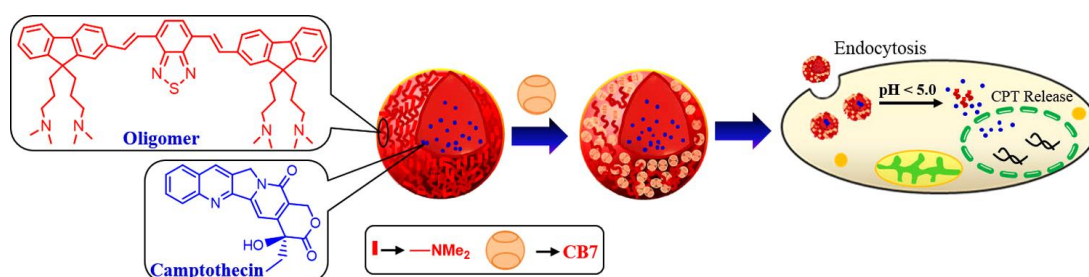


Figure 2.3 Cucurbituril capped, red emitting conjugated oligomer nanoparticles for pH responsive camptothecin delivery and cell imaging (adopted from Pennakalathil et al. *Biomacromolecules* **2014**, 15, 3366-3374)

Though these fluorophores are excellent probes for cellular imaging; unfortunately, the highly rigid C-C or C-N backbone in these polymers renders no biodegradation under physiological conditions. As a result, the cleavage of the polymer scaffold was impossible to achieve in these fluorophore containing polymers

as a drug carrier while imaging. Hence, the development of new dual functional polymer nano-carriers by combining the design principles of biodegradable polymer and π -conjugated luminescent fluorophore in a single polymer system would open up new opportunity for simultaneous delivery and imaging in cancer treatment which is yet to be known in the literature. To accomplish this goal, the present investigation is emphasized to develop new class of block copolymer nano-carrier design consisting of π -conjugated fluorophore as a fixed core and variable length biodegradable arms as self-organization building blocks for cellular imaging and drug delivery vehicle (two-in-one design) in cancer cells. This concept is schematically shown in figure 2.4.

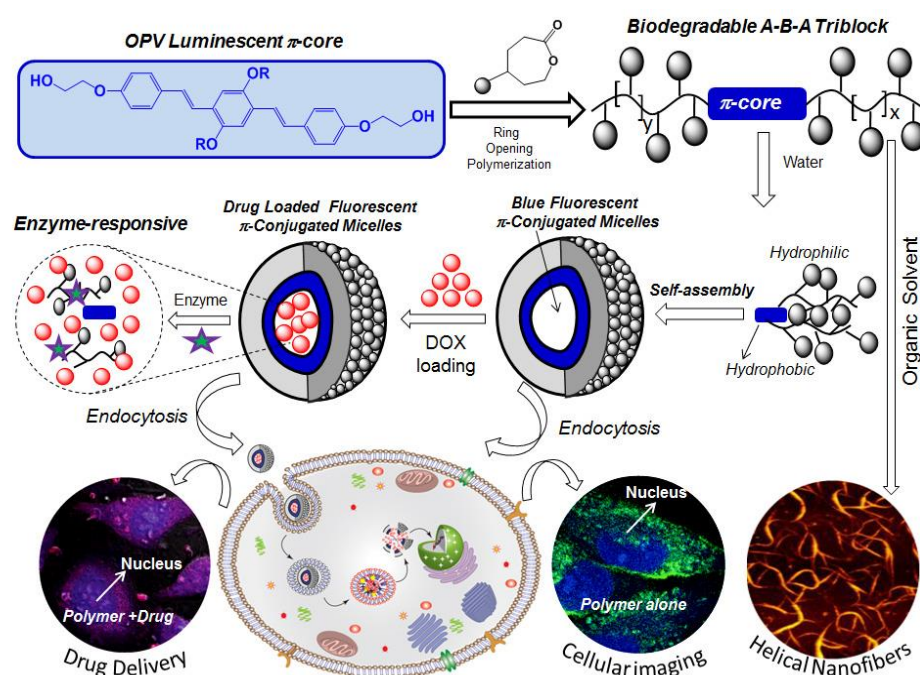


Figure 2.4. New biodegradable polymer- π conjugated chromophore block copolymers approach for drug delivery and imaging in cancer treatment.

For this purpose, biodegradable carboxylic substituted PCL backbone (developed from our laboratory) is employed as self-assembling building blocks and it was attached on the highly fluorescent OPV fluorophore to make unique luminescent nano-carrier having biodegradability for cellular imaging and drug delivery in cancer cells. Polycaprolactone (PCL) is an excellent aliphatic polyester for enzymatic cleavage at physiological conditions.³⁸ Recently, we have developed new carboxylic functional PCL-*b*-PEG copolymers as pH responsive vesicular scaffolds for oral delivery of drugs under GI track.³⁹ These block copolymers were also employed as nano-carrier for producing biodegradable core-shell cisplatin nanoparticles to

overcome the glutathione drug detoxification in breast cancer cells.⁴⁰⁻⁴¹ Our expertise in biodegradable polycaprolactone (PCL) in drug delivery³⁹⁻⁴¹ and the development of π -conjugated optical probes based on oligo-phenylenevinylene chromophores in supramolecular chemistry and sensing⁴²⁻²⁶ is cleverly combined here to make new nano-carrier for both cellular imaging and enzyme-responsive delivering drugs at the intracellular compartments in cancer cells. This new design is very unique and has following features: (i) new series of block copolymer design was adapted and supramolecular building blocks having fluorescent π -core with variable chain length biodegradable arms were tailor-made, (ii) the hydrophilic arm facilitated the self-assembly of the block copolymers into blue luminescent nanoparticles (size ~ 150 nm) in water and these polymer nanoparticles was employed for encapsulating water insoluble anticancer drug doxorubicin (DOX), (iii) the PCL arm is biocompatible and enzyme-responsive (i.e, biodegradable); thus, the nano-carrier ruptured at intracellular compartment by the lysosomal enzymes at intracellular compartment to deliver the loaded anticancer drugs and facilitated the cell killing and (iv) there is no cross-talking between the OPV and DOX chromophores and their optical purity was retained in the nanoparticle assembly which facilitated the cellular imaging while carrying out drug delivery. The DOX loaded polymer nanoparticles exhibited more than 80 % cell death in cervical cancer (HeLa) cell lines. Confocal microscopic imaging confirmed the cellular uptake and the accumulation of DOX at the perinuclear environment. The present investigation opens up new diagnostic-cum-drug delivery approach and demonstrated the proof-of-concept for the first time based on enzyme-responsive π -conjugated biodegradable nano-carrier approach for delivering DOX to cancer cells.

2.2. Experimental Section

2.2.1. Materials: Hydroquinone, ethylhexyl bromide, triethylphosphite, 4-hydroxybenzaldehyde, 2-chloroethanol, potassium *tert*-butoxide, (1 M in THF), potassium iodide, 1,4-cyclohexane diol, *tert*-butyl acrylate, pyridiniumchlorochromate (PCC), *m*-chloroperbenzoic acid, tin(II) 2-ethylhexanoate, caprolactone, Nile red, esterase were purchased from Aldrich chemicals and used without further purification. Paraformaldehyde, HBr in glacial acetic acid, K₂CO₃, KOH, NaHCO₃ were purchased locally. Tetrahydrofuran (THF), dimethylformamide (DMF) and all other solvents were purchased locally and purified using standard procedures. Cervical cancer (HeLa cells) were maintained in DMEM (with phenol red medium: Gibco) containing 10 % (v/v) fetal bovine serum (FBS) and 1 % (v/v) penicillin-streptomycin at 37 °C under a 5 % CO₂ humidified atmosphere. Cells were washed with 40 % DPBS (Gibco), trypsinised using 0.05 % trypsin (Gibco) and seeded in 96- or 6- well (as per experiment) flat-bottomed plastic plates (Costar) for all assays. Tetrazolium salt, 3,4,5-dimethylthiazol-2,5-diphenyltetrazolium bromide (MTT), DMSO, and 4 % paraformaldehyde were purchased from Sigma. Fluoromount was obtained from Southern Biotech.

2.2.2. General Procedures: Structure of the monomers and polymers were characterized by ¹H and ¹³C NMR using 400 MHz JEOL NMR spectrophotometer. All the NMR spectra were recorded in CDCl₃ and TMS as internal standard. Mass of all intermediate compounds was determined by using HRMS-ESI-Q-time-of-flight LCMS and Applied Bio system 4800 PLUS MALDI TOF/TOF Analyzer. Purity of polymers was determined by Gel Permeation Chromatography GPC using Viscotek VE 1122 pump, Viscotek column T6000 M (THF; two column in series), Viscotek VE 3580 RI detector and Viscotek VE 3210 UV-Vis detector in THF using polystyrene as standards for calibration. For GPC analysis concentration of all the polymers was 1 mg/mL in THF. Thermogravimetric analysis (TGA) was performed to determine the thermal stability of the polymers using Perkin Elmer thermal analyzer STA 6000 model at a heating rate of 10 °C/minute under nitrogen atmosphere. Thermal analysis of the polymers was carried out using TA Q20 Differential Scanning Calorimeter at heating and cooling rate of 10 °C/minute. Indium standards were used to calibrate the instrument before measurements. Polymers were heated to melt before recording their thermograms to remove thermal prehistory of the samples. Absorption

spectra were recorded using Perkin Elmer Lambda 45 UV-Vis spectrophotometer. The emission studies and were performed using SPEX Fluorolog HORIBA JOBINVYON fluorescence spectrophotometer. The steady state emission spectra were recorded using 450 W Xe lamp as excitation source. Dynamic light scattering (DLS) of the polymers was carried out using Nano ZS-90 apparatus utilizing 633 nm red laser (at 90° angle) from Malvern Instruments. FESEM images were recorded using Zeiss Ultra plus scanning electron microscope and the samples were prepared by drop-casting on to silicon wafers. Atomic force microscope (AFM) images were taken by using Veeco Nanoscope IV instrument and samples were recorded in tapping mode using SiN probe. Fluorescence microscope images collected using a Carl Zeiss Axiovert 200 microscope. LSM 710 confocal microscope was used for imaging the cells.

2.2.3. Synthesis of 1, 4-bis(2-ethylhexyloxy) benzene (1): Hydroquinone (10.0 g, 91.0 mmol) was dissolved in dry DMSO (60 mL) and KOH (20.4 g, 364.0 mmol) was added to it. The reaction mixture was heated at 80 °C for 30 minutes then 2-ethylhexyl bromide (35.5 mL, 199.0 mmol) was added drop wise to this reaction mixture and heating was continued for 48 h under nitrogen atmosphere. After 48 h, the reaction mixture was cooled and extracted into dichloromethane, washed with 5% NaOH. The organic layer was separated and dried over anhydrous Na₂SO₄. The crude product was purified by passing through silica gel column using ethyl acetate in pet ether as eluent. Yield = 16.8 g (55 %). ¹H-NMR (CDCl₃, 400MHz) δppm: 6.83 ppm (s, 4H, Ar-**H**), 3.80 (m, 4H, OCH₂), 1.70(m, 2H, OCH₂CH), 1.56-1.30 (m, 16H, aliphatic **H**) and 0.95-0.89 (t, 12H, CH₃). ¹³C-NMR (CDCl₃, 100MHz) δppm: 153.4, 115.3, 71.1, 39.4, 30.5, 29.1, 23.8, 23.0, 14.1 and 11.1 FT-IR (cm⁻¹): 2960, 2924, 2869, 1516, 1462, 1382, 1279, 1215, 1110 and 1031. MALDI-TOF-MS: *m/z* calculated for C₂₂H₃₈O₂: 334.54 and found 357.23 [M⁺+Na⁺].

2.2.4. Synthesis of 1,4-bis(bromomethyl)-2,5bis(2-ethyloxy)benzene (2): Compound (1) (8.0 g, 23.9 mmol) was taken in glacial acetic acid (60 mL) and paraformaldehyde (2.9 g, 95.6 mmol) was added. HBr in glacial acetic acid (23.9 mL, 47.8 mmol) was slowly added to this reaction mixture using dropping funnel. The reaction mixture was stirred at 80 °C for 6 h. It was cooled to room temperature and poured into large excess of water. The product was obtained as white precipitate and it was purified by recrystallization from hot isopropanol. Yield = 7.5 g (60 %). ¹H-

NMR (CDCl₃, 400 MHz) δ ppm: 6.86 (s, 2H, Ar-**H**), 4.53 (s, 4H, CH₂Br), 3.88 (d, 4H, OCH₂), 1.76 (m, 2H, OCH₂CH), 1.55-1.34 (m, 16H, aliphatic **H**) and 0.96 (t, 12H, CH₃). ¹³C-NMR (CDCl₃, 100MHz) δ ppm: 150.6, 127.3, 114.1, 70.9, 39.6, 30.6, 29.1, 28.7, 24.0, 23.1, 14.2 and 11.2. FT-IR (cm⁻¹): 2955, 2927, 2865, 1509, 1462, 1440, 1310, 1225, 1116, 1086, 1030 and 910.

2.2.5. Synthesis of tetraethyl (2,5-bis(2-ethylhexyloxy)-1,4-phenylene) bis(methylene) diphosphonate (3): Compound (2) (4.0 g, 7.7 mmol) and triethylphosphite (2.9 mL, 16.9 mmol) was heated at 150 °C for 10 h in nitrogen atmosphere. Then excess of triethylphosphite was removed by vacuum distillation. The crude product was purified by column chromatography using ethyl acetate and pet ether as eluent. Yield = 4.5 g (90%). ¹H-NMR(CDCl₃, 400 MHz) δ ppm: 6.94 (s, 2H, Ar-**H**), 4.02 (m, 8H, POCH₂CH₃), 3.82-3.80 (t, 4H OCH₂), 3.25-3.20 (d, 4H, CH₂P), 1.71 (m, 2H OCH₂CH), 1.54-1.29 (m, 16H, aliphatic CH₂), 1.23 (t, 12H, POCH₂CH₃) and 0.95-0.90 (t, 12H CH₃). ¹³C-NMR (CDCl₃, 100MHz) δ ppm: 150.5, 137.7, 119.4, 114.7, 71.2, 62.1, 53.7, 39.7, 30.6, 29.2, 27.0, 25.5, 24.1, 16.4, 14.1 and 11.2. FT-IR (cm⁻¹): 3478, 2940, 2868, 1645, 1515, 1465, 1250, 1160 and 1025. MALDI-TOF-MS: *m/z* calculated for C₃₂H₆₀O₈P₂: 634.77 and found 657.28 [M⁺+Na⁺].

2.2.6. Synthesis of 4-(2-Hydroxyethoxy) benzaldehyde (4): K₂CO₃ (4.5 g, 32.6 mmol) was added to dry DMF and heated at 80 °C for 10 minutes. 4-hydroxy benzaldehyde (2.0 g, 16.3 mmol) was added and it was stirred for 1 h. 2-Chloroethanol (1.3 mL, 32.6 mmol) and catalytic amount of KI was added and the reaction mixture was heated for 48 h. Excess DMF was removed by vacuum distillation and the crude product was cooled and poured into water. The product was extracted into chloroform and washed with 10% NaOH, brine solution, dried over anhydrous Na₂SO₄. The crude product was further purified by passing through silica gel column using ethyl acetate in pet ether as eluent. Yield = 1.3 g (45 %). ¹H-NMR (CDCl₃, 400 MHz) δ ppm: 9.76 (s, 1H, CHO), 7.73 (d, 2H, Ar-**H**), 6.93(d, 2H, Ar-H), 4.09(t, 2H, ArOCH₂), 3.94 (t, 2H, CH₂OH) and 3.30 (s, 1H, OH). ¹³C-NMR (CDCl₃, 100MHz) δ ppm: 190.9, 163.7, 132.1, 130.4, 114.9, 69.7 and 61.3. FT-IR (cm⁻¹): 3373, 3070, 1663, 1597, 1503, 1397, 1251, 1155 and 1077. HR-MS (ESI⁺): *m/z* calculated for C₉H₁₀O₃: 166.17 and found 189.10 [M⁺+Na⁺].

2.2.7. Synthesis of hydroxyl functionalized oligo-phenylenevinylene (HO-OPV-OH) (5): Bisphosphonate ester (3) (2.0 g, 3.1 mmol) and compound (4) (1.1 g, 6.6 mmol) were taken in dry THF (20 mL) and purged with nitrogen for 20 minutes. This reaction mixture was kept in ice cold condition. Potassium *tert*-butoxide was added drop wise in nitrogen atmosphere and the stirring was continued at 30 °C for 12 h under nitrogen atmosphere. The reaction mixture was concentrated, poured into water and extracted into chloroform. The organic layer was separated and dried using anhydrous Na₂SO₄. The crude product was purified by column chromatography using ethyl acetate and pet ether as eluent. Yield = 1.0 g (50 %). ¹H-NMR (CDCl₃, 400 MHz) δppm: 7.46 (d, 4H, Ar-H), 7.35 (d, 2H, CH=CH), 7.11(s, 2H, CH=CH), 7.11(s, 2H, Ar-H), 6.92 (d, 4H, Ar-H), 4.13 (d, 2H, CH₂OH), 3.99 (d, 2H, Ar-CH₂), 3.96 (d, 4H, OCH₂), 1.82 (m, 2H, CH), 1.60-1.33 (m 16H CH₂) and 1.00-0.90 (t, 12H, CH₃). ¹³C-NMR (CDCl₃, 100MHz) δppm: 151.2, 138.0, 128.6, 127.3, 126.8, 126.4, 123.5, 110.1, 71.7, 39.7, 30.8, 29.3, 24.2, 23.1, 14.1 and 11.3. FT-IR (cm⁻¹): 3435, 2924, 2864, 1688, 1600, 1457, 1418, 1292, 1172 and 1076. MALDI-TOF-MS: *m/z* calculated for C₄₂H₅₀O₆: 658.92 and found 658.46 [M⁺].

2.2.8. Synthesis of *t*-butyl-3-((4-hydroxycyclohexyl)oxy)-propionate (6): 1,4Cyclohexanediol (30.0 g, 259.0 mmol) and Potassium *tert*-butoxide (catalytic amount) were taken in dry THF (90.0 mL) and purged with nitrogen for 15 minutes. *tert*-Butyl acrylate (30.3 mL, 206.0 mmol) was added drop wise using dropping funnel. The reaction mixture was refluxed for 24 h in nitrogen atmosphere. The reaction mixture was concentrated and neutralized with dilute HCl. The content was extracted into dichloromethane, organic layer was separated and dried over anhydrous Na₂SO₄. The crude product was purified by passing through silica gel column using ethyl acetate and pet ether as eluent. Yield = 27.2 g (60 %). ¹H-NMR (CDCl₃, 400 MHz) δppm: 3.64 (m, 3H, OCH₂& OCH), 3.29-3.39(m, 1H, CHOH), 2.40 (t, 2H, CH₂CO), 1.96-1.81 (m, 4H, OCH(CH₂)₂), 1.64-1.32 (m, 4H, CO(CH₂)₂) and 1.45 (s, 9H, C(CH₃)₃). ¹³C-NMR (CDCl₃, 100MHz): 171.1, 80.4, 69.5, 63.9, 63.5, 32.5, 30.1, 29.3 and 27.4. FT-IR (cm⁻¹): 3420, 2980, 2935, 2860, 1715, 1450, 1395, 1270, 1255, 1160 and 1035. HR-MS (ESI⁺): *m/z* calculated for C₁₃H₂₄O₄: 244.56 and found 267.72 [M⁺+Na⁺].

2.2.9. Synthesis of *tert*-butyl-3-((4-oxocyclohexyl) oxy) propanoate (7): Compound (6) (10.0 g, 40.9 mmol) was taken in DCM (100.0 mL) and PCC (13.2 g, 61.4 mmol)

was added. The reaction mixture was stirred at 30 °C under nitrogen atmosphere for 6 h. PCC salts formed during the reaction was removed by filtration. The resultant filtrate was condensed by evaporating the solvent. The crude liquid product was purified by passing through silica gel column using ethyl acetate and pet ether as eluent. Yield = 8.5g (85 %). ¹H-NMR (CDCl₃, 400 MHz) δppm: 3.56 (m, 3H, OCH₂ and OCH), 2.58 (t, 2H, CH₂CO), 2.64 (m, 2H, COCH₂), 2.26 (m, 2H, COCH₂), 2.09 (m, 2H, COCH₂), 1.90 (m, 2H, COCH₂) and 1.45 (s, 9H, C(CH₃)₃). ¹³C-NMR (CDCl₃, 100MHz) δppm: 211.4, 171.1, 80.5, 72.7, 64.1, 37.2, 36.5, 30.5 and 20.0. FT-IR (cm⁻¹): 2970, 2871, 2365, 1716, 1450, 1410, 1395, 1210, 1160 and 1105. HR-MS (ESI⁺): *m/z* calculated for C₁₃H₂₂O₄: 242.32 and found 265.48 [M⁺+Na⁺].

2.2.10. Synthesis of tert-butyl-3-((7-oxooxepan-4-yl)oxy)propanoate (8): Compound (7) (8.0 g, 33.0 mmol) was dissolved in dry DCM and purged with nitrogen for 10 minutes. *m*-CPBA (11.4 g, 66.1 mmol) was added slowly followed by adding anhydrous NaHCO₃(5.5 g, 66.1 mmol) The reaction mixture was stirred at 30 °C for 12 h under nitrogen atmosphere. Solvent was removed by rota evaporator, saturated aqueous NaHCO₃ solution and saturated aqueous Na₂S₂O₃ solution were added. It was extracted into ethyl acetate, organic layer was separated and dried using anhydrous Na₂SO₄. The crude product was further purified by passing through silica gel column ethyl acetate in pet ether as eluent. Yield = 6.5 g (75 %). ¹H-NMR (CDCl₃, 400 MHz) δppm: 4.40 (dd, 1H, COOCH), 4.06(dd, 1H, COOCH), 3.60 (m, 4H, OCH₂, OCH& COCH), 2.98 (dd, 1H, COCH), 2.48 (t, 2H, COCH₂), 2.42-1.81 (m, 4H OCH(CH₂)₂) and 1.46 (s, 9H, C(CH₃)₃). ¹³C-NMR (CDCl₃, 100MHz) δppm: 176.5, 171.3, 80.8, 74.3, 64.3, 63.5, 36.8, 34.2, 28.5, 27.9 and 27.5. FT-IR (cm⁻¹): 2925, 1725, 1460, 1393, 1210, 1160 and 1105. HR-MS (ESI⁺): *m/z* calculated for C₁₃H₂₂O₅: 258.31 and found 281.52 [M⁺+Na⁺].

2.2.11. Ring-Opening Polymerization of substituted caprolactone: The representative procedure of ROP is described for substituted caprolactone monomer (8) and HO-OPV-OH (as initiator) for the ratio of [M]/[I] = 50 in neat. Substituted caprolactone monomer (8) (500 mg, 1.93 mmol), HO-OPV-OH (5) (25.50 mg, 0.038 mmol), and Sn(Oct)₂ (7.84 mg, 0.019 mmol) as catalyst was taken in flame- dried schlenk tube. The content was evacuated by applying high vacuum for 30 minutes. Then the polymerization mixture was heated at 130 °C for 12 h with constant stirring under vacuum. After completion of polymerization THF (1 mL) was added. The

solution was precipitated in cold hexane. The procedure was repeated twice to obtain pure polymer. Yield = 290 mg (58 %). $^1\text{H-NMR}(\text{CDCl}_3, 400 \text{ MHz})$ δppm : 7.47-6.91 (m, 14 Ar-H), 4.44 (t, 4H), 4.14 (t, 6H), 3.96 (d, 4H), 3.75 (t, 2H), 3.66 (t, 1H), 2.45 (t, 4H), 1.85 (t, 4H), 1.44 (s, 9H), 0.98 (t, 6H) and 0.93 (t, 6H). $^{13}\text{C-NMR}(\text{CDCl}_3, 100\text{MHz})$ δppm : 173.3, 170.7, 127.5, 114.6, 80.4, 75.3, 65.8, 64.6, 61.1, 36.1, 32.7, 29.1, 22.9 and 14.0. FT-IR (cm^{-1}): 3580, 2974, 2875, 2361, 1884, 1731, 1632, 1473, 1363, 1252. GPC molecular weights: $M_n = 7200$, $M_w = 18100$; $M_w/M_n = 2.5$.

Following the above polymerization procedure, different block copolymers were synthesized by varying the $[\text{M}]/[\text{I}]$ as = 5, 10, 20, 35 and 100. The details are provided below.

2.2.12. Synthesis of BPCL8: HO-OPV-OH (212.57 mg, 0.32 mmol), monomer 8 (500 mg, 1.93 mmol), $\text{Sn}(\text{Oct})_2$ (65.34 mg, 0.16 mmol). Yield 300 mg (60%). $^1\text{H-NMR}(\text{CDCl}_3, 400 \text{ MHz})$ δppm : 7.46-6.92 (m, 14 Ar-H), 4.45 (t, 4H), 4.13 (t, 6H), 3.96 (d, 4H), 3.75 (t, 2H), 3.66 (t, 1H), 2.45 (t, 4H), 1.86 (t, 4H), 1.44 (s, 9H), 0.99 (t, 6H) and 0.92 (t, 6H). $^{13}\text{C-NMR}(\text{CDCl}_3, 100\text{MHz})$ δppm : 173.9, 171.3, 158.3, 151.4, 131.8, 128.0, 122.1, 115.2, 110.5, 81.0, 75.9, 72.1, 65.2, 61.6, 40.2, 36.9, 33.3, 31.3, 29.3, 23.5, 14.5 and 11.7. FT-IR (cm^{-1}): 3530, 2968, 2874, 2361, 2008, 1731, 1630, 1508, 1470, 1366 and 1250. GPC molecular weights: $M_n = 1500$, $M_w = 4000$ & $M_w/M_n = 2.6$

2.2.13. Synthesis of BPC10: HO-OPV-OH (127.54 mg, 0.19 mmol), monomer 8 (500 mg, 1.93 mmol), $\text{Sn}(\text{oct})_2$ (39.20 mg, 0.09 mmol). Yield = 300 mg (60%). $^1\text{H-NMR}(\text{CDCl}_3, 400 \text{ MHz})$ δppm : 7.45-6.91 (m, 14H, Ar-H), 4.43 (t, 4H), 4.12 (t, 6H), 3.95 (d, 4H), 3.75 (t, 2H), 3.66 (t, 1H), 2.45 (t, 4H), 1.86 (t, 4H), 1.44 (s, 9H), 0.99 (t, 6H) and 0.93 (t, 6H). $^{13}\text{C-NMR}(\text{CDCl}_3, 100\text{MHz})$ δppm : 173.9, 171.3, 158.4, 151.4, 131.8, 128.1, 122.1, 115.2, 110.5, 81.0, 75.9, 72.2, 65.2, 60.4, 40.2, 36.9, 33.3, 29.3, 23.5, 14.5 and 11.7. FT-IR (cm^{-1}): 3536, 3968, 2875, 2361, 2006, 1730, 1630, 1460, 1366 and 1250. GPC molecular weights: $M_n = 2200$, $M_w = 6500$ & $M_w/M_n = 2.9$

2.2.14. Synthesis of BPCL22: HO-OPV-OH (63.77 mg, 0.096 mmol), monomer 8 (500 mg, 1.93 mmol), $\text{Sn}(\text{Oct})_2$ (19.60 mg, 0.048 mmol). Yield = 270 mg (54%). $^1\text{H-NMR}(\text{CDCl}_3, 400 \text{ MHz})$ δppm : 7.46-6.92 (m, 14 Ar-H), 4.45 (t, 4H), 4.14 (t, 6H), 3.96 (d, 4H), 3.76 (t, 2H), 3.66 (t, 1H), 2.45 (t, 4H), 1.85 (t, 4H), 1.44 (s, 9H), 0.99 (t, 6H) and 0.93 (t, 6H). $^{13}\text{C-NMR}(\text{CDCl}_3, 100\text{MHz})$ δppm : 173.6, 170.6, 80.7, 75.5,

64.9, 61.3, 36.5, 33.0, 30.4 and 29.0. FT-IR (cm^{-1}): 3408, 2970, 2870, 2362, 2168, 2006, 1731, 1632, 1472, 1366 and 1251. GPC molecular weights: $M_n = 4700$, $M_w = 14800$ & $M_w/M_n = 3.1$

2.2.15. Synthesis of BPCL40: HO-OPV-OH (35.42 mg, 0.053 mmol), monomer 8 (500 mg, 1.93 mmol), $\text{Sn}(\text{Oct})_2$ (10.89 mg, 0.026 mmol). Yield = 320 mg (65%). $^1\text{H-NMR}(\text{CDCl}_3, 400 \text{ MHz})$ δ ppm: 7.45-6.92 (m, 14 Ar-H), 4.45 (t, 4H), 4.13 (t, 6H), 3.96 (d, 4H), 3.76 (t, 2H), 3.66 (t, 1H), 2.44 (t, 4H), 1.84 (t, 4H), 1.44 (s, 9H), 0.99 (t, 6H) and 0.93 (t, 6H). $^{13}\text{C-NMR}(\text{CDCl}_3, 100\text{MHz})$ δ ppm: 173.3, 170.7, 127.5, 80.4, 75.3, 64.6, 61.1, 36.1, 32.7, 29.5, 14.0 and 11.5. FT-IR (cm^{-1}): 3581, 2973, 2875, 2361, 1884, 1730, 1632, 1473, 1365 and 1251. GPC molecular weights: $M_n = 6000$, $M_w = 13500$ & $M_w/M_n = 2.2$

2.2.16. Synthesis of BPCL100: HO-OPV-OH (12.75 mg, 0.019 mmol), monomer 8 (500 mg, 1.93 mmol), $\text{Sn}(\text{Oct})_2$ (3.92 mg, 0.0096 mmol). Yield = 240 mg (48%). $^1\text{H-NMR}(\text{CDCl}_3, 400 \text{ MHz})$ δ ppm: 7.47-6.92 (m, 14 Ar-H), 4.45 (t, 4H), 4.14 (t, 6H), 3.95 (d, 4H), 3.76 (t, 2H), 3.66 (t, 1H), 2.45 (t, 4H), 1.85 (t, 4H), 1.44 (s, 9H), 0.98 (t, 6H) and 0.93 (t, 6H). $^{13}\text{C-NMR}(\text{CDCl}_3, 100\text{MHz})$ δ ppm: 173.6, 170.6, 80.7, 75.5, 64.9, 61.3, 36.5, 33.0, and 29.0. FT-IR (cm^{-1}): 3581, 2974, 2875, 2361, 1884, 1731, 1632, 1473, 1363 and 1252. GPC molecular weights: $M_n = 12,700$, $M_w = 35,600$ & $M_w/M_n = 2.8$

2.2.17. Encapsulation of doxorubicin (DOX) into BPCLx nanoparticles: The anticancer drug, DOX was loaded into the BPCLx nanoparticles by the dialysis method. DOX.HCl was neutralized with triethyl amine prior to loading. In a typical experiment 2.0 mg of the polymer and 0.5 mg of DOX were dissolved in DMSO (2.0 mL). Deionized water (3.0 mL) was added drop wise into the polymer solution. The resulting solution was stirred at 25 °C under dark conditions for 4 h. The solution was transferred to the semi-permeable membrane having MWCO 1000 and then dialyzed against large amount of deionized water for 48 h. Fresh water was replenished periodically to ensure the removal of un-encapsulated DOX and DMSO from the dialysis membrane. The dialyzed solution was filtered, lyophilized and stored at 4 °C for further usage.

The drug loading content and drug loading efficiency were determined by absorption spectroscopy. The absorbance of the DOX in DOX loaded BPCLx

nanoparticles at 480 nm was used to determine the DLC and DLE. The amount of DOX loaded into the polymer nanoparticles was determined by the molar extinction coefficient of DOX as $11500 \text{ L mol}^{-1} \text{ cm}^{-1}$. Drug loading content (DLC) and drug loading efficiency (DLE) were calculated using the following equations.⁴¹

$$\text{DLC (\%)} = \left\{ \frac{\text{weight of drug encapsulated in nanoparticles}}{\text{weight of drug loaded nanoparticles}} \right\} \times 100\%$$

$$\text{DLE (\%)} = \left\{ \frac{\text{weight of drug encapsulated in nanoparticles}}{\text{weight of drug in feed}} \right\} \times 100\%$$

2.2.18. *In vitro* drug release studies: The release profile of DOX from polymer nanoparticles was studied using dialysis method under physiological conditions. DOX loaded nanoparticles (1.0 mL) were taken in semi-permeable membrane. The membrane was immersed in PBS (10.0 mL) (at pH 7.4) and it was incubated at 37 °C. At specific time intervals PBS (2.0 mL) was withdrawn and replaced with equal volume of fresh PBS buffer. The absorbance of each aliquot was measured using absorption spectroscopy. The absorbance at 480 nm was used to determine the amount of DOX released from the nanoparticles. Esterase assisted drug release studies were carried out by adding 10 U esterase enzyme following the above mentioned procedure. The cumulative release of the drug was calculated by using following equation.⁴¹

$$\text{Cumulative drug release} = \left(\frac{\text{amount of drug release at time } t}{\text{total amount of drug in the nanoparticle taken in dialysis tube}} \right) \times 100$$

2.2.19. Cell-viability assay (MTT assay): The cytotoxicity of DOX loaded polymer nanoparticles and polymer nanoparticles alone was studied in HeLa cell line using the tetrazolium salt, 3,4,5-dimethylthiazol-2,5-diphenyltetrazolium bromide (MTT). In a 96-well plate (Corning, USA), 1000 cells were seeded per well in 100 μL of DMEM with 10% FBS (fetal bovine serum) and allowed to adhere for 16 h. Prior to drug treatment, media from the cells was aspirated and various concentrations of DOX and drug loaded polymer nanoparticles were added as feed. A blank control, DMEM with FBS in the absence of cells and an untreated control, cells with DMEM containing FBS, were used in each experiment. All control and treated experiment wells were in triplicate. Cells were incubated for 24 h without a change in medium and after 24 h

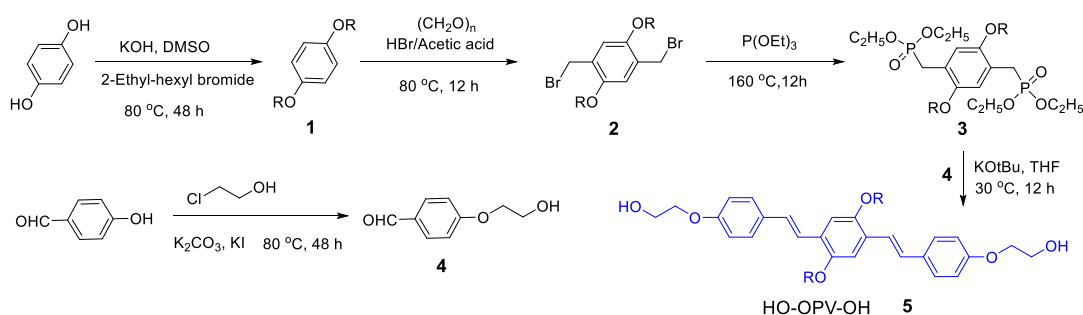
the drug containing medium was aspirated. A freshly prepared stock solution of MTT in sterile PBS (5 mg/mL) was diluted to 50 µg/mL in DMEM. 100 µL of this solution was added to each well. Cells were then incubated with MTT for 4 h at 37 °C. medium with MTT was then aspirated from the wells and the purple formazan crystals that formed as a result of reduction of MTT by mitochondrial dehydrogenase enzyme from the cells were dissolved in 100 µL of DMSO (added per well). The absorbance from the formazan crystals was immediately measured using a micro plate reader at 570 nm (Varioskan Flash) and was representative of the number of viable cells per well. Values from triplicate run for each control and treated set were noted and their mean value was used for calculations.

2.2.20. Cellular uptake studies using confocal microscopy: HeLa cells were seeded at a density of 1×10^5 cells on flame dried cover slips coated placed in 6 well plates containing DMEM medium with 10 % FBS. The cells were incubated at 37 °C for 16 hours and then exposed to the required concentrations of free DOX, BPCLx polymer nanoparticles alone and DOX loaded polymer nanoparticles for 4 h in a CO₂ incubator at 37 °C. After incubation, drug-containing medium was aspirated from each well, and cells were washed twice with PBS (1 mL per wash) and fixed with 4 % paraformaldehyde solution in PBS for 10 minutes at room temperature. The cells were washed twice with PBS (1 mL per wash) and stained with phalloidin conjugated to Alexa 488 (invitrogen) diluted 1: 100 in 5 % BSA solution in PBS. This incubation was performed in the dark and excess of dye was washed from the cells with PBS. The cover slips were mounted on slides using Fluoromount-G mounting medium (Southern Biotech). Slides were then dried overnight at room temperature in the dark. The cells were imaged using a LSM 710 confocal microscope with the λ 420 nm (blue channel), λ 560 nm (red channel) and λ 488 nm (green channel) lasers. Images thus obtained were analyzed using Image J analysis software and the image for each channel was separated.

2.3. Results and Discussion

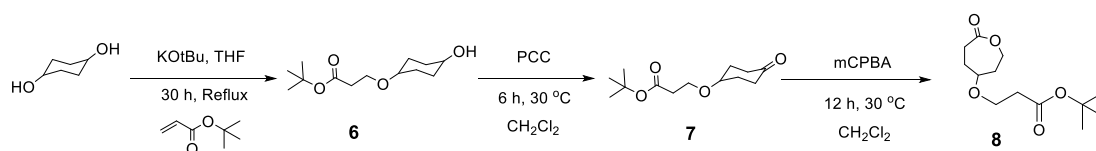
2.3.1. Synthesis and Characterization of Polymers

The hydroxyl functionalized OPV and substituted caprolactone monomer were synthesized through multi-step reaction as shown in scheme 2.1. Hydroquinone was converted into 1-methoxy-4-(2-ethylhexyloxy) benzene (**1**) and it was subjected to bromomethylation to give compound **2**. Compound **2** was converted into bisphosphonate ester (**3**).⁴²⁻⁴³ 2-Chloroethanol was coupled with 4-hydroxybenzaldehyde to yield **4**. Compounds **3** and **4** were reacted together using potassium *tert*-butoxide by Wittig-Horner reaction to produce bishydroxyl functionalized HO-OPV-OH (**5**).



Scheme 2.1. Synthetic scheme of hydroxyl functionalized Oligo (phenylenevinylene).

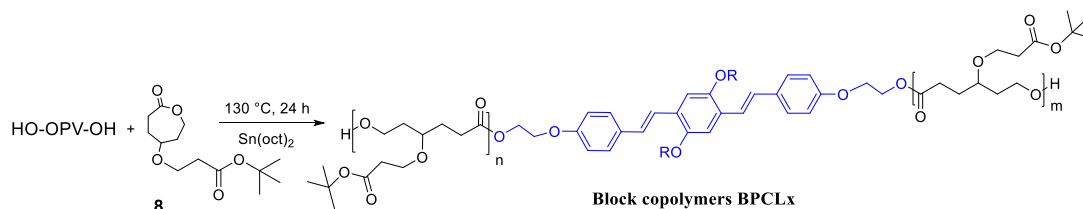
The *t*-butyl carboxylic ester substituted caprolactone monomer was synthesized starting from 1,4-cyclohexanediol in multistep synthesis.³⁹ Michael addition reaction of *t*-butyl acrylate to 1,4-cyclohexanediol and the subsequent oxidation of mono alcohol (**6**) by PCC yielded the ketone derivative (**7**). It was then subjected to Bayer-Veliger oxidation to give substituted caprolactone monomer (**8**) (see Scheme 2.2). All these compounds are characterized by $^1\text{H-NMR}$, $^{13}\text{C-NMR}$ and Mass analysis.



Scheme 2.2. Synthetic scheme of *t*-butyl carboxylic ester substituted caprolactone monomer.

The ring opening polymerization was carried out using HO-OPV-OH as initiator and $\text{Sn}(\text{Oct})_2$ as catalyst in a solvent free melt route (or neat) as shown in

scheme 2.3. The polymerization of substituted caprolactone monomer **8** produced a new OPV containing block copolymers in which the substituted polycaprolactone arms are projected at both sides of the π -core.



Scheme 2.3. Synthetic scheme of block copolymers from *t*-butyl carboxylic ester substituted caprolactone monomer.

These block copolymers were named as BPCL x , where x -represents the total number of BPCL repeating units at both side of the OPV-core and B refers the *t*-butyloxy substitution in PCL backbone. The monomer to initiator ratio $[M]/[I_0]$ was varied from 5 to 100 in the feed to produce different BPCL x chain lengths (or arms) in the block copolymers. The structures of the BPCL x polymers were characterized by ^1H and ^{13}C NMR analysis. ^1H -NMR spectra of HO-OPV-OH and representative example for BPCL x copolymers are given in figure 2.5.

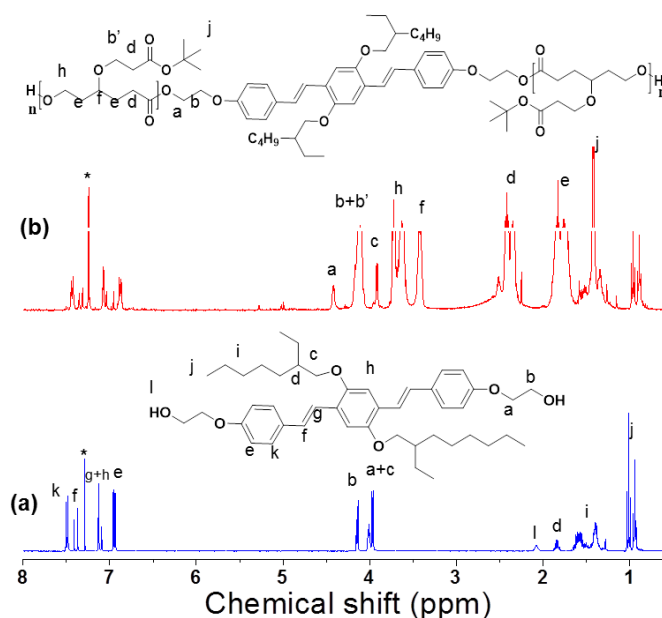


Figure 2.5. ^1H -NMR spectra of HO-OPV-OH (a) and BPCL x (b) in CDCl_3 .

In figure 2.5a, the OPV exhibited typical aromatic peak splitting pattern with respect to bis-stilbene chromophore.⁴² In figure 2.5b, the BPCL x polymer showed

protons corresponding to both OPV core (see the region 6.8 to 7.6 ppm) as well as polycaprolactone units (see region below 5.00 ppm). The comparison of the peak integrals of proton-a (from OPV part) with proton-f (from BPCL part) gave the number of the BPCL units attached on the OPV core. For example for the feed ratio of $[M]/[I_0] = 20$, the $^1\text{H-NMR}$ spectra accounted for total 22 BPCL (see figure 2.5b) units and this polymer sample is referred as BPCL22. A similar NMR analysis was done for other polymer compositions. The plot of $[M]/[I_0]$ in the feed versus their actual incorporation determined by $^1\text{H-NMR}$ (see figure 2.6a) revealed that the BPCL $_x$ polymer series followed linear trend with increase in $[M]/[I_0]$ in the ROP process.

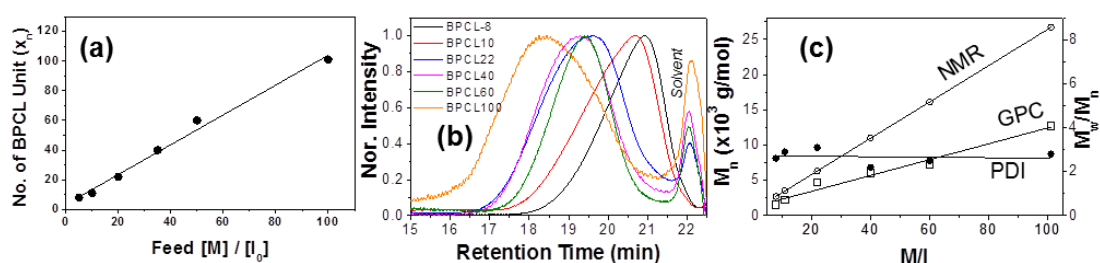


Figure 2.6. The plot of feed $[M]/[I_0]$ versus X_n (no of repeating units) from $^1\text{H-NMR}$ (a). GPC chromatograms of BPCL $_x$ in tetrahydrofuran (b). Plots of M_n (determined by $^1\text{H-NMR}$ and GPC) and M_w/M_n versus the monomer-to-initiator ratio in feed (c).

Table 2.1: Molecular weights of BPCL $_x$ polymers determined by GPC and NMR

Polymer	Feed	X_n^a (NMR)	M_n^a (NMR)	X_n^b (GPC)	M_n^b (GPC) (g/mol)	M_w^b (GPC) (g/mol)	M_w/M_n^b
BPCL8	6	8	2714	3	1500	4000	2.6
BPCL10	10	10	3228	5	2200	6600	3.0
BPCL22	20	22	6312	17	5100	15900	3.1
BPCL40	36	40	10938	30	7200	17900	2.5
BPCL60	50	60	16078	27	7700	13900	1.8
BPCL100	100	100	26358	47	12700	35600	2.8

^(a) Number of repeating units are determined by $^1\text{H-NMR}$ and M_n was calculated as $M_n = (\text{repeating unit mass}) \times n$. ^(b) Molecular weights and PDI determined by GPC in THF.

Molecular weights of the polymers were determined by gel permeation chromatography and their molecular weights are given in table 2.1. GPC plots for BPCLx polymers are given in figure 2.6b. All the polymers showed mono-modal distribution in the GPC plot and the retention time of the polymers decreased with increase in the $[M]/[I_0]$ ratio in the feed. The plots of M_n versus the BPCL chain length (see figure 2.6c) suggested that the linear trend for the formation of higher molecular weight polymers at higher $[M]/[I_0]$ ratio. The polydispersity of the BPCL polymers was found to be in the range of 1.8 to 2.9 as shown in figure 2.6c. To further confirm the controlled ROP process; the polymerization kinetic was carried out for the substituted caprolactone monomer **8** at $[M]/[I_0] = 50$. The aliquots were taken at regular intervals and their molecular weights were determined by GPC. As shown in figure 2.7a the GPC chromatograms showed mono-modal distribution for the aliquots collected up to 120 minutes. The plots of the M_n versus polymerization time (see figure 2.7b) showed linear trend and the M_w/M_n also did not change much. Thus, it can be concluded that polymer with desired molecular weight can be synthesized by controlled ring opening polymerization of newly designed monomer **8** and HO-OPV-OH initiator in the ROP process.

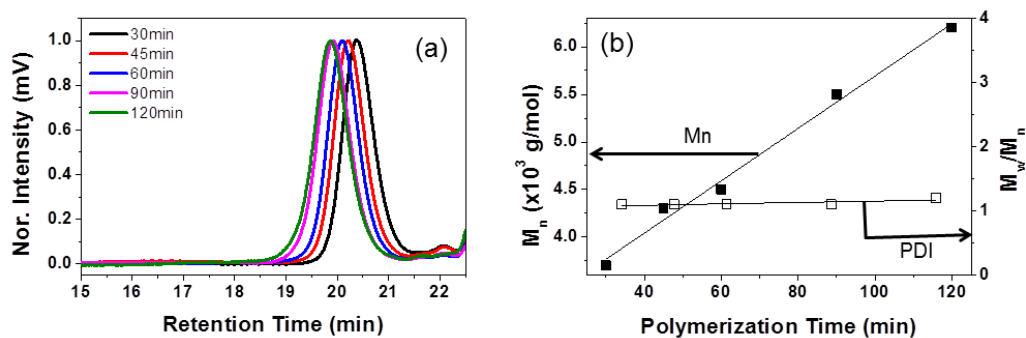


Figure 2.7. GPC chromatogram of aliquots of ROP kinetics for BPCL50 polymer (a), Plot of molecular weight and polydispersity index versus (reaction) time.

The thermal properties of BPCLx polymers were investigated by TGA and DSC analysis. TGA analysis of the polymers (see figure 2.7a) confirmed the thermal stability of BPCLx from 200 °C to 230 °C. DSC thermograms of heating and cooling cycles of the BPCL polymers are shown in figures 2.8b and 2.8c. The DSC thermograms of BPCL-x series polymers were found to be sluggish to crystallize and became completely amorphous. This trend was attributed to the steric hindrance induced by the bulky *t*-butyl groups attached in the BPCLx polymers which hampered the PCL chain folding for crystallization.

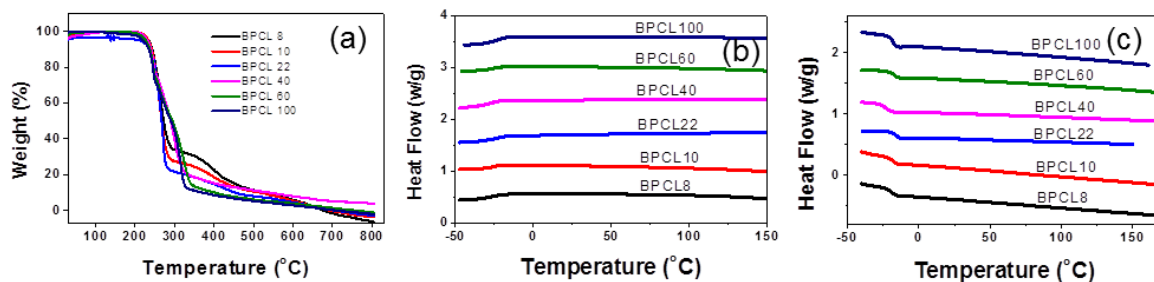


Figure 2.8. TGA profile (a), DSC thermograms of BPCL_x polymers, cooling cycle (b), Heating cycle (c).

2.3.2. Self-assembly of polymers in Organic and Aqueous Medium

The polymers were designed with rigid OPV central π -core and flexible BPCL_x arm at both ends. The self-assemblies of these new classes of polymeric building blocks were studied both in organic solvent (in THF) and in water. The polymer samples BPCL_x with 10, 60, and 100 units were dissolved in THF (0.1 mg/mL) and their dropcasted films were subjected to imaging by field-emission scanning electron microscopy (FESEM) and the images are shown in figure 2.9.

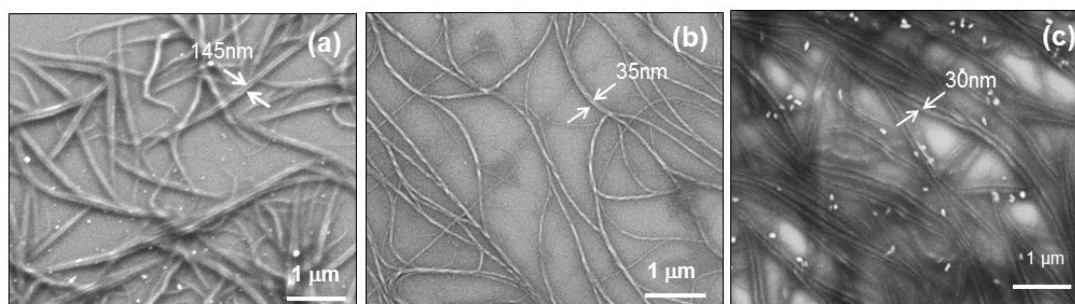


Figure 2.9. FE-SEM images of BPCL10 (a) and BPCL100 (b), and BPCL60 (c). The polymer concentration was maintained as 1.0 mg/mL and the images were recorded for dropcasted films.

FE-SEM image of the BPCL10 and BPCL100 showed the formation of nanofibrous morphology. The average thickness of fiber was found to be 145 ± 10 nm, 30 ± 5 , and 45 ± 10 nm for BPCL10, BPCL60, and BPCL100, respectively. The length of the fibrils were found to be much longer in BPCL60 ($6.8 \pm 2 \mu\text{m}$), BPCL100 ($7.4 \pm 1 \mu\text{m}$) compared to BPCL10 ($4.0 \pm 0.6 \mu\text{m}$). The aspect ratios of the fibers were determined to be ~ 30 , 120 and 135 for BPCL10, BPCL60, and BPCL100, respectively. This confirmed the existence of long range self-assembly of the polymer chains for the exhibition of nanofibers. Atomic force microscope images of BPCL10 and BPCL100 are shown in figures 2.9a and 2.9b, respectively. BPCL10 showed the

existence of curved nanofibers (see figure 2.9a) and their thickness were calculated to be 400 ± 50 nm with length up to $5.3 \pm 0.7 \mu\text{m}$. On the other hand, BPCL100 produced straight nano-fibers with thickness 70 ± 5 nm and length up to $(3.0 \pm 0.5 \mu\text{m})$. Thus, the self-organization of newly designed π -conjugated BPCL polymers were very unique to produce variable length nanofibres which was indirectly controlled by the BPCLx arm lengths.

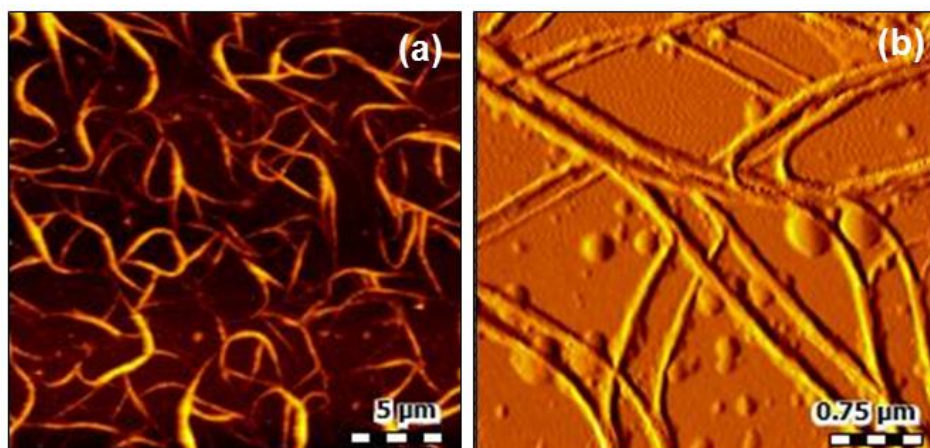


Figure 2.9. Tapping mode AFM images of the BPCL10 (a) and BPCL100 (b) (polymer concentration 1.0 mg/mL).

To investigate the self-assembly of π -conjugated BPCLx polymers in aqueous media; the samples were dissolved in DMSO + water mixture and dialyzed using semi-permeable membrane having MWCO = 1000 for 48 h. The reservoir was continuously replenished with fresh water to ensure the removal of DMSO. The BPCLx polymers were found to produce very stable water solution (very stable for more than 30 days at ambient conditions).

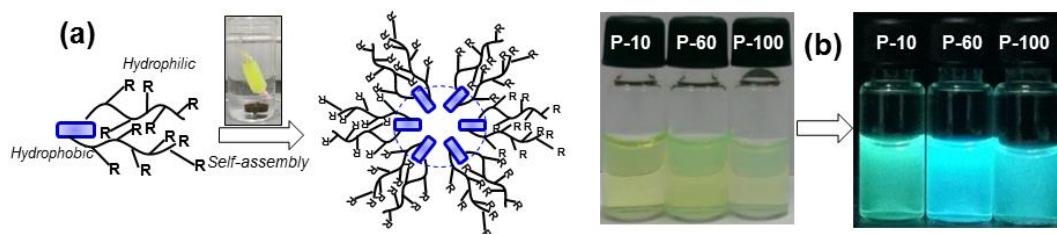


Figure 2.10: Schematic representation of self-assembly of BPCLx polymer in aqueous medium (a), Photographs of vials containing the dialyzed polymer solutions of BPCLx under normal light and upon exposure to photoexcitation (b).

The schematic representation of formation of self-assembly of BPCLx polymers in aqueous medium is shown in figure 2.10a and it is attributed to the hydrophobic rigid OPV core in the polymer which tries to stay away from the aqueous medium. The photographs of vials containing BPCLx polymer dialyzed solutions are shown in figure 2.10b. Upon exposure to UV-light irradiation, they showed high intense blue fluorescence originated from the OPV core. This study clearly indicates that the BOC substituted PCLx units are very good in producing stable aqueous nanoparticles of π -conjugated luminescent OPVs for many newer applications.

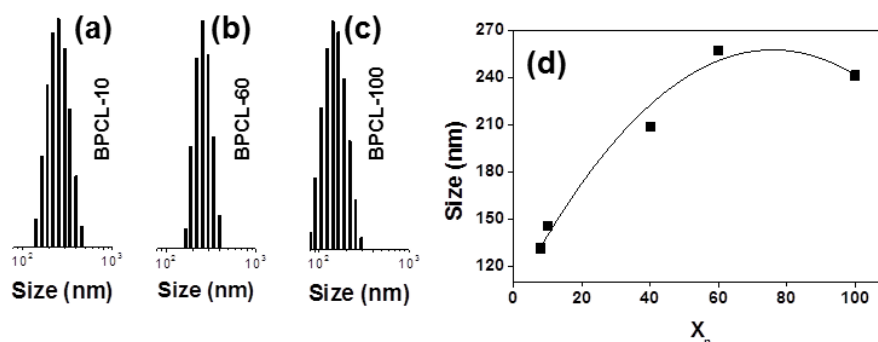


Figure 2.11. DLS histograms of BPCL10 (a), BPCL60 (b) and BPCL 100 (c) at 0.4 mg/mL, Plot of BPCLx polymer nanoparticles size (DLS) in water versus no. of BPCL units (d)

The polymer solutions were subjected to dynamic light scattering (DLS) analysis to determine the size of the BPCLx polymer aggregates in water. DLS histograms of BPCL10, BPCL60 and BPCL100 are shown in figure 2.11. These samples showed mono-model distribution with the average sizes of the assemblies as 145 ± 10 nm, 250 ± 5 and 240 ± 5 nm, respectively. The average particle size of the aqueous dispersion of BPCLx polymers were plotted against the number of BPCL units (x -values) in the arms and the plot is shown in figure 2.11d. It is very clear from the plot that the size of the particle increased with increase in the arm length and it attained a plateau about 50-60 BPCLx units.

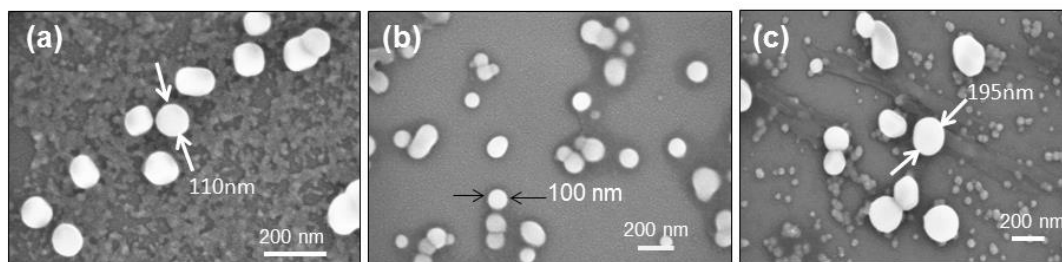


Figure 2.12. *BPCL10 (a), BPCL60 (b), and BPCL 100 from their aqueous dialysis solution.*

FE-SEM image of BPCL10, BPCL60 and BPCL100 are shown in figure 2.12 which revealed the formation of spherical nanoparticle morphology. The average sizes of these nanoparticles were obtained as 100 ± 10 nm and 195 ± 10 nm for BPCL10 and BPCL100, respectively. AFM analysis of BPCL60 and BPCL100 also showed the formation of spherical nanoparticles of 165 ± 15 nm 200 ± 15 respectively (see figure 2.13). All three independent techniques DLS, FE-SEM and AFM confirmed the formation of spherical nanoparticles in the newly designed BPCLx polymers in water. The sizes of the nanoparticles were precisely increased from 120 to 250 nm by systematically varying the length of the BPCLx arms at either side of the OPV core (see plot in figure 2.11d)

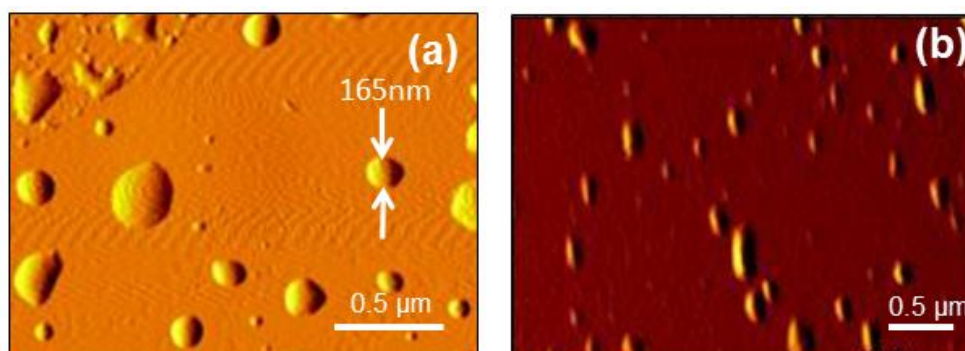


Figure 2.13. *AFM images of BPCL60 (a) and BPCL100 (b) in aqueous medium.*

To study the photo-physical properties of the OPV chromophores in the polymers, their absorbance and emission spectra were recorded. The absorption and emission spectra of BPCLx polymer nanoparticles in the aqueous solution are shown in figures 2.14a and 2.14b. The concentration of BPCLx polymers were maintained at 0.1 O.D with respect to OPV chromophore in solution state.

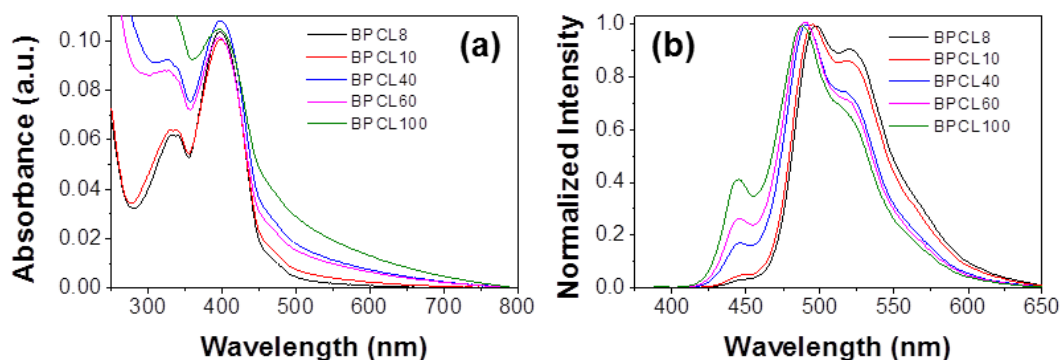


Figure 2.14: Absorbance (a) and emission (b) spectra of dialyzed polymer solutions of BPCLx.

The absorption spectra showed maxima at 395 nm with respect to the OPV chromophore and also a broad peak at 450 nm with respect to OPV chromophore aggregation in water. The emission spectra were recorded by exciting at absorbance maxima ($\lambda_{\text{ex}} = 395$ nm) and the OPV chromophore showed emission maxima at 490 nm. Based on the above analysis, it may be concluded that the newly designed polymers having fixed OPV core and variable BPCLx arms are very interesting classes of π -conjugated fluorescent materials to produce nano-fibrous morphology in the organic solvents and also capable of producing luminescent nanoparticles in water. Since, the aim of the present investigation is to explore these copolymers for biomedical application; further, studies with respect to their nano-fibrous morphology in thin film are not included.

2.3.3 Encapsulation Capabilities of BPCLx Nanoparticles

The loading capacity of the polymer nanoparticles was tested by anticancer drug doxorubicin (DOX). DOX and polymer were dissolved in DMSO + water and the solution was dialyzed against water using semi-permeable membrane for 48 h. The reservoir was replenished with fresh water to remove the un-encapsulated DOX. At the end of the dialysis, stable DOX encapsulated nanoparticles were produced. The short armed polymer BPCL10 was unable to load the DOX into the nanoparticle which suggest that minimum 50 unit arm length is required to produce stable self-assembled nano-scaffold to load the drug into their nanocavity (see figure 2.15a for schematic representation of encapsulation of DOX).

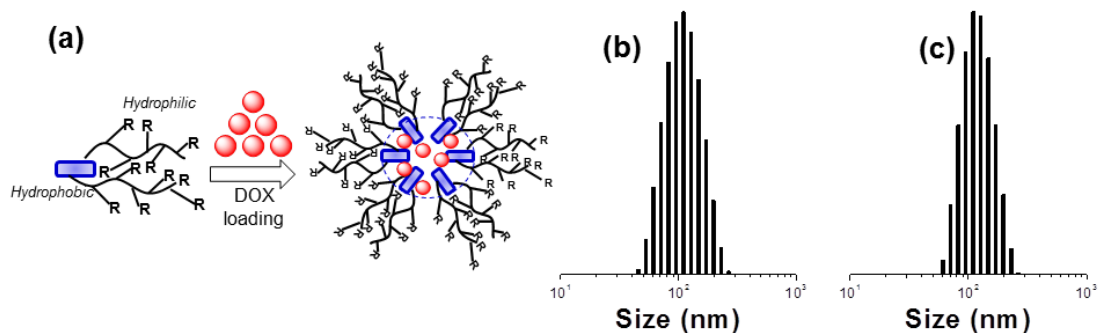


Figure 2.15: Schematic representation of DOX loading in the BPCLx nanoparticles. DLS histograms of DOX loaded BPCL60 (b) and BPCL100 (c).

These DOX loaded nanoparticles are named as BPCLx-DOX. Drug loading content was estimated using absorption spectroscopy. The DLCs were found to be 6.5 % and 8.3 % for BPCL60-DOX and BPCL100-DOX, respectively. Their DLEs were calculated as 13.0 % and 16.7 %, respectively. The DLEs are little lower side; however, the DLCs are moderate to high in the range of 5 to 8 % which is normally observed for most of the polymer scaffolds in the literature.^{36,39,47} The block copolymers reported in the present investigation is very good in encapsulating DOX with good DLCs of 5.0 to 8.0 % for testing in cancer cell lines. It is necessary to further optimize the length of the π -core as well as varying the types of substituted PCL derivative to enhance drug loading efficiency. The DLS histograms for BPCL60-DOX and BPCL100-DOX are given in figures 2.15b and 2.15c, respectively. They showed mono-modal distribution and the size of the nanoparticles was found to be 200 ± 10 nm and 230 ± 10 nm for BPCL60-DOX and BPCL100-DOX, respectively.

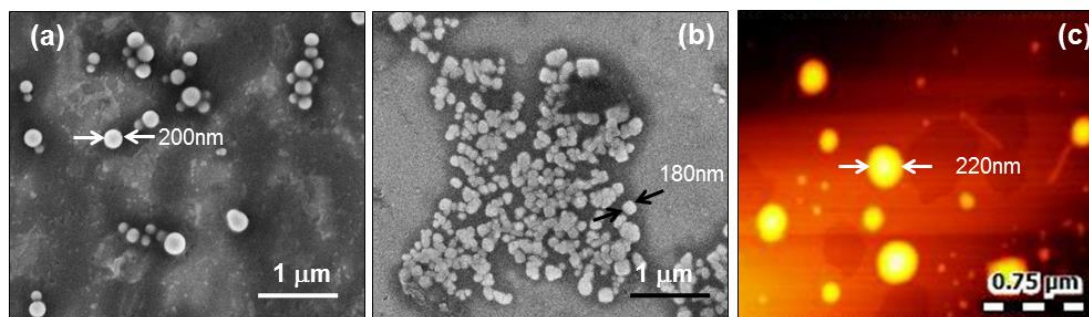


Figure 2.16: FE-SEM images of DOX loaded BPCL100 (a) and BPCL60 (b), AFM image of BPCL60-DOX (c).

FESEM image of BPCL60-DOX and BPCL100-DOX confirmed the formation of spherical nanoparticle. AFM image of BPCL60-DOX is shown in figure 2.16c and it confirmed the nanoparticle formation. It is also important to mention that

the loading of DOX did not alter the size and morphology of the nascent polymer nanoparticles.

The photo-physical properties of the DOX loaded polymer nanoparticles (aqueous solution) were studied by recording their absorption and emission spectra (see figure 2.17). The optical density of BPCLx chromophore was maintained at 0.1 O.D with respect to OPV chromophore. In figure 2.17a, the absorption spectra of BPCL60-DOX and BPCL100-DOX showed two maxima at 395 nm with respect to OPV absorption and a broad peak at 480 nm with respect to DOX absorption. The emission spectra of these polymers were recorded by exciting at 395 nm (with respect to OPV excitation) (see figure 2.17b). BPCL100 (nascent polymer), BPCL60-DOX and BPCL100-DOX showed emission with respect to OPV. At this excitation wavelength, the free DOX showed negligible emission (see figure 2.17b). Interestingly, there is no excitation energy transfer from OPV chromophore to DOX; thus no FRET process occurred between the OPV in the polymer backbone to the DOX present in the nanoparticles. The emission spectra recorded at DOX excitation wavelength (excited at 480 nm) are shown in figure 2.17c. Both free DOX and DOX loaded nanoparticles BPCL60-DOX and BPCL100-DOX showed broad emission at 530 to 600 nm region with respect to DOX

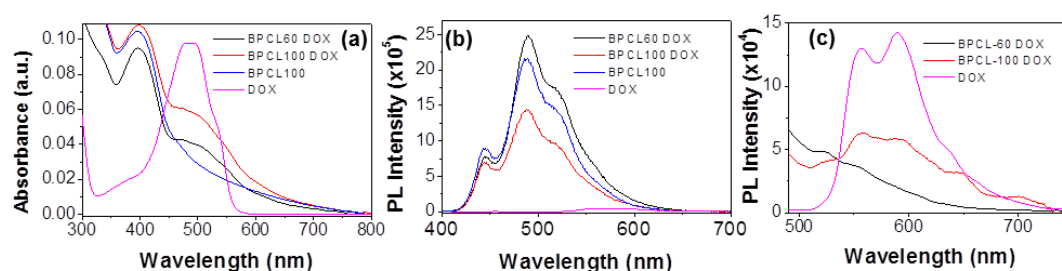


Figure 2.17. Absorbance spectra of free DOX, BPCL100 nanoparticles and DOX loaded polymer nanoparticles (a), Emission spectra of DOX, BPCL100 nanoparticles and DOX loaded polymer nanoparticles for $\lambda_{excitation}$ at 395 nm (at OPV absorbance) (b), Emission spectra of DOX, BPCL100 nanoparticles and DOX loaded polymer nanoparticles for $\lambda_{excitation}$ at 480 nm (at DOX absorbance) (c)

The loading of the DOX in the polymer nanoparticles was further conformed using fluorescence microscopy imaging. Figures 2.18a-2.18d showed the FLM images of BPCL60 DOX polymer. The blue fluorescence of OPV chromophore was observed using 420 nm laser and red fluorescence from DOX was visualized using 568 nm laser. The merged image in figure 2.18d showed very good overlap between red and blue fluorescence from same nanoparticles. To further confirm, the nanoparticles were subjected to confocal microscopic analysis (see figure 2.18e-2.18h). The Confocal images represented the distribution of the blue OPV core as well as DOX in the entire nanoparticles and directly supported the schematic representation of the solid nanoparticle design as shown in figure 2.15a. Based on the above photo-physical experiments as well as fluorescence and confocal microscope images, it may be concluded that the OPV chromophore in the polymer scaffold and loaded DOX drug in the interior do not exhibit any optical inference and they showed their independent photo-physical characteristics.

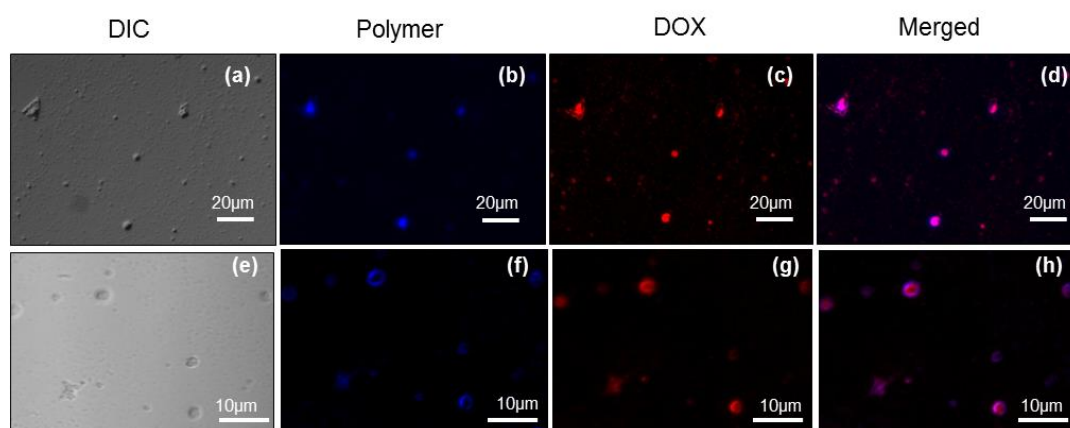


Figure 2.18. Fluorescence and confocal microscopic images of DOX loaded BPCL60 nanoparticles in DIC (a,e); visualized through blue channel (λ 420 nm) (b,f); visualized through red channel (λ 568nm) (c,g) and their merged image (d,h).

2.3.4 In vitro Drug Release and Cytotoxicity

The PCL backbone is constituted by the aliphatic ester linkage; thus, it is susceptible to lysosomal enzymatic cleavage upon taken up by the cells.^{41,48} Therefore, one would expect the enzyme-responsive biodegradation of the substituted PCL part would disassembly the nanoparticles. In this process, the rupturing of the nanoparticles leads to delivery of the loaded cargoes (DOX in the present case) to the intracellular environment (see figure 2.19a).

To study this phenomenon, *in vitro* drug release studies were carried out in PBS in absence and presence of esterase enzyme at pH 7.4 and 37 °C. The cumulative release was studied by absorption spectroscopy. The plot of cumulative drug release in absence and presence of esterase enzyme (10 U)⁴⁸ for BPCL60-DOX are shown in figure 219b. In the absence of esterase enzyme the scaffold showed very good stability for the DOX loaded nanoparticles with less than 15 % release up to 48 h. This suggests that the newly designed nanoparticles are very stable for intravenous circulation. In the presence of esterase enzyme, the PCL part underwent enzymatic biodegradation to release more than 80 % of the drugs in 48 h. This *in vitro* experiment clearly demonstrates that the newly designed polymer scaffold was stable in normal conditions and highly responsive to enzymatic cleavage at the intracellular compartment to deliver the drugs.

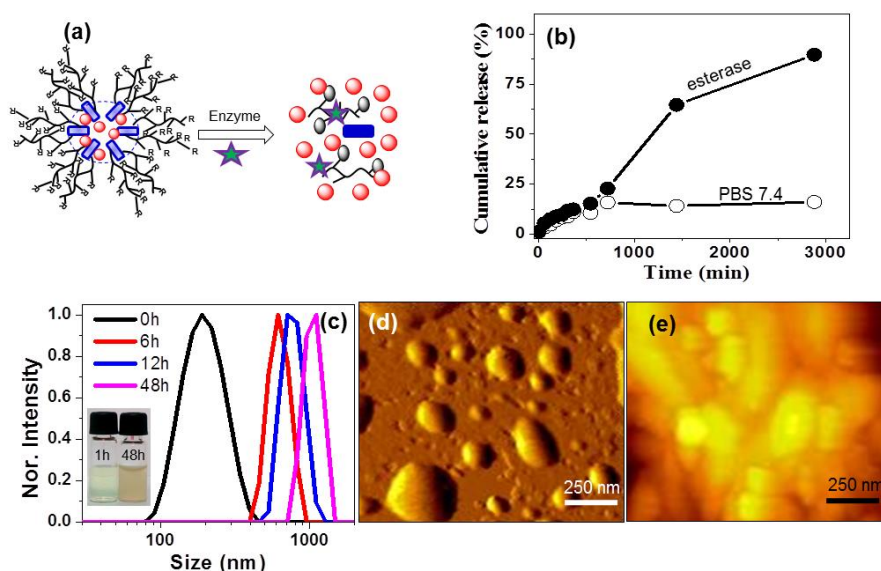


Figure 2.19. Schematic representation of enzyme-responsive cleavage of the DOX loaded BPCLx nanoparticles (a). Cumulative drug release profiles of DOX loaded BPCL60 nanoparticles in the absence and presence of esterase at 37 °C in PBS (b). DLS histograms of BPCL-60 polymer in the presence of 10 U esterase enzyme at various time interval (c). AFM images of BPCL60 polymer nanoparticle at the initial (d) and after 12h (e) of exposure to esterase enzyme.

To prove the biodegradation of the block copolymer nanoparticles, three control experiments were carried out: (i) DLS studies of the polymer nanoparticle degradation in the presence of esterase enzyme at 37 °C in PBS buffer, (ii) the morphology of the polymer degraded product recorded by AFM and (iii) the degraded products were analyzed by MALDI-TOF to identify the mass of the degraded units

and their structures. The data from the first two experiments are given in figures 2.19c to 2.19e. The DLS histograms of the polymer nanoparticles were recorded in the presence of 10 U esterase for a period of 48 h at 37 °C in PBS (see figure 2.19c). The initial data showed mono-modal distribution with average size of the particles ~ 190 nm. With increase in time, the esterase enzyme cleaved the aliphatic ester backbone in the PCL chain; as a result, the self-assembly of nanoparticles was disturbed. The chopped PCL oligomer units were precipitated and turned the solution to turbid. The photographs of the vials in figure 2.19c showed the formation of turbid solution at 48 h. With increase in the incubation time, the size of the particles increased from nanometer to micron-sized particles as evident from the DLS histograms (see figure 2.19c). AFM images of the initial and 12 h esterase enzyme treated samples are shown in figures 2.19d and 2.19e, respectively. The sample exhibited the spherical morphology at the initial stage; however, the nanoparticle features were completely lost in the 12 h of esterase enzyme action. This supported the cleavage of the nanoparticles by esterase enzyme. The turbid solution was lyophilized and the degraded polymer sample was subjected to MALDI-TOF analysis. The MALDI-TOF spectra showed the peaks with respect to the dimer and trimer species in the degraded samples (see figure 2.20). The MALDI-TOF mass analysis along with DLS and AFM images provided direct evidence for the biodegradation of the tri-block polymer scaffold by esterase enzyme.

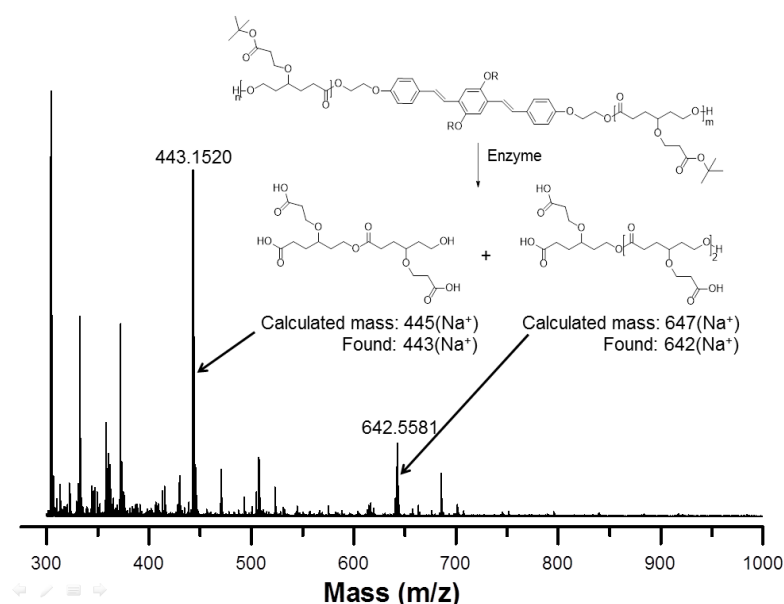


Figure 2.20. MALDI-TOF spectrum of BPCL-60 polymer in the presence of 10 U esterase enzyme after 48 h.

The cytotoxicity of the nascent and DOX loaded BPCL60 and BPCL100 nanoparticles were investigated in cervical cancer (HeLa) cell line. The cytotoxicity of the nascent polymer was tested in HeLa by varying their concentration up to 60 $\mu\text{g/mL}$. In figures 2.21a and 2.21b, the nascent polymer BPCL60 and BPCL100 nanoparticles, showed more than 80 % cell viability upto 30 $\mu\text{g/mL}$ concentrations. The cytotoxicity of the free DOX and DOX loaded BPCL60 and BPCL100 were investigated and the data are shown in figure 2.21c and 2.21d, respectively. The free drug concentration was maintained as equivalent to drug loaded in the polymer. The concentration of the DOX was varied from 0.2 to 1.5 $\mu\text{g/mL}$. The DOX loaded polymer nanoparticles exhibited about 50 % killing of cells at 0.8 and 1.0 $\mu\text{g/mL}$ drug concentration for BPCL60-DOX and BPCL100-DOX, respectively. The free DOX showed much better killing compare to DOX loaded polymer nanoparticles. The effect of polymer nanoparticles on the cell killing would be better visible in the *in vivo* studies as supported by the EPR effect⁴⁸ for macromolecular drug carriers. Nevertheless, the present *in vitro* investigation provides direct evidence that the newly developed DOX loaded polymer nanoparticles are promising candidate for killing cancer cells more than 60-70 % which is very significant for any newly designed polymer scaffold.

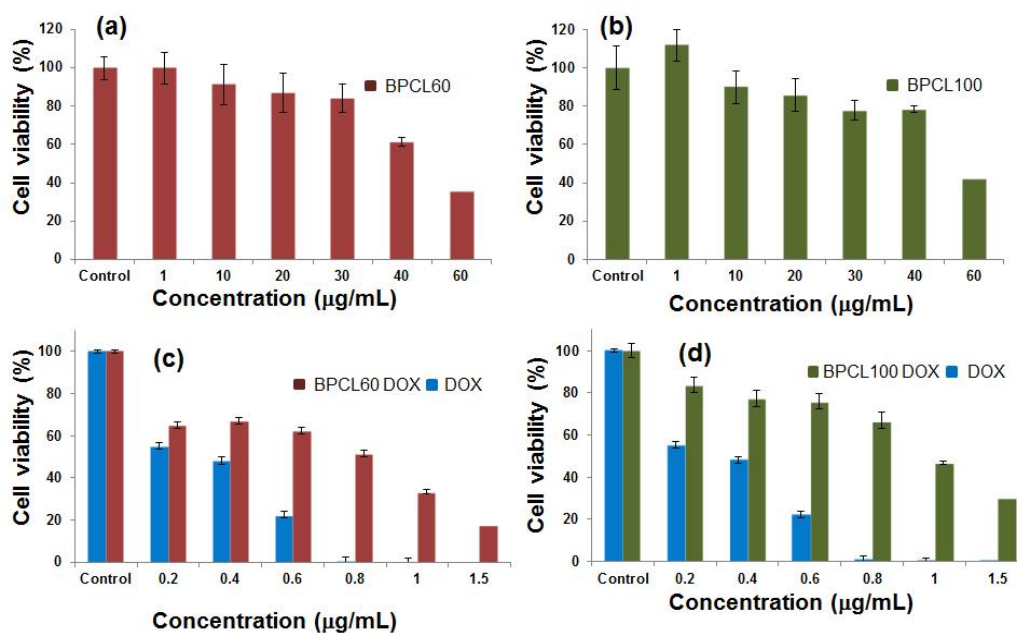


Figure 2.21. Histograms showing cytotoxicity of BPCLx polymer nanoparticles (alone) BPCL60 (a), BPCL100 (b), and DOX loaded BPCLx polymer nanoparticles BPCL60 DOX (c), BPCL100 DOX (d) in HeLa cells at various concentrations.

2.3.5. Confocal Microscope Imaging and Cellular uptake

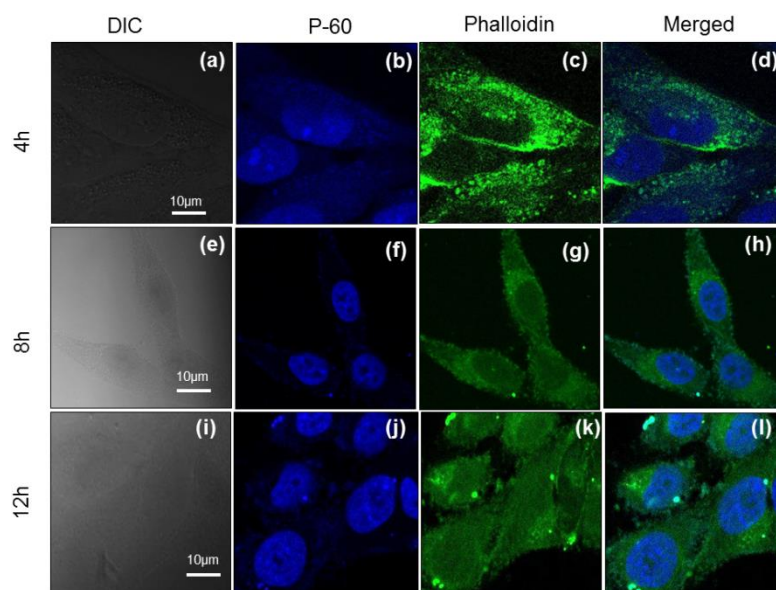


Figure 2.22. CLSM images of HeLa cells incubated with BPCL60 polymer nanoparticles for 4h (a-d), 8h (e-h) and 12 h (i-l). The cells were observed through the blue channel to locate the polymer (OPV chromophore) fluorescence. The actin cytoskeleton network in cells is stained with phalloidin (green).

The cellular uptake and internalization of the nascent polymer and DOX loaded nanoparticles were investigated in HeLa cells by confocal laser scanning microscopy (CLSM). The nascent polymer nanoparticles are blue fluorescent in nature; thus, they were tested for their uptake and detection for long term cellular imaging applications. For this purpose, the BPCL60 nanoparticle was administered to HeLa cells and their confocal images were recorded and shown in figure 2.22. Since the polymer nanoparticles are blue fluorescent, the cells were stained with Phalloidin (green fluorescent). The images in figure 2.22 are clearly evident for the uptake of the polymer nanoparticles in the cytoplasm and perinuclear environment. The merged image in figure 2.22d is further support this claim. To study the influence of the incubation period on the polymer nanoparticles uptake by the cells, the cells were treated at various time intervals of 4h, 8h and 12 h. The Confocal images of cellular uptake of 8 h and 12 h incubated cells are given in figure 2.22e to 2.22l along with 4h images. The comparison of these images revealed that the cellular uptake of the polymer nanoparticles at 4h is almost similar to that of 8h and 12 h. This implies that the tri-block copolymer was capable of undergoing cleavage within 4h in the cytoplasm. These experiments confirmed that the blue luminescent nascent polymer

nanoparticles are highly cell penetrable and may be very useful for cellular imaging applications.

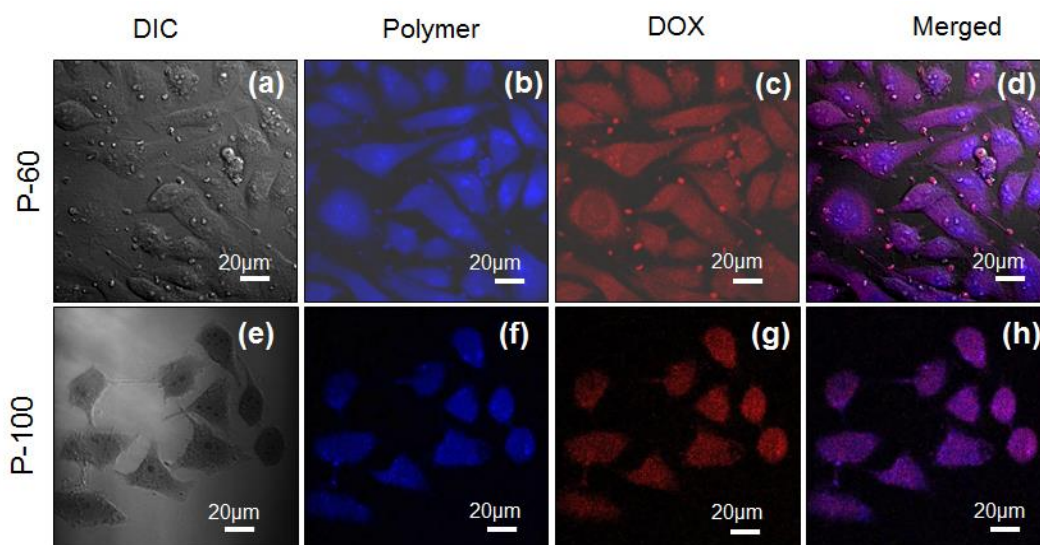


Figure 2.23. Confocal microscopic images of DOX loaded polymer nanoparticles BPCL60 DOX polymer nanoparticles (a-d), BPCL100 DOX (e-h) in treated HeLa cells. The cells were observed through the blue channel to locate the polymer (OPV chromophore) fluorescence and red channel to locate DOX fluorescence.

Figure 2.23 shows the CLSM images corresponding to DOX loaded nanoparticles for BPCL60- DOX and BPCL100-DOX. The blue fluorescence produced by the OPV chromophore was observed through blue channel (at λ 420 nm) and the red fluorescence from DOX was monitored through red channel (at λ 568 nm). The merged images clearly showed magenta emission at the nucleus with respect to the mixture of polymer blue emission and DOX red emission. The closer observation in the merged panel further revealed that the DOX-loaded nanoparticles preferentially accumulate at the nucleus of the cells. The red emission from DOX and blue emission from OPV fluorophores were very clearly visible in the cytoplasm of the cells (see figure 2.23b and 2.23c). This revealed that the current π -conjugated chromophore containing polymer nanoparticle (alone) is very efficient for cellular imaging in cancer cells. The OPV chromophores do not undergo any cross-talk (energy transfer process) with loaded fluorescent drugs like DOX. Thus the optical purity of the chromophores (OPV and DOX) is retained for the simultaneous visualization of drug administration as well as nascent OPV polymer nanoparticle uptake from single polymer dose. This new simultaneous imaging concept is not restricted to this particular system; in principle, it can be expanded to other drugs and

π -chromophores as long as there is no cross-talk between their optical properties. The present investigation reports the development of new luminescent enzyme-responsive (biodegradable) polymer nano-scaffolds for polymer drug delivery applications and demonstrates the proof-of-concept for DOX delivery and cellular imaging in cervical cancer cells.

2.4. Conclusion

In conclusion, a highly luminescent oligo-phenylenevinylene (OPV) chromophore and biodegradable polycaprolactones were cleverly chosen to make new series of luminescent π -conjugated chromophore containing biodegradable polymer nano-scaffold for cellular imaging-cum-drug delivery vehicle for administration to cancer cells. For this purpose, a t-butyl ester substituted caprolactone monomer and bis-hydroxyl functionalized OPV chromophore were custom designed through multi-step synthesis and employed them as monomer and initiator, respectively, in the ring opening polymerization methodology. The biodegradable arm length in the A-B-A triblock species was precisely controlled by varying the monomer-to-initiator ratio in the ring ROP process. It was found that the new series of block copolymers were self-assembled as helical nanofibres in THF drop cast films. In water, the polymer amphiphilic PCL arms facilitated the formation of spherical nanoparticle aggregates. These nanoparticles were found to be blue luminescent and not toxic to cancer cells. The loading of doxorubicin was accomplished in the hydrophobic core of the nanoparticles. The detailed photo-physical studies revealed that there is no cross-talking among the DOX and OPV chromophores in the photo-excitation process. *In vitro* drug release kinetics revealed that the nanoparticles were stable in PBS buffer and the PCL arm was found to undergo enzymatic bio-degradation to rapture the nanoparticles to release the loaded drugs at the intracellular compartments. Cytotoxicity studies indicated that DOX loaded polymer nanoparticles exhibited more than 80 % cell killing in HeLa cell lines. Confocal microscopic analyses further establish the cellular uptake of the nascent blue luminescent nanoparticles as well as DOX loaded nanoparticles in the cytoplasm and peri-nuclear environment. Here, the new concept is demonstrated exclusively for OPV fluorophore and biodegradable PCL system, and in general, this approach could be adapted to wide range of other fluorophores and biodegradable polymers for better cancer therapy.

2.5 References

1. Wu, C.; Chiu, D. T. *Angew. Chem. Int. Ed.* **2013**, *52*, 3086-3109.
2. Nilsson, K.P.R.; Hammarstrom, P. *Adv. Mater.* **2008**, *20*, 2639-2645.
3. Tian, Z.; Yu, J.; Wu, C.; Szymanski, C.; McNeill, J. *Nanoscale* **2010**, *2*, 1999-2011.
4. Zhu, C.; Liu, L.; Yang, Q.; Lv, F.; Wang, S. *Chem, Rev.* **2012**, *112*, 4687-4735.
5. Li, K.; Liu, B. *Chem. Soc. Rev.* **2014**, *43*, 6570-6597.
6. Liu, Z.; Chen, N.; Dong, C.; Li, W.; Guo, W.; Wang, H.; Wang, S.; Tan, J.; Tu, Y.; Chang, J. *ACS Appl. Mater. Interfaces* **2015**, *5*, 18997-19005.
7. Wu, C.; Bull, B.; Szymanski, C.; Christensen, K.; Mc Neill, J. *ACS Nano* **2008**, *2* (11), 2415-2423.
8. Liu, B.; Bazan, G. C. *Chem. Mater.* **2004**, *16*, 4467-4476.
9. Liu, B.; Li, K.; *J. Mater. Chem.* **2012**, *22*, 1257-1264.
10. Feng, G.; Ding, D.; Liu, B. *Nanoscale* **2012**, *4*, 6150-6165.
11. Pu, K-Y.; Li, K.; Shi, J.; Liu, B. *Chem. Mater.* **2009**, *21*, 3816-3822.
12. Liu, J.; Geng, J.; Liu, B. *Chem. Commun.* **2013**, *49*, 1491-1493.
13. Feng, G.; Ding, D.; Li, K.; Liu, J.; Liu, B. *Nanoscale* **2014**, *6*, 4141-4147.
14. Liu, L.; Yu, M.; Duan, X.; Wang, S. *J. Mater. Chem.* **2010**, *20*, 6942-6947.
15. Pu, K-Y.; Liu, B. *Adv. Funct. Mater.* **2010**, *19*, 277-284.
16. Pu, K-Y.; Li, Kai.; Liu, B. *Ad., Funct. Mater.* **2010**, *20*, 2770-2777.
17. Liu, J.; Feng, G.; Ding, D.; Liu, B. *Polym. Chem.* **2013**, *4*, 4326-4334.
18. Moon, J. H.; McDaniel, W.; MacLean, P.; Hancock, L. *Angew. Chem. Int. Ed.* **2007**, *46*, 8223-8225.
19. McRae, R. L.; Phillips, R. L.; Kim, I-B.; Bunz, U. H. F.; Fahrni, C. J. *J. Am. Chem. Soc.* **2008**, *130*, 7851-7853.
20. Gwozdzińska, P.; Pawłowska, R.; Milczarek, J.; Garner, L.E.; Thomas, A. W.; Bazan, G. C.; Chworos, A. *Chem. Commun.* **2014**, *50*, 14859-14861.
21. Yin, C.; Song, W.; Jiang, R.; Lu, X.; Hu, W.; Shen, Q.; Li, X.; Li, J.; Fan, Q. Huang, W. *Polym. Chem.* **2014**, *5*, 5598-5608.
22. Chen, T.; Xu, W.; Huang, Z.; Peng, H.; Ke, Z.; Lu, X.; Yan, Y.; Liu, R. *J. Mater. Chem. B* **2015**, *3*, 3564-3572.
23. Howes, P.; Green, M.; Bowers, A.; Parker, D.; Varma, G.; Kallumadil, M.; Hughes, M.; Warley, A.; Brain, A.; Botnar, R. *J. Am. Chem. Soc.* **2010**, *132*, 9833-9842.
24. Howes, P.; Green, M.; Levitt, J.; Suhling, K.; Hughes, M. *J. Am. Chem. Soc.* **2010**, *132*, 3989-3996.
25. Howes, P.; Thorogate, R.; Green, M.; Jickells, S.; Daniel, B. *Chem. Commun.* **2009**, 2490-2492.
26. Ceperaga, C.; Gallavardin, T.; Marotte, S.; Lanoe, P-H.; Mulatier, J-C.; Lerogue, F.; Parola, S.; Lindgren, M.; Baldeck, P. L.; Marvel, J.; Maury, O.; Monnereau, C.; Favier, A.; Andraud, C.; Leverrier, Y.; Charreyre, M-T. *Polym. Chem.* **2013**, *4*, 61-67.

27. Aparicio-Ixta, L.; Ramos-Ortiz, G.; Pichardo-Molina, J. L.; Maldonado, J. L.; Rodriguez, M.; Tellez-Lopez, V. M.; Martinez-Fong, D.; Zolotukhin, M. G.; Fomine, S.; Meneses-Nava M. A.; Barbosa-Garcia, O. *Nanoscale* **2012**, *4*, 7751-7759.
28. Shen, X.; Li, L.; Wu, H.; Yao, S. Q.; Xu, Q. H. *Nanoscale* **2011**, *3*, 5140-5146.
29. Yin, C.; Hong, B.; Gong, Z.; Zhao, H.; Hu, W.; Lu, X.; Li, J.; Li, X.; Yang, Z.; Fan, Q.; Yao, Y.; Huang, W. *Nanoscale* **2015**, *7*, 8907-8919.
30. Yuan, H.; Chong, H.; Wang, B.; Zhu, C.; Liu, L.; Yang, Q.; Lv, F.; Wang, S. *J. Am. Chem. Soc.* **2012**, *134*, 13184-13187.
31. Wang, B.; Yuan, H.; Liu, Z.; Nie, C.; Liu, L.; Lv, F.; Wang, Y.; Wang, S. *Adv. Mater.* **2014**, *26*, 5986-5990.
32. Wu, C.; Jin, Y.; Schneider, T.; Burnham, D. R.; Smith, P. B.; Chiu, D. T. *Angew. Chem. Int. Ed.* **2010**, *49*, 9436-9440.
33. Feng, X.; Lv, F.; Liu, L.; Tang, H.; Xing, C.; Yang, Q.; Wang, S. *ACS Appl. Mater. Interfaces* **2010**, *2* (8), 2429-2435.
34. Feng, X.; Tang, Y.; Duan, X.; Liu, L.; Wang, S. *J. Mater. Chem.* **2010**, *20*, 1312-1316.
35. Feng, L.; Liu, L.; Lv, F.; Bazan, G.C.; Wang, S. *Adv. Mater.* **2014**, *26*, 3926-3930.
36. Pennakalathil, J.; Jahja, E.; Ozdemir, E.S.; Konu, O.; Tuncel, D. *Biomacromolecules*, **2014**, *15*, 3366-3374.
37. Ding, D.; Li, K.; Zhu, Zhenshu.; Pu, K-Y.; Hu, Y.; Jiang, X.; Liu, B. *Nanoscale* **2011**, *3*, 1997-2002.
38. Jerome, C.; Lacomte, P. *Adv. Drug Delivery Rev.* **2008**, *60*, 1056-1076.
39. Surnar, B.; Jayakannan, M. *Biomacromolecules*, **2013**, *14*, 4377-4387.
40. Surnar, B.; Subhash, P. P.; Jayakannan, M. *Z. Anorg. Allg. Chem.*, **2014**, *640*(6), 1119-1126.
41. Surnar, B.; Sharma, K.; Jayakannan, M. *Nanoscale* **2015**, *7*, 17964-17979.
42. Karnati, N.; Jayakannan, M. *ACS Appl. Mater. Interfaces.*, **2014**, *6*, 19385-19396
43. Goel, M.; Narasimha, K.; Jayakannan, M. *Macromolecules*, **2014**, *47*, 2592-2603.
44. Balamurugan, A.; Vikash Kumar; Jayakannan, M. *Chem. Commun.* **2014**, *50*, 842-845
45. Singh, H.; Balamurugan, A.; Jayakannan, M. *ACS Appl. Mater. Interfaces.*, **2013**, *5*, 5578 – 5591
46. Mahima, G.; Jayakannan, M. *Chem. Eur. J.* **2012**, *18*, 11987-11993.
47. Chang, L.; Deng, L.; Wang, W.; Lv, Z.; Hu, F.; Dong, A.; Zhang, J.; *Biomacromolecules*, **2012**, *13*, 3301-3310.
48. Pramod, P. S.; Takamura, K.; Chaphekar, S.; Balasubramanian, N.; Jayakannan, M. *Biomacromolecules* **2012**, *13*, 3627.

Chapter 3

Fluorescent-Tagged Biodegradable Polycaprolactone Block Copolymer FRET Probe for Intracellular Imaging in Cancer Cells

Abstract

The present investigation reports a new fluorophore-tagged biodegradable polycaprolactone (PCL) block copolymer FRET-probe for intracellular imaging in cancer therapy. Hydroxyl functionalized π -conjugated oligo-phenylenevinylene (OPV) chromophore was tailor-made and it was incorporated in *t*-butyl ester substituted polycaprolactone block copolymer via ring opening polymerization. This blue-luminescent OPV-PCL triblock self-assembled as < 200 nm spherical nanoparticles (FRET donor) and it encapsulated water insoluble Nile red (NR, FRET acceptor) to yield OPV-NR FRET probe. Selective photo excitation of OPV chromophore in block copolymer nano-assemblies enabled the excitation energy transfer from the OPV to NR and facilitated the efficient FRET process in aqueous medium. Time-correlated fluorescent decay dynamics and detail photophysical studies were carried out to estimate the Förster distance, donor-acceptor distance and the excitation energy transfer efficiency. These parameters confirmed the occurrence of FRET process within the confined nano-particle environment. The PCL chains in the FRET probe was susceptible for enzymatic biodegradation at the intracellular environment and the degradation process controlled the FRET on/off mechanism. Cytotoxicity studies revealed that the FRET probe was biocompatible and non-toxic to cells and the FRET-probe was found to be readily taken up by the cancer cells and it was internalized in the cytoplasm and peri-nuclear environment. Selective photo excitation of OPV chromophore in confocal microscope exhibited dual emission from the FRET probe. The cancer cells exhibited blue luminescence (self-emission) with respect to the OPV chromophore (in blue channel) and bright red-luminescence from the NR dye followed by the FRET process at the cellular level (in red channel). The dual luminescence characteristics, biodegradation and biocompatibility makes the newly designed PCL-OPV-NR FRET probe as an excellent biomedical nano-device for bioimaging application and the proof-of-concept was established in cervical (HeLa) and breast cancer (MCF 7) cell lines.

3.1 Introduction

Fluorescent probe tagged polymer nano-carriers are emerging as multi-purpose biomaterials for both delivering anticancer drugs/genes and also as luminescent probes for cellular imaging in cancer therapy.¹⁻³ Macromolecular nano-carriers have additional advantages of passive selective accumulation through EPR effect and also capable of enhancing the bioavailability and biodistribution of loaded cargoes at the cancer tissues.⁴⁻⁵ Among the various fluorescence techniques; Förster resonance energy transfer (FRET) process⁶ is one of the most powerful noninvasive tool and it was employed to study protein folding⁷ and monitoring real-time drug release kinetics at the cellular level (see figure 3.1).⁸⁻⁹

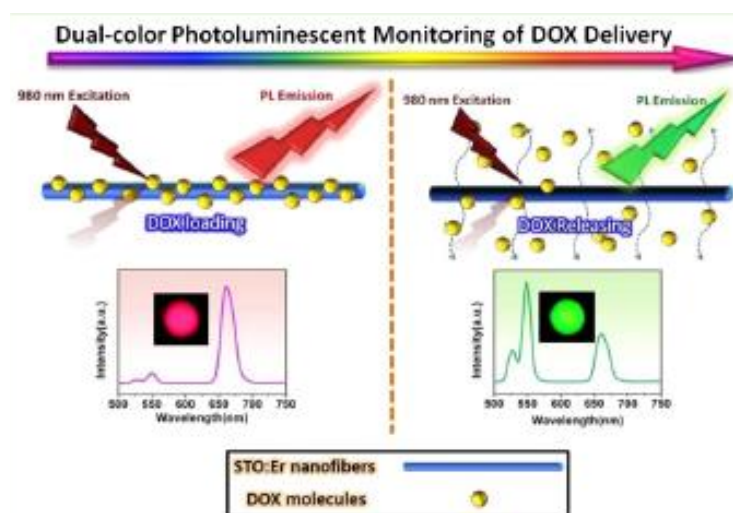


Figure 3.1. Schematic representation of dual color, luminescent nano-fibers based on FRET mechanism between DOX molecules and upconversion nanofibers for ratiometric monitoring of DOX release (Adopted from Fu et al. *ACS Biomater. Sci. Eng.* **2016**, 2, 652-661)

The development of FRET probes for biological application is relatively challenging task since geometry of the polymer nano-carriers should be capable of confining the donor-acceptor chromophores within the Förster distance of 20-60 Å under physiological conditions.⁶ Three types of polymeric systems were explored in the construction of FRET probes: (i) FRET donor-acceptor chromophores either chemically conjugated on the non-luminescent polymers¹⁰⁻¹³ or physically encapsulated in their nano-scaffold,¹⁴⁻¹⁵ (ii) luminescent π -conjugated cationic polymer nano-assemblies as FRET donor which encapsulated FRET acceptor dyes or drugs,¹⁶⁻¹⁹ and (iii) both FRET donor and FRET acceptor π -conjugated chromophores

constituted as part of the backbone.^{3,20} Cationic polyfluorene^{16,17} and poly(fluorene-benzothiadiazole) random copolymers,^{3,21} poly(p-phenylenevinylene)s¹⁸ and poly(p-phenyleneethylene)s²² (see figure 3.2) are some of the very good examples for the π -conjugated FRET systems.

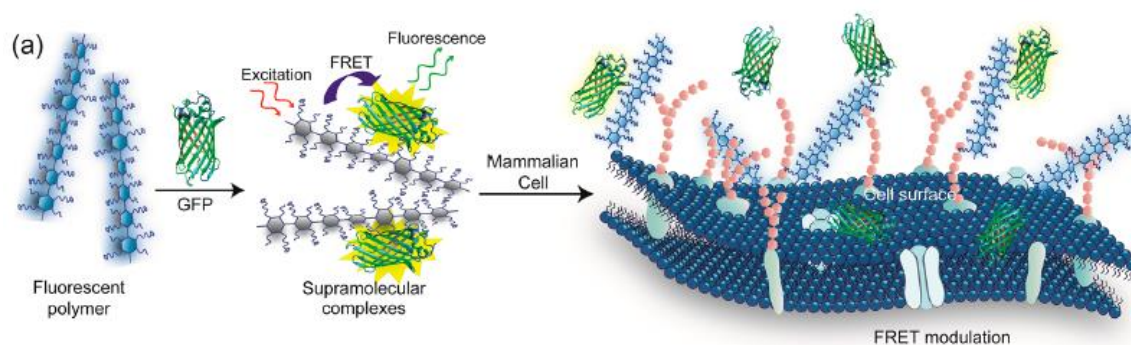


Figure 3.2. Schematic illustration of FRET-based cell sensing using conjugated polymer-GFP complexes. The polymer and GFP form supramolecular complexes through electrostatic interactions, giving rise to FRET responses that are modulated when the complexes interact with cell surface (adopted from et al. *J. Am. Chem. Soc.* **2016**,*138*, 4522-4529)

The tunability of HOMO-LUMO band gap in the π -conjugated chromophores²³ provided unlimited opportunity to make FRET probes ranging from visible to NIR region.²⁴ The π -conjugated polymer FRET probes were employed as biological sensors,^{22,25} detection of DNA methylation in cancer,¹⁶⁻¹⁷ spermine,²⁶ microbial pathogens (see figure 3.3),¹⁸ nucleic acid,²⁷ G-quadruplex,²⁸⁻²⁹ intracellular release of siRNA²⁰ and imaging of protein-specific glycons in cell surface,³⁰ etc. Despite these many advantages of FRET process; still the non-biodegradability of C-C bond in the π -conjugated polymer backbone is still one of the major concerns for the biomedical applications.

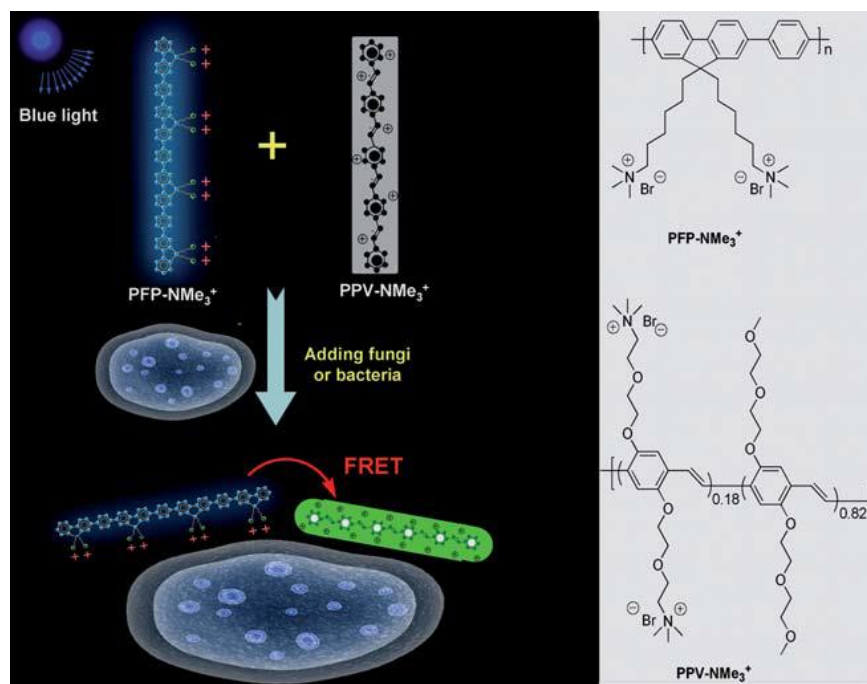


Figure 3.3. Schematic representation of pathogen detection based on FRET between cationic conjugated polymers and chemical structures of PFPNMe_3^+ and PPVNMe_3^+ (adopted from Zhu *et al. J. Mater. Chem.* **2011**, 7905-7912)

Biodegradable polyesters based on poly(L-lactide),³¹ poly(L-glycolide)³² and polycaprolactone (PCL)³³ are emerging as new generation biomaterials due to their excellent enzyme-responsive cleavage of aliphatic ester-backbone by lysosomal enzymes at the intracellular level. Among these polymers, functional polycaprolactone (PCL) block copolymers having hydroxyl,³⁴ azide,³⁵ alkyl,³⁶ alkyloxy,³⁷ oligoethyleneoxy,³⁸ chlorstyryl³⁹ and ketone⁴⁰ were widely studied for anticancer drug and gene delivery in cancer therapy. From our group, we reported carboxylic functional PCL block copolymers as pH responsive nano-carriers under GI track.⁴¹ The role of random and block copolymer polymer topology,⁴² hydrogen bond-controlled drug release,⁴³ and incorporation of π -conjugated fluorophore for imaging-cum-delivery⁴⁴ were also investigated. PEG-*b*-CPCL diblocks⁴⁵⁻⁴⁶ copolymers and PEG-*b*-PCL-*b*-CPCL triblock⁴⁷ copolymers were stitched with cisplatin for synergistic combination therapy in GSH-over expressed breast cancer cells. Recently, few efforts have taken by other groups to encapsulate FRET donor-acceptor molecules in the PCL to study DOX release aspects,⁴⁸ *in vivo* siRNA + quantum dot delivery⁴⁹ and DOX delivery to peritumoral chemotherapy.⁵⁰ This survey revealed that until now there is no effort has been taken to construct fluorophore-tagged PCL block copolymer nano-assemblies as FRET probes in the literature. The approaches

towards the development of new PCL based FRET probe is very important for both fundamental understanding of enzyme-responsiveness on FRET process and also the construction of biocompatible and biodegradable FRET diagnostic device for cancer therapy. Our efforts towards achieving this goal on PCL based FRET probe and the concept is shown in figure 3.4.

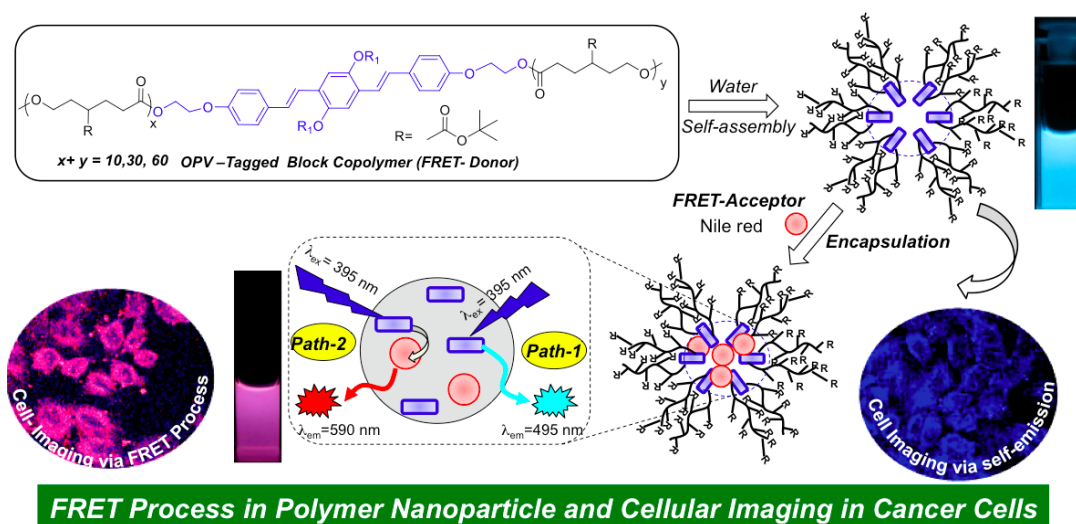


Figure 3.4. Development of biodegradable PCL polymer FRET Probe for imaging in cancer.

The present investigation is emphasized to develop one of the first PCL based FRET probes, study the FRET process by photophysical techniques and demonstrate the proof-of-concept of FRET at the cellular level in cancer cells. For this purpose, π -conjugated oligo-phenylenevinylene (OPV) fluorophore was chosen as FRET donor and it was conjugated as part of the PCL triblock copolymer (see Figure 1). This OPV block copolymer self-assembled into aqueous blue luminescent nanoparticle (FRET donor) which encapsulated water insoluble Nile red (NR) as FRET acceptor. The PCL block copolymer assemblies acted as nano-container for photo excitation energy transfer from OPV to NR and chromophores enabled the construction of efficient FRET probe. Detail photophysical studies such as absorption, emission and time correlated fluorescence decay profiles were done to establish the close vicinity of donor-acceptor chromophores within the Förster distance for the occurrence of FRET process. Cytotoxicity data confirmed that the new PCL-FRET probe was highly biocompatible and it was non-toxic to cells. The FRET probe was readily internalized in the cancer cells through endocytosis and selective photo excitation in the confocal microscope provided direct evidence of the

3.2 Experimental Section

3.2.1 Materials: Horse liver esterase enzyme, Nile red (NR), 3-(4,5-dimethylthiazole-2-yl)-2,5-diphenyltetrazolium bromide (MTT), 4 % paraformaldehyde, DMSO were purchased from Sigma Aldrich and used without further purification. Wild type mouse embryonic fibroblasts (WTMEF) cells, cervical (HeLa) and breast (MCF 7) cancer cells were maintained in DMEM (Gibco) containing FBS (fetal bovine serum) 10 % (v/v) and penicillin-streptomycin 1 % (v/v) at 37 °C in CO₂ (5 %) atmosphere. Cells were washed with DPBS (40 %) and trypsinized using 0.05 % trypsin (Gibco). The cells were seeded in 96-well or 6-well flat bottom plastic plates (as per the experiment) for all assays. The *t*-butyl carboxylic ester substituted caprolactone monomer (1) and fluorescent HO-OPV-OH initiator were synthesized following our earlier report.⁴⁴

3.2.2 Methods: Absorption studies were carried out using Perkin Elmer Lambda 45 UV-vis spectrophotometer. The emission spectra and time resolved fluorescence lifetime measurements (TCSPC) were recorded using SPEX Fluorolog HORIBA JOBINVYON fluorescence spectrophotometer. The 450 W Xe lamp was used as excitation source to record steady state emission spectra. All photophysical measurements were carried out by maintaining the optical density of OPV chromophore at 0.1. The emission spectra were recorded at excitation wavelength of 395 nm and 550 nm corresponding to OPV and NR excitation, respectively. TCSPC measurements were carried out using nano-LED source with wavelength 371nm was used for excitation and life time was collected at emission maxima of 495 nm and 595 nm. The lifetime decay data was fitted using DAS6 software. Average particle size of the polymer nanoparticles were investigated by dynamic light scattering (DLS) using Nano ZS-90 apparatus utilizing 633 nm red laser (at 90° angle) from Malvern Instruments. Nanoparticles were characterized using Zeiss Ultra plus scanning electron microscope. Atomic force microscopic (AFM) images were recorded using Veeco Nanoscope IV instrument and samples were drop casted on mica sheets and recorded in tapping mode. Confocal laser microscope analysis was carried out using Carl Zeiss Axiovert 200 microscope.

3.2.3. Synthesis of OPV-PCL block copolymers: *t*-Butyl substituted caprolactone monomer (400.0 mg, 1.55 mmol), hydroxyl functionalized HO-OPV-OH initiator (34.0 mg, 0.051 mmol), for monomer to initiator ratio, [M]/[I] = 30) and Sn(Oct)₂ as

catalyst (10.4 mg, 0.025 mmol) were taken in schlenk tube. The polymerization mixture was evacuated under high vacuum for 30 minutes and the polymerization was continued by immersing the tube at 130 °C with stirring for 12 h under vacuum (1 mm of Hg). After the completion of polymerization, the viscous mass was dissolved in tetrahydrofuran and precipitated in hexane. The polymer precipitate was filtered and dried in vacuum oven. Yield = 230 mg (58 %). ¹H-NMR (CDCl₃, 400 MHz) δ ppm: 7.46-6.89 (m, 14H), 4.45 (t, 4H), 4.13(t, 6H), 3.95 (d, 4H), 3.74 (t, 2H), 3.67 (t, 1H), 2.46 (t, 4H), 1.85 (t, 4H), 1.43 (s, 9H), 0.98-0.93 (t, 12H). ¹³C-NMR (CDCl₃, 400 MHz) δ ppm: 173.2, 170.6, 127.6, 114.3, 80.5, 75.2, 65.8, 64.5, 61.2, 39.2, 32.5, 29.0, 22.8,14.1.FT-IR (cm⁻¹):3585, 2970, 2871, 2360, 1885, 1735, 1630, 1472, 1365, 1255.

3.2.4 Preparation of luminescent polymer nanoparticles: The OPV-PCL block copolymer (2.0 mg) was dissolved in 1.0 mL of DMSO and 4.0 mL distilled water was added drop wise into the solution. The resulting solution was stirred at 25 °C under dark for 4 h. This polymer solution was dialyzed against distilled water using commercial cellulose ester semipermeable membrane (MW 3500) for 48 h. Fresh water was replenished periodically to ensure the removal of DMSO from dialysis membrane. The dialyzed solution was filtered, lyophilized and stored at 4 °C.

3.2.5. Encapsulation of Nile red (NR) in polymer nanoparticles: To encapsulate Nile red (NR) in the polymer nanoparticles; 2.0 mg of the polymer and 0.2 mg of NR were dissolved in DMSO (2.0 mL) and distilled water (3.0 mL). The solution was stirred at 25 °C under dark for 4 h and dialyzed using semi-permeable membrane as described above. The dialyzed solution was filtered, lyophilized and stored at 4 °C. The absorption spectra of these NR encapsulated block copolymers were recorded with 0.4 mg/mL concentration of the polymers and the optical density was found to be 0.21 at 550 nm (NR absorption maxima) which was sufficient enough to determine the DLC and DLE of NR. The dye loading content (DLC) and dye loading efficiency (DLE) were calculated using the equations:⁴⁴

$$\text{DLC (\%)} = \left\{ \frac{\text{weight of NR encapsulated in nanoparticles}}{\text{weight of NR loaded nanoparticles}} \right\} \times 100\%$$

$$\text{DLE (\%)} = \left\{ \frac{\text{weight of NR encapsulated in nanoparticles}}{\text{weight of NR in feed}} \right\} \times 100\%$$

3.2.6. Enzymatic biodegradation of Nile red encapsulated OPV-PCL block copolymers: Nile red (NR) encapsulated block copolymer P30-NR was subjected for enzymatic biodegradation study in order to understand the enzyme responsive behavior of polymer nanoparticles and its effect on the FRET process between OPV and NR. For this purpose P30-NR polymer nanoparticle solution (2.3×10^{-6} M with respect to OPV) in PBS pH = 7.4 was taken in a vial and esterase enzyme was added to it followed by incubation at 37 °C. The steady state fluorescence spectra were recorded at different time intervals and change in the NR emission intensity at 595 nm was monitored with time. The same experiment was carried out in absence of esterase enzyme in PBS pH=7.4 at 37 °C to determine the stability of NR encapsulated polymer nanoparticle.

3.2.7. Cell-viability assay (MTT assay): The cytotoxicity of nascent polymer nanoparticles and NR loaded polymer nanoparticles was investigated in HeLa cell line using MTT assay.⁴⁴ 10^3 cells were seeded per well in a 96-well plate in 100 μ L of DMEM with 10% FBS. The cells were adhered for 16 h. Medium from the cells was removed. Various concentrations of polymers and NR loaded polymer nanoparticles were added to the cells. Experiment was carried out using medium with FBS without cells and an untreated control, medium with FBS containing cells. Cells were incubated for 24 h without changing medium followed by aspirating the compound containing medium. A fresh 100 μ L solution of MTT (prepared from stock solution) was added into each well followed by incubating the cells with MTT for 4 h at 37 °C. MTT was reduced by dehydrogenase enzyme present in the cells to form purple formazan crystals. 100 μ L of DMSO was added in each well to dissolve these formazan crystals. The number of viable cells in each well was determined by measuring absorbance of formazan crystals at 570 nm using a micro plate reader at (Varioskan Flash).

3.2.8. Cellular uptake studies using confocal microscopy: HeLa cells, Wild-type MEF cells and MCF 7 cells at a density of 10^5 cells were seeded on cover slips placed in 6 well plates containing DMEM medium⁴⁴ followed by incubation of cells at 37 °C for 16 h. The cells were treated with desired concentrations of polymer nanoparticles and NR encapsulated polymer nanoparticles for 2 h in a CO₂ incubator at 37 °C. Post incubation, medium was aspirated from Cells were washed with 1 mL of PBS and

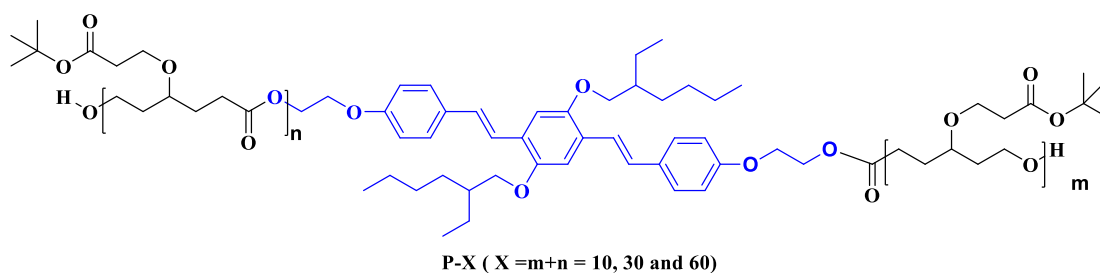
fixed with 4 % PFA solution in PBS (10 minutes) followed by washing the cells with 1 mL of PBS. Fluoromount-G was used to mount the cover slips on slides. Slides were allowed to dry at room temperature for overnight. The cell imaging was done using a LSM 710 confocal microscope with the λ 405 nm and λ 561 nm lasers. Image J analysis software was used to analyze the images. To determine the cellular uptake of the polymer nanoparticles and NR encapsulated polymer nanoparticles the images were recorded in lambda mode wherein the cells were excited by 405 nm laser source and the intensity was recorded at each 5 nm interval from 415 to 725 nm range. Further an area of the cell was chosen and the mean intensity was generated using Image J analysis software and was plotted against wavelength.

3.2.9 Flow Cytometry Measurements: Flow cytometry analysis was carried out to study the cellular uptake of P30 and P30-NR polymer nanoparticles in cervical cancer cells following our earlier procedure.⁴² 1×10^5 HeLa cells were seeded in 6 well plate containing DMEM media. The incubation of cells at 37 °C was carried out for 16 h. The cells were treated with P30 and P30-NR nanoparticles and incubated for 4 h. After incubation the cells were washed with PBS and digested with 500 μ L of trypsin and incubated for 1 min. The suspension was subjected to centrifugation at 10000 rpm for 5 min and pellet was resuspended in PBS (1 mL). BD LSR Fortessa SORP cell analyzer equipped with five lasers and 18 color detectors was employed for the flow cytometry studies. 405 and 561 nm lasers were used for excitation of OPV and NR and band-pass filters were chosen as 450 ± 50 and 610 ± 10 respectively.

3.3 Results and Discussion

3.3.1. Synthesis and Self-assembly of Fluorescent-Block Copolymers

The *t*-butyl carboxylic substituted caprolactone monomer and the fluorescent hydroxyl functionalized oligo-phenylenevinylene (HO-OPV-OH) initiator as well as the fluorescent-tagged polycaprolactone block copolymers (P30) were prepared via ring opening polymerization using HO-OPV-OH as initiator and Sn(Oct)₂ as catalyst at 130 °C (see Scheme-3.1 for the structure of PX polymer). following synthetic procedures given in chapter 2.



Scheme 3.1. Chemical structure OPV containing of block capolmer

These polymers are referred as P-X (X= 10, 30 and 60) where X-represents the total number of PCL units present at the either side of the OPV chromophores in the block copolymer. P10 and P60 polymers were used from chapter 2. The no of repeating units for P30 polymer were estimated from ¹H NMR as described in previous chapter (chapter 2).

The aqueous self-assembly of the fluorescent-tagged block polymer nanoparticles was studied by dissolving the polymer in DMSO+ water and dialyzed in distilled water using semipermeable membrane. Fresh water was replenished periodically to ensure the removal of DMSO. The polymer structure possessed a rigid hydrophobic aromatic OPV core in the centre and flexible carboxylic ester bearing hydrophilic segments as arms at either side of the OPV part. The PCL chains are highly hydrophobic and expected to be water insoluble; however, the *t*-butyl ester substitution anchored as pendants in the PCL backbone enhanced the water dispersability of the block copolymer nano-assemblies. Earlier, we proved that these polymer nano-assemblies were very stable and capable of loading anticancer drug molecules and deliver them to cancer cells.⁴⁴ In the present study to confirm the formation of polymer aggregates, the dialyzed block copolymer solution was subjected to dynamic light scattering (DLS) studies. The DLS histograms exhibited

mono-modal distribution with respect to the formation of 180 ± 10 nm sized aggregates (see Figure 3.5b). Further to visualize the shape of the polymer aggregates, they were subjected to electron microscope (FESEM) and atomic force microscope (AFM) imaging. FESEM image in figure 3.6c showed the formation of spherical nanoparticle morphology with average particle size as 150 ± 30 nm. AFM images also confirmed the formation of spherical nanoparticles of size 170 ± 10 nm (see figure 3.5d). The sizes of the dialyzed polymer nano-aggregate in DLS matched very well with the FESEM and AFM images and confirmed the formation of nanoparticles for the OPV-PCL block copolymers model as shown the in figure 3.6a. Polymer nanoparticles of size up to 250 nm range were reported to be readily taken up by the cancer cells; ^[41,44,47,49,52] thus, the custom designed polymer nanoparticles (< 200 nm) were within the PL acceptable range for cellular uptake studies.

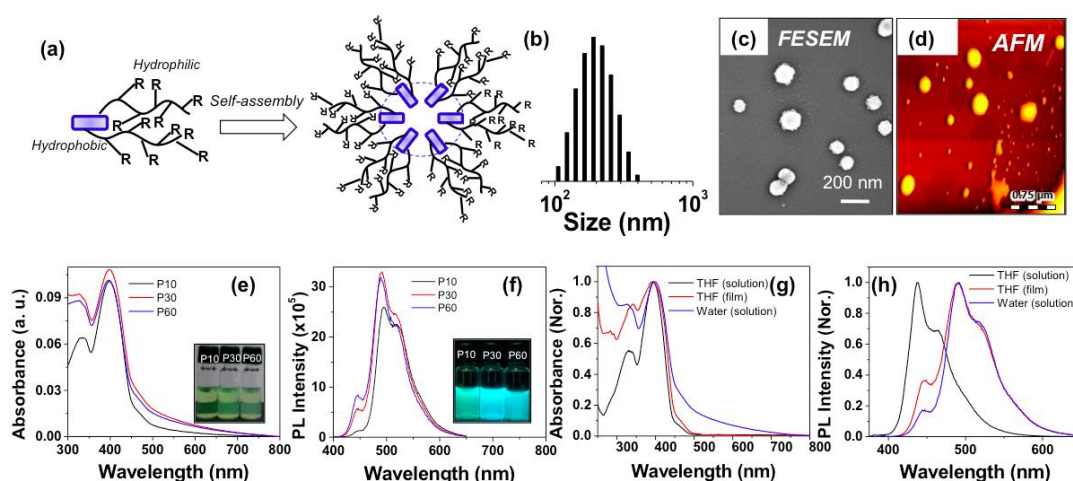


Figure 3.5. (a) Schematic representation of polymer nanoparticle formation. (b) DLS histogram, (c) FESEM and (d) AFM images of P-30 aqueous nanoparticles. Absorbance (e) and emission spectra (f) of the OPV-PCL block copolymers in water. The photographs in the vials showed under normal light and upon photo excitation by UV-lamp. Absorbance (g) and emission spectra (h) of P-30 polymer in THF, water and thin-film state.

Since the block copolymers have OPV chromophore, they were subjected to photophysical studies. The absorption spectra of aqueous polymer nano-aggregates showed maxima at 395 nm corresponding to OPV chromophore (see figure 3.6e). The emission spectra of the polymers were recorded by exciting at absorption maxima of OPV in the polymer (at 395 nm) and it showed maxima at 495 nm corresponding to OPV chromophore. The photographs of the polymers under the hand-held UV lamp

photo excitation (at $\lambda=365$ nm) showed bright blue-luminescence (see Figure 3.6f) and confirmed the strong emission characteristics in the nanoparticle. Thus, the custom designed OPV fluorophore containing PCL block copolymers self-assembled in water and produced stable fluorescent nanoparticles in aqueous medium. To study the formation of types of OPV aggregates, the absorption and emission spectra of OPV-PCL block copolymer (P30 polymer) were recorded in THF, aqueous medium and solid state (in thin-film) and they are shown in figures 3.6f and 3.6g. The molar extinction coefficient of the OPV chromophore containing P-10 block copolymer was determined in both tetrahydrofuran (THF) and dialyzed aqueous solution. The hydroxyl substituted HO-OPV-OH chromophore was not soluble in water; thus, its molar extinction coefficient was determined in THF. To determine the molar extinction coefficient, the sample concentrations were varied from 4×10^{-7} to 2×10^{-6} M (see Figure 3.6). Using absorption spectroscopy, the molar extinction coefficient of the P-10 block copolymer and HO-OPV-OH in THF were determined as $53,000 \text{ M}^{-1} \text{ cm}^{-1}$ and $61,000 \text{ M}^{-1} \text{ cm}^{-1}$ respectively. The molar extinction coefficient of the P-10 block copolymer in water was determined as $42,000 \text{ M}^{-1} \text{ cm}^{-1}$. The molar extinction coefficient values of the polymer samples were almost similar in both water and THF; thus, it confirmed that the OPV chromophore has significant absorption in the visible region. The photographs of the dialyzed sample polymer P-10 are shown in figure 3.6d and it is very clear that the samples were very well dispersed in water without any turbidity or scattering.

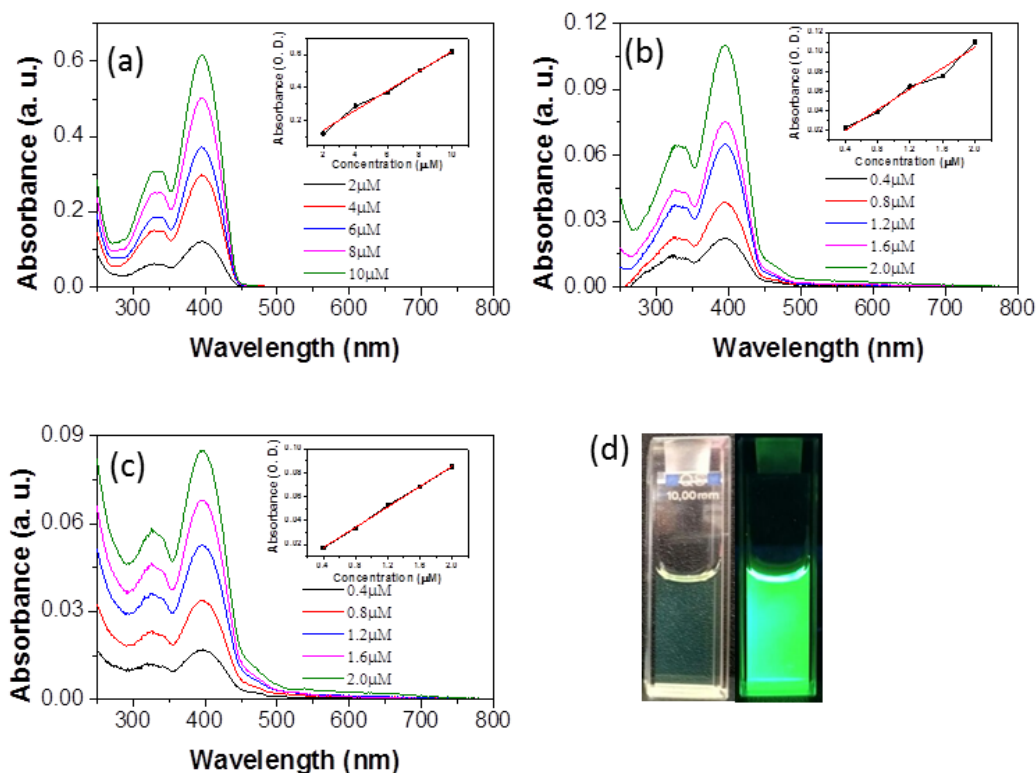


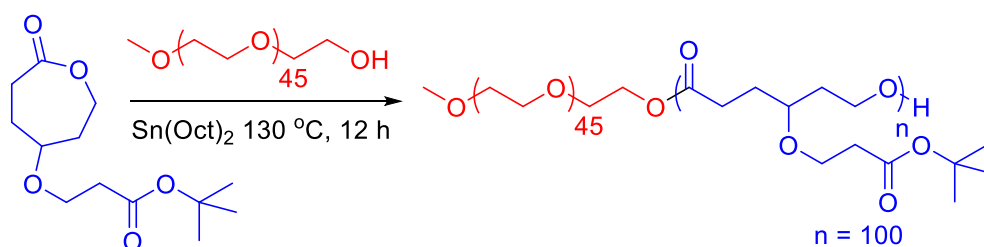
Figure 3.6. (a) Absorption spectra at different concentrations of HO-OPV-OH in THF. (b) Absorption spectra at different concentrations of polymer P10 in THF (b) and dialyzed aqueous medium (c). Inset figure shows optical density versus concentration plot in linear fit for respective plot to calculate the molar extinction coefficient. (d) Photograph of vials under normal light and UV light for P10 polymer.

The block copolymer showed identical absorption spectra with maxima at 395 nm with respect to OPV chromophore in THF, water and thin-film. On the other hand, the emission spectra exhibited significant difference with respect to their self-assembly in THF and water (or thin-film). In THF, the polymers showed emission maxima at 445 nm with respect to isolated OPV chromophores. On the other hand, the polymers showed 50 nm red-shift in water (maxima at 495 nm) followed by strong aggregation. Aromatic π -conjugated chromophores such as OPV were well known to undergo π - π stacking depending upon the solvent environment.^[53,54] Thus, the large red-shift in the emission maxima was attributed to the emission from the J-type aggregates by the hair-pin like micellar self-assembly of OPV chromophores. Further, the emission spectra in thin film showed maxima at 495 nm which was almost identical to that of their emission spectra in water. The π - π aggregation is typically found to be maximum in the solid state; thus, the identical emission spectra of OPV-PCL block polymers in water and thin film suggested that the OPV cores attained

maximum aggregation in aqueous dialyzed nanoparticles as similar to that of solid state.

3.3.2. Encapsulation of Acceptor and FRET Process

The OPV fluorophore tagged block copolymers were subjected for donor-acceptor self-assembly study in aqueous medium. The OPV block copolymer and acceptor molecules were dissolved in DMSO + water mixture and dialyzed using semipermeable membrane. The NR loaded polymer nanoparticles were named as P10-NR, P30-NR and P60-NR. In order to study the encapsulation of polymer backbone, a diblock copolymer PEG-*b*-BPCL without OPV chromophores and having 100 repeating units (reported by us in earlier studies⁴³) was chosen as a non-luminescent PCL polymer counterpart (see scheme 3.2). This polymer was donated by Ms. Mehak Malhotra from our laboratory. It was encapsulated with NR and the resultant non-luminescent polymer nanoparticles were employed as a reference.



Scheme 3.2. Non-luminescent carboxylic PCL block copolymer (PEG-*b*-BPCL) for encapsulating NR

The DLS histogram of P30-NR (see figure 3.7a) exhibited mono-modal distribution and the size of the nanoparticles was found to be 185 ± 10 nm. Further the FESEM and AFM morphologies of these NR dye loaded polymer sample was found to be spherical nanoparticles with sizes ranging as 160 ± 10 nm. Thus, the loading of NR did not alter the morphology of the polymer nanoparticles. Absorption spectra of NR loaded polymer donor-acceptor pair (see figure 3.7b) showed polymer absorption maxima at 395 nm corresponding to OPV chromophore and NR maxima as shoulder at 550 nm. This confirmed the loading of the NR dye in the OPV block copolymer nanoparticle. Dye loading content (DLC) and dye loading efficiency (DLE) were estimated by absorption spectroscopy and it was found to be in the range of 0.36 to 0.45 % and 3.61 to 4.56 % respectively as shown in table 3.1. The DLC and DLE of

this non-luminescent PEG-*b*-BPCL polymer was determined to be 0.44 % and 4.47 % respectively, which were almost similar to that of the luminescent OPV-PCL block copolymer nanoparticles.

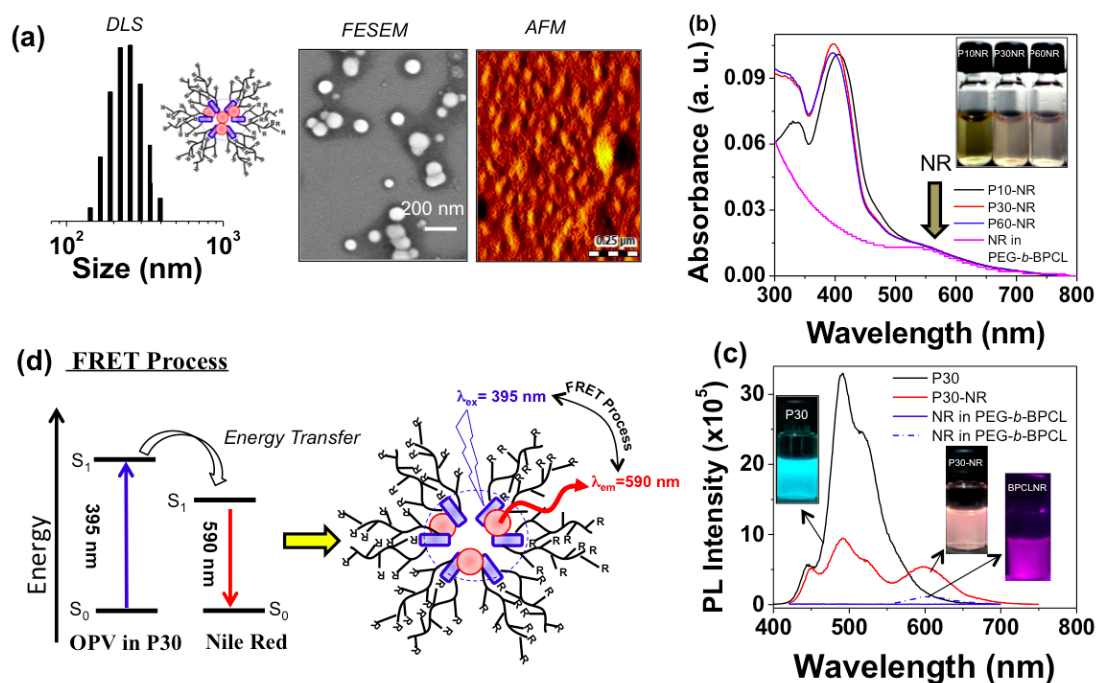


Figure 3.7. (a) DLS histogram, FE-SEM and AFM images of NR loaded P30 nanoparticles. (b) Absorbance spectra of NR loaded polymers P10, P30 and P60 nanoparticles in aqueous medium. (c) Emission spectra of the nanoparticles (solid line) recorded at OPV excitation ($\lambda_{ex} = 395$ nm) NR excitation ($\lambda_{ex} = 550$ nm, dotted line). (d) Photo excitation energy transfer from OPV to NR and the occurrence of FRET process in the nanoparticles. The OPV and NR concentrations are 2.3×10^{-6} M and 5.0×10^{-7} M, respectively for photophysical studies

Table 3.1. DLC and DLE of NR-loaded polymers.

Polymer	DLC(wt %)	DLE(wt %)
P10-NR	0.43	4.34
P30-NR	0.45	4.56
P60-NR	0.36	3.61
PEG- <i>b</i> -BPCL ₁₀₀	0.44	4.47

The concentration of NR present in the NR loaded block copolymer nanoparticles was determined by absorption spectra as 5.7×10^{-6} M. The

concentration of OPV chromophores was determined as 2.7×10^{-5} M. This estimated the molar ratio between OPV in the polymer and NR in the nanoparticles as 1.0 : 0.21. The NR dye has molar extinction coefficient as $38,000 \text{ M}^{-1} \text{ cm}^{-1}$;⁵⁵ thus, it has good absorption characteristics as fluorophore. The loading capability could be increased by further optimizing the block copolymer structures. Nevertheless, the quantity of the NR dye encapsulated in the polymer nanoparticle was sufficient enough for bioimaging application. The OPV-PCL block copolymers were employed as donor and various electron deficient fluorophores such as fluorescein, Nile red (NR), perylenebisimides, and Rose Bengal were used as acceptors. It was found that only NR loaded sample was found to be stable in aqueous medium and other donor-acceptor combinations were precipitated during the dialysis process. Thus, the present polymer micellar assemblies are suitable exclusively for NR loading.

The emission studies of the NR loaded polymers were carried out by exciting at absorption maxima of OPV at 395 nm as shown in figure 3.7c. The optical density of OPV chromospheres was maintained as 0.1 OD for this study. The emission spectra of nascent OPV block polymer nanoparticle (without NR loading), and NR loaded non-luminescent PEG-*b*-PCL block copolymer (without OPV chromophore) and P30-NR (having both OPV and NR chromophores) were compared in figure 3.7c. At 395 nm excitation, the OPV containing polymer P-30 exhibited emission maxima at 495 nm with respect to OPV self-emission. In this sample there is no emission with respect to NR. At 395 nm excitation, the NR loaded in non-luminescent PEG-*b*-PCL nanoparticle (without OPV) showed almost no emission at 595 nm. At 550 nm excitation (with respect to NR absorption); this sample showed little enhancement in the NR emission at 595 nm (shown dotted line, see figure 3.7c). This suggested that the NR dye does not have significant amount of emission from the nanoparticles at 395 nm excitation. The emission spectra of OPV and NR containing sample (P30-NR) exhibited two emission maxima at 495 nm and 595 nm corresponding to the self-emission from OPV chromophore and FRET induced emission from NR chromophore, respectively (see Figure 3.7c). The comparison of emission spectra of P-30 and P-30-NR samples revealed that the excitation energy transfer from OPV chromospheres to NR in the P30-NR sample. Thus, the sample P30-NR exhibited emission from NR at 595 nm followed by the FRET process. Based on the density functional theory calculation in the literature; the LUMO (or S_1) state of the OPV chromophore and NR dye were found to be -2.60 eV ⁵⁶⁻⁵⁷ and -3.56 eV ⁵⁸, respectively,

for the vacuum level. This suggested that S_1 state of the OPV was very well below the S_1 state of the NR which provided ample opportunity for the energy transfer process in the present system for FRET process. This process is explained by schematic energy model as shown in figure 3.7d.

The FRET between donor and acceptor resulted in the different emission color than original color of either donor (OPV) or acceptor (nile red). Ideally OPV chromophore is blue emitting molecule; hence, the nascent polymer showed blue light emission in absence of Nile red (acceptor) (see vials in figure 3.5f). Upon encapsulation of NR, the OPV polymer exhibited the donor acceptor interaction which resulted in the orange-pink emission in the visible region (see vials in figure 3.7c). This difference in the emission color further confirmed from occurrence of the FRET process. To further visualize the color difference, the OPV block copolymer and its NR loaded sample were subjected to fluorescence microscope images and the images are shown in figure 3.8.

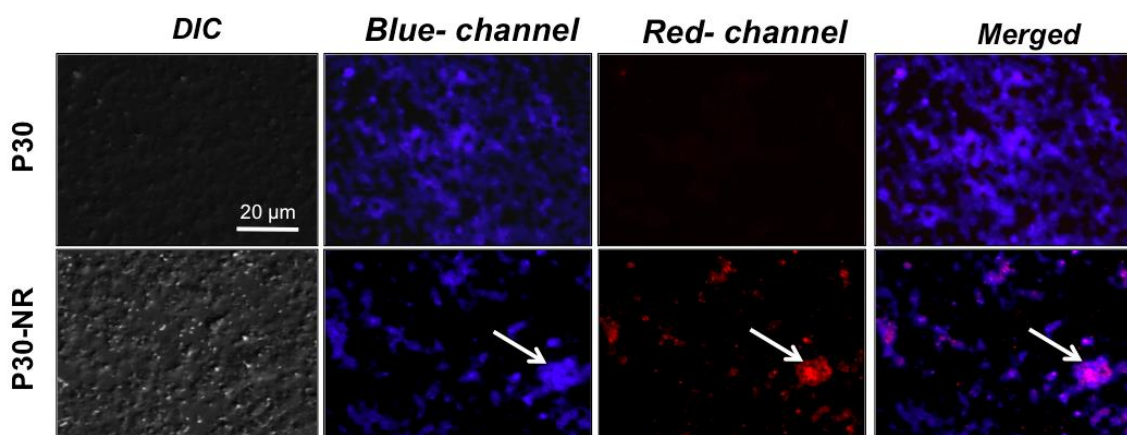


Figure 3.8. Fluorescence microscope imaging of P30 and P-30-NR sample and the images were captured in the blue and red-channels for the photoexcitation of OPV chromophore using 405 nm LED Laser. The merged images are produced by overlaying the blue and red channel images together. The OPV and NR concentrations are $2.7 \times 10^{-5} M$ and $5.7 \times 10^{-6} M$, respectively.

The images were recorded by exciting the sample at 405 nm laser source and visualizing through both blue and red channel. The nascent OPV polymer P30 showed bright blue emission (in blue channel) and it did not show any red fluorescence (in the red channel) (see the first panel). On the other hand, the NR loaded OPV block copolymer exhibited bright red emission (in red channel) in addition to the self blue emission. The merged image for the NR loaded sample showed magenta emission

followed by the merging of blue+red colors. Further, the merged image also showed the magenta color at the particle domain where the red and blue color observed in respective channels confirming that FRET process between OPV and NR within the nanoparticle domain (shown by arrows). These studies confirmed the excitation energy transfer from OPV chromophore in the polymer (donor) to the NR (acceptor).

3.3.3. Energy Transfer and FRET Distance

FRET is a distance dependent process and depends upon the intermolecular distance between donor and acceptor and the distance at which the FRET is 50% efficient is called Förster distance (R_0).⁶ and determined by equation:

$$R_0 = [8.79 \times 10^{-5} (\kappa^2 \eta^{-4} Q_D J(\lambda))]^{1/6}$$

where κ^2 is the angle between the dipole moments of donor and acceptor, Q_D is the quantum yield of donor, η is refractive index of the medium and $J(\lambda)$, the overlap integral from the emission spectrum of donor with the absorption spectrum of acceptor is given as;⁶

$$J(\lambda) = \int_0^\infty F_D(\lambda) \mathcal{E}_A(\lambda) \lambda^4 d\lambda$$

where F_D is the corrected fluorescence intensity of donor and $\mathcal{E}_A(\lambda)$ is the molar extinction coefficient of the acceptor.

The FRET efficiency can be determined from the equation:

$$E_{\text{FRET}} = (R_0^6) / [R_0^6 + R^6]$$

where R is the distance between donor and acceptor molecules. The parameter R_0 is also dependent on the $J(\lambda)$, the overlap integral of the emission spectrum of donor and absorption spectrum of acceptor. E_{FRET} is determined from the fluorescence life of donor molecule as follows:⁶

$$E = 1 - [\tau_{\text{DA}} / \tau_{\text{D}}]$$

where τ_{D} is the average fluorescence lifetime of donor in absence of acceptor and τ_{DA} is the average fluorescence lifetime of donor in presence of acceptor. The values of

$J(\lambda)$ and R_0 determined as above were computationally determined using the programme as per the literature report.⁵⁹

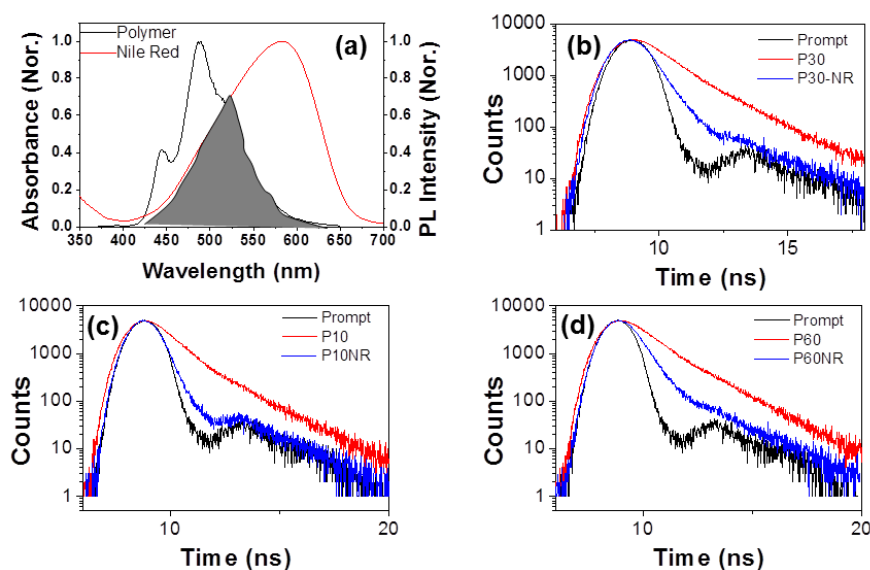


Figure 3.9. (a) Overlap between the OPV emission spectrum of P-30 and absorbance spectrum of NR in aqueous medium. TCSPC life time data for (b) P30 and P30-NR (c) P10 and P10-NR and (d) P60 and P60-NR recorded by 371 nm LED source and collected at OPV emission at 495 nm

Table 3.2 TCSPC life time data recorded by 371 nm LED source and collected at OPV emission at 495 nm for OPV-PCL block copolymers and NR encapsulated OPV-PCL block copolymers. The TCSPC decay data was fitted using DAS6 software and bi-exponential fit was observed for all the polymers.

Polymer	τ_1 (ns)	τ_2 (ns)	Average τ (ns)	χ^2	B_1	B_2
P10	0.84	1.73	1.00	0.92	68.74	31.26
P30	1.0	1.65	1.21	0.75	56.85	43.15
P60	1.08	1.73	1.28	0.86	56.84	43.16
Polymer	τ_1 (ns)	τ_2 (ns)	Average τ (ns)	χ^2	B_1	B_2
P10-NR	0.04	0.69	0.04	1.09	87.84	12.16
P30-NR	0.12	0.74	0.18	0.97	61.98	38.02
P60-NR	0.16	0.83	0.24	1.03	58.97	41.03

There was significant overlap (> 75 %) between the emission spectrum of OPV in the polymer (FRET donor) and the absorption spectrum of NR (FRET acceptor) (see figure 3.9a). Further, the energy transfer between donor and acceptor was determined by time correlated single photon count (TCSPC) techniques. The average fluorescence lifetime of the polymers was determined in absence and presence of NR (acceptor). The TCSPC studies were done using 371 nm nano-LED excitation source and the data were collected at emission maxima of OPV at 495 nm. For the NR loaded polymer sample, the data were collected at both OPV emission maxima at 495 nm and at NR maxima at 595 nm. All the polymers and NR encapsulated polymers collected at OPV emission maxima are shown in figure 3.9b to 3.9d. The TCSPC decay data was fitted using DAS6 software and bi-exponential fit was observed for all the polymers and the life time, amplitude and other details are provided in table 3.2. The average life time data $[(\tau_1 + \tau_2) / 2]$ was used for the D-A energy calculations and the determination of E_{FRET} by following reported procedure.^[6] The average lifetime values are summarized in table 3.2. The decay profiles clearly evident that the OPV chromophores exhibited much faster decay in the presence of NR. The comparison of the fluorescence lifetime data of the polymers in absence and presence of acceptor showed that average fluorescence lifetime of the polymers has been changed in the presence of the acceptor. There was significant decrease in the average lifetime of the polymers in presence of acceptor which further confirmed the energy transfer from OPV in the polymer (donor) to Nile red (acceptor). The energy transfer efficiency (E) was calculated for each combination of the donor acceptor pair. The E_{FRET} values were obtained 82 to 95 % (see table 3.3) revealed the excellent energy transfer between OPV and NR chromophores. The distance at which the FRET is 50% efficient is called Förster distance (R_0) between energy donor and acceptor and the distance should be in the range of 20 to 60 Å.⁶ From the table it is clear that the Förster distance (R_0) for all the donor acceptor pairs was almost identical and they were found to be < 42 Å for the present system. Both the Förster distance (R_0) and E_{FRET} values were used to determine the intermolecular distance (R) between the OPV and NR in the nanoparticle domain. The values of R were found to be < 32 Å (see table 3.3) which is much below the Förster distance (R_0) and provide direct evidence for the efficient FRET process at the nanoparticle domain. The size of the NR encapsulated polymer nanoparticles was in the range of ~180 nm (obtained from DLS

measurements at concentration of 0.4 mg/mL) and this particle size corresponds to the aggregation of few nanoparticles together in the aqueous medium. The donor-acceptor distance determined by the photophysical experiments represent the actual OPV and NR distance within the isolated nanoparticles in the aqueous medium. The detail photophysical analysis confirmed that the custom designed OPV fluorophore bearing PCL block copolymers are efficient nano-container for facilitating FRET process between OPV and NR.

Table 3.3. *all the parameters determined for the FRET process*

Polymer	$J(\lambda)$ ($M^{-1} cm^{-1} nm^4$)	R_0 (\AA)	τ_D (ns)	τ_{DA} (ns)	E	R (\AA)
P10-NR	1.96×10^{15}	41.82	1.00	0.04	0.95	25.89
P30-NR	1.67×10^{15}	41.56	1.21	0.18	0.86	31.08
P60-NR	1.56×10^{15}	41.48	1.28	0.24	0.82	32.54

3.3.4. Enzyme-responsiveness and FRET Process

The polycaprolactone arms in the block copolymer is aliphatic polyester in nature; thus it is readily susceptible for enzymatic biodegradation under physiological conditions.⁴³ The biodegradation of PCL segments in the block copolymer would bring the hydrophilic-hydrophobic imbalance thereby the nanoparticle undergo disassembly as shown in figure 3.10a. This process is expected to induce large separation of OPV donor and NR acceptor more than Förster distance (R_0); thus the FRET process is expected to be turn-off in the NR loaded nanoparticle assembly. In order to study the effect of enzyme-responsiveness of the block copolymer nanoparticles on the FRET process; esterase enzyme was chosen to biodegrade PCL segments.⁴² The steady state fluorescence spectra of the P30-NR nanoparticle were recorded at different time intervals in the presence or absence of esterase enzyme in PBS 7.4 at 37 °C. In the absence of esterase enzyme, the nanoparticle was very stable and there is no change in the intensity of NR emission maxima at 595 nm (see Figure 3.10b). In presence of esterase enzyme, the cleavage of nanoparticle and separation of OPV and NR chromophores apart reflected on the decrease in the NR emission intensity at 595 nm (see Figure 3.10c). The decrease in the FRET intensity was attributed to the separation of OPV and NR chromophores upon the biodegradation of PCL chain by enzymes. The isolation of OPV and NR would increase the donor-acceptor distance more than the Förster distance (R_0); thus, hampered the FRET

process. To quantify the enzyme action on the FRET process; the plot of $[F_0 - F_t]/F_0 \times 100$ was plotted against incubation time and shown in figure 3.10d. In this plot F_0 is the fluorescence intensity at initial time and F_t is the fluorescence intensity at time t . From this plot it can be concluded that FRET efficiency decreased drastically at initial 2 h and then it decreased slowly up to 12 h. In this process only 65% of FRET intensity was lost; however, remaining 35 % of the FRET was retained. The NR emission was not completely vanished even after 24 h indicated that there may be partial association of OPV and NR even after the biodegradation of PCL arms from the nanoparticles.

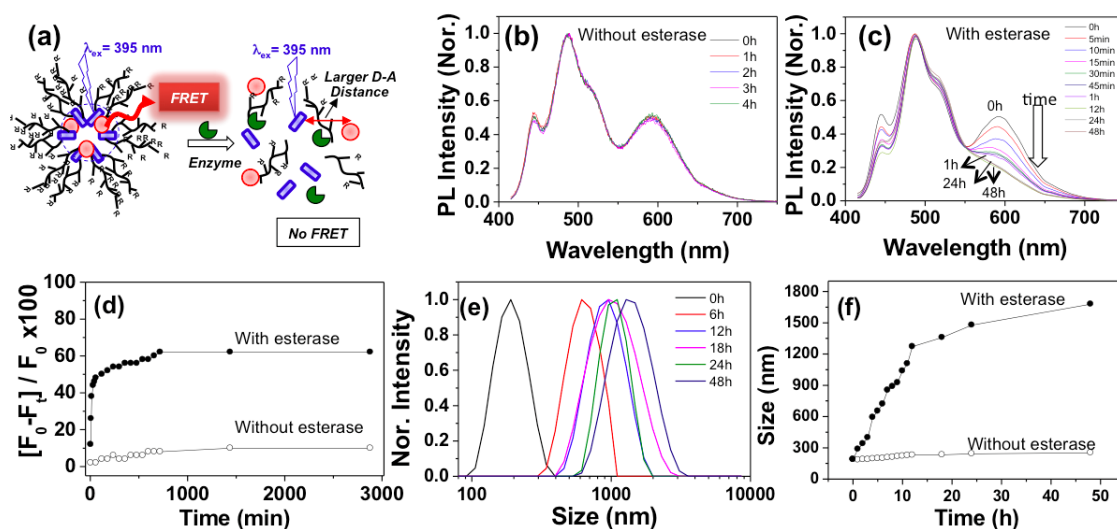


Figure 3.10. (a) Enzymatic biodegradation of PCL segments in the block copolymers and its influence on FRET Process. (b) Emission spectra of P-30-NR sample in PBS at 37 °C. (c) Emission spectra of P-30-NR sample in the presence of 10 U esterase enzyme in PBS at 37 °C. (d) Plot of $[F_0 - F_t]/F_0 \times 100$ versus incubation time in the absence or presence of esterase enzyme. The emission spectra were recorded using excitation wavelength at 395 nm. (e) Time dependent DLS histograms of P30-NR polymer in presence of esterase enzyme in PBS 7.4 at 37 °C. (f) Plot of DLS size versus time for P30-NR polymer in absence and presence of esterase enzyme in PBS 7.4 at 37 °C. The OPV and NR concentrations are 2.3×10^{-6} M and 5.0×10^{-7} M, respectively.

To further confirm the biodegradability of these block copolymers time-dependent DLS studies were carried out for P30-NR polymer nanoparticles. For this purpose P30-NR polymer nanoparticles were incubated in the absence and presence of esterase enzyme at 37 °C and PBS pH 7.4 buffer and the DLS histograms were recorded at regular time intervals (see figure 3.10e). The average sizes of the polymer nanoparticles obtained at various time intervals were plotted against incubation time

as shown in figure 3.10f. In absence of esterase enzyme, the polymer nanoparticles were found to be stable and hence size of the nanoparticles did not changed with time. In presence of esterase enzyme, the aliphatic ester backbone in the PCL chain was cleaved and disturbed the self-assembly of the polymer nanoparticles. Hence with increase in incubation time, the size of the nanoparticle was changed from nanometer to micron sized particles which is evident from the DLS histograms. A similar experiment was carried out wherein DLS histograms were recorded in pH 5 PBS buffer at 37 °C over a period of 48 h (see figure 3.11) With increase in the time of incubation, a slight increase in the size of polymer nanoparticle was observed and the nanoparticles were found to be stable at pH=5. At pH =5.0, in the presence of enzyme, the release occurred more than 80 %. This confirmed that the nanoparticles were not disassembled or degraded under lysosomal acidic-environment and the enzymes present in the endo-lysosomal compartment are responsible for cleavage of the nanoparticle. The above study revealed that the NR loaded OPV polymer nanoparticles behaved as efficient FRET probe and are stable at extracellular conditions (at 37 °C and pH 7.4). The FRET probes partially lose its activity at the intracellular environment due to the dissociation by the lysosomal enzymes. This experiment suggests that once the imaging is done at the intracellular level; the FRET probe can be completely degraded by the enzymes to clear from the site of action under physiological conditions.

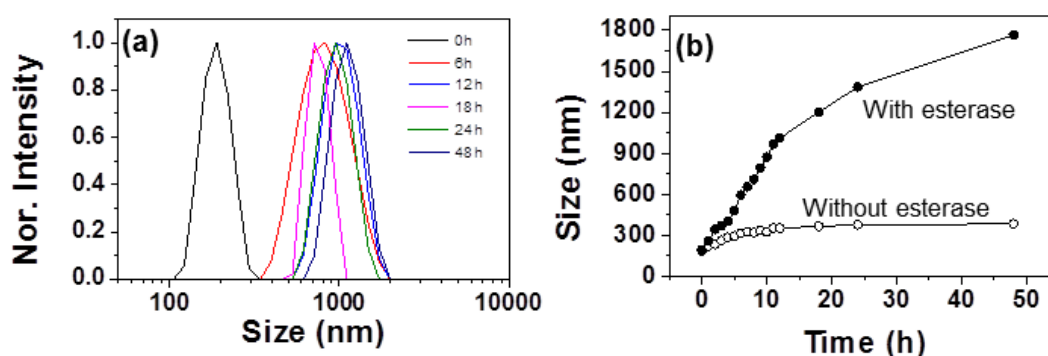


Figure 3.11: Time dependent DLS histograms of P30-NR polymer in presence of esterase enzyme in PBS 5 at 37 °C. (f) Plot of DLS size versus time for P30-NR polymer in absence and presence of esterase enzyme in PBS 5 at 37 °C

3.3.5. Cytotoxicity and FRET Process in Cancer Cells

To determine the biocompatibility of the polymer nanoparticles; cytotoxicity studies were done for P-30 and P30-NR nanoparticles by MTT assay method. HeLa cell line was used and the sample concentrations were varied up to 60 $\mu\text{g/mL}$ and the histograms are shown in figures 3.12a and 3.12b. The cell viability results showed that nascent polymer as well as its NR loaded nanoparticles is biocompatible and non-toxic to cells up to 40 $\mu\text{g/mL}$. This data clearly supports that the custom designed FRET probe nanoparticles were biocompatible and it may not harm the tissue environment while employing them for bioimaging.

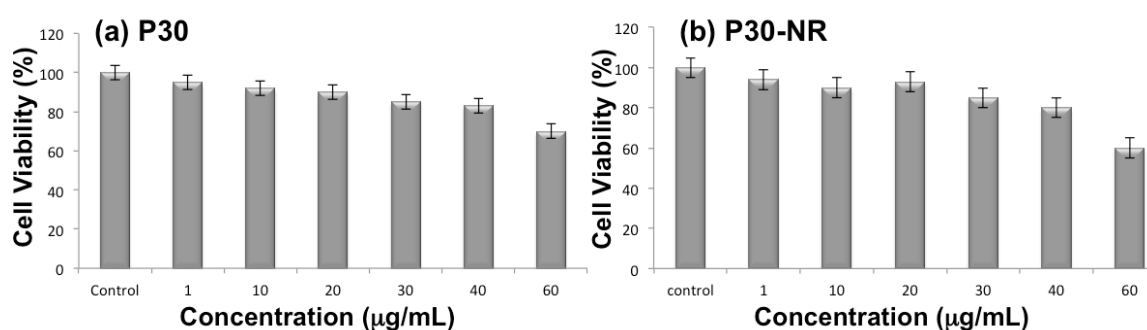


Figure 3.12: Cytotoxicity data of (a) P30 polymer and (b) P30-NR polymer in HeLa Cells at various concentrations

The FRET process between OPV in polymer and NR was investigated in HeLa cells by confocal microscopy. P30 and P30-NR polymer nanoparticles were incubated in HeLa cells for 2 h and the CLSM images are shown in figure 3.13a. Confocal images showed the uptake of the polymer nanoparticles and these nanoparticles were accumulated in the cytoplasm. The polymer nanoparticles are blue fluorescent in nature due to OPV chromophore; and thus, the OPV fluorescence was observed through blue channel ($\lambda = 405 \text{ nm}$). These images are shown in the first panel and the cells are clearly blue luminescent with respect to the OPV in blue channel and the signals were completely absent in the red-channel. NR loaded non-luminescent block polymer nanoparticle (without OPV) was also subjected to cellular uptake and these nanoparticles showed signals only in the red channel. Interestingly, the NR loaded OPV block copolymer showed bright blue emission upon excited by blue laser source and visualized through blue channel. For the same excitation source, this sample also showed strong signal in the red channel (560 nm) and the merged images showed magenta color emission with very good overlap. Hence, it may be

concluded that the occurrence of FRET process at OPV excitation enabled the OPV self-emission in the blue channel and also showed red emission with respect to the energy transfer from OPV to NR. The comparison of photophysical process in polymer nanoparticles in figure 3.7, fluorescence microscopy images in figure 3.8 and the confocal images of HeLa cells in figure 3.13a revealed that the occurrence of FRET process in the custom designed NR loaded OPV-block copolymer nanoparticles. To further, support the cellular internalization of P-30 and P30-NR polymer nanoparticles, they were subjected to flow cytometry analysis in HeLa cells (see Figures 3.13b and 3.13c). These plots clearly showed that P30 and P30-NR nanoparticles were taken up by the cells and fluorescence intensity clearly indicated high levels of cellular uptake of the nanoparticles.

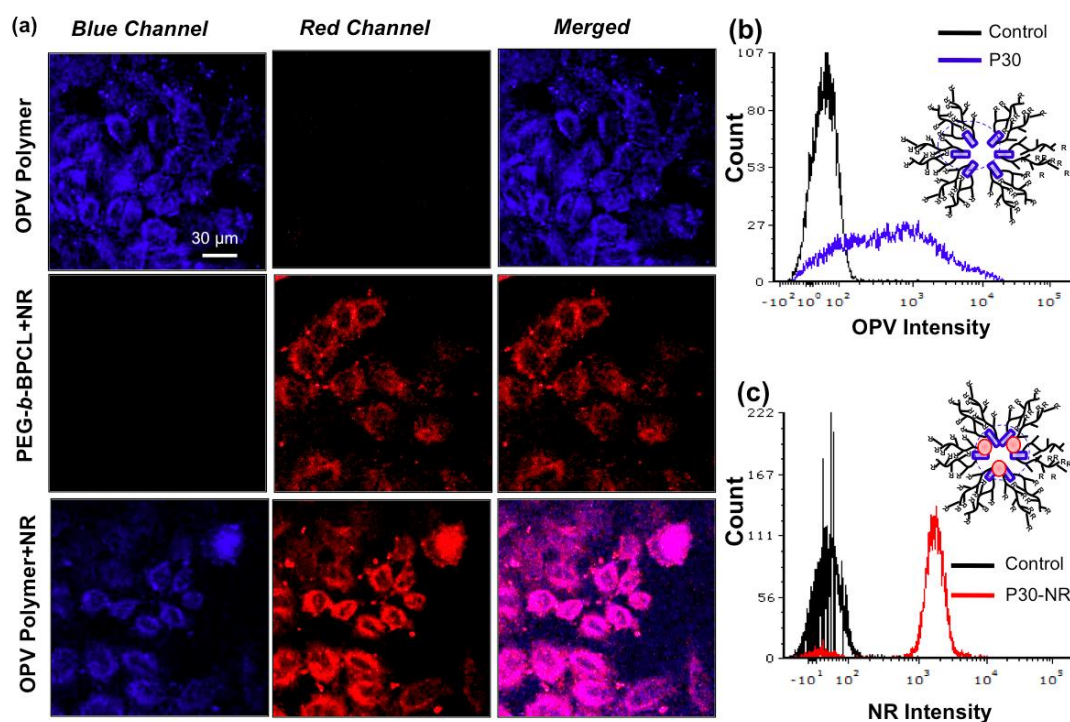


Figure 3.13. CLSM images of P30 polymer, NR encapsulated control polymer (polymer+NR) and P30-NR polymer (a) Incubated with HeLa cells and cells were excited using blue laser (λ 405 nm) and observed through blue and red channel and their merged images. Flow cytometry plots for P30 (b) and P30-NR nanoparticles (c) in HeLa cell lines (10000 cells were used). The OPV and NR concentrations are 2.7×10^{-5} M and 5.7×10^{-6} M, respectively.

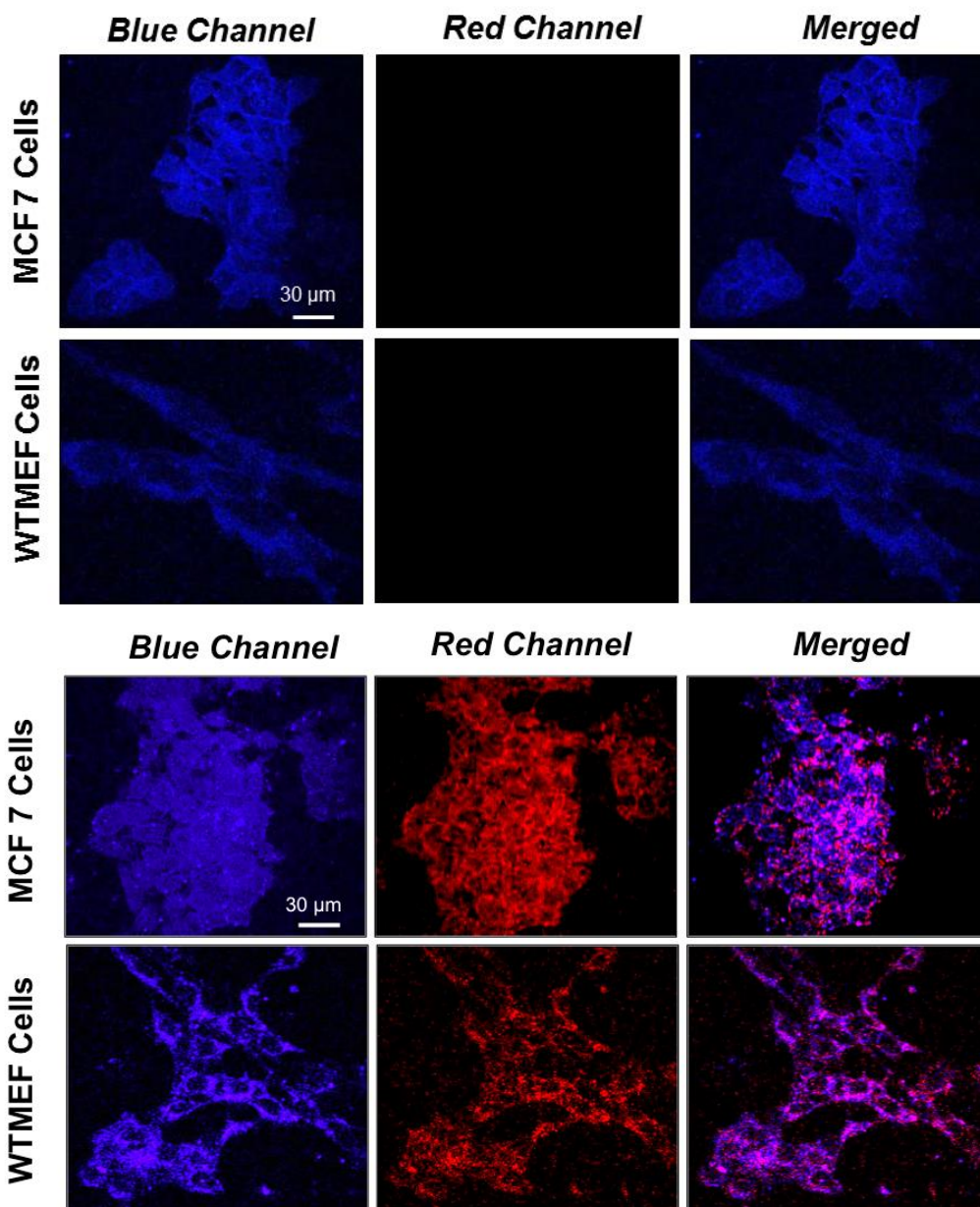


Figure 3.14: CLSM images of P30 polymer in MCF 7 and WT-MEF cells (upper two panels). The cells were excited using blue laser (λ 405 nm) and observed through blue and red channel and their merged images. The OPV concentration is 2.7×10^{-5} M. CLSM images of P30-NR polymer in MCF 7 and WT-MEF cells (lower two panels). The cells were excited using blue laser (λ 405 nm) and observed through blue and red channel and their merged images. The OPV and NR concentrations are 2.7×10^{-5} M and 5.7×10^{-6} M, respectively.

The FRET process was also investigated in breast cancer (MCF 7) and wild-type MEF cells (normal) cell lines. The FRET process was observed using the 405 nm excitation and the CLSM images for samples incubated with P30-NR are shown in Figure 3.14. Both these cell line images showed bright blue emission with respect to OPV chromophore in blue channel and red-emission form NR followed by the

occurrence of FRET between OPV and NR. The merged images showed magenta color with respect to the overlap of chromophores from same nanoparticles.

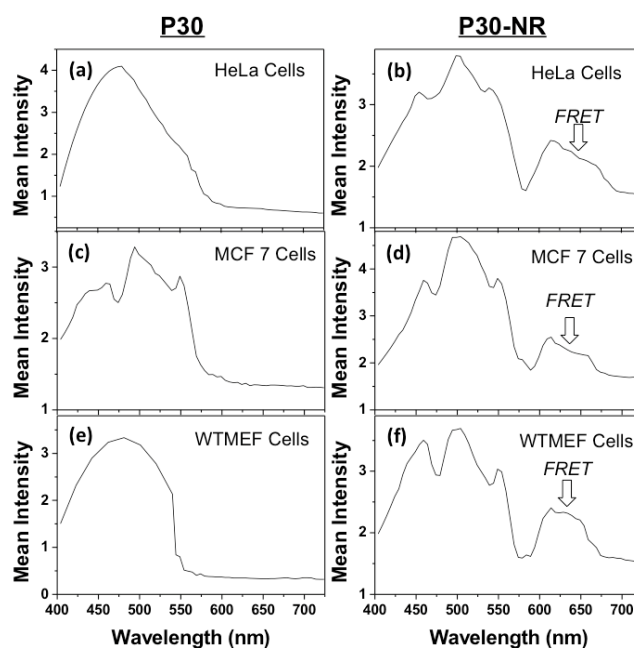


Figure 3.15. Mean fluorescence intensity from CLSM images of P30 and P30-NR nanoparticles in HeLa (a and b), MCF 7 (c and d) and WT-MEF (e and f) cells. The cells were excited using blue laser (λ 405 nm) and observed through blue channel (for spectra a, c and e) and red channel (for spectra b, d and f) for OPV and NR chromophores, respectively. The OPV and NR concentrations are 2.7×10^{-5} M and 5.7×10^{-6} M, respectively.

Further, fluorescence spectra for the in vitro CLSM images were constructed by exciting the cells using 405 nm laser source and recording the emission intensity at 5 nm interval from 415 to 725 nm. The mean fluorescence intensity was determined by image J software and plotted against the emission wavelength. The resultant spectra in HeLa, MCF 7 and WT-MEF cells for the P-30 and P30-NR samples are shown in figure 10. The P30 polymer showed emission peak with respect to OPV whereas the P30-NR showed peaks for self-emission from OPV and also FRET induced red-emission from NR at 590 to 700 nm (see Figure 3.15). The FRET process between OPV and NR was observed in both cancer (MCF 7 and HeLa) as well as normal cells indicating that new OPV-NR FRET probe is versatile to exhibit FRET based bioimaging in diverse cell lines. In the present investigation, we have designed and developed a new FRET probe based on OPV fluorophore conjugated PCL based diblocks copolymers and employed them as nano-scaffold for stabilizing NR to make new FRET donor-acceptor pair in aqueous medium. The FRET process as established

by detail spectroscopic and proof-of-concept of the occurrence of the FRET process was also successfully demonstrated in the cancer cell. The new FRET probe is biodegradable, non-toxic, cell penetrable and retained the chromophore photophysical process to enable their action at the intracellular level.

3.4. Conclusion

In summary, we have developed new FRET probes based on biodegradable and biocompatible and blue luminescent OPV-PCL block copolymer nanoparticles as FRET donor and Nile red (NR) as FRET acceptor. Biodegradable substituted caprolactone monomer was subjected to ring opening polymerization by luminescent hydroxyl functionalized OPV as initiator. These polymers were self-assembled as aqueous, luminescent nanoparticles and further encapsulated with NR dye. The polymer nanoparticles and NR loaded polymer nanoparticles were characterized by DLS and spherical morphology was confirmed by FESEM and AFM. The photophysical studies revealed that the block copolymer nano-assemblies provided appropriate geometry for close vicinity for OPV chromophores in the polymer and physically encapsulated NR dye for efficient excitation energy transfer from OPV to NR. The Förster distance and spatial distance between OPV and NR was found to be $\sim 42 \text{ \AA}$ and 32 \AA , respectively for efficient FRET process. The photoexcitation energy transfer between donor and acceptor was determined to be $> 85 \%$ which is very good for imaging applications. The new OPV-NR FRET probe was enzyme-degradable, biocompatible and non-toxic to cells. Intracellular visualization of FRET process between OPV and NR was accomplished by confocal microscopic imaging. The CLSM images were exhibited bright blue luminescence from OPV self-emission and bright red-luminescence from NR followed by the FRET process between OPV and NR. This observation supports that the newly developed FRET probe can be used for dual imaging process in cancer cells depending upon the requirement. Though, the PCL block copolymer approach here demonstrated exclusively for OPV and NR donor-acceptor pair, it is not restricted to only these two examples, in principle, it may be extended to other FRET chromophores as well. The OPV-NR FRET probe based on PCL nanoparticles can be employed for many futuristic applications including bioimaging in cancer cells for diagnostic purpose.

3.5. References

1. Li, C.; Liu, S.. *Chem. Commun.* **2012**, *48*, 3262-3278.
2. Lv, F.; Qiu, T.; Liu, L.; Ying, J.; Wang, S. *Small* **2016**, *12*, 696-705.
3. Ciu, Q.; Wang, X.; Yang, Y.; Li, S.; Li, L.; Wang, S *Chem. Mater.* **2016**, *28*, 4661-4669.
4. Matsumura, Y.; Maeda, H. *Cancer. Res.* **1986**, *46*, 6387-6392.
5. Maruyama, K. *Adv. Drug Delivery Rev.* **2011**, *63*, 161-169.
6. Sahoo, H. *J. Photochem. Photobiol. C* **2011**, *12*, 20-30.
7. Fruhwirth, G. O.; Fernandes, L. P.; Weitsman, G.; Patel, G.; Kelleher, M.; Lawler, K.; Brock, A.; Poland, S. P.; Matthews, D. R.; Kéri, G.; Barber, P. R.; Vojnovic, B.; Ameer-Beg, S. M.; Coolen, A. C. C.; Fraternali, F.; Ng, T. *ChemPhysChem* **2011**, *12*, 442-461.
8. Yu, J. C.; Chen, Y. L.; Zhang, Y. Q.; Yao, X. K.; Qian, C. G.; Huang, J.; Zhu, S.; Jiang, X. Q.; Shen, Q. D.; Gu, Z. *Chem. Commun.* **2014**, *50*, 4699-4702.
9. Fu, Y.; Chen, X.; Mou, X.; Ren, Z.; Li, X.; Han, G. *ACS Biomater. Sci. Eng.* **2016**, *2*, 652-661.
10. Kim, H. J.; Miyata, K.; Nomoto, T.; Zheng, M.; Kim, A.; Liu, X.; Cabral, H.; Christie, R. J.; Nishiyama, N.; Kataoka, K. *Biomaterials* **2014**, *35*, 4548-4556.
11. Matsuoka, K.; Arai, H.; Oka, H.; Koyama, T.; Hatano, K. *ACS Macro Lett.* **2012**, *1*, 266-269.
12. Mitra, K.; Singh, S.; Hira, S. K.; Patel, V. K.; Singh, D.; Vishwakarma, S.; Singh, R.; Kumari, A.; Manna, P. P.; Ray, B. *ACS Biomater. Sci. Eng.* **2016**, *2*, 1630-1640.
13. Wang, X.; Yang, Y.; Zhuang, Y.; Gao, P.; Yang, F.; Shen, H.; Guo, H.; Wu, D.. *Biomacromolecules* **2016**, *17*, 2920-2929.
14. Sakai-Kato, K.; Un, K.; Nanjo, K.; Nishiyama, N.; Kusuhara, H.; Kataoka, K.; Kawanishi, T.; Goda, Y.; Okuda, H. *Biomaterials* **2014**, *35*, 1347-1358.
15. Han, X.; Liu, D.; Wang, T.; Lu, H.; Ma, J.; Chen, Q.; Gao, H. *ACS Appl. Mater. Interfaces* **2015**, *7*, 23760-23766.
16. Duan, X.; Liu, L.; Feng, F.; Wang, S. *Acc. Chem. Res.* **2010**, *43*, 260-270.
17. Zhang, G.; Xing, B.; Song, J.; Zhang, F.; Nie, C.; Jioa, L.; Liu, L.; Lv, F.; Wang, S. *Anal. Chem.* **2014**, *86*, 346-350.
18. Zhu, C.; Yang, Q.; Liu, L.; wang, S.; *J. Mater. Chem.* **2011**, 7905-7912.
19. Wang, Y.; Li, S.; Feng, L.; Nie, C.; Liu, L.; Lv, F.; Wang, S. *ACS Appl. Mater. Interfaces* **2015**, *7*, 24110-24118.
20. Yu, J.; Zhu, S.; Feng, P.; Qian, C.; Huang, J.; Sun. M.; Shen, Q. *Chem. Commun.* **2015**, *51*, 2976-2979.
21. Cui, Q.; Yang, Y.; Yao, C.; Liu, R.; Li, L. *ACS Appl. Mater. Interfaces* **2016**, *8*, 35578-35586.
22. Rana, S.; Elci, S. G.; Mout, R.; Singla, A. K.; Yazdani, M.; Bender, M.; Bajaj, A.; Saha, K.; Bunz, U. H. F.; Jirik, F. R. Rotello, V. M. *J. Am. Chem. Soc.* **2016**, *138*, 4522-4529.
23. Li, K.; Liu, B. *Polym. Chem.* **2010**, *1*, 252-259.

24. Huang, Y.; Qiu, F.; Shen, L.; Chen, D.; Su, Y.; Yang, C.; Li, B.; Yan, D.; Zhu, X. *ACS Nano* **2016**, *10*, 10489-10499.
25. Wasin, T.; Enomoto, K.; Sakurai, T.; Padalkar, V. S.; Cheng, H. L.; Tang, M. T.; Horio, A.; Sakamaki, D.; Omicgi, M.; Saeki, A.; Kikuchi, K.; Hori, Y.; Chiba, A.; Saito, Y.; Kamiya, T.; Sugumoto, M.; Seki, S. *ACS Sens.* **2016**, *1*, 766-774.
26. Malik, A. H.; Hussain, S.; Iyer, P. K. *Anal. Chem.* **2016**, *88*, 7358-7364.
27. He, X. W. F.; Li, L.; Wang, H.; Yan, R.; Li, L. *ACS Appl. Mater. Interfaces* **2013**, *5*, 5700-5708.
28. Liu, X.; Shi, L.; Hua, X.; Huang, Y.; Su, S.; Fan, Q.; Wang, L.; Huang, W. *ACS Appl. Mater. Interfaces* **2014**, *6*, 3406-3412.
29. Xu, H.; Gao, S.; Yang, Q.; Pan, D.; Wang, L.; Fan, C. *ACS Appl. Mater. Interfaces* **2010**, *2*, 3211-3216.
30. Lin, W.; Zhu, Y.; Chen, X. A Cis-Membrane *J. Am. Chem. Soc.* **2014**, *136*, 679-687.
31. Al-Itiry, R.; Lamnawar K.; Maazouz, A. *Polym. Degrad. Stab.* **2012**, *97*, 1898-1914.
32. Kaihara, S.; Matsumura, S.; Mikos, A. G.; Fisher, J. P. *Nat. Protoc.* **2007**, *2*, 2767-2771.
33. M, Labet.; W. Thielemans. *Chem. Soc. Rev.* **2009**, *38*, 3484-3504
34. Chang, L.; Deng, L.; Wang, W.; Lv, Z.; Hu, F.; Dong, A.; Zhang, J. *Biomacromolecules* **2012**, *13*, 3301-3310.
35. Yao, K.; Wang, J.; Zhang, W.; Lee, J. S.; Wang, C.; Chu, F.; He, X.; Tang, C. *Biomacromolecules* **2011**, *12*, 2171-2177.
36. Hao, J.; Servello, J.; Sista, P.; Biewer, M. C.; Stefan, M. C. *J. Mater. Chem.* **2011**, *21*, 10623-10628.
37. Hao, J.; Cheng, Y.; Ranatunga, R. J. K. U.; Senevirathne, S.; Biewer, M. C.; Nielsen, S. O.; Wang, Q.; Stefan, M. C. *Macromolecules* **2013**, *46*, 4829-4838.
38. Rieger, J.; Bernaerts, K. V.; Prez, F. E. D.; Jerome, R.; Jerome, C. *Macromolecules* **2004**, *37*, 9738-9745.
39. Mahmud, A.; Patel S.; Molavi, O.; Choi, P.; Samuel, J.; Lavasanifar A. *Biomacromolecules* **2009**, *10*, 471-478.
40. Tian, D.; Halleux, O.; Dubois, P.; Jérôme, R. *Macromolecules* **1998**, *31*, 924-927.
41. Surnar, B.; Jayakannan M. *Biomacromolecules* **2013**, *14*, 4377-4387.
42. Malhotra, M.; Surnar, B.; Jayakannan, M. *Macromolecules* **2016**, *49*, 8098-8112.
43. Surnar, B.; Jayakannan, M. *ACS Biomater. Sci. Eng.* **2016**, *2*, 1926-1941.
44. Kulkarni, B.; Surnar, B.; Jayakannan, M. *Biomacromolecules* **2016**, *17*, 1004-1016.
45. Surnar, B.; Subash, P. P.; Jayakannan, M. *Z. Anorg. Allg. Chem.* **2014**, *640*, 1119-1126.
46. Surnar, B.; Sharma, K.; Jayakannan, M. *Nanoscale* **2015**, *7*, 17964-17979.
47. Surnar, B.; Jayakannan, M. *Biomacromolecules* **2016**, *17*, 4075-4085.

48. Deng, H.; Zhao, X.; Liu, J.; Zhang, J.; Deng, L.; Liu, J.; Dong, *Nanoscale* **2016**, *8*, 1737-1450.
49. Endres, T.; Zheng, M.; Kilic, A.; Turowska, A.; Beck-Broichsitter, M.; Renz, H.; Merkel, O. M.; Kissel, T. *Mol. Pharmaceutics* **2014**, *11*, 1273-1281.
50. Huang, P.; Song, H.; Zhang, Y.; Liu, J.; Zhang, J.; Wang, W.; Liu, J.; Kong, D. *ACS Appl. Mater. Interfaces* **2016**, *8*, 2923-2933
51. Aluri, R.; Jayakannan, M.. *Biomacromolecules* **2017**, *18*, 189-200.
52. Li, X.; Mu, J.; Liu, F; Tan, E. W. P.; Khezri, B.; Webster, R. D.; Yeow, E. K. L.; Xing, B. *Bioconjugate Chem.* **2015**, *26*, 955-961.
53. Narashima, K.; Jayakannan, M. *Macromolecules* **2016**, *49*, 4102-4114.
54. Goel, M.; Narashima, K.; Jayakannan, M. *Macromolecules* **2014**, *47*, 2592-2603.
55. Karpenko, I. A.; Klymchenko, A. S.; Gioria, S.; Kreder, R.; Shulov, I.; Villa, P.; Mely, Y.; Hibert, M.; Bonnet, D. *Chem. Commun.* **2015**, *51*, 2960-2963.
56. Peeters, E.; Hal, P. A. van.; Knol, J.; Brabec, C. J.; Sariciftci, N. S.; Hummelen, J. C.; Janssen, R. A. J.. *J. Phys. Chem. B.* **2004**, *104*, 10174-10190.
57. Neuteboom E. E.; Meskers, S. C.; P. A. van.; Duren, J. K. J. van.; Meijer, E. W.; Janssen. R. A. J.; Dupin, H.; Pourtois, G.; Cornil, J.; Lazzaroni, R.; Bredas, J-L.; Beijonne, D. *J. Am. Chem. Soc.*, **2003**, *125*, 8625-8638.
58. Liu, Y-X.; Summers, M. A.; Scully, S. R.; McGehee, M. D. *J. Apply. Phys.* **2006**, *99*, 935211-935214.
59. Hink et al. <http://www.photobiology.info/Visser-Rolinski.html>.

Chapter 4

Enzymatically-Biodegradable Perylene bisimide-Carboxylic Polycaprolactone Fluorescent Block Copolymers for Bio-imaging in Cancer Cells

Abstract

Water soluble perylene bisimide derivatives are becoming increasingly attractive for various biomedical applications. However preserving their exceptional properties in aqueous medium is one of the great challenges. The present work is focused to prepare water soluble highly fluorescent PBI derivatives with enzyme responsive amphiphilic biodegradable block copolymer for cellular imaging in cancer cells. The carboxyl substituted polycaprolactone was incorporated as hydrophilic and biodegradable substituent on the imide position of PBI via ring opening polymerization. The amphiphilic block copolymers self-assembled as spherical nanoparticles of ~ 100 nm in aqueous medium. The hydrophilic PCL arms ensured the water solubility and expected to hinder the aggregation of PBI chromophore in block copolymers. Importantly the desired photophysical properties of the PBI chromophore were retained in aqueous medium. Enzyme responsive biodegradation studies revealed the possible degradation of polymer nanoparticles into small molecules which can be subsequently removed from the body after the intended purpose. The block copolymer nanoparticles with prominent features including high fluorescence, biodegradability and low toxicity were demonstrated for bioimaging application in cancer cells and exhibited good cellular uptake concurrently observed by inherent red fluorescence for the PBI chromophore. Hence, current polymer design with attractive photophysical properties of PBI and biodegradability of PCL backbone provided new opportunity for development of efficient nano-assemblies for bioimaging application.

4.1 Introduction

π -Conjugated oligomers and polymers have been extensively investigated for optoelectronic devices application as well as biomedical applications such as bioimaging, biosensing, diagnosis etc owing to their excellent photophysical properties.^{1,2} In this regard, perylenebisimide (PBI) derivatives have been well recognized π -conjugated chromophores with outstanding chemical, thermal, and photostability. PBI derivatives are also characterized by exceptional electrochemical properties and unique photophysical properties such as high molar extinction coefficient, high fluorescence quantum yield intense photoluminescence, and long fluorescence lifetime.^{3,4} Thus, scientific interest is driven by the remarkable highly versatile PBI derivatives which find potential applications in broad range of different fields such as OLEDs,⁵ molecular switches and wires⁶, light harvesting arrays⁷, photoreactive thin films⁸, solar cells⁹, sensor materials¹⁰, supramolecular architectures¹¹ and so on. Amphiphilic PBI derivatives have also gained significant interest in biological applications for cellular imaging and drug delivery.¹² Most of the π -conjugated polyaromatic chromophores encounter three important problems for biomedical applications: (i) insoluble, (ii) aggregation-induced fluorescent quenching even at low concentrations in aqueous medium and (iii) non-biodegradability under physiological conditions. Hence, potential biomedical applications of PBI derivatives have so far been limited by their poor water solubility and low quantum yield in aqueous medium.¹³

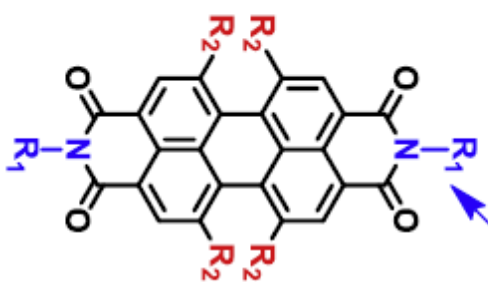


Figure 4.1. Imide position and bay region of Perylene bisimide (adopted from k. Liu et al. *Prog. Polym. Sci.* **2015**, 46,25-54)

Thus, it is highly desirable to prepare water soluble PBI derivatives for biological applications. In order to overcome insolubility of the PBI chromophores in water many successful efforts have been taken to develop water soluble PBI derivatives. The derivatization of PBI core was done both at the bay region and imide substitution position as shown in figure 4.1. The substitution at the imide position provide unlimited choice via imide chemistry and this approach was extended to make charged or uncharged substituents such as dendritic newkome type carboxylates,¹⁴ polyethylene glycol chains,¹⁵ cyclodextrines,¹⁶ phosphate surfactants,¹⁷ poly(vinyl alcohol)¹⁸ and crown ethers¹⁹, etc. All these PBI derivatives exhibited water solubility but high fluorescence quantum yields could not be achieved perhaps due to the aggregation induced fluorescence quenching.

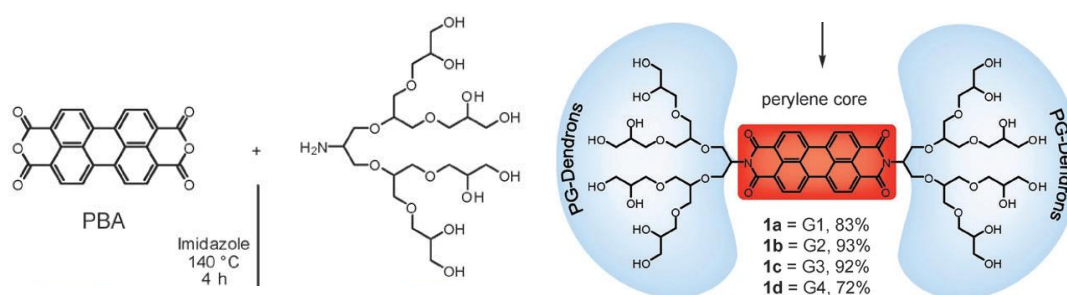


Figure 4.2 Water soluble , highly fluorescent polyglycerol dendronized Perylene bisimide (adopted from Heek et al. *Chem. Commun.* **2010**, 46, 1884-1886)

To circumvent this Haag and co-workers synthesized highly water soluble polyglycerol dendronized PBI as shown in figure 4.2 with high fluorescence quantum yields in water.²⁰ Amino acid substituents such as alanine,²¹ aspartic acid,²² histidine,²³ and lysine²⁴ have been introduced to achieve water soluble PBI. Water soluble core substituted, imide substituted nitrilotriacetic acid functionalized PBI derivatives and monofunctional polyglycerol dendronized PBI and were developed for highly specific protein labelling.^{25,26} Mullen and co-worker synthesized core shell nanoparticles consist of central PBI chromophore, a rigid polyphenylene dendrimer and flexible polymer shell with multiple carboxylic acid groups and monofunctional amine groups for inducing water solubility as shown in Figure 4.3. These core shell nanoparticles were demonstrated for different biological applications such as cellular membrane transport,²⁷ staining of extracellular matrix²⁸ and specific cell-nucleus staining.²⁹ Hg⁺² detection via imaging in live cells have been reported for dithioacetal

functionalized PBI and N-acetylated urea derivatives of PBI which serve as selective fluorescent chemo sensor of recyclable Hg^{+2} detection and ‘turn on’ fluorescent chemodosimeter respectively.^{30,31}

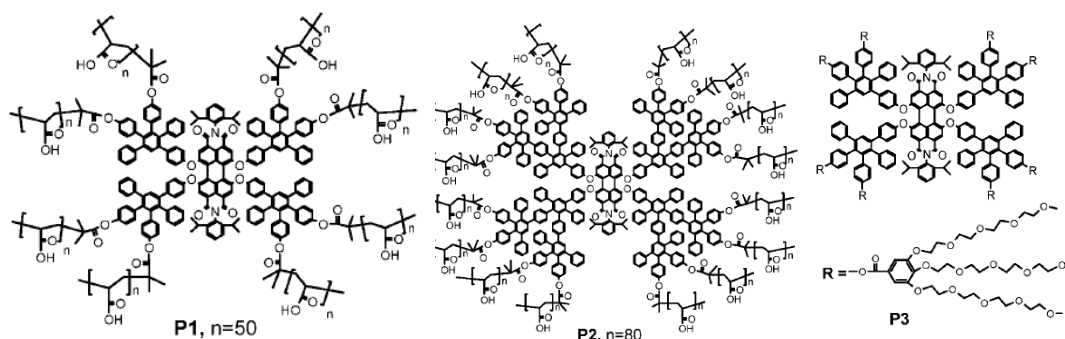


Figure 4.3. PDI-labeled core/shell nanoparticles containing multiple carboxylic groups (P1 and P2) and PEO groups (adopted from Yin et al. *Small* **2008**, 4, 894-898)

Maizen Yin and Jie group reported highly water soluble PBI cored cationic polyesters and polyamidiamine (PBI-PAmAm) dendrimers with peripheral amine groups for efficient *in vitro* and *in vivo* gene transfection.³² PBI cored acrylate star polymers poly(2-(dimethylamino ethyl methacrylate)) were synthesized and further employed to prepare bifunctional magnetic fluorescent $\text{Fe}_3\text{O}_4\text{SiO}_2\text{-PDI-PAA/Ca}^{+2}$ nanoparticles as shown in Figure 4.4. These star polymers and the magnetic nanoparticles were demonstrated for gene delivery and bioimaging.^{33,34}

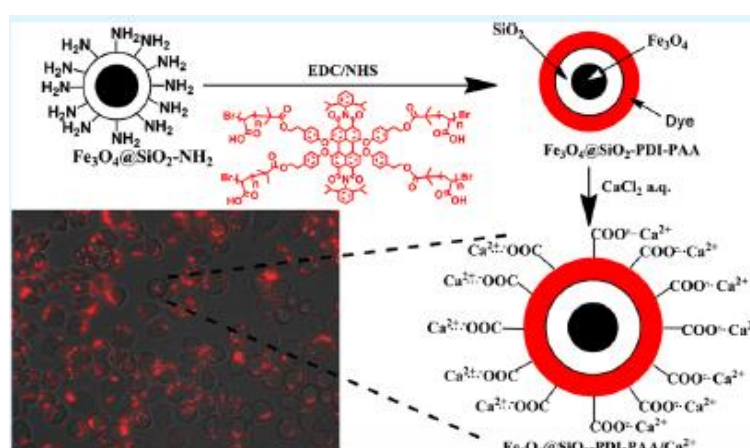


Figure 4.4. Fluorescent, magnetic PBI cored star polymer for cell imaging (adopted from Lu et al. *ACS Appl. Mater. Interface* **2015**, 7, 5226-5232)

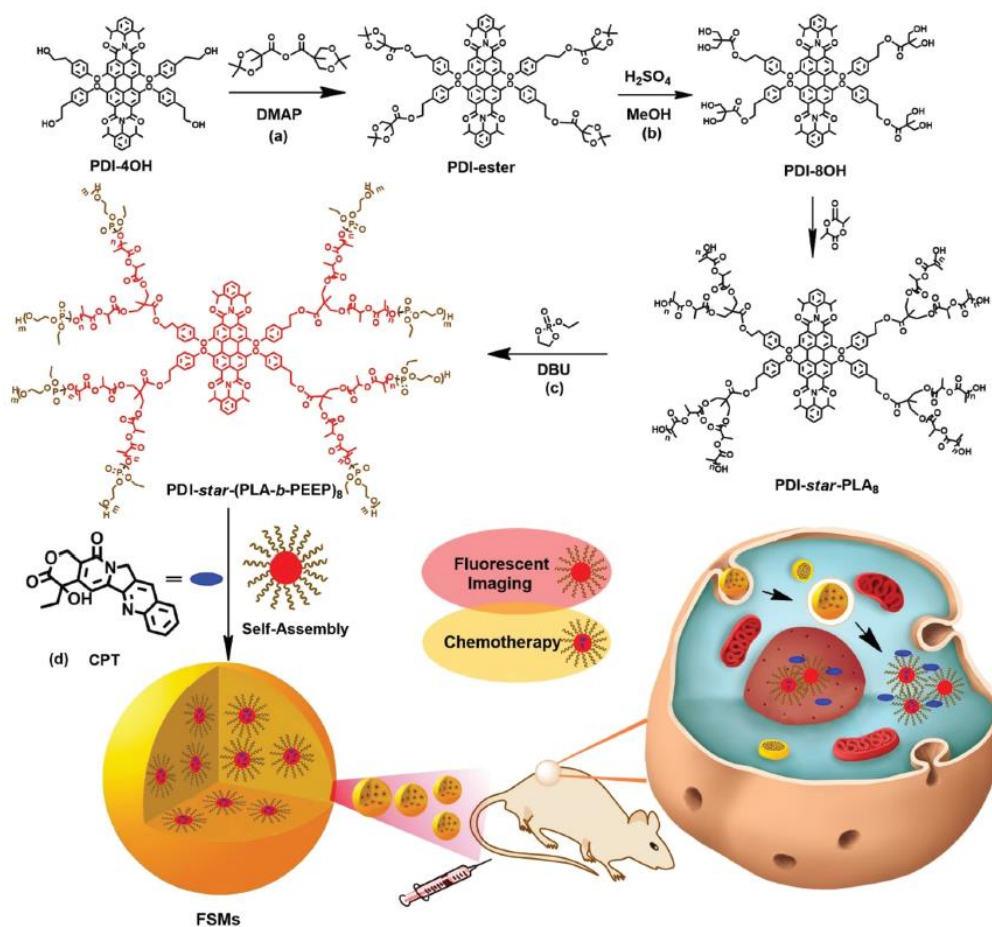


Figure 4.5. Schematic illustration of the formation of CPT-loaded PDI-star-(PLA15-b-PEEP25)₈ nanomicelles and the fluorescence imaging-guided intracellular drug release (adopted from *Nanoscale* **2016**, 8, 5302-5312)

The imide position of PBI was modified with poly(ethylene glycol) monomethyl ether methacrylate (PEGMA) based on ATRP to obtain brush like fluorescent labelled polymer for imaging different types of cells.³⁵ Asha and co-workers developed fluorescent polystyrene nanobeads by incorporating PBI and/or OPV chromophores and successfully demonstrated for multicolour bioimaging application in HeLa cells.³⁶ Further, Xu et al. reported water soluble rigid PBI derivative was designed as DNA intercalator by introduction of two tertiary ammonium salts at imide position which localized into cell nuclei and intercalated into DNA thereby suppressing cancer cells and tumour.³⁷ Ionic pyridinol substituted highly water soluble PBI was employed for biolabeling.³⁸ *In vitro* bioimaging in HeLa cells was carried out by perylene monoimide (PeIm) nanoparticles and *ortho* substituted phosphonate functionalized PBI.^{39,40} Haag and co-workers designed and

synthesized amphiphilic dendritic perylene imido dialkylester for imaging of cellular membrane as shown ⁴¹ Fluorescent pH responsive micelles composed of PDI core and poly(D,L-lactide)-*b*-poly(ethyl ethylene phosphate) star polymer was developed for fluorescence imaging-guided cancer therapy as shown in figure in Figure 4.5. ⁴²

Thus, PBI is an excellent fluorophore which is being explored for the potential biomedical application due to its favourable properties including biocompatibility. However, as discussed above majority of the polymer or dendrimeric units attached on the PBI do not possess biodegradability (except the PLLA system) which is of utmost importance for the applications in biological field. The biodegradable material can be broken down either through hydrolytic degradation or by enzymatic means and subsequently removed from the body after the intended purpose. Hence, development of new water soluble PBI derivatives with biodegradable substituents would be of high interest and provide new opportunity for their potential use in various biomedical applications.

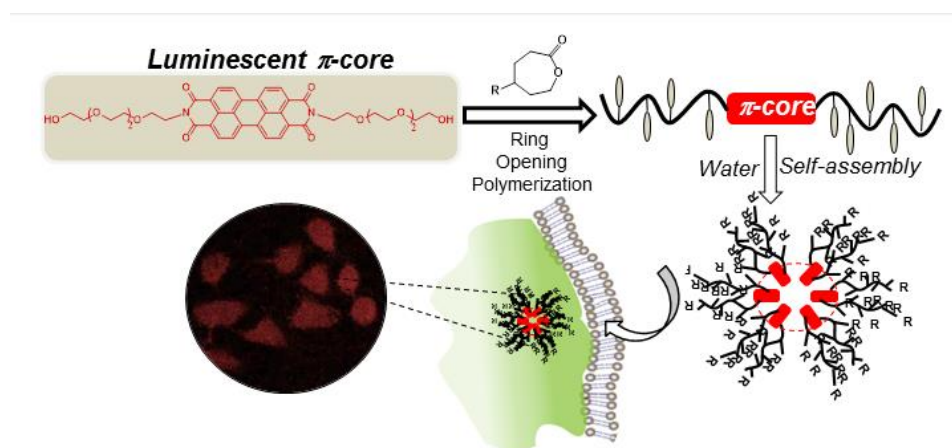


Figure 4.6. New red fluorescent, biodegradable PBI containing block copolymers for cellular imaging in cancer cells.

The goal of the present work is to prepare water soluble highly fluorescent PBI derivatives with hydrophilic biodegradable polymer for cellular imaging in cancer cells. Among various biodegradable polymers enzymatically-degradable polycaprolactone based aliphatic polyesters are extensively used for biomedical applications. PBI with PCL polymer was earlier reported in the literature; however, their water insolubility restricted their exploration in biological systems. ^{43,44,45} In the

present investigation, the unique photophysical properties of PBI were combined with biodegradable carboxyl substituted PCL backbone, for the first time, to make new PBI-PCL amphiphilic nano-scaffolds and employ them for cellular imaging in the literature which is schematically shown in figure 4.6. To achieve this goal carboxyl substituted polycaprolactone which have been reported in the previous chapters (2 and 3) appeared to be promising to introduce water solubility was employed as hydrophilic and biodegradable substituent on the imide position of PBI. Unlike the OPV chromophore (in the chapters 2 and 3), the PBI unit was found to stable under de-protection of BOC-ester groups under acidic conditions which enabled the construction of highly water soluble and fluorescent PBI-carboxylic PCL system for bioimaging application in cancer cells. These polymers were self-assembled in to ~ 100 nm spherical nanoparticles in aqueous medium. Further photophysical properties of PBI chromophore were retained in the aqueous medium so that these polymer nanoparticles could be employed for cellular imaging studies. Enzyme responsive biodegradation was carried out as the polymer backbone consists of aliphatic ester linkages. Cytotoxicity studies confirmed that the newly synthesized luminescent block copolymers were highly biocompatible and cellular internalization was studied by confocal microscope imaging.

4.2. Experimental section

4.2.1. Materials: Tetraethylene glycol, *p*-toluenesulfonylchloride, sodium azide, lithium aluminium hydride, zinc acetate [Zn(OAc)₂], tin (II) 2-ethylhexanoate, and horse liver esterase enzyme were purchased from Sigma Aldrich chemicals and used as received. Dimethyl acetamide (DMAc), tetrahydrofuran (THF), dimethyl formamide (DMF) and all other solvents were purchased locally and used after purification by standard procedures. 3-(4,5-dimethylthiazole-2-yl)-2,5-diphenyltetrazolium bromide salt (MTT), 4 % paraformaldehyde, DMSO were obtained from Sigma Aldrich.

4.2.2. Methods: ¹H and ¹³C NMR spectra were recorded in CDCl₃ and methanol D₄ containing tetramethylsilane (TMS) as internal standard using 400-MHz JEOL NMR spectrophotometer. Mass analysis of all the intermediate compounds was carried out using high resolution mass spectrometry-electrospray ionization-quantitative time-of-flight liquid chromatography-mass spectrometry (HRMS-ESI-Q-TOF LC-MS) and

Applied Biosystem 4800 PLUS MALDI TOF/TOF Analyzer. Gel permeation chromatographic (GPC) analysis of polymers was performed to determine the purity of polymer samples using Viscotek VE 1122 pump, Viscotek VE 3580 RI detector and Viscotek VE 3210 UV-Vis detector. Polymer samples for GPC were prepared in THF (with concentration 0.5 mg mL^{-1}) using polystyrene standards for calibration. Thermogravimetric analysis (TGA) was carried out to determine thermal stability of polymers using Perkin Elmer thermal analyser STA 6000 model at heating rate of $10 \text{ }^\circ\text{C/min}$ under nitrogen atmosphere. Subsequently thermal properties of the polymers were studied using TA Q20 Differential Scanning Calorimeter (DSC) with heating and cooling rate of $10 \text{ }^\circ\text{C/min}$. Size of the nanoparticles was determined by dynamic light scattering using Nano ZS-90 apparatus from Malvern instruments using red laser with 633 nm as light source. Absorption studies were performed using PerkinElmer Lambda 45 UV-Vis spectrophotometer. Steady state fluorescence spectra were recorded using Horiba Jobin Fluoromax fluorescence spectrophotometer. FE-SEM analysis was carried out by using Zeiss Ultra Plus scanning electron microscope. Atomic force microscope (AFM) images of nanoparticle samples drop casted on mica plates were recorded using Veeco Nanoscope IV instrument in tapping mode. Confocal microscope images were collected using LSM 710 confocal microscope.

4.2.3. Synthesis of 2-(2-(2-(2-hydroxyethoxy)ethoxy)ethoxy)ethyl 4-methylbenzenesulphonate (1). Tetraethylene glycol (5.0 g, 25.7 mmol) was dissolved in THF (40.0 mL) and this solution was added to aqueous solution of NaOH (40.0 mL) at room temperature. *p*-toluenesulfonylchloride (2.5 g, 12.8 mmol) was dissolved in THF (40.0 mL) and this solution was slowly added into the reaction mixture using dropping funnel under ice cold conditions followed by stirring under same condition for 2 h. After the completion of reaction, reaction mixture was poured in ice cold water and extracted into chloroform. Organic layer was separated and dried over sodium sulphate. The crude product was purified by column chromatography using chloroform and methanol as eluent. Yield = 6.0 g (67%) $^1\text{H-NMR}$ (CDCl_3 , 400 MHz) δ ppm: 7.78 (d, 2Ar-H), 7.33 (d, 2Ar-H), 4.16 (t, 2H, OH- CH_2), 3.59-3.70 (m, 12H, O- CH_2), 2.52 (t, 2H, O- CH_2), 2.44 (s, 3H, Ar- CH_3). $^{13}\text{C-NMR}$ (CDCl_3 , 100MHz) δ ppm: 140.3, 128.5, 70.4, 67.6, 61.3, 21.4

4.2.4 Synthesis of 2-(2-(2-(2-azidoethoxy)ethoxy)ethoxy)ethanol (2). Compound 1 was dissolved in DMF and sodium azide was added to it. The reaction mixture was

stirred at 80 °C for 12 h. reaction mixture was cooled to room temperature and poured into water followed by extraction with diethyl ether. The organic layer was separated and dried over anhydrous sodium sulphate. The crude compound was used for next step without purification. ¹H-NMR (CDCl₃, 400 MHz) δppm 3.71 (t, 2H, OH-CH₂), 3.36 (m, 10H, O-CH₂), 3.59 (t, 2H, O-CH₂), 3.38 (t, 2H, N₃-CH₂) ¹³C-NMR (CDCl₃, 100MHz) δppm 67.8, 69.5, 70.2, 70.8, 61.5.

4.2.5 Synthesis of 2-(2-(2-(2-aminoethoxy)ethoxy)ethoxy)ethanol (3). Compound 2 was dissolved in dry THF under N₂ atmosphere at room temperature. Lithium aluminium hydride was taken in round bottom flask and dry THF was added to it under N₂ in ice cold condition followed by addition of compound 2 solution in THF to it. Reaction mixture was stirred at 25 °C for 7 h under N₂. Subsequently reaction mixture was filtered and concentrated to get yellow oil which was used without purification for next reaction. ¹H-NMR (CDCl₃, 400 MHz) δppm 3.69 (t, 2H, OH-CH₂), 3.62-3.64 (m, 8H, O-CH₂), 3.58 (t, 2H, O-CH₂), 3.52 (t, 2H, O-CH₂), 2.83 (t, 2H, NH₂-CH₂) ¹³C-NMR (CDCl₃, 100MHz) δppm 67.8, 69.5, 72.3, 70.8, 61.5, 41.2

4.2.6. Synthesis of PBI initiator. PTCDA was taken in round bottom flask and DMAc was added it. Further compound 3 and Zn(OAc)₂ was added to it and the reaction mixture was heated at 140 °C for 12 h. After completion of reaction DMAc was removed by vacuum distillation. The crude product was washed with water, dried over sodium sulphate and purified by column chromatography using chloroform and methanol as eluent. Yield = 40 % ¹H-NMR (CDCl₃, 400 MHz) δppm 8.61 (d, 4Ar-H), 8.52 (d, 4Ar-H), 4.46 (t, 2H, N-CH₂), 3.88 (t, 2H, HO-CH₂), 3.62 (m, 24H, O-CH₂) ¹³C-NMR (CDCl₃, 100MHz) δppm 161.5, 130.1, 127, 9, 125.1, 122.8, 71.9, 69.2, 65.5, 43.9

4.2.7 Synthesis of t-butyl substituted polymers (PBI-BPCL₄₀). Ring opening polymerization was carried out to synthesize PBI-BPCL). The polymer was synthesized with [M]/[I] = 50. Hydroxyl functionalized PBI initiator (22.98 mg, 0.0309 mmol) was dissolved in 0.5 mL of dry THF in a schlenk tube and Sn(Oct)₂ (6.27 mg, 0.0154 mmol) as catalyst was added to it. This polymerization mixture was purged with nitrogen for 30 min. t-butyl substituted caprolactone monomer (400 mg, 1.5485 mmol) was dissolved in 0.5 mL dry THF and added to the polymerization

mixture and the purging was continued for another 30 min. The schlenk tube was immersed into preheated oil bath and the polymerization mixture was refluxed for 48 h under nitrogen atmosphere. After completion of polymerization the content was precipitated in hexane and the procedure was repeated to obtain pure polymer. Yield = 290 mg (58 %). $^1\text{H-NMR}$ (CDCl_3 , 400 MHz) δ ppm: 7.47-6.91 (m, 14 Ar-H), 4.44 (t, 4H), 4.14 (t, 6H), 3.96 (d, 4H), 3.75 (t, 2H), 3.66 (t, 1H), 2.45 (t, 4H), 1.85 (t, 4H), 1.44 (s, 9H), 0.98 (t, 6H) and 0.93 (t, 6H). $^{13}\text{C-NMR}$ (CDCl_3 , 100MHz) δ ppm: 173.3, 170.7, 127.5, 114.6, 80.4, 75.3, 65.8, 64.6, 61.1, 36.1, 32.7, 29.1, 22.9 and 14.0. FT-IR (cm^{-1}): 3580, 2974, 2875, 2361, 1884, 1731, 1632, 1473, 1363, 1252. GPC Mol. Wt

4.2.7. Synthesis of PBI-BPCL₁₅ polymer. The polymer was synthesized by following the above mentioned ROP procedure with $[\text{M}]/[\text{I}] = 25$. PBI initiator (46.01 mg, 0.0620 mmol), t-butyl ester substituted monomer (400 mg, 1.548 mmol), $\text{Sn}(\text{Oct})_2$ (12.51 mg, 0.0309 mmol) and dry THF 1.0 mL. Yield 300 mg (60%). $^1\text{H-NMR}$ (CDCl_3 , 400 MHz) δ ppm: 7.46-6.92 (m, 14 Ar-H), 4.45 (t, 4H), 4.13 (t, 6H), 3.96 (d, 4H), 3.75 (t, 2H), 3.66 (t, 1H), 2.45 (t, 4H), 1.86 (t, 4H), 1.44 (s, 9H), 0.99 (t, 6H) and 0.92 (t, 6H). $^{13}\text{C-NMR}$ (CDCl_3 , 100MHz) δ ppm: 173.9, 171.3, 158.3, 151.4, 131.8, 128.0, 122.1, 115.2, 110.5, 81.0, 75.9, 72.1, 65.2, 61.6, 40.2, 36.9, 33.3, 31.3, 29.3, 23.5, 14.5 and 11.7. FT-IR (cm^{-1}): 3530, 2968, 2874, 2361, 2008, 1731, 1630, 1508, 1470, 1366 and 1250.

Following similar polymerization condition caprolactone monomer was also synthesized to produce PBI-PCL₄₀ polymer with $[\text{M}]/[\text{I}] = 50$ and the details are given below.

4.2.8. Synthesis of PBI-PCL₄₀ polymer: Caprolactone monomer (400 mg, 1.548 mmol), PBI initiator (46.01 mg, 0.0620 mmol), $\text{Sn}(\text{Oct})_2$ (12.51 mg, 0.0309 mmol) and dry THF 1.0 mL. Yield 300 mg (60%). $^1\text{H-NMR}$ (CDCl_3 , 400 MHz) δ ppm: 7.46-6.92 (m, 14 Ar-H), 4.45 (t, 4H), 4.13 (t, 6H), 3.96 (d, 4H), 3.75 (t, 2H), 3.66 (t, 1H), 2.45 (t, 4H), 1.86 (t, 4H), 1.44 (s, 9H), 0.99 (t, 6H) and 0.92 (t, 6H). $^{13}\text{C-NMR}$ (CDCl_3 , 100MHz) δ ppm: 173.9, 171.3, 158.3, 151.4, 131.8, 128.0, 122.1, 115.2, 110.5, 81.0, 75.9, 72.1, 65.2, 61.6, 40.2, 36.9, 33.3, 31.3, 29.3, 23.5, 14.5 and 11.7. FT-IR (cm^{-1}): 3530, 2968, 2874, 2361, 2008, 1731, 1630, 1508, 1470, 1366 and 1250.

4.2.9 Synthesis of carboxylic acid substituted polymers (PBI-CPCL_x). PBI-BPCL₁₅ polymer (300 mg) was dissolved in dry DCM (3.0 mL) and trifluoroacetic acid (3.0 mL) was added slowly into the polymer solution and stirred at 30 °C for 30 min. The polymer content was concentrated and dissolved in THF and precipitated in methanol. ¹H-NMR (CD₃OD, 400 MHz) δppm: 7.47-6.92 (m, 14 Ar-H), 4.45 (t, 4H), 4.14 (t, 6H), 3.95 (d, 4H), 3.76 (t, 2H), 3.66 (t, 1H), 2.45 (t, 4H), 1.85 (t, 4H), 0.98 (t, 6H) and 0.93 (t, 6H). ¹³C-NMR (CDCl₃, 100MHz) δppm: 173.6, 170.6, 80.7, 75.5, 64.9, 61.3, 36.5, 33.0, and 29.0. FT-IR (cm⁻¹): 3581, 2974, 2875, 2361, 1884, 1731, 1632, 1473, 1363 and 1252

Following similar procedure deprotection of PBI-BPCL₄₀ polymer was carried out and the details are given below.

4.2.8. Synthesis of PBI-CPCL₄₀ polymer: ¹H-NMR (CD₃OD, 400 MHz) δppm: 7.45-6.92 (m, 14 Ar-H), 4.45 (t, 4H), 4.13 (t, 4H), 3.96 (d, 4H), 3.76 (t, 2H), 3.66 (t, 1H), 2.44 (t, 4H), 1.84 (t, 4H), 0.99 (t, 6H) and 0.93 (t, 6H). ¹³C-NMR (CDCl₃, 100MHz) δppm: 173.3, 170.7, 127.5, 80.4, 75.3, 64.6, 61.1, 36.1, 32.7, 29.5, 14.0 and 11.5. FT-IR (cm⁻¹): 3581, 2973, 2875, 2361, 1884, 1730, 1632, 1473, 1365 and 1251

4.2.10. Cell-viability assay (MTT assay): The cytotoxicity polymer nanoparticles was studied in HeLa and MCF-7 cell line using the tetrazolium salt, 3,4,5-dimethylthiazol-2,5-diphenyltetrazolium bromide (MTT). In a 96-well plate (Corning, USA), 1000 cells were seeded per well in 100 μL of DMEM with 10% FBS (fetal bovine serum) and allowed to adhere for 16 h. Prior to drug treatment, media from the cells was aspirated and various concentrations of polymer nanoparticles were added as feed. A blank control, DMEM with FBS in the absence of cells and an untreated control, cells with DMEM containing FBS, were used in each experiment. All control and treated experiment wells were in triplicate. Cells were incubated for 24 h without a change in medium and after 24 h the drug containing medium was aspirated. A freshly prepared stock solution of MTT in sterile PBS (5 mg/mL) was diluted to 50 μg/mL in DMEM. 100 μL of this solution was added to each well. Cells were then incubated with MTT for 4 h at 37 °C. medium with MTT was then aspirated from the wells and the purple formazan crystals that formed as a result of reduction of MTT by mitochondrial dehydrogenase enzyme from the cells were dissolved in 100 μL of

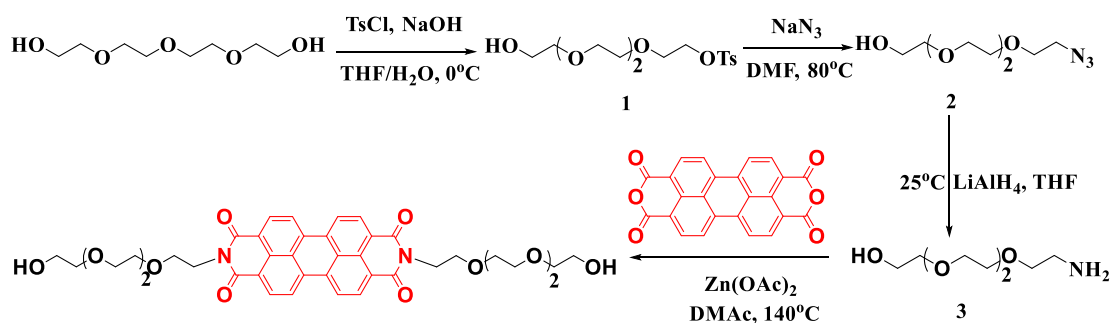
DMSO (added per well). The absorbance from the formazan crystals was immediately measured using a micro plate reader at 570 nm (Varioskan Flash) and was representative of the number of viable cells per well. Values from triplicate run for each control and treated set were noted and their mean value was used for calculations.

4.2.11. Cellular uptake studies using confocal microscopy: HeLa cells were seeded at a density of 1×10^5 cells on flame dried cover slips coated placed in 6 well plates containing DMEM medium with 10 % FBS. The cells were incubated at 37 °C for 16 hours and then exposed to the required concentrations of polymer nanoparticles and for 4 h in a CO₂ incubator at 37 °C. After incubation, drug-containing medium was aspirated from each well, and cells were washed twice with PBS (1 mL per wash) and fixed with 4 % paraformaldehyde solution in PBS for 10 minutes at room temperature. The cells were washed twice with PBS (1 mL per wash) and stained with phalloidin conjugated to Alexa 488 (invitrogen) diluted 1: 100 in 5 % BSA solution in PBS. This incubation was performed in the dark and excess of dye was washed from the cells with PBS. The cover slips were mounted on slides using Fluoromount-G mounting medium (Southern Biotech). Slides were then dried overnight at room temperature in the dark. The cells were imaged using a LSM 710 confocal microscope with the λ 420 nm (blue channel), λ 560 nm (red channel) and lasers. Images thus obtained were analyzed using Image J analysis software and the image for each channel was separated.

4.3 Results and Discussion

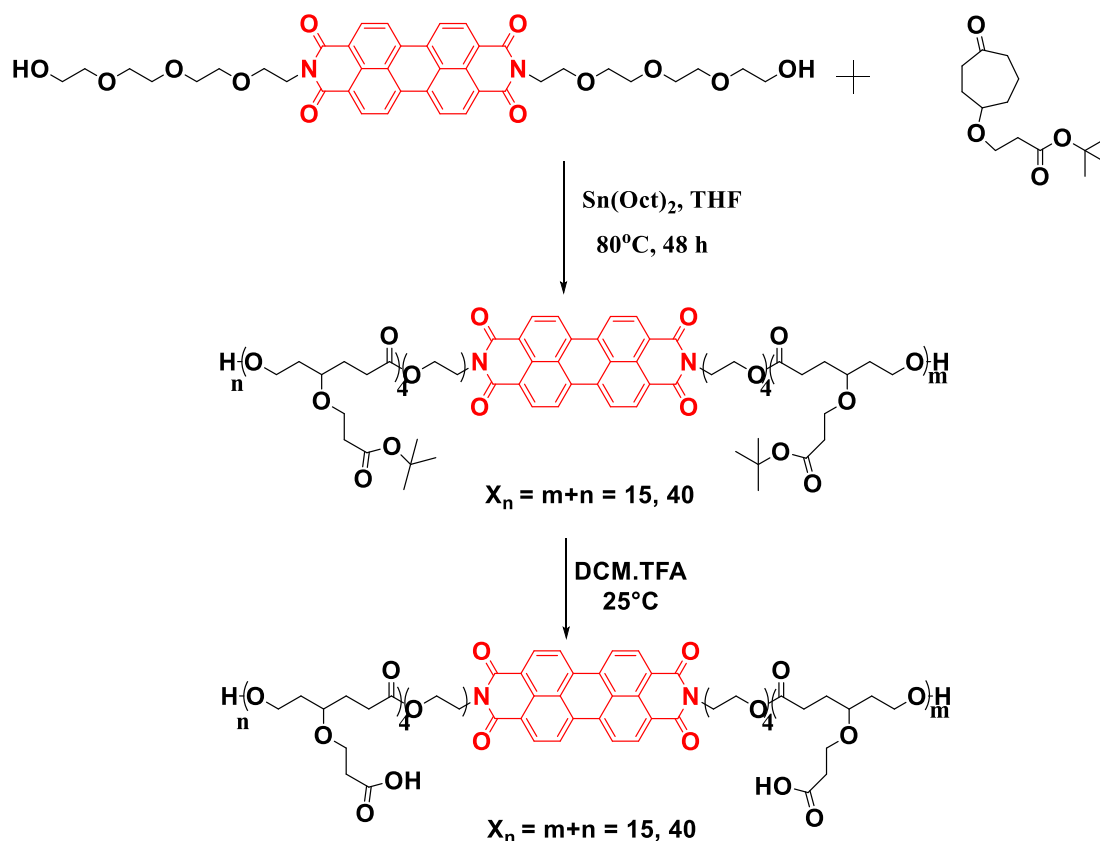
4.3.1. Synthesis of Fluorescent PBI-PCL Block Copolymers

The N-substituted hydroxyl functionalized perylene bisimide (PBI) initiator was synthesized following the steps as shown in scheme 4.1. Tetraethylene glycol was reacted with *p*-toluenesulfonylchloride to give monotosylated product (compound **1**). The monotosylated tetraethylene glycol was converted into azide using sodium azide (compound **2**) followed by reduction with LAH to give amine (compound **3**). The symmetrical N-substituted perylenebisimide was obtained by reacting perylene-3,4,9,10-tetracarboxylic dianhydride (PTCDA) with compound **3**. The resulting PBI initiator was characterized by ¹H, ¹³C NMR, and mass spectrometry analysis.



Scheme 4.1. Synthetic scheme of hydroxyl functionalized perylene bisimide initiator.

t-Butyl substituted caprolactone monomer (compound 8 from chapter 2) was synthesized from 1,4-cyclohexanediol using procedure reported in chapter 2. The ring opening polymerization of t-butyl substituted caprolactone monomer was carried out by employing fluorescent hydroxyl functionalized perylene bisimide (PBI) as initiator and $\text{Sn}(\text{Oct})_2$ as catalyst in THF as shown in Scheme 4.2.



Scheme 4.2. Synthetic scheme of PBI containing block copolymers from t-butyl carboxylic ester substituted caprolactone monomer

Two different polymers were synthesized by varying the t-butyl substituted caprolactone monomer to PBI initiator molar ratio in the feed as $[M]/[I] = 25$, and 50. The polymerization was carried out in THF solvent at 80 °C for 48 h. polymers were purified by repeated precipitation in hexane. Further the polymers were subjected to selective deprotection of t-butyl ester using trifluoroacetic acid to obtain corresponding carboxylic acid functionalized derivatives.

The proton NMR spectra of PBI initiator and PBI-BPCL₄₀ are shown in figure 4.7. The degree of polymerization was determined by comparison of the peak intensities of N-CH₂ proton from PBI initiator which appeared at 4.48 ppm (proton a) with proton 'f' from the PCL part. The degree of polymerization was found to be 40 repeating units for the M/I = 50 in the feed. A similar NMR analysis was carried out for the polymer synthesized with M/I = 50 in the feed and the degree of polymerization was determined to be 15.

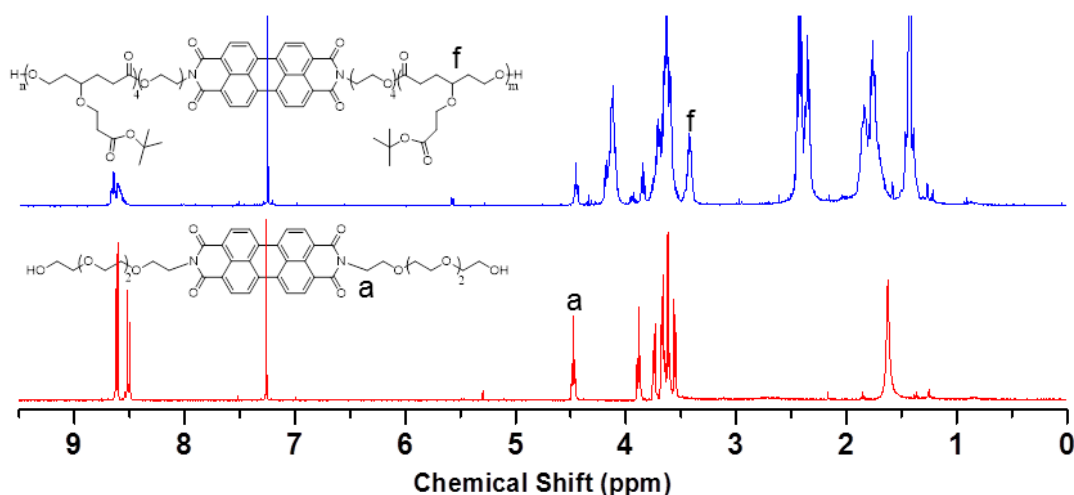


Figure 4.7. ¹H-NMR spectra of PBI initiator and PBI-BPCL₄₀ in CDCl₃.

The deprotection of t-butyl substituted polymers was confirmed by ¹H NMR spectra as shown in figure 4.8 wherein the protons at 1.45 ppm corresponding to t-butyl group were completely disappeared. This analysis further revealed the successful deprotection of t-butyl group to produce carboxyl substituted polymers without disturbing the polymer backbone structure.

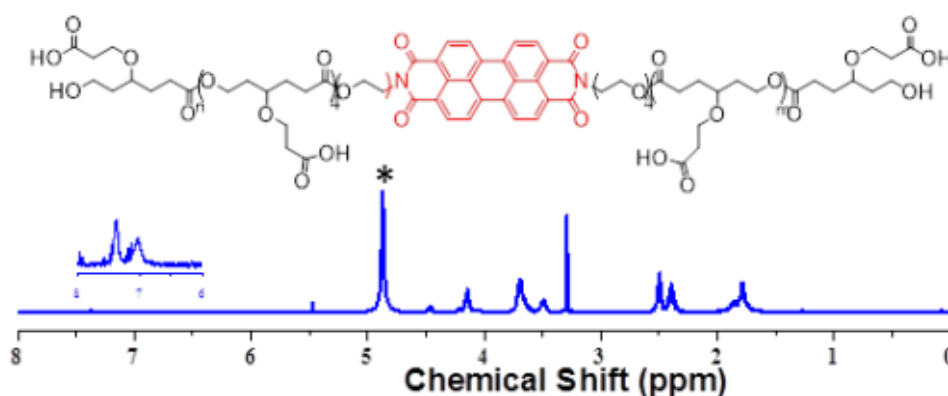


Figure 4.8. $^1\text{H-NMR}$ spectra of PBI-CPCL₄₀ in methanol D_4 .

The molecular weights, polydisperties and the purity of the polymers were determined by size exclusion chromatography using polystyrene standards and the corresponding chromatograms are shown in figure 4.9. The number average (M_n) molecular weight, weight average (M_w) molecular weight and their polydispersity are summarized in table 4.1. All the polymers showed monomodal distribution indicating the purity of polymers and relatively low polydispersities ~ 1.4 . Further distinct difference in the retention time of the polymers and PBI initiator confirmed the formation of polymers. Thus well-defined homogeneous polymers were obtained from ring opening polymerization process. The polymers were referred as PBI-BPCL_x and PBI-CPCL_x wherein x represents the number of t-butyl substituted caprolactone (B) and carboxylic acid monomer repeating unit present at both sides of the PBI core

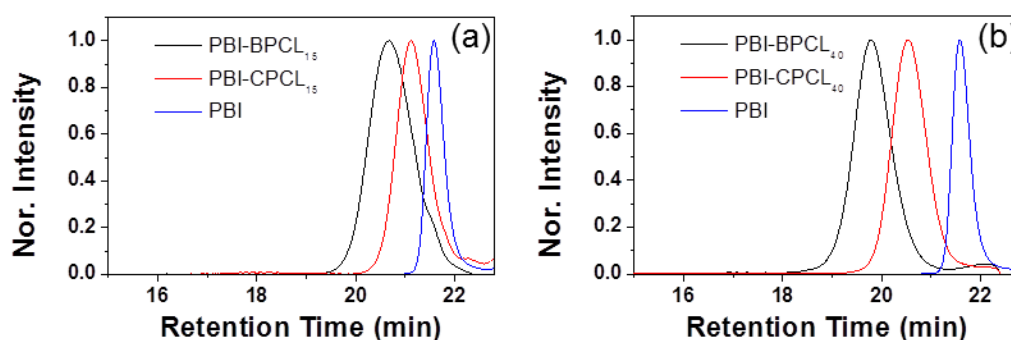


Figure 4.9. GPC chromatograms of PBI containing block copolymers in THF

Table 4.1: Molecular weights of PBI-BPCL_x polymers determined by GPC and NMR

Polymer	M _n ^a	M _n ^b (g/mol)	M _w ^b (g/mol)	M _w /M _n ^b	T _g (°C)	T _D (°C)
PBI-BPCL ₁₅	4600	2600	3600	1.36	-44.1	220
PBI-BPCL ₄₀	11100	7200	9000	1.25	-37.5	220
PBI-CPCL ₁₅	3800	1400	3300	1.28	-38.7	250
PBI-CPCL ₄₀	8700	2900	3700	1.26	-30.8	250
PBI-PCL ₄₀	5300	2500	4000	1.4	-40.7	220

^(a)Molecular weights are determined by ¹H-NMR and calculated as $M_n = (\text{repeating unit mass}) \times n$. ^(b)Molecular weights and PDI determined by GPC.

The ROP process was first optimized for fixed monomer to initiator ratio as $[M]/[I] = 50$ and the optimization was done by varying the polymerization temperature and time. The degree of polymerization (from NMR) and GPC molecular weights of polymer obtained in various reaction conditions are summarized in the table 4.2. A maximum of 40 repeating units were obtained in the ROP process at 80 °C for 48 h polymerization. Hence, these reaction conditions were followed to study the kinetics of ROP. Since the PBI is bifunctional initiator, the ROP initiation occurs at both ends and the polymer chain grows at both sides of the PBI core.

Table 4.2: Molecular weights of PBI-BPCL_x polymers determined by GPC and NMR

Sr. No.	Temp (°C)	Time (h)	No. of Repeating units (NMR) ^a	M _n (g/mol) ^b	M _w (g/mol) ^b	PDI ^b
1	80	20	17	2600	3400	1.29
2	80	36	30	6800	8600	1.24
3	80	48	40	7200	9000	1.25
4	80	72	34	6300	9200	1.47
5	60	48	22	2800	4500	1.56
6	70	48	25	2900	3700	1.26

^(a)no. of repeating units are determined by ¹H-NMR. ^(b)Molecular weights and PDI determined by GPC.

The polymerization kinetics was carried out for t-butyl substituted caprolactone monomer with $M/I = 50$. For this purpose, aliquots were taken at regular intervals up to 48 h and for these aliquots were subjected to NMR and GPC analysis. The GPC plot (figure 4.10a) showed gradual increase in molecular weight with polymerization time. Similarly, the plot for molecular weight M_n obtained from NMR versus polymerization time (figure 4.10b) also showed liner trend and polydispersity values obtained as ≈ 1.4 and did not change much with reaction time (figure 4.10c). These results confirmed that desired molecular weight polymers can be produced by controlled ROP process.

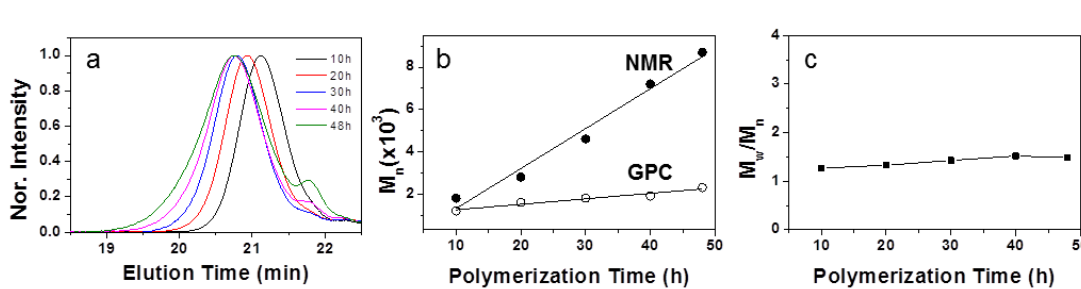
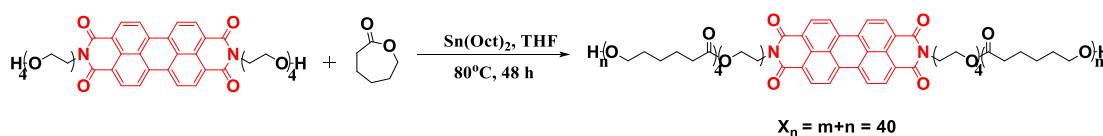


Figure 4.10. GPC chromatograms of PBI-BPCL_x in tetrahydrofuran (a). Plots of M_n (determined by $^1\text{H-NMR}$ and GPC) vs polymerization time (b) and M_w/M_n versus the polymerization time (c).

Following a similar ROP methodology, a polymer from ϵ -caprolactone was also synthesized with monomer to initiator ratio as 40 as shown in scheme 4.3. This non-substituted analogue was named as PBI-PCL_x.



Scheme 4.3. Synthetic scheme of PBI containing block copolymers from caprolactone monomer

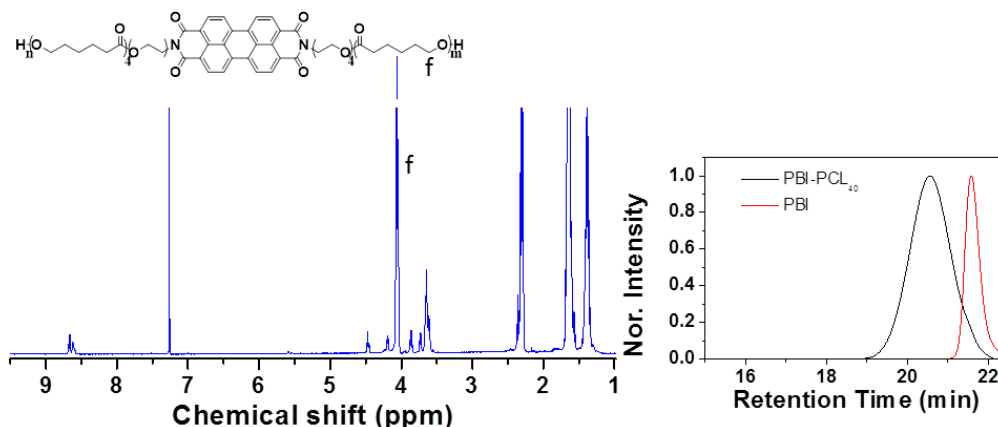


Figure 4.11. $^1\text{H-NMR}$ spectra and GPC chromatogram of PBI-PCL_{40} in CDCl_3 .

The proton NMR spectra of PBI-PCL_{40} are shown in figure 4.5. The degree of polymerization was determined by comparison of the peak intensities of N- CH_2 proton from PBI initiator which appeared at 4.48 ppm (proton a) (as shown in figure 4.1) with proton 'f' from the PCL part. The degree of polymerization was found to be 40 repeating units for the $M/I = 50$ in the feed. The comparison of no of repeating units obtained for t-butyl ester substituted ϵ -caprolactone and ϵ -caprolactone for the feed $[M]/[I]$ ratio are equal which shows that reactivity of PBI initiator is similar towards both the monomers for ROP process. The molecular weights, polydisperties and the purity of the polymers were determined by gel permeation chromatography and the corresponding chromatograms are shown in figure 4.11. The number average (M_n) molecular weight, weight average (M_w) molecular weight and their polydispersity are summarized in table 4.1. The polymer showed monomodal distribution indicating the purity of polymer.

Thermal properties of the newly synthesized polymers were investigated by TGA and DSC with $10\text{ }^\circ\text{C}/\text{min}$ heating rate under nitrogen atmosphere and the plots are shown in figure 4.12. From TGA plots it is evident that all the polymers were stable up to $220\text{-}250\text{ }^\circ\text{C}$. The DSC thermograms in figures 4.12b and 4.12c clearly showed that t-butyl ester substituted block copolymers and their deprotected analogues were completely amorphous in nature due to the bulky substitution on the polymer backbone which hampered the packing of the polymer chains. Interestingly, non-substituted PCL block copolymer PBI-PCL_{40} was found to be semi-crystalline.

The degradation temperatures and glass transition temperatures of the polymers are summarized in table 4.2.

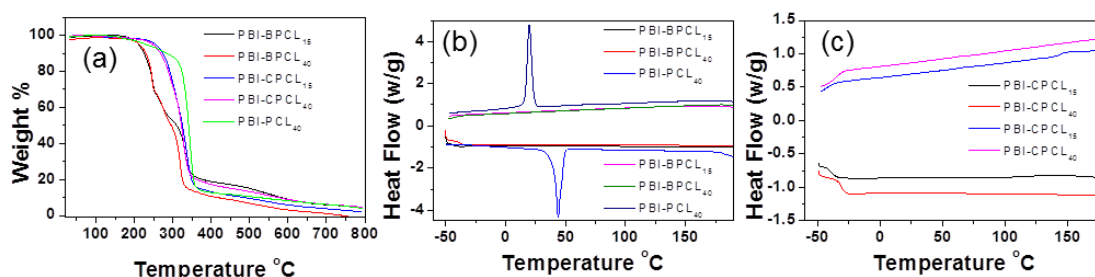


Figure 4.12. TGA profile (a), DSC thermograms of PBI-BPCL_x and PBI-PCL_x polymers (b), PBI-CPCL_x polymers (c).

4.3.2. Self-Assembly of PBI-CPCL Amphiphilic block copolymers

In the present investigation, the block copolymer was engineered rigid hydrophobic PBI unit in the middle which was sandwiched between the hydrophilic carbocyclic functionalize PCL chains. This unique design provide optimum geometry to self-assembly the polymer chains differently in organic and in aqueous medium. While evaporating the dropcast the polymer samples from the organic solvent such as THF on substrate, the polymer chains underwent long-range phase segregation of like-like interactions to produce nano-fibrous morphology. On the other hand, it is anticipated that the phase segregation of hydrophilic-hydrophobic segments in the block is expected to align as hair-pin bend type amphiphiles in water. Subsequent aggregation of these hair-pin type amphiphiles produces compact spherical nanoparticle assemblies. In these arrangements, the PBI units occupy at the middle of the nanoparticle core; thus, it could able to retain the fluorescence characteristics in aqueous medium for several applications including bio-imaging. The self-assembly phenomena of the PBI-CPCL blocks are shown schematically Figure 4.13.

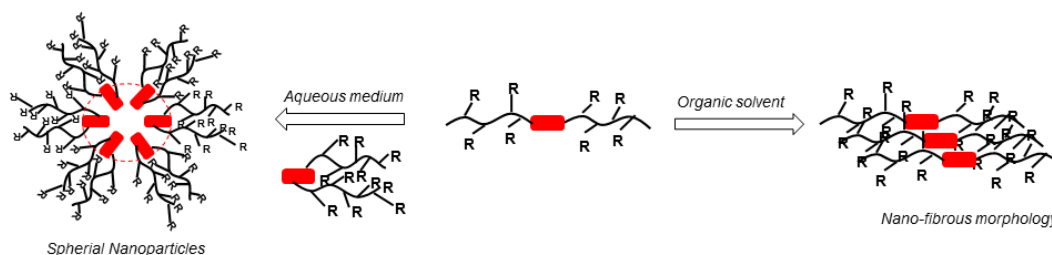


Figure 4.13. Schematic representation of self-assembly phenomenon of block copolymers in organic and aqueous medium.

The self-assemblies of these newly synthesized fluorescent block copolymers were investigated in organic solvent (THF) and in aqueous medium. Electron and atomic force microscopic analysis was carried out to visualize the morphology of the polymer films drop-caste from organic solvent (THF). The field emission scanning electron microscope images of PBI-CPCL₁₅ and PBI-CPCL₄₀ are shown in figure 4.14a and 4.14b and AFM image for PBI-CPCL₁₅ is shown in figure 4.14c. FESEM images clearly showed the formation of helical nano-fibres. The average thickness and length of the nano-fibers were estimated to be 20 ± 5 nm and $3 \pm 0.5 \mu\text{m}$ respectively for PBI-BPCL₁₅. Similarly PBI-BPCL₄₀ produced nano-fibers with average thickness and length of 45 ± 5 nm and $4 \pm 1 \mu\text{m}$ respectively.

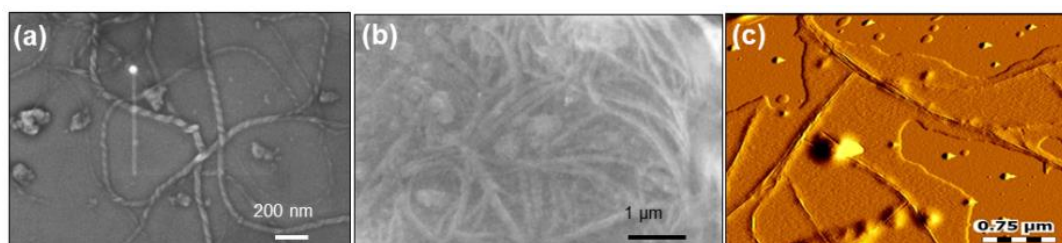


Figure 4.14. FE-SEM images of PBI-BPCL₁₅ (a) and PBI-BPCL₄₀ (b), and AFM image of PBI-BPCL₁₅ (c). The polymer concentration was maintained as 0.1 mg/mL and the images were recorded for dropcaste films.

The ability of these PBI-CPCL polymers to produce stable self-assemblies in aqueous medium was investigated. For this purpose, the polymer was dissolved in DMSO+water (2:3 v/v/) and the resultant solution was dialyzed against large excess of water for 48 h using semipermeable membrane having MWCO of 3500 g/mol. Fresh water was relished in the reservoir periodically to remove the DMSO completely. In this process, the polymer chains self-assembled as shown in Figure

4.15 to produce stable nano-aggregates. A red colour clear aqueous polymer solution was obtained at the end of the dialysis (photograph of vials shown in figure 4.15

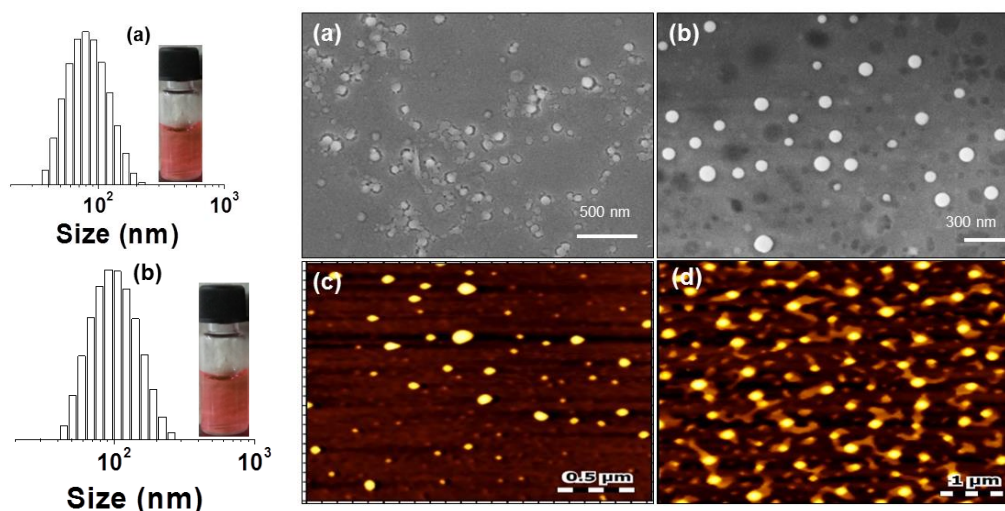


Figure 4.15. DLS histograms of PBI-CPCL15 (a), and PBI-CPCL40 (b). FE-SEM and AFM images of PBI-CPCL15 (a,c) and PBI-CPCL40 (b,d), respectively (aqueous dialysis solution).

The size of the polymer aggregates was determined by dynamic light scattering (DLS) analysis and their DLS histograms are shown in figure 4.15a and 4.15b. The histograms clearly showed the existence of uniform mono-modal distribution of nanoparticles with average sizes 90 ± 5 nm and 110 ± 5 nm for PBI-CPCL₁₅ and PBI-CPCL₄₀ polymer, respectively. The morphology and size of these polymer nano-aggregates were investigated by FESEM and AFM analysis. FE-SEM images of PBI-CPCL₁₅ and PBI-CPCL₄₀ are shown in figure 4.15c and 4.15d, respectively, which indicates the existence of soft spherical nano-aggregates. The nanoparticles exhibited average size of 80 ± 10 nm and 100 ± 15 nm for PBI-CPCL₁₅ and PBI-CPCL₄₀, respectively. The spherical morphology was further confirmed by AFM analysis (see figure 4.15) and the sizes of the polymer nanoparticles are in good agreement with FESEM analysis. The nanoparticle size of the aqueous aggregates were found to almost identical both in the DLS and FE-SEM (or AFM) indicating that these aggregates indeed stabilized in the aqueous solution and they were not disturbed during the morphological analysis. These results confirmed that the newly designed PBI-CPCL block copolymer is unique to produce stable spherical nano-assemblies of in aqueous environment.

4.3.3. Photophysical Characterization

To investigate the photophysical properties of PBI chromophore absorption and emission spectra of the PCL block copolymers were recorded in organic solvent as well as in aqueous medium. Figure 4.16 shows the absorption and emission spectra of block copolymers in THF. The absorption band between 450 to 530 nm can be assigned to $0 \rightarrow 0$, $0 \rightarrow 1$, $0 \rightarrow 2$, $0 \rightarrow 3$ transitions of $S_0 \rightarrow S_1$ band. Thus, PBI chromophore exhibit well resolved vibronic structure corresponding to $S_0 \rightarrow S_1$ transitions with transition dipole moment along the long axis of PBI molecule.⁴⁶ The emission spectra of the polymers were (recorded at $\lambda_{\text{excitation}}$ of 485 nm) mirror images corresponding to $S_0 \rightarrow S_1$ absorption band indicating the well resolved fine structure of PBI chromophore. The absorption and emission spectra of the block copolymer nano-assemblies were also recorded in aqueous medium as shown in figure 4.16. It can be seen from the figure 4.16c that spectra became broader and less structured in aqueous medium which may be attributed to the electronic coupling between the PBI chromophores. The emission spectra of these polymers at $\lambda_{\text{excitation}}$ of 495 nm showed the characteristic fluorescence of PBI.

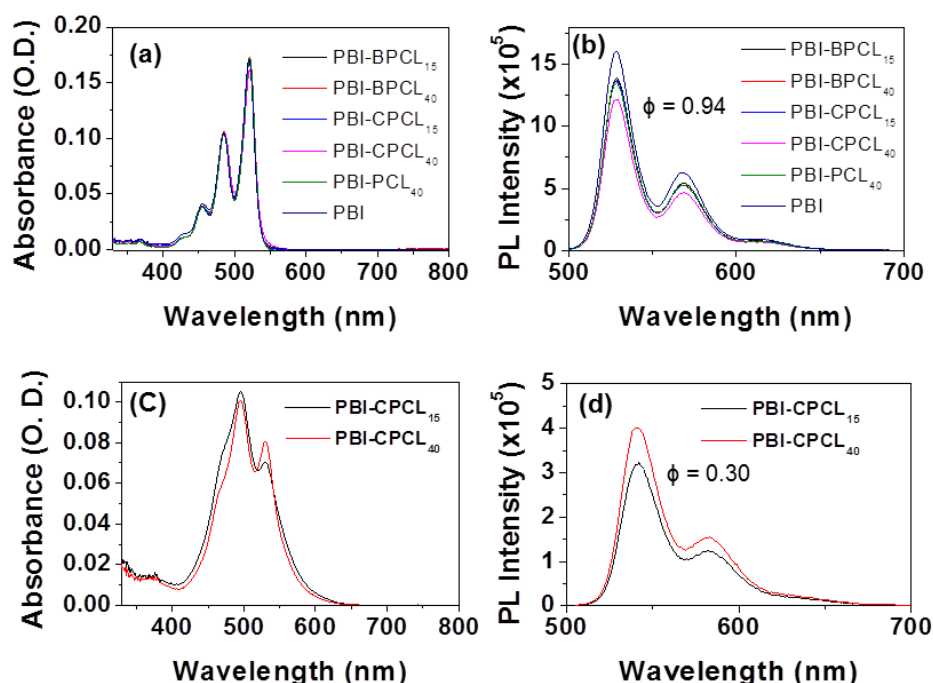


Figure 4.16. Absorbance (a) and emission (b) spectra of block copolymers in THF. Absorbance (c) and emission (d) spectra of aqueous dialysed block copolymers.

The fluorescence quantum yield of the block copolymers was in THF and water using *N,N'*-bis(hexyl heptyl)perylene-3,4,9,10-bis(dicarboximide) as standard in

chloroform.³⁶ In THF the fluorescence quantum yields were found to be 0.90 and 0.93 for PBI-CPCL₁₅ and PBI-CPCL₄₀, respectively. In aqueous medium the quantum yields were found to be 0.23 and 0.30 for PBI-CPCL₁₅ and PBI-CPCL₄₀, respectively. The quantum yields of the PBI-CPCL nanoparticles in aqueous solution are in the similar range of other PBI systems reported for bio-imaging application (ref).^{25,47} In the present case, the good fluorescence quantum yield of PBI in the block copolymer may be attributed to the fact that the polymer structure consist of rigid hydrophobic PBI in the middle and hydrophilic carboxylic acid substituted caprolactone units at both the ends which are expected to reduce the possible aggregation of PBI chromophore in aqueous medium.

Time resolved fluorescence life time measurements of PBI-CPCL polymer were carried out in organic solvent THF and in aqueous medium. The decay measurements were carried out at 460 nm LED as excitation source and the decay were collected at respective emission maxima. The decay profile and the life time data are given in figure 4.17 Polymer in THF showed single exponential fit with life time of 4.43 ns corresponding to isolated species in excited state. The polymer nanoparticles in aqueous medium exhibited biexponential decay corresponding to isolated and aggregated species in the excited state. Moreover, polymer showed similar decay profile and the average life time of polymer in THF and water is almost similar which indicated that in water the aggregated excited species did not lose the excitation energy by nonradiative processes and retained its delayed emission which is beneficial for bioimaging application.

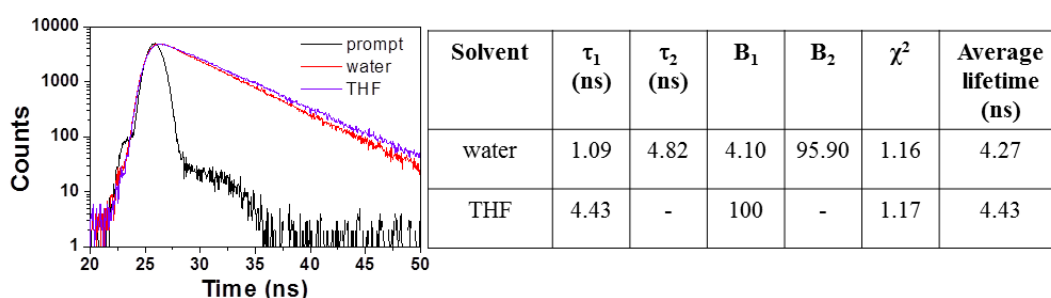


Figure 4.17. TCSPC decay profile and life time data for PBI-CPCL40 in organic and aqueous medium recorded by 460 nm LED source and collected at emission maxima 540 nm.

To get more insight into the aggregation behaviour of PBI, solvent dependent UV-Vis spectroscopic studies were carried out for PBI-CPCL40 block copolymer. Figure 4.18 shows UV-Vis spectra recorded for the block copolymer in THF/water solvent combination. The absorption spectra revealed well resolved vibronic structure corresponding to $S_0 \rightarrow S_1$ transition with most intense band at 520 nm indicating that PBI is in molecularly dissolved (nonaggregated) state in THF. Upon increasing the amount of water, a gradual decrease in the absorption coefficient was observed. Further spectral features were also changed and spectra became broader and less structured which is attributed to the electronic interactions between the chromophores. As seen in figure 4.18, a gradual decrease in the emission intensity (excited at 495 nm) of PBI with concomitant decrease in the absorption coefficient was observed which was further confirmed from the plot of PL intensity versus THF/ Water composition. Hence, all these photophysical studies conclude that the PBI containing block copolymers can be utilized for bio-imaging application as they exhibit desired water solubility and quantum yield in aqueous medium.

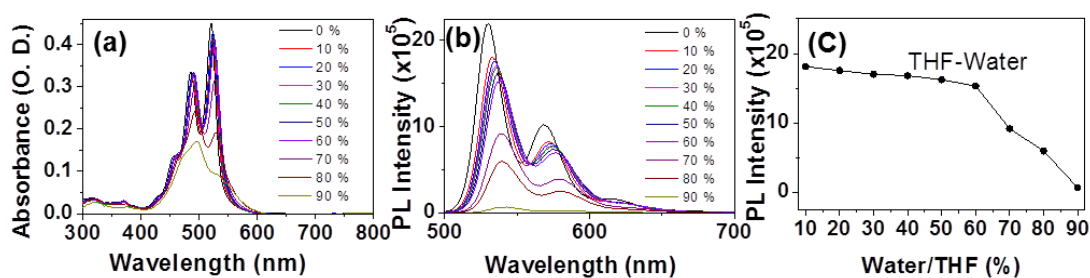


Figure 4.18. Absorption (a) and emission (b) spectra of PBI-CP4.4CL40 polymer in THF/water combination, plot of PL intensity versus solvent composition (c).

4.3.4. Enzyme-responsive Biodegradation of PBI-CPCL

Florescent polymer nanoparticles encounter two important challenges while employing them for cellular imaging in biological system; (i) they should possess significant stability under extracellular conditions, and (ii) should be capable of biodegradable into smaller segments under intracellular stimuli so that they can be excreted from the cellular environment once the action is performed. These two steps are shown in Figure 4.19a. In the present investigation, the PBI-CPCL blocks are designed with biodegrade aliphatic polyester chains (PCL chains); hence, they can be readily enzymatically-biodegraded by intracellular enzymes such as esterase present

in the lysosomal compartments. Stability of polymer nanoparticles under physiological conditions is the desirable property for the bio-imaging application. Therefore, stability of the block copolymer nanoparticles was investigated in PBS 7.4 at 37 °C by monitoring change in the size of the nanoparticle utilizing DLS up to 48h. Figure 4.19b represents the DLS histograms at various time points and it is evident that mean diameter of the polymer nanoparticle did not change over the period of time. Hence the block copolymer nanoparticles are stable under physiological condition. The backbone of the fluorescent PCL block copolymer constitute with aliphatic ester linkage therefore they are prone to degrade in presence of esterase enzyme under physiological conditions. DLS was utilized to evaluated enzymatic biodegradation of the block copolymers.

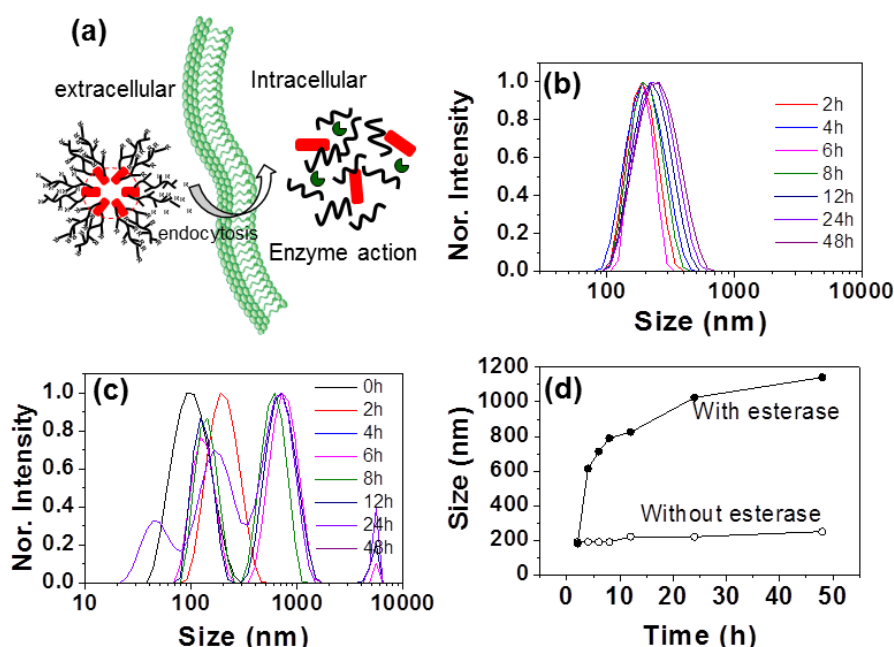


Figure 4.19. The DLS histograms of PBI-CPCL40 polymer nanoparticles incubated in PBS 7.4 at 37 °C in absence of esterase (a), in presence of esterase (b), plot for size of the polymer nanoparticles vs incubation time (c).

To demonstrate the enzymatic biodegradation, polymer nanoparticles were incubated with esterase enzyme in PBS 7.4 at 37 °C and DLS measurements were carried out at regular time interval as shown in figure. A gradual change from mono-modal to multi-modal size distribution with increase in mean diameter was observed. Increase in the size of the polymer nanoparticle was attributed to cleavage of the polymer backbone by esterase enzyme to produce oligomer species. As a result, polymer nanoparticle disassembled due to the disturbance in amphiphilicity and the

resulting oligomer species lose the hydrophobic-hydrophilic balance to form large size aggregates in the aqueous medium. Further size of the nanoparticle vs incubation time plot as shown in figure 4.19c demonstrates the stability of block copolymer under physiological conditions as there is no appreciable change in the size of the polymer NP with incubation time. On the other hand size of the nanoparticle increased gradually due to the enzymatic biodegradation of the polymer.

The enzymatic biodegradability of block copolymers was also investigated by GPC analysis. For this purpose, block copolymer PBI-CPCL₄₀ was dissolved in PBS 7.4 in presence of esterase enzyme and stirred at 37 °C for 48 h. Aliquots were taken periodically and GPC analysis was performed and the GPC plots are shown in Figure 4.20a. The molecular weight (M_n) obtained from GPC analysis was plotted against esterase incubation time as shown in figure 4.19b. The plot revealed gradual decrease in the molecular weight of the polymer due to the degradation of long polymeric chain by esterase enzyme which results in the formation of low molecular weight fragments. Thus, the newly synthesized fluorescent PCL block copolymers were stable at extracellular conditions and undergo enzymatic biodegradation at intracellular conditions.

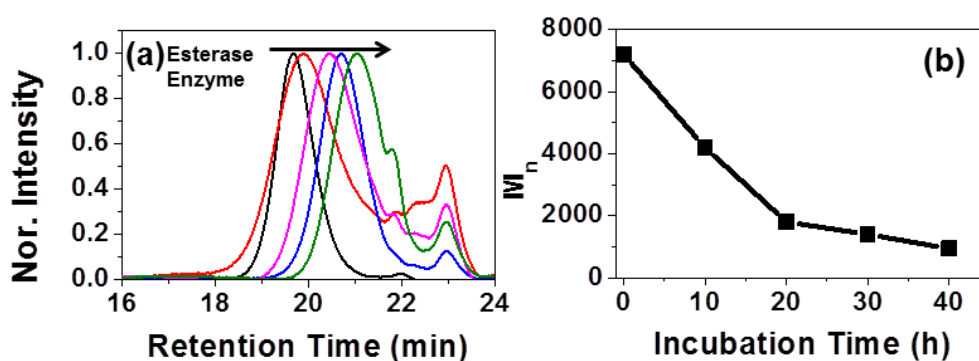


Figure 4.20. GPC chromatograms of aliquots of polymer incubated with esterase enzyme at various time points (a) and plot for molecular weight (M_n) obtained from GPC versus incubation time (b).

4.3.5. Cytotoxicity and Cellular Uptake of Polymer Nanoparticles

Biocompatibility of polymer nanoparticle is a primary concern for their potential use in biomedical application. In order to demonstrate the biocompatibility, cervical cancer (HeLa) and breast cancer (MCF-7) cells were incubated with block copolymer nanoparticles at various concentrations (from 1 to 100 $\mu\text{g/mL}$) for 48 h and MTT assay was carried out in HeLa and MCF-7 cell line. MTT is colorimetric assay wherein the cell viability is evaluated by reduction of MTT in to formazan and figure 4.21 shows the cell viabilities of PBI-CPCL₁₅ and PBI-CPCL₄₀ polymer nanoparticles in HeLa and MCF-7 cells. The results showed that more than 80 % cell viability was retained up to 100 $\mu\text{g/mL}$ concentration of the polymer nanoparticles. Thus the low cytotoxicity of block copolymer nanoparticles further confirmed that they are potential candidates for biomedical applications.

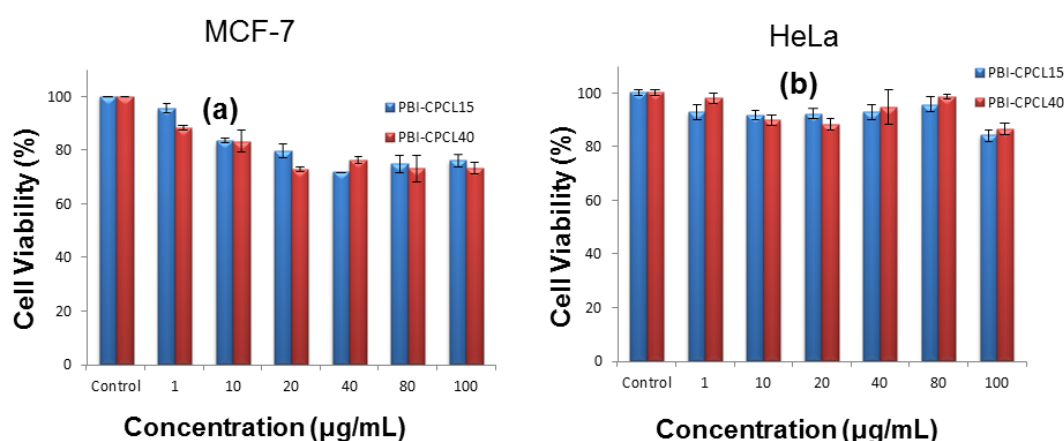


Figure 4.21. Cytotoxicity studies of PBI-CPCL_x block copolymers in MCF-7 cells (a) and HeLa cells (b).

Therefore, the highly biocompatible, biodegradable red luminescent polymer nanoparticles were demonstrated for the *in vitro* cellular imaging in cervical cancer HeLa cell line. The cellular uptake was studied by incubating the polymer nanoparticles with HeLa cells and the imaging was performed using confocal laser scanning microscope (CLSM). The polymer nanoparticles were stained with DAPI to visualize the nuclei of the cells. The CLSM images of the polymer nanoparticles are shown in figure 4.22. The cells were observed for the red luminescence (λ 514 nm laser) from the PBI chromophore in the polymer NP as shown in figure 4.19c and 4.19g which confirmed that the polymer NP was taken up by the cells and mainly

localized in the cytoplasm and perinuclear region. The cells were also observed through blue channel (λ 405 nm laser) for DAPI stain (figure 4.22b,f). The merged images again confirmed that the polymer NP was preferably accumulated in the cytoplasm. Thus the cellular uptake studies revealed that these PBI containing polymer nanoparticles were readily internalized into the HeLa cells and red fluorescence of PBI chromophore was preserved at the intracellular conditions hence current polymer design is very efficient for cellular imaging in cancer cells.

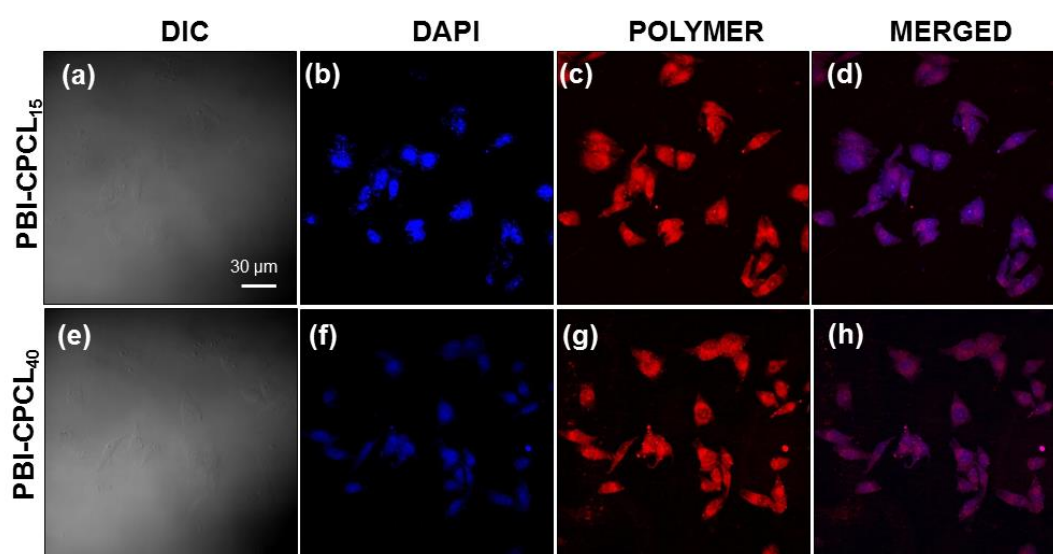


Figure 4.22. CLSM images of HeLa cells incubated with block copolymer nanoparticles. Cells were stained with DAPI (b, f) and observed for red fluorescence of PBI (c, g),

4.4 Conclusion

In conclusion, novel highly luminescent, enzyme responsive, amphiphilic PCL block copolymers were successfully synthesized and demonstrated for the cellular imaging application in the cancer cells. For this purpose, ROP process was optimized for t-butyl ester substituted caprolactone monomer and hydroxyl functionalized red fluorescent PBI chromophore as initiator. Molecular weight of the polymers was controlled by monomer to initiator ratio in the ROP process. Further t-butyl ester substituted PCL polymers were successfully converted into carboxyl substituted PCL polymers which rendered the amphiphilicity to the block copolymers. The PCL block

copolymers exhibited nanofibrous morphology in organic solvent THF and in aqueous medium spherical nanoparticles of ~100 nm were observed. The photophysical properties of PBI chromophore in the block copolymer were studied in detail. The hydrophilic PCL arms ensured the water solubility thereby reducing the aggregation of PBI chromophore in block copolymers which resulted in retaining the desirable photophysical properties in aqueous medium. The PCL block copolymers were studied for their enzyme responsive biodegradation as the polymer backbone constituent aliphatic ester linkages which are cleaved in presence of esterase enzyme present in the lysosomal compartment. The enzymatic biodegradation studies revealed that block copolymer NP were stable at extracellular condition and degrade at intracellular conditions in presence of esterase enzyme. Further biocompatibility was studied by MTT assay and the block copolymer NPs were nontoxic to cells. Thus, desired water solubility, strong red fluorescence from PBI chromophore along with biodegradability and low cytotoxicity were the key attractions for bioimaging application of the novel PBI containing PCL block copolymers. The cellular uptake studies revealed that the polymer NPs were rapidly internalized in to the cells and inherent red fluorescence for the PBI chromophore was observed inside the cells confirming the potential use of the polymer NPs for cellular imaging application. The present polymer design combined attractive photophysical properties of PBI in aqueous medium and biodegradability of PCL backbone which provided new opportunity for development of efficient nano-assemblies for biological applications such as drug delivery and bioimaging.

4.5 References

1. Zhan, X.; Zhu, D. *Polym. Chem.* **2010**, *1*, 409–419.
2. Zhu, C.; Liu, L.; Yang, Q.; Lv, F.; Wang, S. *Chem. Rev.* **2012**, *112*, 4687–4735.
3. Yilmaz, M. D.; Bozdemir, O. A.; Akkaya, E. U. *Org. Lett.*, **2006**, *8*, 2871-2873.
4. Weil, T.; Vosch, T.; Hofkens, J.; Peneva, K.; Müllen, K. *Angew. Chem. Int. Ed.*, **2010**, *49*, 9068-9093.
5. J. Pan; W. Zhu; S. Li; W. Zeng; Y. Cao; H. Tian. *Polymer*.**2005**, *46*, 7658.
6. T. M. Wilson; M. J. Tauber; M. R. Wasielewski. *J. Am. Chem. Soc.* **2009**, *131*, 8952.
7. T. Ishi-I; K. Murakami; Y. Imai; S. Mataka. *Org. Lett.* 2005, *7*, 3175.
8. R. Gvishi; R. Reisfeld; Z. Burshtein. *Chem. Phys. Lett.* **1993**, *213*, 338.
9. C.W. Tang. *Appl. Phys. Lett.* **1986**, *48*, 183.
10. Y. Liu; K. R. Wang; D. S. Guo; B. P. Jiang. *Adv. Funct. Mater.* **2009**, *19*, 2230.
11. R. Dobrawa; M. Lysetska; P. Ballester; M. Grune; F. Wurthner. *Macromolecules*, **2005**, *38*, 1315.
12. Liu, K.; Xu, Z.; Yin, M. *Prog. Polym. Sci.* **2015**, *46*, 25-54.
13. Sun, M.; Mullan, K.; Yin, M. *Chem. Soc. Rev.* **2016**, *45*, 1513-1528.
14. C. Backes; C. D. Schmidt; F. Hauke; C. Bottcher; A. Hirsch. *J. Am. Chem. Soc.*, **2009**, *131*, 2172
15. X. Zhang; Z. J. Chen; F. Wurthner. *J. Am. Chem. Soc.*, **2007**, *129*, 4886.
16. L. Zang, R. C. Liu; M. W. Holman; K. T. Nguyen; D. M. Adams. *J. Am. Chem. Soc.* **2002**, *125*, 10640.
17. Y. W. Huang; Y. Yan; B. M. Smarsly; Z. X. Wei; C. F. J. Faul; *J. Mater. Chem.* **2009**, *19*, 2356
18. H. J. Salavagione; G. Martinez; R. Gomez; J. L. Segura. *J. Polym. Sci., part A: Polym. Chem.* **2010**, *48*, 3613
19. H. Langhals; W. Jona; F. Einsiedl; S. Wohnlich. *Adv. Mater.*, **1998**, *10*, 1022
20. Heek, T.; Fasting, C.; Rest, C.; Zhang, X.; Würthner, F.; Haag, R. *Chem Commun.*, **2010**, *46*, 1884-1886.
21. Xu, Y.; Leng, S.; Xue, C.; Sun, R.; Pan, J.; Ford, J.; Jin, S. *Angew Chem. Int. Ed.* **2007**, *46*, 3896-3899.
22. Zhong, L.; Xing, F.; Shi, W.; Yan, L.; Xie, L.; Zhu, S. *ACS Appl. Mater. Interfaces* **2013**, *5*, 3401-3407.
23. Tuntiwechapikul, W.; Taka, T.; Béthencourt, M.; Makonkawkeyoon, L.; Randall Lee, T.; *Med. Chem. Lett.* **2006**, *16*, 4120-4126.
24. Sun, Y.; Li, Z.; Wang, Z. *J. Mater. Chem.* **2012**, *22*, 4312-4318.
25. Peneva, K.; Mihov, G.; Herrmann, A.; Zarrabi, N.; Börsch, M.; Dunan, T. M.; Müllen; K. *J. Am. Chem. Soc.* **2008**, *130*, 5398-5399.
26. Yang, S. K.; Shi, X.; Park, S.; Doganay, S.; Ha, T.; Zimmerman, S. C. *J. Am. Chem. Soc.* **2011**, *133*, 9964-9967.
27. Yin, M.; Kuhlmann, C. R. W.; Sorokina, K.; Li, C.; Mihov, G.; Pietrowski, E.; Koynov, K.; Klapper, M.; Luhmann, H. J.; Müllen; K.; Weil, T. *Biomacromolecules* **2008**, *9*, 1381-1389.
28. Yin, M.; Shen, J.; Pflugfelder, G. O.; Müllen; K. *J. Am. Chem. Soc.* **2008**, *130*, 7806-7807.
29. Yin, M.; Shen, J.; Gropeanu, R.; Pflugfelder, G. O.; Weil, T.; Müllen; K. *Small* **2008**, *4*, 894-898.

30. Liu, K.; Xu, J.; Yin, M.; Yang, W.; He, B.; Wei, W.; Shen, J. *J. Mater. Chem. B* **2014**, *2*, 2093-2096.
31. Lu, X.; Guo, Z.; Feng, M.; Zhu, W. *ACS Appl. Mater. Interfaces* **2012**, *4*, 3657-3662.
32. Xu, Z.; He, B.; Wei, W.; Liu, K.; Yin, M.; Yang, W.; Shen, J. *J. Mater. Chem. B* **2014**, *2*, 3079-3086.
33. Lu, Y.; Zheng, Y.; You, S.; Wang, F.; Gao, Z.; Shen, J.; Yang, W.; Yin, M. *ACS Appl. Mater. Interfaces* **2015**, *7*, 5226-5232.
34. You, S.; Cai, Q.; Zheng, Y.; He, B.; Shen, J.; Yang, W.; Yin, M. *ACS Appl. Mater. Interfaces* **2014**, *6*, 16327-16334.
35. Wang, L.; Xu, L.; Neoh, K. G.; Kang, E-T. *J. Mater. Chem.* **2011**, *21*, 6502-6505.
36. Makkad, S. K.; Asha, S. K. *ACS Biomater. Sci. Eng.* **2017**, *3*, 1788-1798.
37. Xu, Z.; Guo, K.; Yu, J.; Sun, H.; Tang, J.; Shen, J.; Müllen; K.; Yang, W.; Yin, M. *Small* **2014**, *10*, 4087-4092.
38. Qu, J.; Kohl, C.; Pottek, M.; Müllen; K. *Angew. Chem. Int. Ed.* **2004**, *43*, 1528-1531.
39. Jana, A.; Bai, L.; Li, X.; Ågren, H.; Zhao, Y. *ACS Appl. Mater. Interfaces* **2016**, *8*, 2336-2347.
40. Battagliarin, G.; Davies, M.; Mackowiak, S.; Li, C.; Müllen; K. *ChemPhysChem* **2012**, *13*, 923-926.
41. Heek, T.; Nikolaus, J.; Schwarzer, R.; Fasting, C.; Welker, P.; Licha, K.; Herrmann, A.; Haag, R. *Bioconjugate Chem.* **2013**, *24*, 153-158.
42. Sun, M.; Yin, W.; Dong, X.; Yang, W.; Zhao, Y.; Yin, M. *Nanoscale* **2016**, *8*, 5302-5312.
43. Xu, X.; Li, Y.; Xiong, Z.; Yang, J.; Pan, L.; Wu, Y.; Wei, C.; Lu, S. *RSC Adv.* **2016**, *6*, 110329-110336.
44. Klok, H-A.; Becker, S.; Schuch, F.; Pakula, T.; Müllen; K. *Macromol. Biosci.* **2003**, *3*, 729-741.
45. Zhang, X.; Gong, T.; Chi, H.; Li, T. *R. Soc. open sci* **2018**, *5*, 171686-171696.
46. Chen, Z.; Fimmel, B.; Würthner, F. *Org. Biomol. Chem.* **2012**, *10*, 5845-5855.
47. Xu, Z.; He, B.; Shen, J.; Yang, W.; Yin, M. *Chem. Commun.* **2013**, *49*, 3646-3648.

Chapter 5

Perylene-Tagged Triblock Theranostic Fluorescent Nanocarriers for Pt-drug Delivery in Cancer Cells

Abstract

The development of smart nanocarriers system for simultaneous delivery and direct monitoring of cisplatin to elicit improved therapeutic efficiency from cisplatin is highly desirable. Therefore, dual functional highly luminescent, biodegradable, cisplatin conjugated amphiphilic block copolymer nanocarriers have been developed and demonstrated for therapeutic and diagnostic application in cancer cells. Novel PBI-CPCL-PEGPCL block copolymer was designed and synthesized by ring opening polymerization. The polymer design comprises carboxylic acid is functionalized polycaprolactone block to facilitate chemical conjugation of cisplatin and hydrophilic PEG substituted polycaprolactone block to obtain required amphiphilicity in the block copolymer. Moreover, highly fluorescent PBI chromophore provides opportunity to directly monitor fate of the drug inside the cells. The polymer nanocarriers prevented undesirable interactions of cisplatin with PBS, saline and GSH and protected the drug inside polymer-cisplatin conjugated nanoparticles. The *in vitro* drug release studies demonstrated that esterase enzyme triggered the cleavage of polymer-cisplatin conjugated nanoparticles to release cisplatin in to the medium. Cytotoxicity studies confirmed high biocompatibility of the nascent polymer and hence utilized as fluorescent probe to track the non-fluorescent cisplatin delivery inside the cancer cells using non-invasive bioimaging tool. Further, Polymer-cisplatin conjugated NP exhibited comparable cell killing to that of free cisplatin in cancer cells The cellular uptake followed by accumulation of the drug conjugated nanoparticles inside the cytoplasm was confirmed from the red fluorescence of PBI chromophore in the polymer by CLSM imaging. Thus, the multifunctional block copolymer nanocarriers are promising candidates for simultaneous delivery and direct tracking of cisplatin inside the cancer cells.

5.1 Introduction

The serendipitous discovery of anticancer properties of cisplatin by Rosenberg and Vancamp in 1969 has revolutionized the cancer treatment. FDA approved cisplatin to treat ovarian and testicular cancer in 1978, since then it has become one of the oldest and most efficient clinical drugs employed to treat wide range of cancers including ovarian, breast, testicular, head and neck, small cell and non-small cell lung, bladder, liver because of its broad spectrum of antitumor activity.^{1,2} Cisplatin (cis-diamminedichloridoplatinum (II) (CDDP) is platinum based neutral, inorganic, square planar complex and its antitumor property is mainly associated with binding of cisplatin to DNA in cell nucleus to form un-repairable platinum DNA adducts ultimately resulting in DNA damage to trigger cellular apoptosis.^{3,4,5} The mechanism of action of cisplatin is depicted in figure 5.1.

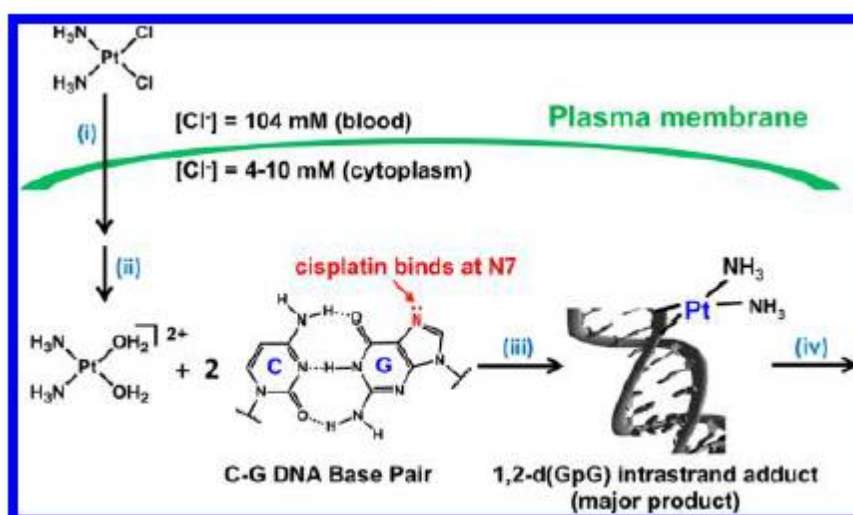


Figure 5.1. Four steps of the mechanism of action of cisplatin (i) cellular uptake, (ii) aquation/ activation, (iii) DNA binding, and (iv) cellular processing of DNA lesions leading to apoptosis (adopted from Johnstone et al. *Chem. Reviews* **2016**, 116, 3436-3486)

The cisplatin drug is neutral in bloodstream and enters the cell via both passive and active pathways. At intracellular conditions the chloride leaving group is displaced by water molecule to form aquated cisplatin and thus the drug is in activated form. The aquo complex of cisplatin covalently binds to the nitrogen in N^7 position of purine bases which subsequently cross link to adjacent purine. This platinum DNA adduct interfere with normal DNA replication and transcription which trigger DNA damage and culminate in cell apoptosis.^{2,4} However, cisplatin treatment suffers severe side

effects including neurotoxicity, nephrotoxicity, ototoxicity, emetogenesis, nausea, vomiting, fatigue. This systemic toxicity is due to the poor specificity of cisplatin which limits the therapeutic efficacy. In addition, cisplatin efficacy is mainly restricted by inherent and acquired resistance in cancer cells. The major mechanisms by which the cells become resistant to cisplatin are; (1) Reduced drug accumulation due to change in the uptake or efflux profile, (2) Cytoplasmic detoxification of cisplatin by sulphur containing molecules, (3) enhanced repair of cisplatin-DNA adduct. (4) Increased tolerance to DNA damage and change in the molecular pathways leading to failure of apoptosis pathways.^{6,7} To circumvent the limitations of cisplatin, second generation Platinum analogues such as oxaliplatin, carboplatin, and nedaplatin have been prepared and are in clinical use. These platinum derivatives are safer and show improved therapeutic efficacy in cancer treatment. Despite the better performance of these drugs, their use is also associated with more acceptable side effects as they possess similar mechanism of action to that of cisplatin.^{6,8} Recent advances in nanotechnology have enabled the development of smart nanocarriers to alleviate the side effects of cisplatin in cancer treatment. Using this approach, the encapsulation of drug in the nanocarriers temporarily passivates the drug during the transport to reduce systemic toxicity and targeted delivery of the nanocarriers promotes drug uptake thereby improving the therapeutic efficacy.⁴ A range of nanocarriers including liposomes, inorganic, and polymeric nanoparticles have been investigated for the cisplatin delivery in the cancer treatment.

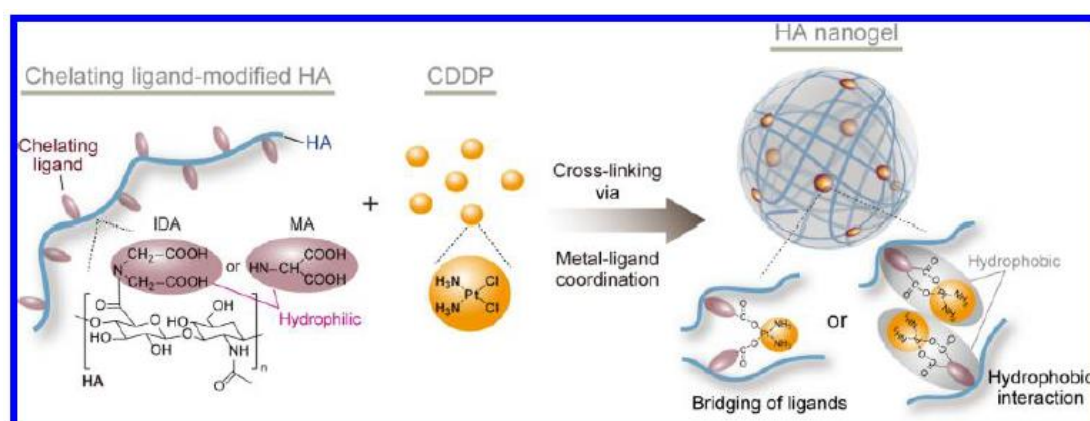


Figure 5.2. Illustration of nanogel formation from chelating ligand-conjugated HA, induced by ligand-cisplatin coordination. The ligand conjugated HA is cross-linked via bridging of ligands by cisplatin or hydrophobic interaction of cisplatin coordinated ligands that lose their hydrophilicity through coordination of action of cisplatin (adopted from Ohta *et al. Bioconjugate Chem.* **2016**, 27, 504-508)

Ohta *et al.* developed cisplatin encapsulated hyaluronan nanogels through cheating ligand metal coordination as shown in figure 5.2 for pH responsive cisplatin delivery.⁹ Similarly, pH responsive luteinizing hormone-releasing hormone (LHRH)-targeted nanogels and laponite nanodisc based nanohydrogels were demonstrated for in vitro as well as in vivo cisplatin delivery to ovarian cancer and cervical cancer respectively.^{10,11} Anish Babu *et al.* prepared multifunctional chitosan coated lactic acid nanoparticle for codelivery of cisplatin and siRNA/Plasmid DNA and tested for its efficacy in cisplatin resistant 2008/C13 ovarian cancer cells.¹² Xinming Li and co-workers used multifunctional grapheme oxide conjugated Pt(IV) prodrug to enhance the in vivo therapeutic efficacy.¹³ Shribin *et al.* developed folic acid conjugated polypeptide based cisplatin encapsulated vesicles for targeted drug delivery.¹⁴ Lioposome-conjugated cisplatin (IV) prodrug nanomedicine was developed for in vivo cancer therapy.¹⁵ Johnson and coworkers synthesized brush-arm star polymer via convergent synthetic approach and demonstrated for single nanoparticle based combination cancer therapy of cisplatin, doxorubicin, and camptothecin.¹⁶

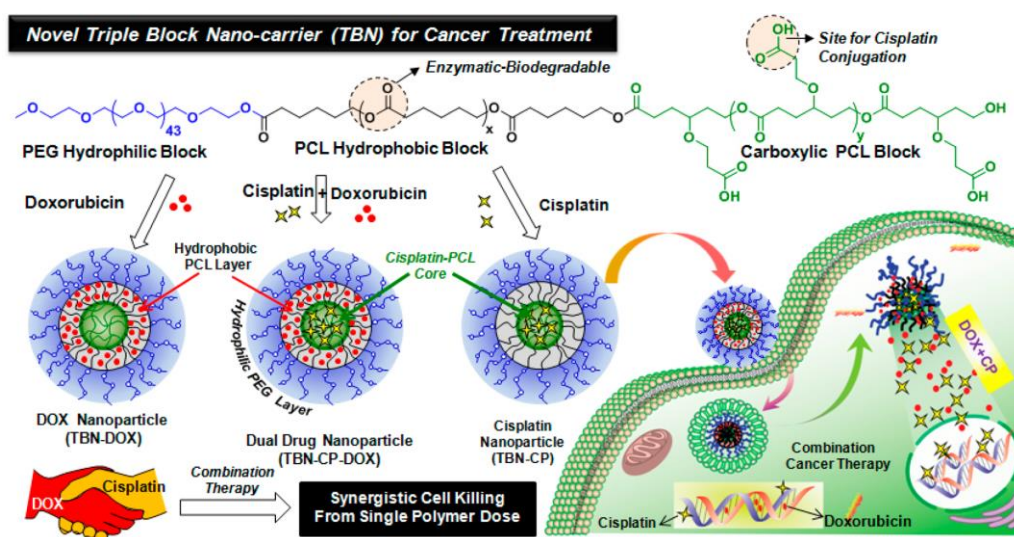


Figure 5.3. Triple block nanocarrier (TBN) design for combination therapy of cisplatin and DOX and accomplishing synergistic cancer therapy from single polymer platform (adopted from Bapurao *et al* *Biomacromolecules* **2016**, *17*, 4075-4085)

Bapurao *et al.* from our laboratory reported biodegradable PEG-CPCL block copolymer core shell nanoparticles to overcome cisplatin detoxification against GSH overexpressed breast cancer cells.^{17,18} Bapurao *et al.* from our laboratory has also demonstrated biodegradable triblock copolymers as triple block nanocarriers for codelivery of antagonistic drugs cisplatin and doxorubicin for synergistic cancer therapy as shown in figure 5.3.¹⁹

Nilesh *et al.* from our laboratory developed cisplatin-conjugated polysaccharide vesicles as single nanoscaffold for combination therapy of triple antagonistic cisplatin, doxorubicin, and camptothecin drugs.²⁰ The aforementioned cisplatin nanocarriers are important in demonstrating improved therapeutic efficacy of cisplatin in cancer therapy.

Theranostic polymer nano-carriers are one of the fast growing research areas in cancer treatment in which the nano-system is tagged with unique molecular property for tracking their administration in the biological system (diagnostics) as well as deliver desirable cargoes to carryout particular action (therapeutics) in single polymer platform. Therefore, several efforts were taken to coformulate Pt-drug imaging agent with therapeutic agent in a single platform which allows simultaneous delivery as well as non-invasive visualization of the drug to improve cancer treatment. Among these approaches Kabanov and co-workers developed magnetic nanoparticles with luteinizing hormone-releasing hormone (LHRH)-targeted poly(glutamic acid)-b-(ethylene glycol) block copolymer conjugated with cisplatin as shown in figure 5.4 and demonstrated for simultaneous MR imaging and ovarian cancer chemotherapy.²¹

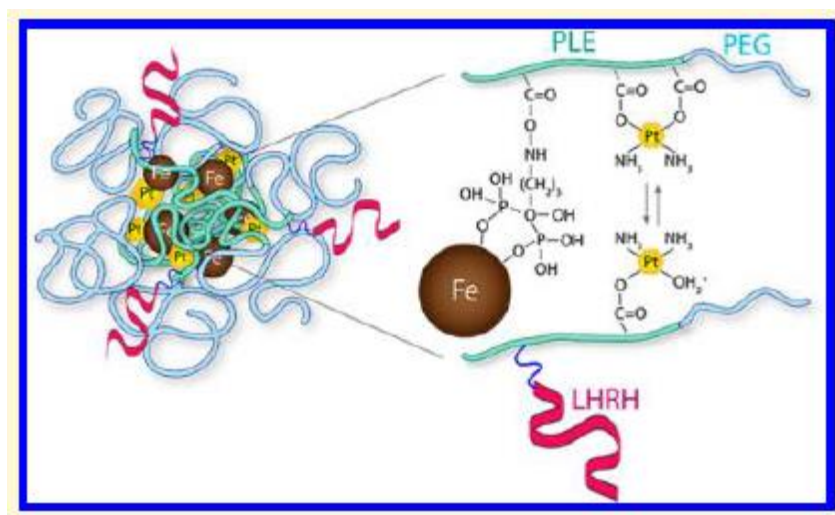


Figure 5.4. Cisplatin loaded magnetite nanoclusters for simultaneous MR imaging and cancer chemotherapy (adopted from Vishwasrao H.M. *et al Chem. Mater.* **2016**, 28, 3024-3040)

Lipoic acid functionalized PEGylated dendritic system was developed with bio-reducible disulphide bond to generate pH/redox dual responsive supramolecular nanoplatform for cisplatin delivery. Moreover, the nanocarriers were endowed with NIR fluorescence probe to visualized in vitro and in vivo fate of the cisplatin

delivery.²² Yubin Huang and co-workers developed dual sensitive dual drug (demethylcantharidin (DMC) and cisplatin) backboneed nanoparticles (DD-NP) as shown in figure 5.5 which trigger release of the drugs in chain-shattering manner under reduction/acidic intracellular environment. Further DD-NP was applied as contrast agent to directly track the drug and NP via DMCT and ICP-MS both in vitro and in vivo.²³

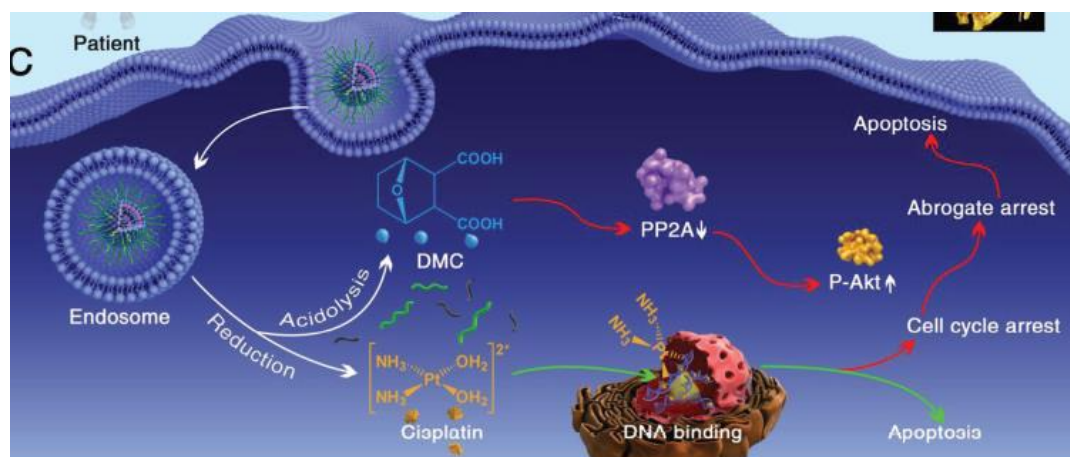


Figure 5.5. Schematic illustration of dual drug backboneed shattering polymeric nanoparticle possible dual anticancer mechanism after endocytosis by cancer cells (adopted from Cong *et al Adv. Mater.* **2018**, *30*, 1706220)

Patel *et al.* demonstrated nanoemulsions for encapsulation of difatty acid platins (cisplatin prodrug) and C6 ceramide an apoptosis enhancer in the lipid core and the surface was decorated with lipidated FA and lipidated Gd-DTPA to improve targeting ability and Gd-DTPA enabled monitoring of tumor uptake by noninvasive MR imaging.²⁴ Poly(methacrylic acid)-grafted-poly(ethylene glycol methacrylate) polymer nano-assemblies were investigated with *in situ* coating of magnetite nanocrystallites and this magnetic drug delivery system was investigated for cisplatin delivery. The anticancer properties of the drug nanocarriers were monitored with PET-CT (positron emission tomography/computed tomography) in cisplatin resistant HT-29 human colon adenocarcinoma model.²⁵ Xiaoyong Wang and co-workers explored Pt(IV) prodrug loaded superparamagnetic iron oxide nanoparticles (SPIONs) which exhibited GSH promoted cytotoxicity against tumor cells and therapeutic response of the NP was monitored by MR imaging.²⁶ Multifunctional FA-grafted PEGylated yolk like Fe₃O₄@Gd₂O₃ pH responsive nanoparticle for in vivo cisplatin delivery and MR imaging diagnostic was investigated by Zhengyan Wu and co-workers.²⁷

Unfortunately, cisplatin is non-fluorescent drug therefore these nanocarrier designs depend upon the labelling of fluorescent molecules or the fluorescent drug used in the combination therapy for tracking of the intracellular cisplatin delivery as a compromise as this approach does not give the direct information about fate of the drug at intracellular level. Fluorescent polymer nano-carriers are unique system which allows to track their pathway in the biological system by confocal microscopy imaging as well as image dependent spectroscopy tools such as FRET. Yen Wei and co-workers prepared AIE based fluorescent amphiphilic copolymer (ATPHE-co-BTDA) synthesized via ROP of amine terminated AIE dyes (ATPHE) with BDTA followed by conjugation with hydrazide terminated PEG to form dynamic hydrazine. These nano-assemblies were developed for in vitro cisplatin delivery and biological imaging in HeLa cells.²⁸ Upconversion nanoparticles consisting of lanthanides coated with polyethyleneimine for Pt(IV) drug conjugation (UCNP@PEI-Pt-PEG@siRNA) were demonstrated for in vitro as well as in vivo cisplatin delivery and to track the fate of the nanoparticles.²⁹ Wang *et al.* developed structure switching aptamer triggered hybridization chain reaction (HCR) on cell surface which enabled real time activation and signal amplification for fluorescence imaging and efficient targeted tumor therapy.³⁰ Chatterjee *et al* developed cisplatin encapsulated gold nanoparticles for simultaneous cell imaging and drug delivery in cervical cancer HeLa cells.^{31,32} Gold nanoclusters conjugated with cisplatin prodrug and folic acid were reported for fluorescence imaging and targeted chemotherapy of breast cancer.³³ Polydopamine coated gold nanorods were investigated for image guided tumor therapy which targets tumor angiogenesis enhancing therapeutic efficacy.³⁴ Bin Liu and co-workers synthesized PEG substituted conjugated polyelectrolyte (CPE) conjugated with cisplatin to develop nanoparticles (CPE-PEG-Pt) for simultaneous cisplatin delivery and drug tracking in HepG2 cancer cells.³⁵ Lipoic acid functionalized PEGylated dendritic system was developed with bio-reducible disulphide bond to generate pH/redox dual responsive supramolecular nanoplatform for cisplatin delivery. Moreover, the nanocarriers were endowed with NIR fluorescence probe to visualize in vitro and in vivo fate of the cisplatin delivery.³⁶ With very few exceptions, above mentioned cisplatin delivering and imaging nanocarriers are biocompatible but not biodegradable. The development of biodegradable dual functional nanocarriers would facilitate the targeted delivery of cisplatin to tumor and allow non-invasive visualization of fate of the drug at intracellular condition. Hence, developing

biodegradable nanocarriers which is capable of simultaneously delivering cisplatin and monitoring fate of the drug inside the cells is highly desirable. However, major challenge in developing such biodegradable nano-scaffold is to maintain balance between therapeutic and diagnostic properties to achieve optimum effect.

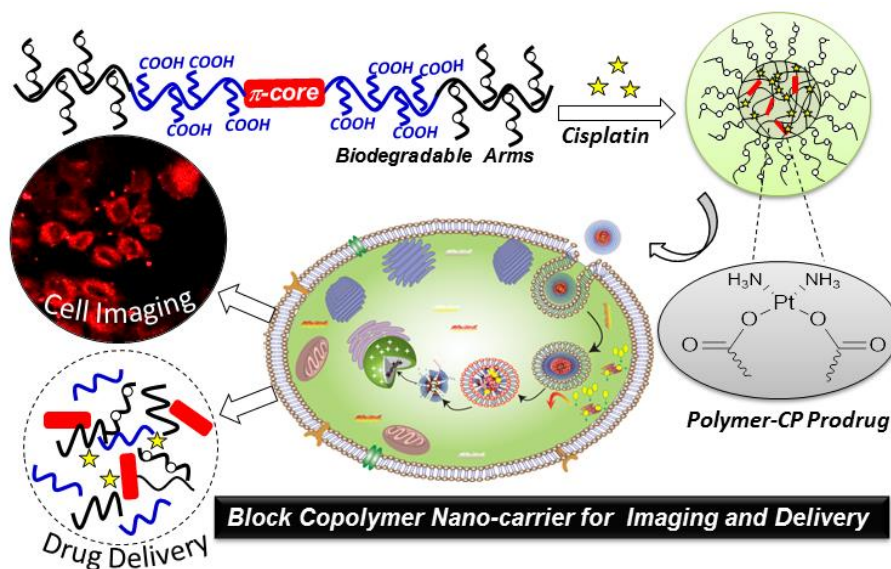


Figure 5.6. Dual functional block copolymer nanocarriers design for simultaneous cisplatin delivery and cell imaging in cancer therapy.

In order to accomplish this goal new biodegradable block copolymer design was proposed with following features. (i) carboxylic acid substituted PCL for CP conjugation, (ii) PEG substituted PCL block for aqueous solubility of the nanocarriers (iii) red fluorescent perylene bisimide (PBI) chromophore for fluorescence bioimaging to monitor cisplatin delivery to cancer cells. In this design, PCL block copolymer undergo enzymatic cleavage at intracellular environment to trigger cisplatin release and PBI chromophore utilized for bioimaging purpose is biocompatible and has negligible mass in comparison with total biodegradable polymeric mass. This nanocarriers design for simultaneous delivery and imaging is schematically shown in figure 5.6. In the present investigation novel PBI-CPCL-PEGPCL block copolymer was designed and synthesized by ring opening polymerization. For this purpose, PEG substituted caprolactone monomer was custom designed and synthesized to improve the solubility of block copolymer in aqueous medium. The polymer design is functionalized with carboxylic acid groups for chemical conjugation of cisplatin. The resulting polymer-cisplatin conjugate self-

assembled in aqueous medium to form spherical nanoparticles. The desirable photophysical properties of PBI chromophore were retained in polymer-cisplatin conjugates which enabled to utilize them for cellular imaging to monitor the delivery of cisplatin to cancer cells. The stability of polymer-cisplatin conjugated nanoparticles was investigated in detail. In vitro drug release studies demonstrated that esterase enzyme present in the lysosomal compartment triggered the cleavage of polymer-cisplatin conjugated nanoparticles to release cisplatin. Polymer-cisplatin conjugated NP exhibited comparable cell killing to that of free cisplatin in cancer cells. The fluorescent PBI chromophore enabled to monitor the cellular uptake of NP by CLSM imaging which confirmed the successful internalization of NP inside the cells and preferably accumulated in cytoplasm and peri-nuclear region. Hence, present investigation demonstrated that multifunctional block copolymer nanocarriers are efficient for simultaneous imaging and drug delivery in cancer treatment.

5.2 . Experimental section

5.2.1. Materials: Tetraethylene glycol, *p*-toluenesulfonylchloride, sodium azide, lithium aluminium hydride, zinc acetate [Zn(OAc)₂], 1,4-cyclohexane diol, *tert*-butyl acrylate, pyridiniumchlorochromate (PCC), *m*-chloroperbenzoic acid, caprolactone, polyethylene glycol monomethyl ether (molecular weight = 350), cisplatin, tin (II) 2-ethylhexanoate, orthophenylenediamine (OPD), silver nitrate, glutathione (GSH) and horse liver esterase enzyme were purchased from Sigma Aldrich chemicals and used as received. Dimethyl acetamide (DMAc), tetrahydrofuran (THF), dimethyl formamide (DMF), chloroform, trifluoroacetic acid and all other solvents were purchased locally and used after purification by standard procedures. Human breast cancer cells (MCF-7) and Cervical cancer (HeLa) cells were maintained in DMEM (with phenol red medium: Gibco) supplemented with 10 % (v/v) fetal bovin serum (FBS) and 1 % (v/v) penicillin-streptomycin at 37 °C under a 5 % CO₂ humidified atmosphere. Cells were washed with 40 % DPBS (Gibco), trypsinised using 0.05 % trypsin (Gibco) and seeded in 96- or 6- well flat-bottomed plastic plates (Costar) for all assays. 3-(4,5-dimethylthiazole-2-yl)-2,5-diphenyltetrazolium bromide salt (MTT), 4 % paraformaldehyde, DAPI, and DMSO were obtained from Sigma Aldrich.

5.2.2. Synthesis of 3-((4-oxocyclohexyl)oxy)propanoic acid (3): compound (7 from chapter 2) (14.0 g, 57.85 mmol) was dissolved in dry DCM (50.0 mL) and stirred for

5 minutes. TFA (50.0 mL) was added slowly to the reaction mixture and continued to stir for 2 h at 30 °C. Solvent and TFA were removed by evaporation to get yellow liquid. The crude product was purified by column chromatography using ethyl acetate in pet ether as eluent. Yield = 10.0 g (90.0 %). ¹H-NMR (400MHz, CDCl₃) δ ppm: 3.77 (m, 3H, -CH₂ and -O-CH), 2.55 (t, 2H, -CH₂-CO-), 2.48 (m, 2H, -CH₂), 2.22 (m, 2H, -CH₂), 2.06 (m, 2H, -CH₂) and 1.87 (m, 2H, -CH₂). ¹³C-NMR (100MHz, CDCl₃) δ ppm: 211.9, 177.4, 72.7, 63.3, 36.8, 36.0 and 30.2 FT-IR (cm⁻¹): 3440, 2930, 2365, 1700, 1420, 1340, 1310, 1240, 1185, 1105 and 1063. HRMS (ESI+): m/z [M+Na⁺] calcd. for C₉H₁₄O₄[M⁺] = 209.07; found = 209.15

5.2.3. Synthesis of tert-butyl-3-((7-oxooxepan-4-yl)oxy)propanoate (4):

Compound (3) (10.0 g, 53.5 mmol) and catalytic amount of DMAP were dissolved in dry DCM (150.0 mL) and deoxygenated by purging with nitrogen with stirring for 10 minutes. EDC.HCl (15.4 g, 80.0 mmol) was added to it and stirring was continued for 15 minutes followed by addition of DIPEA (28.1 mL, 16.1 mmol). PEG monomethyl ether (molecular weight 350) (15.0 g, 43.0 mmol) was dissolved in dry DCM (50.0mL) separately and deoxygenated by purging with nitrogen for 15 minutes. The PEG solution was added to the reaction mixture and continued to stir for 48 h at 30 °C under nitrogen atmosphere. DCM was evaporated and crude reaction mixture was dissolved in ethyl acetate followed by washing with sodium bicarbonate and brine solution. The organic layer was separated and dried over sodium sulphate. Crude product was purified by passing through silica gel column using DCM and methanol as eluent. Yield = 13.5 g (50 %). ¹H-NMR (400MHz, CDCl₃) δ ppm: 4.24 (t, 2H, CH₂-OOC-), 3.76 (t, 2H, -CH₂-O-), 3.68 (m, 3H, -CH-O and -CH₂-O-), 3.63 (m, 2H, -CH₂-O-), 3.53 (t, 2H, -CH₂-O-), 3.36 (s, 3H, -O-CH₃), 2.62 (t, 2H, -CH₂-CO-), 2.55 (m, 2H, -CH₂), 2.22 (m, 2H, -CH₂), 2.05 (m, 2H, -CH₂) and 1.88 (m, 2H, -CH₂). ¹³C-NMR (100MHz, CDCl₃) δ ppm: 211.9, 177.4, 72.7, 63.3, 36.8, 36.0 and 30.2 FT-IR (cm⁻¹): 3445, 2925, 2362, 1725, 1422, 1345, 1310, 1240, 1185, 1105 and 1063.

5.2.4. Synthesis of tert-butyl-3-((7-oxooxepan-4-yl)oxy)propanoate (PEG-CL-Monomer):

Compound (4) (5.0 g, 9.65 mmol) was dissolved in dry DCM (100.0 mL) and *m*-chloroperbenzoic acid (3.3 g, 19.3 mmol) and sodium bicarbonate (1.6 g, 19.3 mmol) were added sequentially and the reaction mixture was stirred at 30 °C for 72 h under nitrogen atmosphere. Reaction mixture was concentrated and saturated aqueous

NaHCO₃ solution and saturated aqueous Na₂S₂O₃ solution was added to it. The crude product was extracted into ethyl acetate and dried over anhydrous sodium sulphate. Pure product was obtained by column chromatography using DCM and methanol as eluent. Yield = 3.2 g (60 %). ¹H-NMR (CDCl₃, 400 MHz) δppm: 4.45 (dd, 1H, COOCH), 4.24 (t, 2H, CH₂-OOC-), 4.04(dd, 1H, COOCH), 3.64 (m, 4H, OCH₂, OCH& COCH), 3.53 (t, 2H, -CH₂-O-), 3.36 (s, 3H, -O-CH₃), 2.95 (dd, 1H, COCH), 2.50 (t, 2H, COCH₂), 2.42-1.79 (m, 4H OCH(CH₂)₂) ¹³C-NMR (CDCl₃, 100MHz) δppm: 176.5, 171.3, 80.8, 74.3, 64.3, 63.5, 36.8, 34.2, 28.5, 27.9 and 27.5. FT-IR (cm⁻¹): 2925, 1725, 1460, 1393, 1210, 1160 and 1105.

5.2.5. Synthesis of PBI-BPCL₄₀ Macroinitiator: Macroinitiator was synthesized by ring opening polymerization of t-butyl ester substituted monomer with hydroxyl functionalized perylene bisimide (PBI) initiator following the procedure as described below. The monomer to initiator was taken as [M]/[I] = 50. In a flame dried schlenk tube PBI initiator (22.9 mg, 0.03 mmol) was dissolved in dry THF (0.5 mL) and Sn(Oct)₂ (6.2 mg, 0.01 mmol) as added as catalyst. The polymerization mixture was deoxygenated by purging with nitrogen for 30 minutes. Monomer (400 mg, 1.54 mmol) was dissolved in dry THF (0.5 mL) separately and this monomer solution was added to the schlenk tube and purging was continued for another 30 minutes. The schlenk tube was immersed in preheated oil bath and refluxed for 48 h with constant stirring. The crude polymer mixture was cooled and precipitated in hexane. The procedure was repeated twice to obtain pure polymer. Yield = 270 mg (67 %) ¹H-NMR (400 MHz, CDCl₃) δ ppm: 4.13 (m, 2H), 4.07 (m, 2H), 3.69-3.63 (m, 5.27 H), 3.45 (m, 1H), 2.52 (m, 2H), 3.38 (m, 2H), 1.86-1.78 (m, 4H), 1.45 (m, 9H). ¹³C-NMR (100 MHz, CDCl₃): 173.85, 172.02, 760.99, 65.20, 61.67, 35.73, 33.36, 32.22, 29.65, 29.04, 26.34, 23.06 and 14.51. FT-IR (cm⁻¹): 2935, 2867, 1250,1328, 1463, 1343, 1257, 1172, 1094, 1064, 941 and 720.

5.2.6. Synthesis of PBI-BPCL-PEGPCL Block copolymer. The block copolymer was synthesized by ring opening polymerization of PEG substituted caprolactone monomer (5) with PBI-BPCL polymer synthesized above as macroinitiator for [M]/[I] ratio of 50 as follows. Macroinitiator (165.7 mg, 0.015 mmol) was taken in a flame dried schlenk tube and dissolved in dry THF (0.5 mL) followed by addition of Sn(Oct)₂ (3.1 mg, 0.007 mmol) as added as catalyst. The polymerization mixture was

deoxygenated by purging with nitrogen for 30 minutes. The PEG substituted caprolactone monomer (5) (400 mg, 0.75 mmol) was dissolved in dry THF (0.5 mL) separately and this monomer solution was added to the schlenk tube and purging was continued for another 30 minutes. The schlenk tube was immersed in preheated oil bath and refluxed for 72 h with constant stirring. The crude polymer mixture was cooled and precipitated in diethyl ether. The procedure was repeated twice to obtain pure polymer. Yield = 300 mg (50 %) $^1\text{H-NMR}$ (400 MHz, CDCl_3) δ ppm: 4.24 (t, 2H, $\text{CH}_2\text{-OOC-}$), 4.13 (m, 2H), 4.07 (m, 2H), 3.53 (t, 2H, $-\text{CH}_2\text{-O-}$), 3.36 (s, 3H, $-\text{O-CH}_3$), 3.69-3.63 (m, 5.27 H), 3.45 (m, 1H), 2.52 (m, 2H), 3.38 (m, 2H), 1.86-1.78 (m, 4H), 1.45 (m, 9H). $^{13}\text{C-NMR}$ (100 MHz, CDCl_3): 173.85, 172.02, 760.99, 65.20, 61.67, 35.73, 33.36, 32.22, 29.65, 29.04, 26.34, 23.06 and 14.51. FT-IR (cm^{-1}): 2938, 2870, 1725, 1328, 1463, 1343, 1257, 1172, 1094, 1064.

5.2.7. Synthesis of PBI-CPCL-PEGPCL block copolymer: The t-butyl group was deprotected by adding trifluoroacetic acid (2.0 mL) into the PBI-BPCL-PEGPCL polymer (200 mg) solution in DCM and the reaction mixture was stirred for 30 minutes at 30 °C. The solvents were evaporated and polymer was precipitated from diethyl ether to obtain pure polymer. $^1\text{H-NMR}$ (400 MHz, CDCl_3) δ ppm: 4.24 (t, 2H, $\text{CH}_2\text{-OOC-}$), 4.13 (m, 2H), 4.07 (m, 2H), 3.53 (t, 2H, $-\text{CH}_2\text{-O-}$), 3.36 (s, 3H, $-\text{O-CH}_3$), 3.69-3.63 (m, 5.27 H), 3.45 (m, 1H), 2.52 (m, 2H), 3.38 (m, 2H), 1.86-1.78 (m, 4H), $^{13}\text{C-NMR}$ (100 MHz, CDCl_3): 173.85, 172.02, 760.99, 65.20, 61.67, 35.73, 33.36, 32.22, 29.65, 29.04. FT-IR (cm^{-1}): 3450, 2880, 1720, 1352, 1252, 1180, 1092, 948, 917, 841 and 730.

5.2.8. Preparation of Aquated Cisplatin $[\text{Pt}(\text{NH}_3)_2(\text{OH}_2)_2]^{2+}$: Cisplatin drug (20 mg, 0.066 mmol, 1 equivalent) was suspended in H_2O (20.0 mL) with constant stirring at 37 °C subsequently silver nitrate (22.5 mg, 0.132 mmol, 2 equivalents) was added and stirring was continued for 24 h under dark conditions. Cisplatin aquo complex formation was confirmed by milky white silver chloride precipitate formation which was removed by centrifuging at 10,000 rpm for 1 h. the resulting solution was filtered through 0.45 μm filter and lyophilized and stored at 4°C.

5.2.9. Synthesis of Polymer-Cisplatin Conjugate: PBI-CPCL-PEGPCL block copolymer (10.0 mg) was dissolved in NaOH solution and stirred for 30 minutes at 37 °C followed by addition of cisplatin aquo complex. Stirring was continued for 24 h

under dark condition. The resulting polymer-cisplatin conjugate was dialysed against large excess of Mili-Q water for 48 h to remove the un-encapsulated cisplatin. The solution was filtered through 0.45 μm filters, lyophilized and stored at 4 $^{\circ}\text{C}$. FT-IR (cm^{-1}): 3300, 2920, 2880, 1725, 1660, 1560, 1395, 1360, 1090, 1050, 930, 830 and 548.

5.2.10. Ortho-phenylenediamine (OPD) colorimetric assay: To determine the cisplatin content in the given samples OPD assay was performed. Cisplatin containing samples were added to the OPD solution (2.0 mL) in DMF (1.2 mg/mL) and heated at 80 $^{\circ}\text{C}$ for 2 h to get OPD-Pt complex. The absorbance of the resulting solution was measured at 706 nm (absorption maxima of OPD-Pt complex) to determine the amount of platinum present in the sample. Molar extinction coefficient for OPD-Pt was calculated as 24,310 $\text{L}\cdot\text{mol}^{-1}\cdot\text{cm}^{-1}$.

Drug loading content (DLC) and drug loading efficiency (DLE) of cisplatin in polymer-drug conjugated were determined by OPD assay using absorption spectroscopy as follows.¹⁷

$$\text{DLC (\%)} = \{ \text{weight of drug in NPs} / \text{weight of drug loaded NPs} \} \times 100\%.$$

$$\text{DLE (\%)} = \{ \text{weight of drug in NPs} / \text{weight of drug in feed} \} \times 100\%$$

5.2.11. In vitro drug release studies: In vitro drug release studies of polymer-cisplatin conjugated nanoparticles were carried out in saline, PBS, and esterase enzyme (10 U). The nanoparticles (2.0 mL) were taken in dialysis bag and dialysed against saline and or PBS solution at 37 $^{\circ}\text{C}$. 1.0 mL of the dialysate was collected at regular time intervals and replaced with fresh solution. OPD colorimetric assay was carried out to measure the amount of drug present in each aliquot using absorption spectroscopy and the cumulative release was calculated using following equation:¹⁸

$$\text{Cumulative release (\%)} = C_n \times V_o / m \times 100$$

Where, C_n is the amount of loaded cargo in the n^{th} sample, V_o is total volume, and m is the total amount loaded in nanoparticles.

5.2.12. Cell viability assay: To evaluate the therapeutic effect of cisplatin cytotoxicity of nascent PBI-CPCL-PEGPCL polymer and the polymer-cisplatin conjugated nanoparticles was determined using standard MTT assay. HeLa and MCF-7 cells were seeded (1000 cells/well) in 96 well plate supplemented with 100 μL

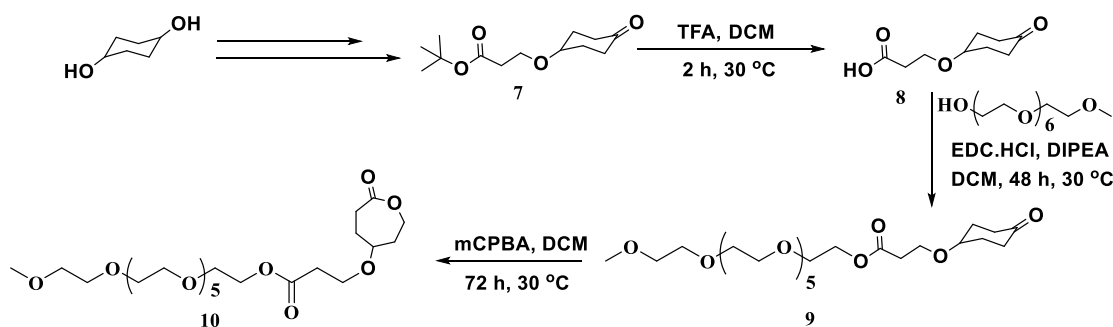
DMEM in 10% FBS and incubated at 37 °C for 16 h. After that the media was discarded and the cells were treated with various concentrations of cisplatin and polymer-cisplatin conjugated nanoparticles for 72 h. DMEM containing FBS with and without cells were used as blank control and untreated control respectively. After 72 h the cell media was removed and 100 µL of MTT (stock solution prepared in sterile PBS (5 mg/mL) and diluted to 50 µg/mL in DMEM) solution was added in each well and the cells were allowed to incubate for 4 h at 37 °C. MTT was reduced to purple formazan crystals by mitochondrial dehydrogenase enzyme. Then the media was replaced with 100 µL of DMSO in each well. The relative cell viabilities were calculated by measuring the absorbance from the formazan crystals at 570 nm using micro plate reader.

5.2.13. Cellular Uptake of polymer-cisplatin conjugated nanoparticles by Confocal microscopy: HeLa cells were seeded at a density of 1×10^5 cells on flame dried cover slips coated placed in 6 well plates containing DMEM medium with 10 % FBS. The cells were incubated at 37 °C for 16 hours and then exposed to the required concentrations of nascent block copolymer nanoparticles polymer-cisplatin conjugated nanoparticles for 4 h in a CO₂ incubator at 37 °C. After incubation, drug-containing medium was aspirated from each well, and cells were washed twice with PBS (1 mL per wash) and fixed with 4 % paraformaldehyde solution in PBS for 10 minutes at room temperature. The cells were washed twice with PBS (1 mL per wash) and stained with DAPI solution in PBS. This incubation was performed in the dark and after 2 min incubation, at room temperature excess of dye was washed from the cells with PBS. The cover slips were mounted on slides using Fluoromount-G mounting medium (Southern Biotech). Slides were then dried overnight at room temperature in the dark. The cells were imaged using a LSM 710 confocal microscope with the λ 420 nm (blue channel), λ 514 nm (red channel) lasers. Images thus obtained were analyzed using Image J analysis software and the image for each channel was separated.

5.3. Results and Discussion

5.3.1. Synthesis of block copolymers

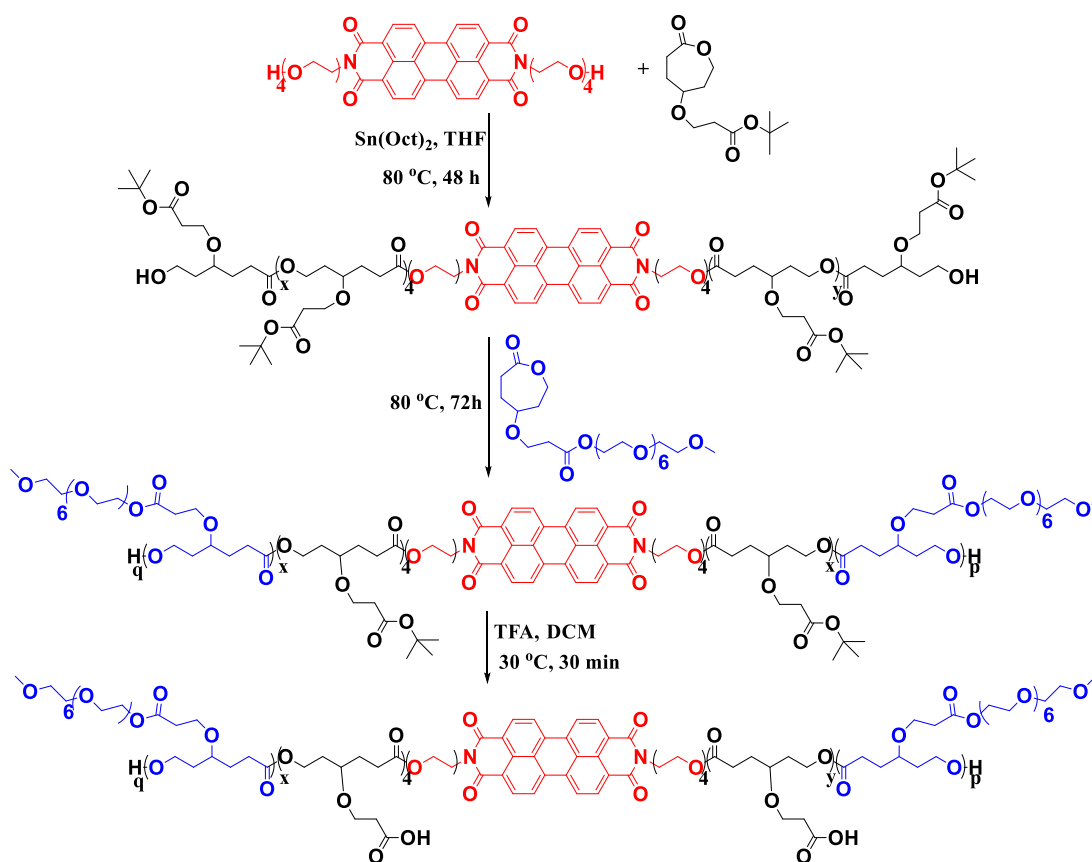
The block copolymers were synthesized via ring opening polymerization of two different t-butyl ester substituted caprolactone and PEG₃₅₀ substituted caprolactone monomers with red fluorescent PBI initiator. The PEG substituted ϵ -caprolactone monomer was synthesized following the steps as shown in scheme 5.1. 1,4-Cyclohexanediol was reacted with t-butyl acrylate by Michael addition reaction to produce monosubstituted alcohol which was subsequently oxidized into ketone with PCC as described in chapter 2. The t-butyl group present in the resulting ketone was deprotected using trifluoroacetic acid (TFA) to give carboxylic acid substituted ketone (8). Esterification of Compound (8) was carried out with polyethylene glycol monomethyl ether (molecular weight 350) to form ester (9). Compound (9) was subsequently oxidized to ϵ -caprolactone (10) by Baeyer viliger oxidation. The ϵ -caprolactone monomer was characterized by ¹H, ¹³C NMR, and mass spectrometry analysis.



Scheme 5.1. Synthesis of PEG-350 substituted ϵ -caprolactone monomer

t-Butyl substituted caprolactone monomer and hydroxyl functionalized fluorescent PBI initiator were synthesized according to the detailed procedure discussed in chapter 2 and chapter 4. The ring opening polymerization of t-butyl substituted caprolactone monomer was carried out by employing fluorescent hydroxyl functionalized perylene bisimide (PBI) as initiator and Sn(Oct)₂ as catalyst in THF as shown in Scheme 5.2. The monomer to PBI initiator molar ratio was fixed as [M]/[I] = 50. The resulting polymer was referred as PBI-BPCL₄₀ with 40 repeating units. Further the block copolymer was synthesized by utilizing PBI-BPCL₄₀ polymer as

macroinitiator in ROP process with PEG₃₅₀ substituted ϵ -caprolactone monomer with monomer to macroinitiator ratio as $[M]/[I] = 50$. The block copolymer was purified by repeated precipitation in diethyl ether and the block copolymer was referred as PBI-BPCL-PEGPCL. The block copolymer was subjected to selective deprotection of t-butyl ester using trifluoroacetic acid to obtain corresponding carboxylic acid functionalized derivative PBI-CPCL-PEGPCL. Thus, the ROP of PEG substituted caprolactone monomer with fluorescent PBI-BPCL₄₀ polymer as macroinitiator resulted in new class fluorescent polymer.



Scheme 5.2. Synthesis of macroinitiator and block copolymer

The structures of these polymers were characterized by ^1H and ^{13}C NMR. The proton NMR spectra of macroinitiator PBI-BPCL₄₀ and PBI-BPCL-PEGPCL block copolymer are shown in figure 5.7. The degree of polymerization was determined by comparison of the peak intensities of N-CH₂ proton from PBI which appeared at 4.45 ppm (proton a) with proton g corresponding to methyl group present on PEG chain on caprolactone monomer. The degree of polymerization was found to be 40 repeating units in the present case. The disappearance of t-butyl proton in the ^1H NMR spectra confirmed the deprotection of t-butyl substituted polymers into carboxylic acid

substituted polymers. Further this analysis also confirmed that the polymer backbone remains undisturbed during the selective deprotection of t-butyl group.

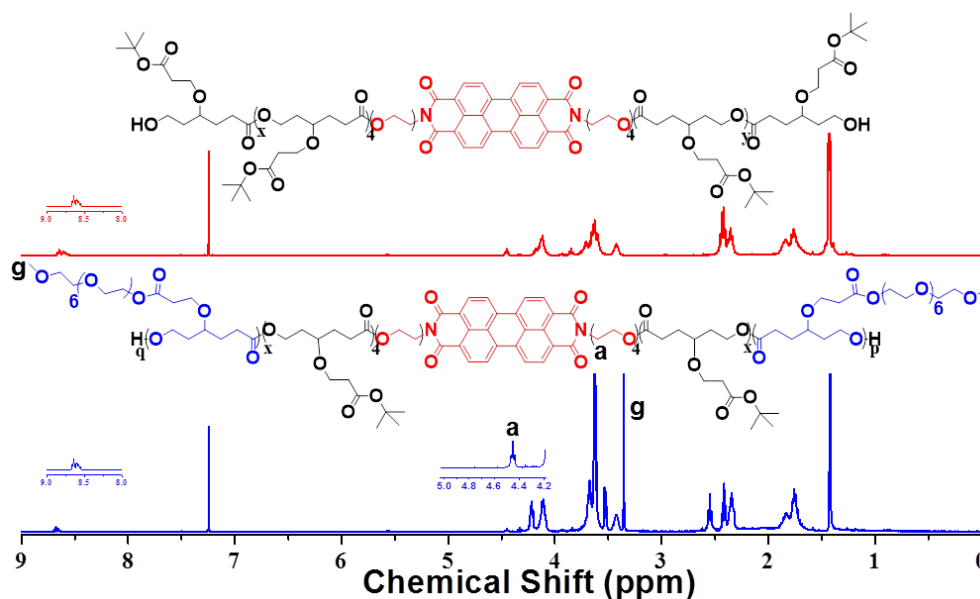


Figure 5.7. ¹H NMR of PBI-BPCL macroinitiator and PBI-BPCL-PEGCPCL block copolymer

The molecular weights and the purity of the polymers were measured by gel permeation chromatography and figure 5.8 shows the GPC chromatograms for corresponding polymers. Standard polystyrene calibration plot was used for estimation of molecular weights of the polymers. The formation of PBI-BPCL-PEGCPCL polymer was confirmed by shift in the retention time of the block copolymer towards high molecular side in comparison with retention time of the PBI-BPCL macroinitiator. The number average (M_n) molecular weight, weight average (M_w) molecular weight and their polydispersity are summarized in table given in figure 5.8. All the polymers showed monomodal distribution indicating the purity of polymers and relatively low polydispersities ~ 1.4 . Thus well-defined homogeneous polymers were obtained from ring opening polymerization process.

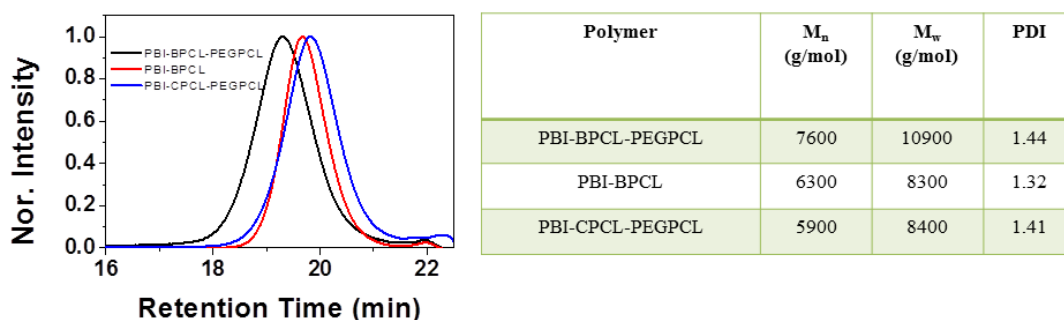


Figure 5.8 GPC chromatograms of macroinitiator and block copolymers in THF. Molecular weights and polydispersity of block copolymers determined by GPC

Thermal gravimetric analysis (TGA) and differential scanning calorimetry (DSC) studies were carried out to investigate the thermal properties of the newly synthesized block polymers. The thermal analysis was carried out with 10 °C/min heating rate under nitrogen atmosphere. The TGA and DSC thermograms are shown in figure 5.9. The TGA plot clearly showed that the block copolymer was stable up to 220-250 °C and the amorphous nature of the polymer was confirmed from the DSC plot.

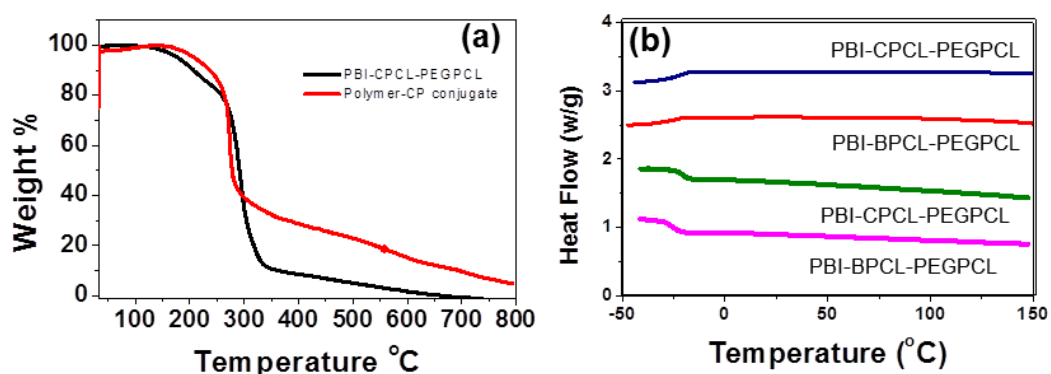


Figure 5.9. TGA (a), DSC (b) thermograms of block copolymers at heating/cooling rate of 10 °C/min under nitrogen atmosphere.

5.3.2. Synthesis of PBI Fluorescent Triblock Pt-prodrug

After the successful synthesis and characterization of PBI-CPCL-PEGPCL block copolymer, further it was tested for the polymer-cisplatin conjugated formation as the polymer backbone is functionalized with carboxylic acids and the PEG350 chains present on the polymer backbone ensures the water solubility after the complex formation. The importance of the current polymer design is that, it provides an opportunity to track the delivery cisplatin drug as the drug is not fluorescent. For this purpose, the cisplatin was converted into its aquo complex *cis*-diamminediaqua platinum (II) by reacting with silver nitrate in Milli-Q water. The silver chloride precipitate formed in this reaction was filtered to get the required cisplatin aquo complex. The carboxylic sodium salt of the block copolymer was treated with cisplatin aquo complex in dark condition for 24 h at 37 °C. 1.0:1.0 molar ratios between aquo complex and block copolymer was maintained to obtain complete complex formation as shown in figure 5.10. After the completion of polymer-cisplatin conjugate formation the resulting solution was filtered and subjected for dialysis for 48 h to ensure the removal of unreacted cisplatin aquo complex. The polymer-cisplatin prodrug was obtained by lyophilisation of the dialyzed solution.

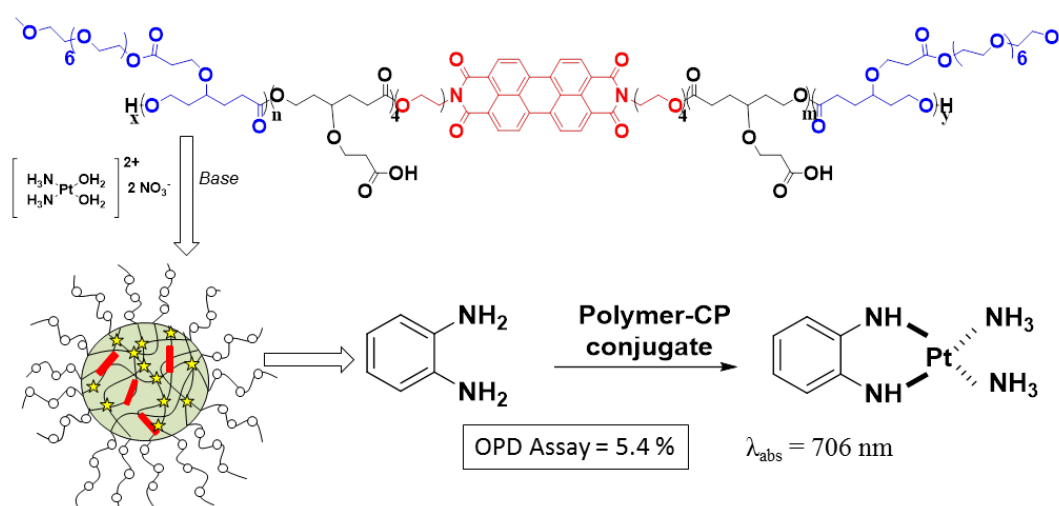


Figure 5.10. Synthesis of Pt-conjugation in the triblock copolymer.

FT-IR spectra of the block copolymer and the polymer-cisplatin prodrug were recorded and shown in figure 5.11 in order to confirm the formation of polymer-cisplatin complex. The nascent polymer showed band at 1725 cm^{-1} corresponding to $C=O$ (carbonyl) stretching frequency. After polymer-cisplatin complex formation a new band around 1565 cm^{-1} was observed corresponding to $(Pt-O-C=O)$ stretching

frequency of the metal carboxylate functional group. A band at 540 cm^{-1} was also observed for Pt-O bond stretching with reference to the formation of polymer-cisplatin drug conjugates.

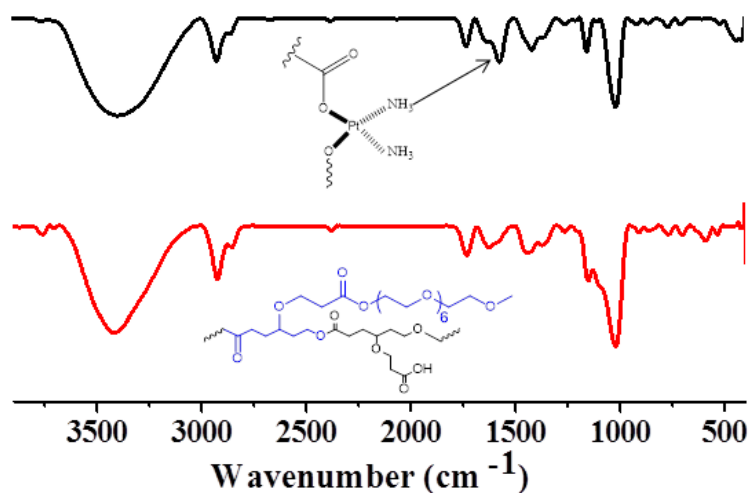


Figure 5.11. FT-IR spectra of PBI-CPCL-PEGPCL block copolymer and polymer-cisplatin conjugate.

Further the drug loading content and the drug loading efficiency of the polymer-cisplatin conjugate was determined by OPD colorimetric assay and was obtained as 5.5 % and 30 % respectively.

5.3.3. Self-assembly of PBI Triblock Pt-Prodrug

The polymer-cisplatin conjugate has rigid PBI and the cisplatin conjugated PCL as hydrophobic part and PCL backbone decorated with PEG chain as flexible hydrophilic part. Hence the polymer-cisplatin drug conjugate is capable of self-organizing to form nano-assembly in water. The size distribution of this nano-assembly was investigated by dynamic light scattering measurements and showed mono-modal distribution as shown in figure 5.12a The mean diameter of the polymer-cisplatin drug conjugate nanoparticles was measured to be 165 ± 10 nm in aqueous solution. The morphology of the polymer-drug conjugate was studied by field emission- scanning electron microscope and atomic force microscope techniques. The FE-SEM and AFM images of the polymer-drug nanoparticles are shown in figure 5.12 which exhibited the formation of spherical nanoparticles with average size of 160 ± 10 . Thus, the amphiphilic polymer cisplatin complex revealed the formation of

uniform spherical nanoparticles as obtained from DLS, FE-SEM and AFM studies which can be utilized for cisplatin delivery to the cancer cells.

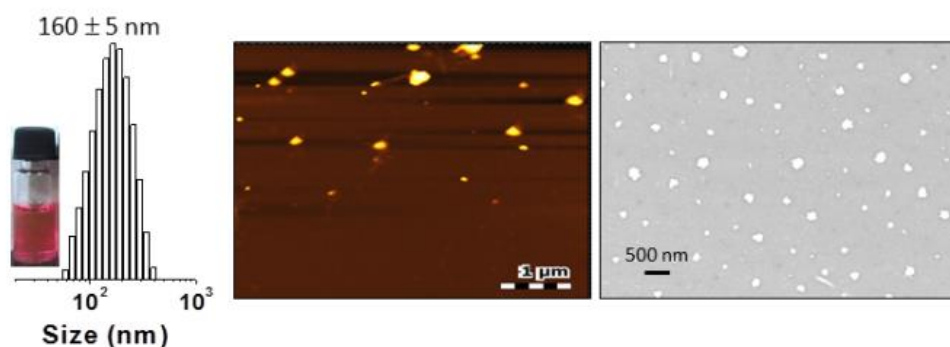


Figure 5.12. DLS histogram AFM image and FESEM image of polymer cisplatin conjugated nanoparticles.

The UV-vis absorption and emission spectra of the PBI-CPCL-PEGPCL polymer was recorded in THF solution to study the photo-physical properties of the perylene bisimide chromophore. The absorption and emission spectra of the block copolymer are shown in figure 5.13. The absorption spectra revealed the absorption peak ($0 \rightarrow 0$, $0 \rightarrow 1$, $0 \rightarrow 2$, $0 \rightarrow 3$) between 450 to 530 nm regions related to $S_0 \rightarrow S_1$ transition which confirmed the existence of well resolved vibronic structure corresponding to $S_0 \rightarrow S_1$ transitions with transition dipole moment along the long axis of the molecule. The polymer was excited at absorption maxima of 485 nm and emission spectrum was recorded. Emission maximum at 530 nm was obtained along with the well resolved structure of the perylene bisimide chromophore. Further, the absorption spectrum of the polymer-cisplatin conjugate nanoparticles was recorded in aqueous medium and it is shown in figure 5.13c. In aqueous medium the electronic coupling between the perylene bisimide chromophores resulted in the broadening of the absorption spectra along with the loss of the structural features. The emission spectrum recorded at an absorption maximum of 495 nm exhibited a maximum at 540 nm showing characteristic emission of perylene bisimide chromophore.

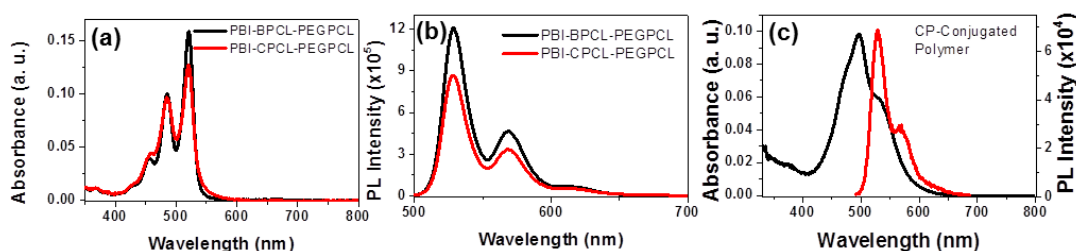


Figure 5.13. Absorption(a) and emission(b) spectra of block copolymers in THF. Absorption and emission (c) spectra of polymer-cisplatin conjugated nanoparticles in aqueous medium.

The fluorescence quantum yield of the PBI-CPCL-PEGPCL polymer and the polymer-cisplatin conjugate were determined in THF and water, respectively using *N,N'*-bis(hexylheptyl)perylene-3,4,9,10-bis(dicarbiximide) as standard in chloroform. The QY of the block copolymer in THF was measured to be 0.90 and that of polymer-cisplatin conjugate in water was measured to be 0.25. The high quantum yield of the polymer-drug conjugate is the result of the decreased possible aggregation of PBI chromophores in aqueous medium due to the hydrophilic PEG chain present on the caprolactone repeating unit facilitating the water solubility of the polymer in aqueous medium. Hence, these studies revealed that loading of cisplatin into the block copolymer through conjugation did not alter the optical properties of perylene bisimide chromophore and therefore it can be employed for the diagnostic purpose.

5.3.4. Stability Against GSH detoxification and Enzyme-responsive Delivery

The stability of the polymer-cisplatin drug conjugate was investigated in presence of chloride ions in saline (0.9%) and phosphate buffer saline as these ions favour the cleavage of platinum-carboxylate (Pt-OOC) linkages and release cisplatin from the polymer-drug conjugate through exchange reaction and is schematically shown in figure 5.14a. For this purpose, polymer-cisplatin complex was incubated in saline (aqueous NaCl, pH = 6.8), and PBS 7.4 at 37 °C for 48 h. The OPD (*o*-phenylenediamine) colorimetric assay was utilized to establish the amount of drug released from polymer-drug conjugate in the media wherein the released drug is treated with OPD solution in DMF at 80 °C. The absorption spectra of the resulting solution (OPD-Pt complex) were recorded and the absorbance at 706 nm determines the amount of drug released in the solution. The cumulative release was calculated using following equation: Cumulative release (%) = $C_n \times V_0 / m \times 100$ %, where C_n is

the amount of drug loaded in the n th sample, V_0 is the total volume and m is total amount loaded in the prodrug.

The absorption spectra of OPD treated samples showed increase in the absorption maxima with respect to drug release time. The cumulative release profile of cisplatin from polymer-cisplatin conjugate in presence of water, saline (0.9%) and PBS pH 7.4 is shown in figure 5.14b. It is clear from the release profile that the polymer drug conjugate was quiet stable in water as less than 10 % of drug was released in 48 h. Hence, the polymer-cisplatin drug conjugate could be stored in water. In presence of chloride ions in saline, polymer-drug conjugate was cleaved due to the de-chelation and 35 % of drug was leached from the nanoparticles. A burst release of 25 % of drug was observed in 12 h followed by very slow release of drug (only 10 %) over a period of 48 h. Thus, more than 60 % of drug was retained in the polymer-cisplatin conjugated nanoparticles.

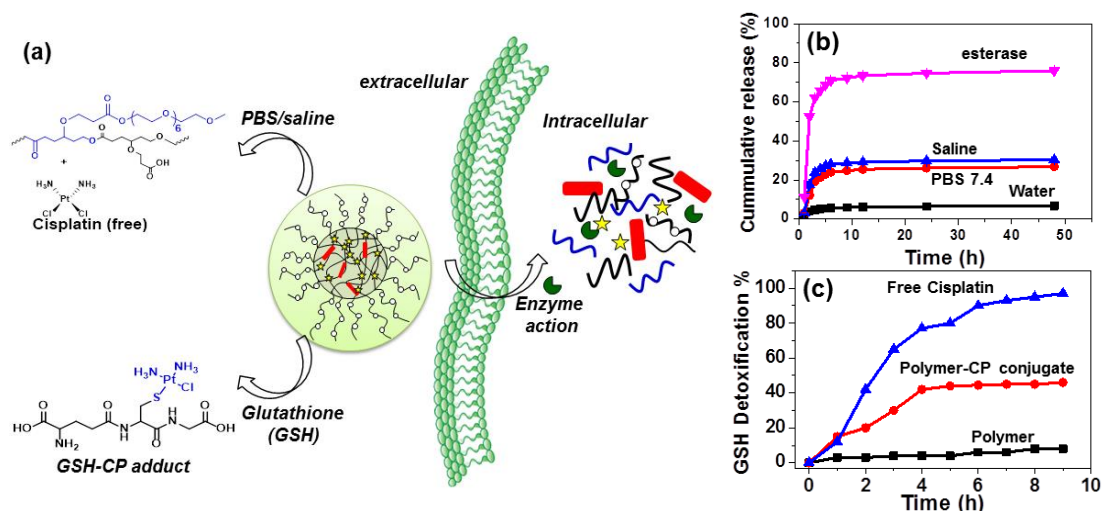


Figure 5.14. Schematic representation of cisplatin release from polymer-cisplatin conjugated nanoparticles in presence of saline/PBS/enzyme and GSH detoxification (a), cumulative release profile of cisplatin in presence of water, PBS 7.4 and (0.9 %) saline and esterase enzyme(b) Extent of GSH reaction on PBI-CPCL-PEGPCL polymer, polymer-cisplatin conjugate and free cisplatin (monitored at 260 nm absorbance for formation of Pt-S bond)(c)

The stability of polymer-cisplatin drug conjugate in saline under physiological conditions is particularly important because the drug carrying nanoparticles are exposed to 5 to 10 times higher chloride ion concentration in extracellular conditions ($[Cl^-] = 100$ mM) compared to intracellular condition ($[Cl^-] = 3-10$ mM). The cisplatin conjugated nanoparticles can also undergo de-chelation in presence of phosphate ions

present in PBS buffer and hence 30 % of drug leaching was observed in PBS pH 7.4 buffer. The drug release kinetics of the cisplatin conjugated nanoparticles in PBS buffer was found to be similar to that in the saline. Thus, these release studies suggested that the polymer-cisplatin conjugated nanoparticles were stable under physiological conditions with more than 60 % of the drug was retained in the polymer nanoparticles and can be employed for the intravenous administration of the drug for cancer therapeutics. Cisplatin encounters the major challenge of detoxification by sulphur containing biological species present in the body such as amino acids like cysteine and tripeptide glutathione (GSH) in cancer therapy. Cisplatin exhibit strong reactivity towards S-donor molecules such as methalothioneins or GSH resulting in the formation of stable S-Pt bond which leads to resistance and toxicity. Thus, the stability of polymer-cisplatin conjugated nanoparticles was studied against GSH detoxification. For this purpose, free cisplatin, PBI-CPCL-PEGPCL polymer and polymer-cisplatin conjugate were treated with GSH in 0.1mM Tris-HCl buffer containing 4.6 mM NaCl at 37 °C in the dark. Reaction between cisplatin and GSH was monitored by absorption spectroscopy which showed new absorption peak at 250 nm corresponding to the formation of Pt-S bond and the intensity of peak increased with time. The plot of percentage detoxification vs reaction time is shown in figure 5.14c. The nascent polymer did not show any detoxification with GSH and thus the polymer is completely stable against GSH. It is clear from the plot that free cisplatin readily reacted with GSH and more than 95 % of drug was detoxified. In case of polymer-cisplatin conjugated nanoparticles more than 55 % of the drug was protected from the detoxification against GSH action as the cisplatin was confined inside the polymer nanoparticles. Thus, this experiment clearly indicates that these newly designed polymer-cisplatin conjugates are capable of stabilizing cisplatin inside the nanoparticles and helps in reducing GSH detoxification.

The intracellular drug delivering capability of the polymer-cisplatin drug conjugated nanoparticles was investigated in presence of lysosomal esterase enzyme owing to the presence of aliphatic ester linkages in the polymer backbone. To study the intracellular fate of the polymer-cisplatin drug conjugated nanoparticles and subsequent cisplatin release the nanoparticles were incubated with 10 U esterase in presence of esterase enzyme in PBS pH 7.4 buffer at 37 °C for 48 h. The polymer nanoparticles were cleaved in presence of esterase enzyme which leads to the release

of cisplatin in to the medium which is schematically shown in figure 5.14a and the amount of cisplatin released was measured by OPD assay. The cumulative cisplatin release pattern is shown in figure 5.14b which exhibited 80 % of cisplatin release from the drug conjugated nanoparticles due to the rupture of nanoparticles in presence of esterase enzyme.

Further the cleavage of polymer-cisplatin conjugated nanoparticles was also demonstrated by dynamic light scattering experiment. Polymer-cisplatin conjugated nanoparticles were incubated in PBS 7.4 buffer at 37 °C for 48 h in absence and presence of esterase enzyme. The size of the nanoparticles was measured by DLS at regular time interval and it was plotted against incubation time which is shown in figure 5.15. In absence of esterase enzyme there was a negligible change in size of the polymer nanoparticles with incubation time suggesting that the nanoparticles were stable in PBS buffer. On the other hand, in presence of esterase enzyme size of the polymer nanoparticles increased with incubation time. The increase in the nanoparticle size was attributed to the disassembly of polymer nanoparticles due to the cleavage of the ester linkage present in the polymer backbone. Hence the present polymer design has demonstrated that the polymer-cisplatin conjugated nanoparticles were efficient for stabilizing the drug inside the nanoparticles at extracellular condition and delivering cisplatin at the intracellular conditions.

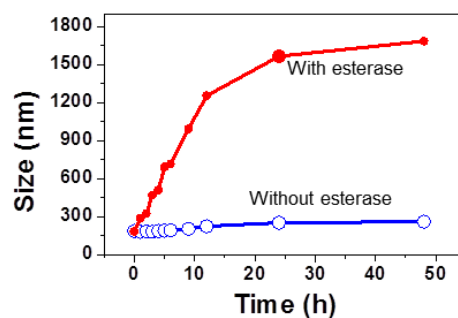


Figure 5.15. Plot for size of the polymer nanoparticles obtained from DLS vs incubation time in absence and presence of esterase enzyme at 37°C.

5.3.5. Cytotoxicity and Cellular Uptake

The *in vitro* cell viability of HeLa and MCF-7 cells incubated with nascent PBI-CPCL-PEGCL polymer was examined in order to employ the polymer nanoparticles for the bioimaging application. The concentration of the polymer was varied upto 100 $\mu\text{g}/\text{mL}$. The cell viability data is shown in figure 5.16 which indicates that more than 80 % cell viability of both HeLa and MCF-7 cells was observed for 100 $\mu\text{g}/\text{mL}$ concentration. These results revealed that the polymer nanoparticles are non-toxic even at 100 $\mu\text{g}/\text{mL}$ suggesting that the newly designed block copolymer are promising for bioimaging application due to the high biocompatibility.

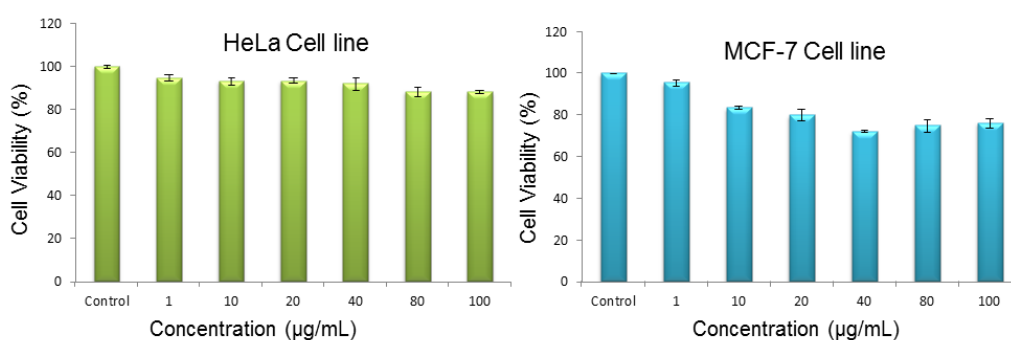


Figure 5.16. Cell viability study of cervical (HeLa) (a) and breast cancer (MCF-7) (b) cells incubated with PBI-CPCL-PEGPCL nascent polymer.

The *in vitro* cytotoxicity of the polymer-cisplatin conjugated nanoparticles and free cisplatin against HeLa and MCF-7 cells were investigated. The equivalent concentration of cisplatin was maintained in free cisplatin and polymer-drug conjugate and the concentration was varied from 0.1 to 8.0 $\mu\text{g}/\text{mL}$. The cytotoxicity data are shown in figure 5.17. In HeLa cells, Polymer-cisplatin conjugate showed 50 % cell killing at 2 $\mu\text{g}/\text{mL}$ whereas free cisplatin showed the same cell killing at 1 $\mu\text{g}/\text{mL}$. This result indicates that polymer-drug conjugate nanoparticles have slightly lower cytotoxicity than free cisplatin but at higher concentration of 8.0 $\mu\text{g}/\text{mL}$ both free cisplatin and polymer-drug conjugated nanoparticles exhibit similar cell killing which may be due to slow release of cisplatin from the polymer-drug conjugate nanoparticles. In MCF-7 cells, both free cisplatin and polymer-drug conjugated nanoparticles showed 50 % cell killing at 2 $\mu\text{g}/\text{mL}$ indicating that polymer-drug conjugated nanoparticles exhibit potential cell killing. Hence, the custom designed polymer-cisplatin conjugated nanoparticles are efficient candidates for cisplatin delivery to the cancer cells. The cellular uptake studies were carried out in HeLa cells

using confocal microscopic imaging. The importance of the current design is that cisplatin conjugated polymer contains PBI chromophore and hence it is red luminescent in nature so it provides an opportunity to monitor the drug release from the polymer nanoparticles as well as the fate of the polymer unlike the other non-luminescent polymer-cisplatin conjugate nano-carrier designs which depend upon the physically encapsulated dyes or the fluorescent drug used in combination therapy as cisplatin is non-fluorescent drug.

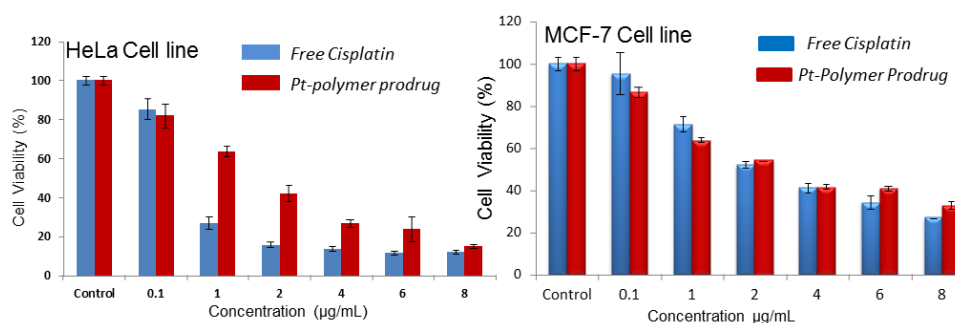


Figure 5.17. Cell viability study of cervical cancer (HeLa) (a) and breast cancer (b) cell line incubated with polymer-cisplatin conjugated nanoparticles and free cisplatin as control.

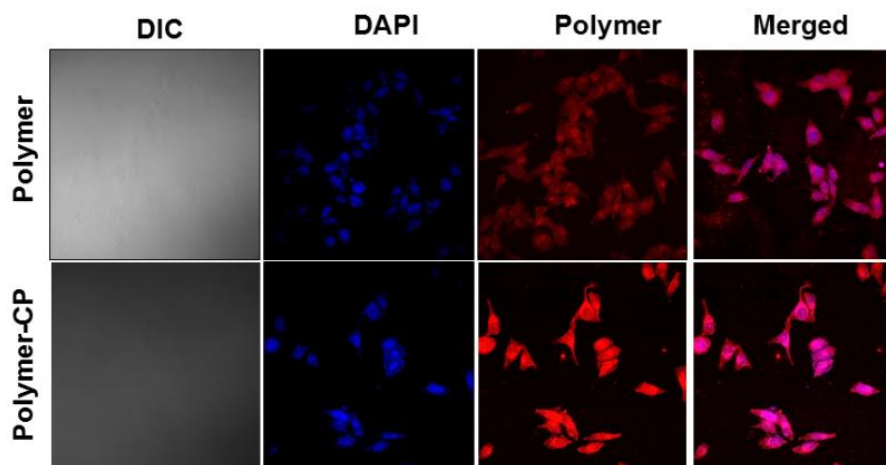


Figure 5.18. CLSM images of HeLa cells incubated with nascent PBI-CPCL-PEGPCL block copolymer and polymer-cisplatin conjugated nanoparticles. Cells were stained with DAPI (b, f) and observed for red fluorescence of PBI (c, g)

The cellular uptake of nascent polymer and the polymer-cisplatin conjugated nanoparticles was demonstrated in HeLa cells. For this purpose, HeLa cells were incubated with nascent polymer and the polymer-cisplatin conjugated nanoparticles for 4 h and then the polymers were stained with DAPI to visualize the cell nuclei in the confocal microscope. Figure 5.18 shows the CLSM images of nascent polymer and the polymer-cisplatin conjugated nanoparticles. The blue fluorescence ($\lambda = 405$ nm) from cell nuclei was observed as the cells were stained with DAPI (figure 5.18b and f). The red fluorescence produced from PBI chromophore present in the polymer was observed through red channel ($\lambda = 514$ nm). Figure 5.18c and g clearly indicated that the red fluorescence coming from the PBI chromophore in the polymer was primarily coming from cytoplasm thus the polymer and cisplatin conjugated polymer nanoparticles were internalized in to the cells and accumulated in the cytoplasm and the peri-nuclear region. The merged images further supported the above observation. Hence, cellular uptake studies revealed that, the polymer-cisplatin conjugated nanoparticles were rapidly internalized into the cells and distributed mainly in the cytoplasm and peri-nuclear environment and importantly the tracking of cisplatin release was possible due to the inherent red fluorescence from the PBI chromophore in the polymer. Thus the current polymer design is efficient candidate for the therapeutics as well as diagnostic purpose.

5.4. Conclusion

In summary, the present investigation demonstrated new classes of dual functional highly luminescent, biodegradable, cisplatin conjugated amphiphilic block copolymer nanocarriers for therapeutic and diagnostic application in cancer cells. Tailor made PEG₃₅₀ substituted caprolactone monomer was prepared by multistep synthesis to employ as monomer for ring opening polymerization. The ROP process was carried out for the macro-initiator synthesis in which the dual hydroxyl functionalized PBI chromophore having inherent red luminescence was employed as initiator and t-butyl ester substituted caprolactone monomer. The block copolymer was synthesized by using t-butyl substituted PCL polymer as macro-initiator and the newly designed PEG substituted caprolactone as monomer in ROP process. The length of the block copolymer was varied by varying monomer to initiator ratio. The PBI-BPCL-PEGPCL block copolymer was converted into carboxylic acid functionalized PBI-CPCL-PEGPCL block copolymer as it was designed to conjugate cisplatin drug through carboxyl acid functional groups. The cisplatin conjugated block copolymer were amphiphilic having cisplatin stitched hydrophobic core and the PEG substituted caprolactone units as hydrophilic shell and hence self-assembled as spherical nanoparticles with average size of 160 nm in aqueous medium. The novel optical properties of PBI chromophore were preserved in the polymer-cisplatin conjugated nanoparticles so that it can be utilized for the bioimaging application in cancer cells. The drug conjugated block copolymers exhibited very good stability in water. Further, in saline and PBS buffer more than 60 % of cisplatin was retained inside the polymer-cisplatin nanoparticles and the cisplatin present inside the nanoparticles were also protected against GSH detoxification. The *in vitro* drug release studies suggested that lysosomal esterase enzyme triggers the cleavage of polymer backbone having aliphatic ester linkages to deliver the drug in the cancer cells. Cytotoxicity studies of the nascent polymer confirmed that the PBI-CPCL-PEGPCL block copolymer was highly biocompatible and hence utilized as fluorescent probe to track the cisplatin delivery inside the cancer cells using bioimaging tool as cisplatin is non-fluorescent drug and difficult to track otherwise. Moreover, the cytotoxicity of the polymer-cisplatin conjugated polymer nanoparticles is comparable to that of free cisplatin in HeLa and MCF-7 cells. Cellular uptake studies of polymer-cisplatin polymer conjugated nanoparticles in HeLa and MCF-7 cells revealed that nanoparticles were

readily internalized inside the cells and preferably distributed in the cytoplasm and the peri-nuclear region to deliver the drug in the cancer cells. The accumulation of the drug conjugated nanoparticles inside the cytoplasm was confirmed from the red fluorescence of PBI chromophore in the polymer by CLSM imaging. Thus, the present biodegradable, luminescent cisplatin conjugated block copolymers are promising nanocarriers for simultaneous drug delivery and fluorescence probe for tracking of the drug inside the cancer cells.

5.5. References

1. Duan, X.; He, C.; Kron, S.; Lin, W. *WIREs Nanobiotechnol.* **2016**, *8*, 776.
2. Johnstone, T.; Suntharalingam, K.; Lippard, S. *Chem. Rev.* **2016**, *116*, 3436.
3. Fuertes, M.; Alonso, C.; Perez, J. *Chemical Reviews.* **2003**, *103*, 647.
4. Browning, R.; Reardon, P.; Parhizkar, M.; Pedley, R.; Edirisinghe, M.; Knowles, J.; Stride, E. *ACS Nano.* **2017**, *11*, 8560.
5. Siddik, Z. *Oncogene*, **2003**, *22*, 7265.
6. Wang, X.; Guo, Z. *Chem. Soc. Rev.* **2013**, *42*, 202.
7. Wang, D.; Lippard, S. *Nature Reviews.* **2005**, *4*, 307.
8. Kelland, L. *Nature Reviews.* **2007**, *7*, 574.
9. Ohta, S.; Hiramoto, S.; Amano, Y.; Sato, M.; Suzuki, Y.; Shinohara, M.; Emoto, S.; Yamaguchi, H.; Ishigami, H.; Sakai, Y.; Kitayama, J.; Ito, T. *Bioconjugate Chem.* **2016**, *27*, 504.
10. Nukolova, N.; Oberoi, H.; Chekhonin, V.; Kabanov, A.; Bronich, T. *Mol. Pharmaceutics* **2013**, *10*, 3913.
11. Becher, T.; Mendonca, M.; Farias, M.; Portugal, R.; Jesus, M.; Ornelas, C. *ACS Appl. Mater. Interfaces.* **2018**, *10*, 21891.
12. Babu, A.; Wang, Q.; Muralidharan, R.; Shanker, M.; Munshi, A.; Ramesh, R. *Mol. Pharmaceutics.* **2014**, *11*, 2720.
13. Li, J.; Lyv, Z.; Li, Y.; Liu, H.; Wang, J.; Zhan, W.; Chen, H.; Chen, H.; Li, X. *Biomaterials.* **2015**, *51*, 12.
14. Shirbin, S.; Ladewig, K.; Fu, Q.; Klimak, M.; Zhang, X.; Duan, W.; Qiao, G. *Biomacromolecules.* **2015**, *16*, 2463.
15. Feng, L.; Gao, M.; Tao, D.; Chen, Q.; Wang, H.; Dong, Z.; Chen, M.; Liu, Z. *Adv. Funct. Mater.* **2016**, *26*, 2207.
16. liao, L.; Liu, J.; Dreaden, E.; Morton, S.; Shopsowitz, K.; Hammond, P.; Johnson, J. *J. Am. Chem. Soc.* **2014**, *136*, 5896.
17. Surnar, B.; Sharma, K.; Jayakannan, M. *Nanoscale* **2015**, *7*, 17964.
18. Surnar, B.; Subash, P.; Jayakannan, M. *Z. Anorg. Allg. Chem.* **2014**, *640*, 1119.
19. Surnar, B.; Jayakannan, M. *Biomacromolecules* **2016**, *17*, 4075.
20. Deshpande, N. U.; Jayakannan, M.; *Biomacromolecules* **2017**, *18*, 113-126.

21. Vishwasrao, H.; Master, A.; Seo, Y.; Liu, X.; Pothayee, N.; Zhou, Z.; Yuan, D.; Boska, M.; Bronich, T.; Davis, R.; Riffle, J.; Papkov, M.; Kabanov, A. *Chem. Mater.* **2016**, *28*, 3024.
22. Li, Y.; Li, Y.; Zhang, X.; Xu, X.; Zhang, Z.; Hu, C.; He, Y.; Gu, Z. *Theranostics*. **2016**, *6*, 1293.
23. Cong, Y.; Xiao, H.; Xiong, H.; Wang, Z.; Ding, J.; Li, C.; Chen, X.; Liang, X.; Zhou, D.; Huang, Y. *Adv. Mater.* **2018**, *30*, 1706220.
24. Patel, N.; Piroyan, A.; Nack, A.; Galati, C.; McHugh, M.; Orosz, S.; Keeler, A.; O'Neal, S.; Zamboni, W.; Davis, B.; Coleman, T. *Mol. Pharmaceutics*. **2016**, *13*, 1996.
25. Voulgari, E.; Bakandritsos, A.; Galtsidis, S.; Zoumpourlis, V.; Burke, B. P.; Clemente, G. S.; Cawthorne, C.; Archibald, S. J.; Tucek, J.; Zbonl, R.; Kantarelou, V.; Karydas, A. G.; Avgoustakis, K. *J. Control. Release* **2016**, *243*, 342-356.
26. Zhu, Z.; Wang, Z.; Hao, Y.; Zhu, C.; Jiao, Y.; Chen, H.; Wang, Y.; Yan, J.; Guo, Z.; Wang, X. *Chem, Sci.* **2016**, *7*, 2864.
27. Sun, X.; Du, R.; Zhang, G.; Zhang, G.; Zheng, X.; Qian, J.; Tian, X.; Zhou, J.; Wang, Y.; Wu, Y.; Zhong, K.; Cai, D.; Zou, D.; Wu, Z. *ACS Nano*. **2017**, *11*, 7049.
28. Wan, Q.; Zeng, G.; He, Z.; Mao, L.; Liu, M.; Huang, H.; Deng, F.; Zhang, X.; Wei, Y. *J. Mater. Chem. B*. **2016**, *4*, 5692-5699.
29. Teng, B.; Ma, P.; Yu, C.; Zhang, X.; Feng, Q.; Wen, L.; Li, C.; Cheng, Z.; Jin, D.; Lin, J. *J. Mater. Chem. B*. **2017**, *5*, 307.
30. Wang, Y.; Wu, Z.; Liu, S.; Chu, X. *Anal. Chem.* **2015**, *87*, 6470.
31. Chatterjee, B.; Sahoo, A.; Ghosh, S.; Chattopadhyay, A. *RSC Adv.* **2016**, *6*, 113053.
32. Chatterjee, B.; Ghoshal, A.; Chattopadhyay, A.; Ghosh, S. S. *ACS Biomater. Sci. Eng.* **2018**, *4*, 1005.
33. Zhou, F.; Feng, B.; Yu, H.; Wang, D.; nag, T.; Liu, J.; Meng, Q.; Wang, S.; Zhang, P.; Zhang, Z.; Li, Y. *Theranostics* **2016**, *6*, 679.
34. Zhang, L.; Su, H.; Cai, J.; Cheng, D.; Ma, Y.; Zhang, J.; Zhou, C.; Liu, S.; Shi, H.; Zhang, Y.; Zhang, C. *ACS Nano*. **2016**, *10*, 10404.
35. Ding, D.; Li, K.; Zhu, Z.; Pu, K-Y.; Hu, Y.; Jiang, X.; Liu, B. *Nanoscale* **2011**, *3*, 1997-2002.
36. Li, Y.; Li, Y.; Zhang, X.; Xu, X.; Zhang, Z.; Hu, C.; He, Y.; Gu, Z. *Theranostics*. **2016**, *6*, 1293.

Overall summary and future directions

6 Overall summary and future directions

This thesis work is focused on design and development of multifunctional fluorescent, biodegradable caprolactone block copolymers for drug delivery and bioimaging in cancer cells to achieve improved cancer treatment. For this purpose, blue fluorescent oligophenylene vinylene (OPV) and red fluorescent perylene bisimide (PBI) were explored imaging agents for bioimaging and carboxylic acid and PEG substituted polycaprolactone nanocarriers were demonstrated for delivery of drug such as DOX and cisplatin to cancer cells. Moreover the OPV forms a FRET probe with NR as acceptor for intracellular bioimaging in cancer cells.

Blue-luminescent biodegradable PCL block copolymers were designed and developed for simultaneous delivery of doxorubicin and bioimaging at the intracellular level. Ring opening polymerization process was adopted to synthesize t-butyl substituted caprolactone polymers using tailor-made blue luminescent oligo-phenylenevinylene chromophore as initiator. The fluorescent caprolactone block copolymers were encapsulated with doxorubicin and demonstrated for enzyme responsive *in vitro* delivery of DOX. The block copolymer nanocarriers also served as fluorescent probe for cancer cell imaging.

The blue fluorescent OPV tagged block copolymer nanoassemblies were encapsulated with NR dye to obtain FRET probe with OPV as donor and NR acceptor. *In vitro* enzyme triggered FRET process was studied by detailed steady state fluorescence and TCSPC measurements. Further the energy transfer process in the FRET probe was also visualized inside the cancer cells.

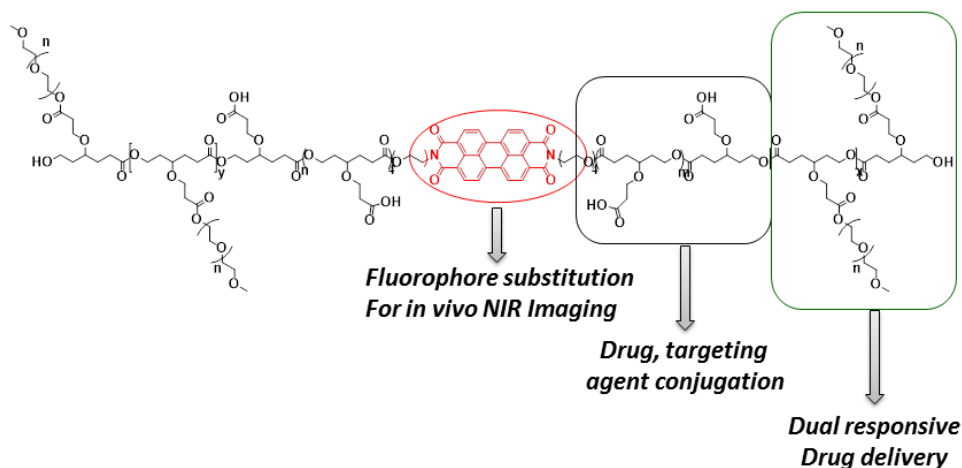
The red luminescent carboxylic acid substituted PCL polymers were developed by ROP process between red luminescent hydroxyl functionalized PBI initiator and t-butyl ester substituted caprolactone monomer. The conversion of t-butyl substituted PCL polymer into carboxylic acid substituted PCL polymers resulted into luminescent amphiphilic block copolymers readily forming nano-assemblies in aqueous medium. The block copolymer nano-assemblies were employed for cell imaging in cancer cells owing to the inherent red luminescence of PBI chromophore.

Novel triblock copolymers were synthesized from t-butyl ester and PEG functionalized monomers and PBI chromophore initiator by ROP process. For this

purpose PEG substituted caprolactone monomer was tailor made to improve the water solubility of the block copolymers. The carboxylic acid functionality in the triblock copolymer was utilized for chemical conjugation of cisplatin. These red fluorescent cisplatin conjugated polymer nanocarriers were demonstrated for simultaneous tracking of cisplatin delivery to cancer cells.

Future direction

This thesis work has combined the smart features of conjugated polymers and biodegradable polymers together to give rise to a plenty of opportunities for the drug delivery of drug and monitoring the fate of the drug as well as nanocarriers within single nano-object to improve the efficacy of the treatment. The perylene bisimide (PBI) is potential chromophore for fluorescence imaging technique as it has emission in the red region of visible spectrum. Further conjugation in PBI can be extended by substitution in the core of the molecule to obtain emission in the near IR region which is beneficial for the deep tissue penetration and biological autofluorescence in *in vivo* imaging. Further the carboxylic group present on the caprolactone backbone can be conjugated with drugs, fluorophore, targeting ligand to improve the cellular uptake of nanocarriers. Further encapsulation of another drug in cisplatin conjugated block copolymer nanoparticles provides opportunity for codelivery of drug for combination therapy. The PEG substituted polycaprolactone block is known to exhibit thermoresponsive behaviour therefore by varying the PEG chain length in the polymer backbone dual (temperature and enzyme) responsive polymer nanocarriers can be developed for controlled drug delivery.



List of Publications

7 List of Publications

1. Kulkarni, B.; Surnar, B.; Jayakannan, M. Dual Functional Nanocarrier for cellular Imaging and Drug Delivery in Cancer Cells Based on π -Conjugated Core and Biodegradable Polymer Arms. *Biomacromolecules* **2016**, *17*, 1004-1016.
2. Kulkarni, B.; Jayakannan, M. Fluorescent-Tagged Biodegradable Polycaprolactone Block Copolymer FRET Probe for Intracellular Bioimaging in Cancer Cells. *ACS Biomaterials Science and Engineering*. **2017**, *3*, 2185-2197.
3. Kulkarni, B.; Jayakannan, M. Enzymatically-Biodegradable Perylene bisimide-Carboxylic Polycaprolactone Fluorescent Block Copolymers for Bioimaging in Cancer Cells *Manuscript Submitted*
4. Kulkarni, B.; Jayakannan, M. Perylene-Tagged Triblock Theranostic Fluorescent Nanocarriers for Pt-drug Delivery in Cancer Cells. *Manuscript under Preparation*

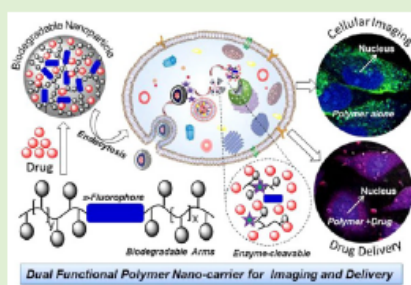
Dual Functional Nanocarrier for Cellular Imaging and Drug Delivery in Cancer Cells Based on π -Conjugated Core and Biodegradable Polymer Arms

Bhagyashree Kulkarni, Bapurao Surnar, and Manickam Jayakannan*

Department of Chemistry, Indian Institute of Science Education and Research, Pune, Dr. Homi Bhabha Road, Pune, 411008 Maharashtra, India

Supporting Information

ABSTRACT: Multipurpose polymer nanoscaffolds for cellular imaging and delivery of anticancer drug are urgently required for the cancer therapy. The present investigation reports a new polymer drug delivery concept based on biodegradable polycaprolactone (PCL) and highly luminescent π -conjugated fluorophore as dual functional nanocarrier for cellular imaging and delivery vehicles for anticancer drug to cancer cells. To accomplish this goal, a new substituted caprolactone monomer was designed, and it was subjected to ring opening polymerization using a blue luminescent bishydroxyloligo-phenylenevinylene (OPV) fluorophore as an initiator. A series of A–B–A triblock copolymer building blocks with a fixed OPV π -core and variable chain biodegradable PCL arm length were tailor-made. These triblocks self-assembled in organic solvents to produce well-defined helical nanofibers, whereas in water they produced spherical nanoparticles (size \sim 150 nm) with blue luminescence. The hydrophobic pocket of the polymer nanoparticle was found to be an efficient host for loading water insoluble anticancer drug such as doxorubicin (DOX). The photophysical studies revealed that there was no cross-talking between the OPV and DOX chromophores, and their optical purity was retained in the nanoparticle assembly for cellular imaging. *In vitro* studies revealed that the biodegradable PCL arm was susceptible to enzymatic cleavage at the intracellular lysosomal esterase under physiological conditions to release the loaded drugs. The nascent nanoparticles were found to be nontoxic to cancer cells, whereas the DOX-loaded nanoparticles accomplished more than 80% killing in HeLa cells. Confocal microscopic analysis confirmed the cell penetrating ability of the blue luminescent polymer nanoparticles and their accumulation preferably in the cytoplasm. The DOX loaded red luminescent polymer nanoparticles were also taken up by the cells, and the drug was found to be accumulated at the perinuclear environment. The new nanocarrier approach reported in the present manuscript accomplishes both cellular imaging and delivering drugs to intracellular compartments in a single polymer system. The present investigation is one of the first examples to demonstrate the dual functional biodegradable luminescence nanocarrier concept in the literature, and the studies established this proof-of-concept in cellular imaging and drug delivery in cancer cells.



INTRODUCTION

Multipurpose polymer nanoscaffolds are urgently required for the simultaneous detection and delivery of anticancer drugs to improve the treatment efficacies in cancer.^{1,2} Recently, self-assembled nanoparticulate dispersion of luminescent π -conjugated polymers (or oligomers) was explored as a fluorescent nanoprobe for cellular imaging and diagnosis.^{3–5} The emission color of these nanoparticles was tuned by manipulating their HOMO–LUMO band gaps of their π -conjugated backbones.^{6,7} To enhance the cellular uptake and imaging, these π -conjugated nanoparticles were further modified with cationic charges to increase their intracellular administration and binding to DNA.⁸ Cationic polyelectrolytes based on polyfluorenes and their copolymers,^{9–14} poly(phenyleneethynylene),^{15,16} and poly(phenylenevinylene)s,^{17–21} are some of the important examples for the above studies. These polymers were employed as probes for Heparin sensing,²² NIR fluorescence imaging,²³ targeted

imaging of HER2-positive cells,²⁴ etc. Two-photon imaging and two-photon photodynamic therapeutic techniques were also developed based on these π -conjugated polymers in living cells.^{25–29} Bioluminescence resonance energy transfer process between luminal and cationic oligo-phenylenevinylene (OPV) chromophores was also achieved for anticancer, antifungal activities and combating drug resistance of cancer cells.^{30,31} Few attempts were also made to blend or complex these π -conjugated polymers (or oligomer) with polystyrene-*co*-maleic anhydride,³² poly(L-glutamic acid),³³ or lipids,³⁴ antibodies,³⁵ or cucurbituril³⁶ to bring appropriate biocompatibility and nanoshape for drug administration. Cationic polyfluorene polyelectrolyte–cisplatin complex was also developed for imaging and drug tracking in

Received: December 8, 2015

Revised: February 3, 2016

Published: February 3, 2016

Fluorescent-Tagged Biodegradable Polycaprolactone Block Copolymer FRET Probe for Intracellular Bioimaging in Cancer Cells

Bhagyashree Kulkarni and Manickam Jayakannan*[✉]

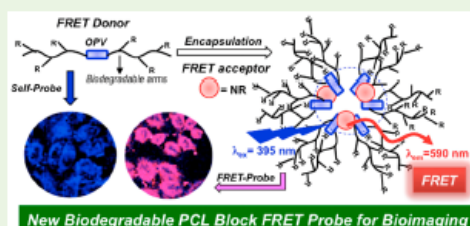
Department of Chemistry, Indian Institute of Science Education and Research (IISER) Pune, Dr. Homi Bhabha Road, Pune 411008, Maharashtra, India

Supporting Information

ABSTRACT: The present investigation reports a new fluorophore-tagged biodegradable polycaprolactone (PCL) block copolymer FRET-probe for intracellular imaging in cancer therapy. A hydroxyl functionalized π -conjugated oligophenylenevinylene (OPV) chromophore was tailor-made, and it was incorporated in a *t*-butyl ester substituted polycaprolactone block copolymer via ring opening polymerization. This blue-luminescent OPV-PCL triblock self-assembled as <200 nm spherical nanoparticles (FRET donor), and it encapsulated water insoluble Nile red (NR, FRET acceptor) to yield an OPV-NR FRET probe. Selective photo excitation of the OPV

chromophore in block nanoassemblies enabled the excitation energy transfer from the OPV to NR and facilitated the efficient FRET process in aqueous medium. Time-correlated fluorescent decay dynamics and detailed photophysical studies were carried out to estimate the Förster distance, donor–acceptor distance, and the excitation energy transfer efficiency. These parameters confirmed the occurrence of the FRET process within the confined nanoparticle environment. The PCL chains in the FRET probe were susceptible to enzymatic biodegradation in intracellular environments, and the degradation process controlled the FRET on/off mechanism. Cytotoxicity studies revealed that the FRET probe was biocompatible and nontoxic to cells, and the FRET-probe was found to be readily taken up by the cancer cells, and it was internalized in the cytoplasm and peri-nuclear environment. Selective photoexcitation of the OPV chromophore in a confocal microscope exhibited dual emission from the FRET probe. The cancer cells exhibited blue luminescence (self-emission) with respect to the OPV chromophore (in the blue channel) and bright red-luminescence from the NR dye followed by the FRET process at the cellular level (in the red channel). The dual luminescence characteristics, biodegradation and biocompatibility, make the newly designed PCL-OPV-NR FRET probe an excellent biomedical nanodevice for bioimaging applications, and the proof-of-concept was established in cervical (HeLa) and breast cancer (MCF 7) cell lines.

KEYWORDS: FRET, block copolymers, enzyme-responsive, polycaprolactone, bioimaging



New Biodegradable PCL Block FRET Probe for Bioimaging

INTRODUCTION

Fluorescent probe tagged polymer nanocarriers are emerging as multipurpose biomaterials for both delivering anticancer drugs/genes and also as luminescent probes for cellular imaging in cancer therapy.^{1–3} Macromolecular nanocarriers have additional advantages of passive selective accumulation through an EPR effect and are also capable of enhancing the bioavailability and biodistribution of loaded cargoes at the cancer tissues.^{4,5} Among the various fluorescence techniques, the Förster resonance energy transfer (FRET) process⁶ is one of the most powerful noninvasive tools, and it was employed to study protein folding⁷ and monitoring real-time drug release kinetics at the cellular level.^{8,9} The development of FRET probes for biological application is a relatively challenging task since the geometry of the polymer nanocarriers should be capable of confining the donor–acceptor chromophores within the Förster distance of 20–60 Å under physiological conditions.⁶ Three types of polymeric systems were explored in the construction of FRET probes: (i) FRET donor–acceptor

chromophores either chemically conjugated on the non-luminescent polymers^{10–13} or physically encapsulated in their nanoscaffold,^{14,15} (ii) luminescent π -conjugated cationic polymer nanoassemblies as a FRET donor which encapsulated FRET acceptor dyes or drugs,^{16–19} and (iii) both FRET donor and FRET acceptor π -conjugated chromophores constituted as part of the backbone.^{3,20} Cationic polyfluorene^{16,17} and poly(fluorene-benzothiadiazole) random copolymers,^{3,21} poly(*p*-phenylenevinylene)s¹⁸ and poly(*p*-phenyleneethylene)s²² are some of the very good examples for the π -conjugated FRET systems. The tunability of the HOMO–LUMO band gap in the π -conjugated chromophores²³ provided unlimited opportunities to make FRET probes functionable from visible to the NIR region.²⁴ The π -conjugated polymer FRET probes were employed as biological sensors,^{22,25} for the detection of

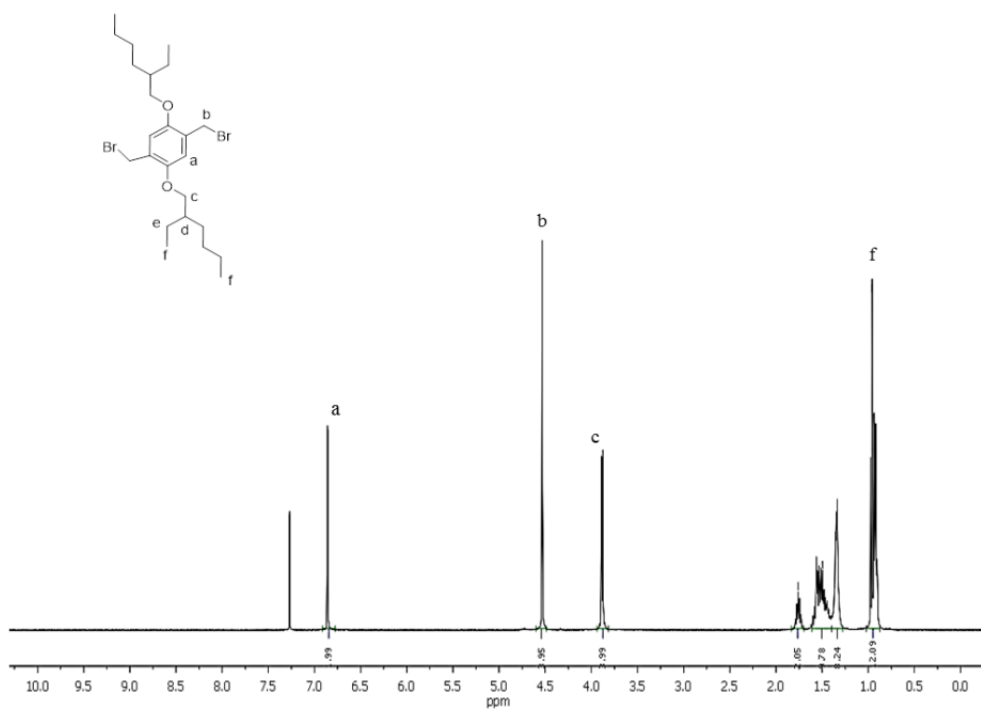
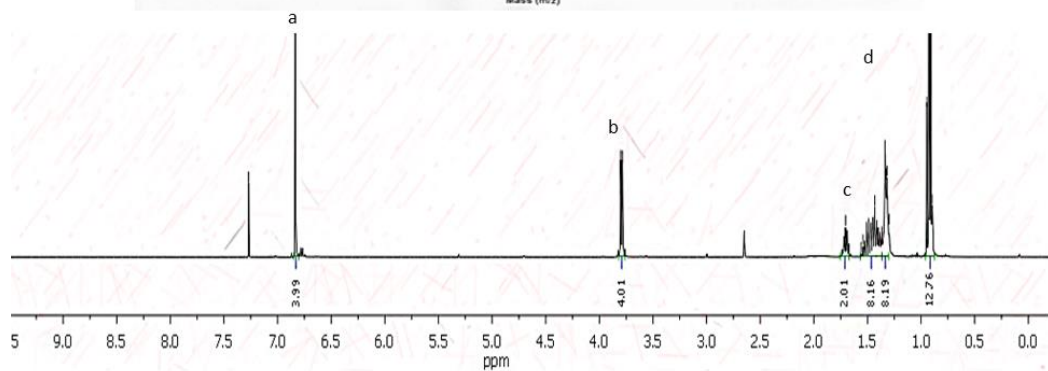
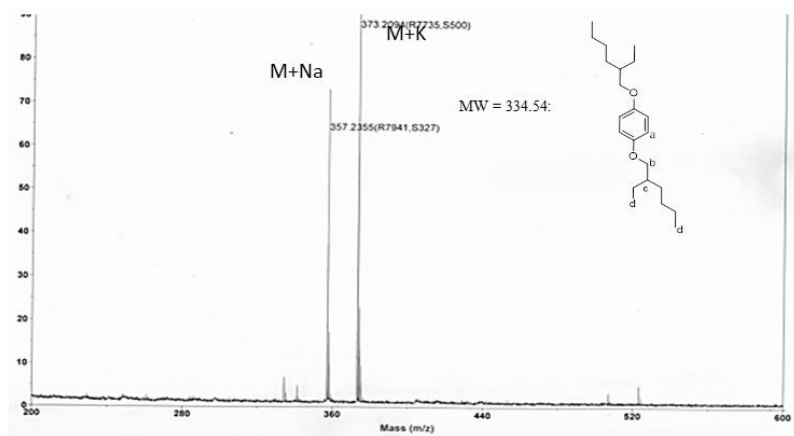
Received: June 29, 2017

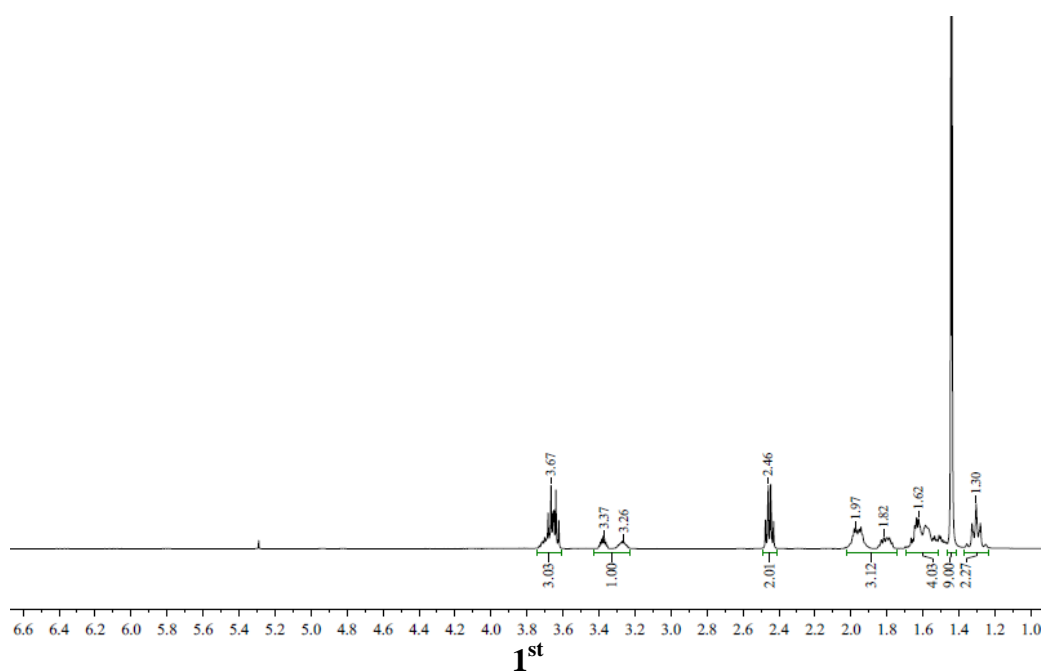
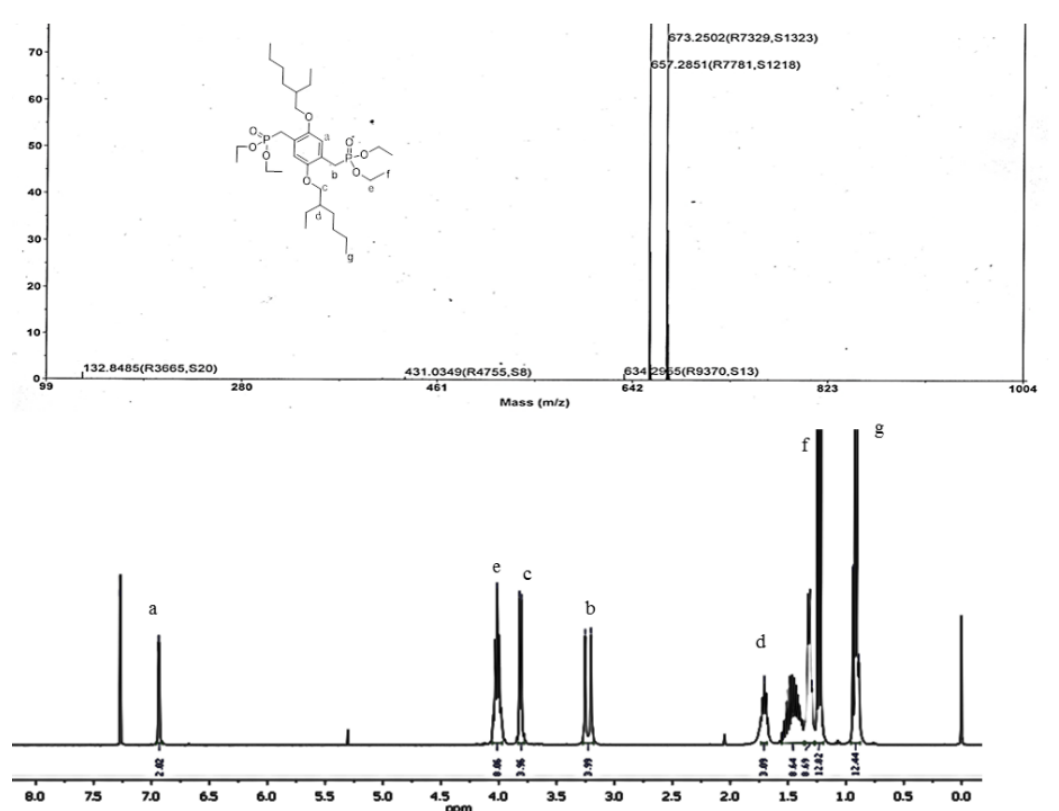
Accepted: July 12, 2017

Published: July 12, 2017

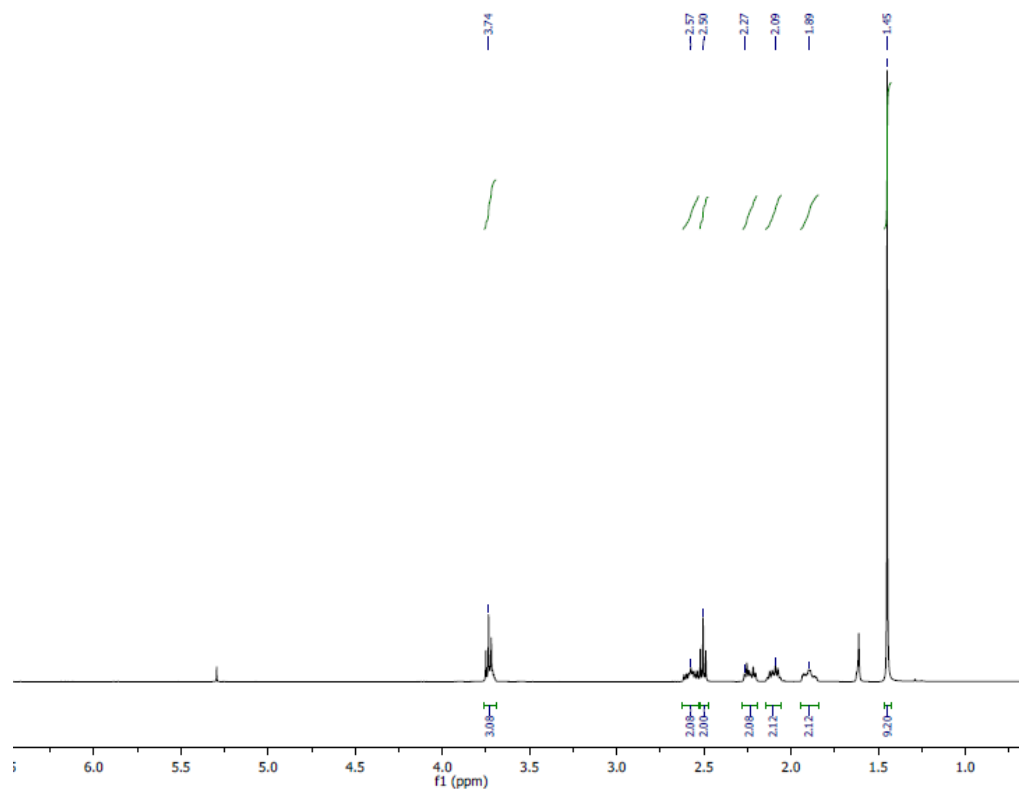
Appendix

8 Appendix

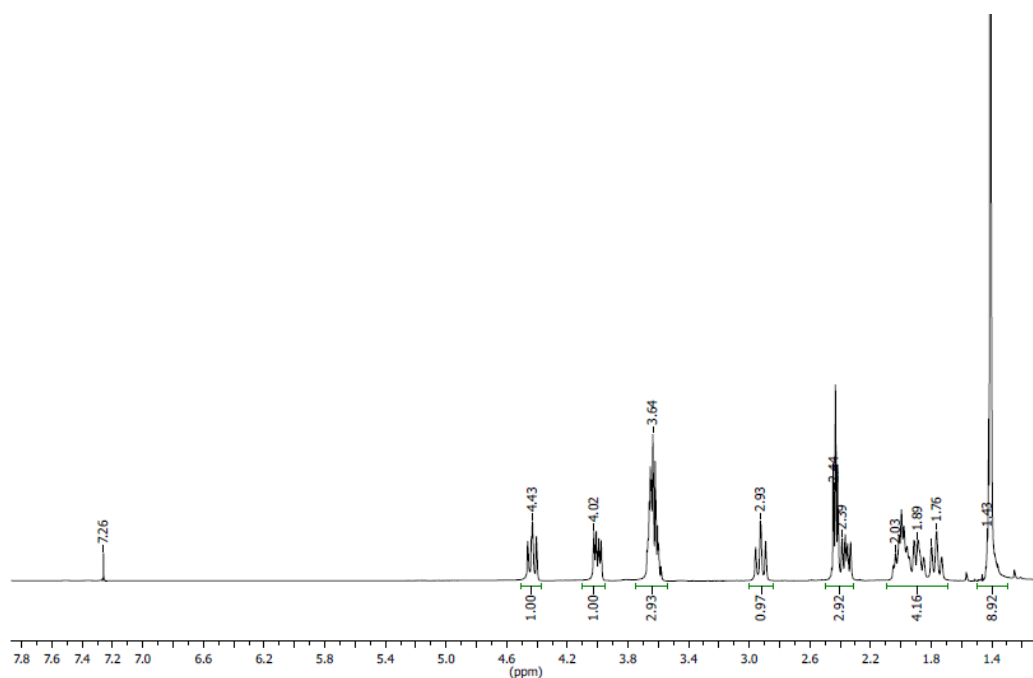




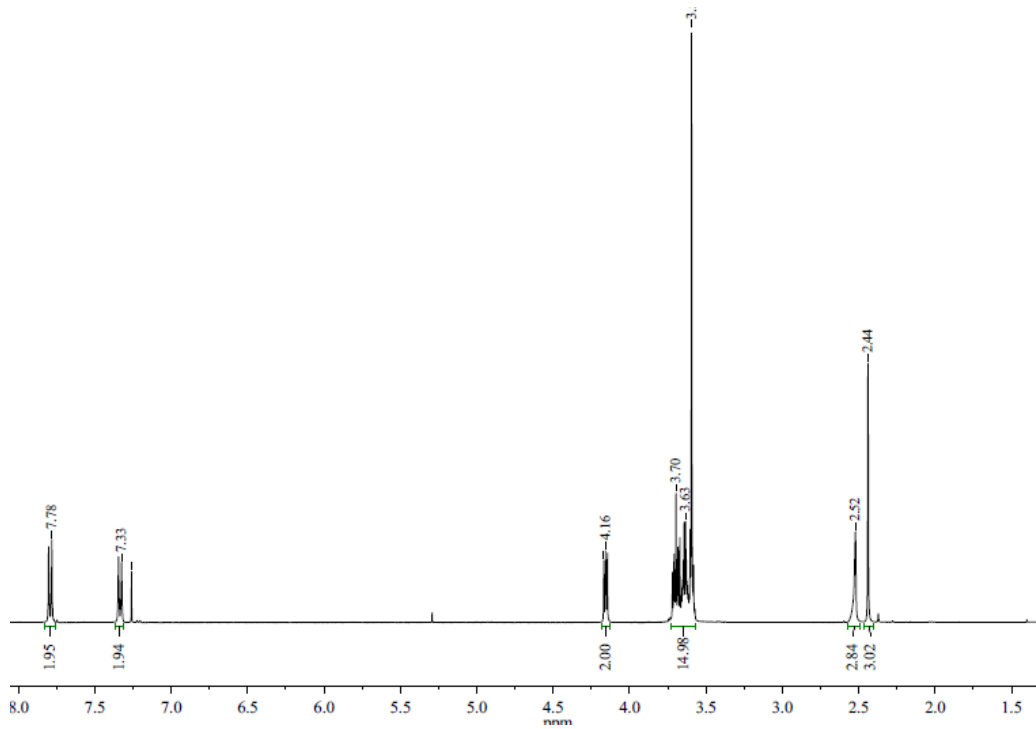
¹H NMR of t-butyl-3-((4-hydroxycyclohexyl)oxy)propionate



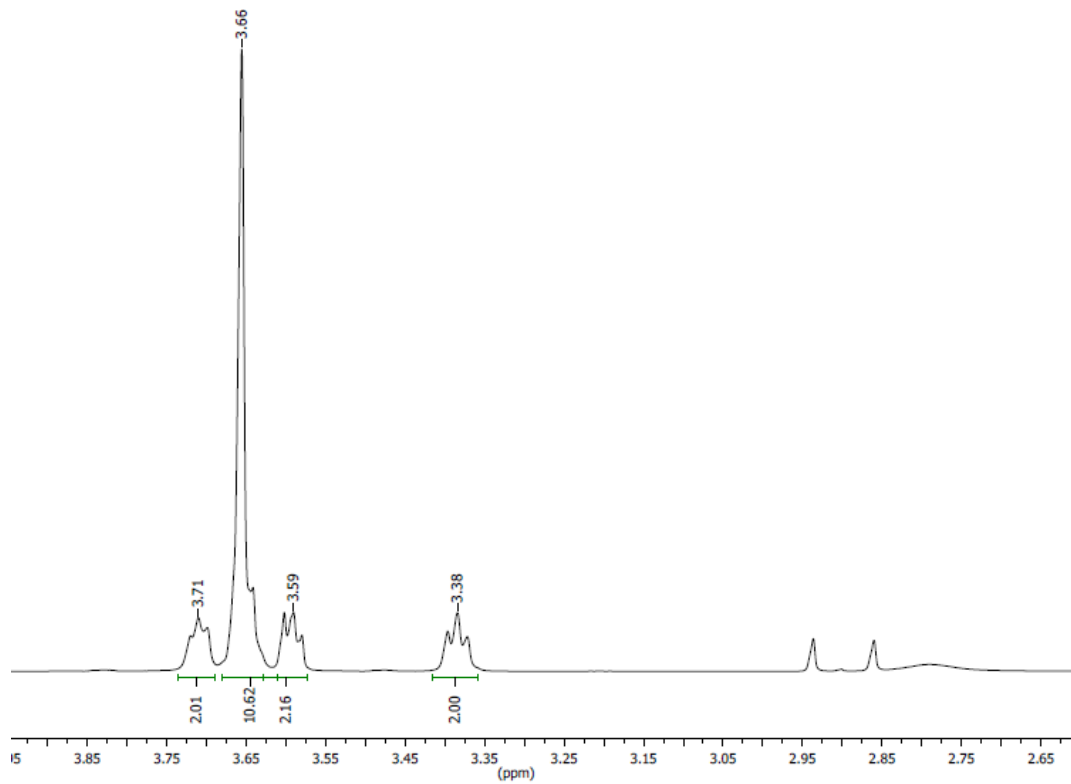
^1H NMR of tert-butyl-3-((4-oxocyclohexyl)oxy)propanoate



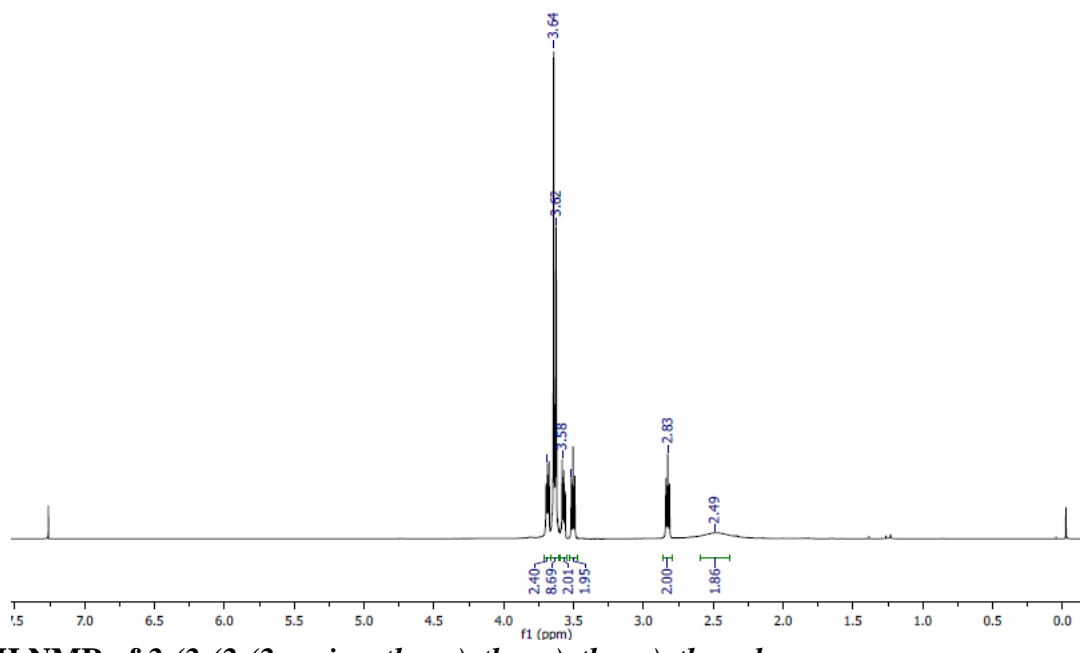
^1H NMR of tert-butyl-3-((7-oxooxepan-4-yl)oxy)propanoate



^1H NMR of *2-(2-(2-(2-hydroxyethoxy)ethoxy)ethoxy)ethyl 4-methylbenzenesulphonate*



^1H NMR of *2-(2-(2-(2-azidoethoxy)ethoxy)ethoxy)ethanol*



1H NMR of 2-(2-(2-(2-aminoethoxy)ethoxy)ethoxy)ethanol



RightsLink®

[Home](#)
[Create Account](#)
[Help](#)


Title: Dual Functional Nanocarrier for Cellular Imaging and Drug Delivery in Cancer Cells Based on n-Conjugated Core and Biodegradable Polymer Arms

Author: Bhagyashree Kulkarni, Bapurao Surnar, Manickam Jayakannan

Publication: Biomacromolecules

Publisher: American Chemical Society

Date: Mar 1, 2016

Copyright © 2016, American Chemical Society

LOGIN

If you're a [copyright.com](#) user, you can login to RightsLink using your [copyright.com](#) credentials. Already a RightsLink user or want to [learn more?](#)

PERMISSION/LICENSE IS GRANTED FOR YOUR ORDER AT NO CHARGE

This type of permission/license, instead of the standard Terms & Conditions, is sent to you because no fee is being charged for your order. Please note the following:

- Permission is granted for your request in both print and electronic formats, and translations.
- If figures and/or tables were requested, they may be adapted or used in part.
- Please print this page for your records and send a copy of it to your publisher/graduate school.
- Appropriate credit for the requested material should be given as follows: "Reprinted (adapted) with permission from (COMPLETE REFERENCE CITATION). Copyright (YEAR) American Chemical Society." Insert appropriate information in place of the capitalized words.
- One-time permission is granted only for the use specified in your request. No additional uses are granted (such as derivative works or other editions). For any other uses, please submit a new request.

[BACK](#)
[CLOSE WINDOW](#)


RightsLink®

[Home](#)
[Create Account](#)
[Help](#)


Title: Fluorescent-Tagged Biodegradable Polycaprolactone Block Copolymer FRET Probe for Intracellular Bioimaging in Cancer Cells

Author: Bhagyashree Kulkarni, Manickam Jayakannan

Publication: ACS Biomaterials Science & Engineering

Publisher: American Chemical Society

Date: Sep 1, 2017

Copyright © 2017, American Chemical Society

LOGIN

If you're a [copyright.com](#) user, you can login to RightsLink using your [copyright.com](#) credentials. Already a RightsLink user or want to [learn more?](#)

PERMISSION/LICENSE IS GRANTED FOR YOUR ORDER AT NO CHARGE

This type of permission/license, instead of the standard Terms & Conditions, is sent to you because no fee is being charged for your order. Please note the following:

- Permission is granted for your request in both print and electronic formats, and translations.
- If figures and/or tables were requested, they may be adapted or used in part.
- Please print this page for your records and send a copy of it to your publisher/graduate school.
- Appropriate credit for the requested material should be given as follows: "Reprinted (adapted) with permission from (COMPLETE REFERENCE CITATION). Copyright (YEAR) American Chemical Society." Insert appropriate information in place of the capitalized words.
- One-time permission is granted only for the use specified in your request. No additional uses are granted (such as derivative works or other editions). For any other uses, please submit a new request.

[BACK](#)
[CLOSE WINDOW](#)